

**Study of the molecular mechanisms  
underlying Bap-mediated cell-cell interactions  
in *Staphylococcus aureus***

AGUSTINA TAGLIALEGNA

Pamplona – Iruña, 2016



**CSIC**

CONSEJO SUPERIOR DE INVESTIGACIONES CIENTÍFICAS

**upna**

Universidad  
Pública de Navarra  
Nafarroako  
Unibertsitate Publikoa



**Gobierno  
de Navarra**



Memoria presentada por

**TAGLIALEGNA AGUSTINA**

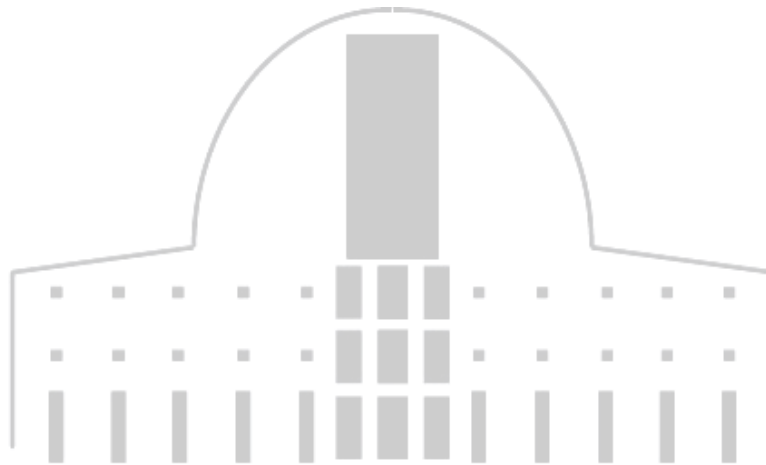
para optar al grado de Doctor por la Universidad Pública de Navarra

**Study of the molecular mechanisms  
underlying Bap-mediated cell-cell interactions  
in *Staphylococcus aureus***

Directores:

Prof. IÑIGO LASA UZCUDUN

Dra. JAIONE VALLE TURRILLAS



**Universidad Pública de Navarra**

Departamento de Producción Agraria

Instituto de Agrobiotecnología

**Nafarroako Unibertsitate Publikoa**

Nekazaritza Ekoizpen Saila

Agrobioteknologiako Institutua



**Prof. ÍÑIGO LASA UZCUDUN**, Catedrático de Microbiología del Departamento del Producción Agraria de la Universidad Pública de Navarra,

**Dra. JAIONE VALLE TURRILLAS**, Investigadora contratada Ramón y Cajal del Consejo Superior de Investigaciones Científicas.

INFORMAN:

Que la presente memoria de Tesis Doctoral “Study of the molecular mechanisms underlying Bap-mediated cell-cell in *Staphylococcus aureus*” elaborada por Doña **AGUSTINA TAGLIALEGNA** ha sido realizada bajo su dirección y que cumple las condiciones exigidas por la legislación vigente para optar al grado de Doctor.

Y para que así conste, firma la presente en Pamplona, a 07 de marzo de 2016.

Fdo. Íñigo Lasa Uzcudun

Fdo. Jaione Valle Turrillas



***A mis padres***





## AGRADECIMIENTOS

*No podría estar más agradecida a todas las personas y entidades que han contribuido a mi crecimiento académico, personal y al desarrollo de esta tesis.*

*Me gustaría empezar agradeciendo a mis directores. A Iñigo, que accedió a tenerme en su labo aún sin conocerme, que ha puesto su confianza en mi y me ha dado la oportunidad de trabajar y aprender en un ambiente científico increíble. Gracias a Jaio, por tener paciencia sobre todo este último tiempo entre tantas idas y venidas y esperas infinitas con el artículo, y por haberme ayudado a aprender todo lo que se.*

*A Salvador Ventura y James Garnett, por su gran implicación y labor científica en la colaboración que mantenemos.*

*A todos los actuales biofilms. Bego, Pedrito, Carmenchu, Bea, Echevel, Amaia, Saio, Solano, y Sonia por tantas risas, excursiones y horas biofilm de tonterías interminables, cada uno con sus montañas rusas emocionales, pero siempre ahí dispuestos a hacernos el aguante y ayudarnos con lo que sea. También quiero agradecer a los ex-biofilms que han pasado por el labo y han coincidido conmigo (Igor, Viol, Villanueva) y por supuesto a Ale: gracias por ayudarme al principio en mi llegada a Pamplona y por estar siempre dispuestísimo a echar una mano en lo que haga falta!*

*A todas las demás personas del IdAB, por su predisposición a ayudar siempre, por los calderetes y las comiditas de navidad! En especial a Victor porque no hay palabras para describir el sol de persona que sos.*

*A Pauletas y su cuadrilla, por habernos hecho un lugarcito en su corazón a Leti y a mi sin dudarlo.*

*A algunas de las personas que conocí en el Master de Agrobiotecnología: Carlitos colombiano, Lili, María Ancin, Ernest, Germán, Saio. Ha sido genial el año que compartimos juntos.*

*A Salo, por haber sido mi mamá navarra y una gran confidente.*

*A algunos de los que han sido mis compañeros de piso: Barbara, Kris, Prea y Lore por ayudarme a desconectar después de largos días en el labo.*

*A mi gran familia española. A Isa, sos una mujer increíble, con una fortaleza única, gracias x tu cariño. A Inma, porque estamos lejos pero seguimos en sintonía como si siguieras en Pamplona. A mi parejita preferida, Argi y Urtzi. Gracias porque por culpa de ustedes a veces me siento más navarra que argentina! Los quiero un montón. A la familia de Argi, porque me han abierto las*

*puertas de su casa innumerables veces y siempre me he sentido una más. A Beita, por las caminatas y charlas después de comer cerca del IdAB. A Arkatiz, Fer y Maribel por compartir tantos momentos divertidos. A Julia, por darme tu apoyo y cariño siempre, por tu gran empatía, las charlas, los viajes y saliditas de sabados. A Charly, por ser ese compañero de poyata y amigo excepcional. Me has hecho reir mucho, también me has hecho enfadar, hemos hablando y reflexionado sobre todo tipo de temas, y siempre me has dado a tu manera el empujon que necesitaba para no bajar los brazos. A Ana y Leti: mis sisters españolas. Gracias. Definitivamente, sin el apoyo cotidiano de ustedes dos en el labo no se si habría podido con todo esto. Las admiro y las quiero. Que nos deparará el futuro después de este doctorado que nos ha unido? Sin dudas algún otro de esos viajes surrealistas en los que cada día es una nueva aventura (tal vez cruzando el charco!?!).*

*A huguito, por tantas sesiones de terapia transatlántica via wasap. Sigamos afinando puntería, que vamos por buen camino!*

*A mi familia de Microbios (Betún, Nocelli, Barquetti, Guillote, Julieta, Julius, Noita, Wasqui, Vanuki, Anita, Orne, Chele, la Vieja y el Flaco). La microbiología nos unió, y una fuerte amistad nos mantiene constantemente conectados. No veo la hora de volverlos a ver y reirme con ustedes a carcajadas sin parar como lo hemos hecho todos estos años, en cada viaje, en cada juntada, en cada congreseada! Los quiero, y gracias a los mini microbios (Bauti, Pia y Emma) por aportar ternura y encanto a este grupo de locos.*

*A Chele. Por miles de audios seca medula a la distancia, filosofando de la vida, del futuro y del presente, haciéndonos el aguante en este periodo de gran cambio para ambas, compartiendo angustias, alegrías y mucho humor. Gracias por tu incondicional apoyo siempre, por ser un pilar fundamental en mi vida.*

*A Anita, Orne, Vani, la Vieja y Vicky B. Gracias por compartir esas ganas de que nuestra amistad permanezca intacta con el tiempo, y por cada palabra de aliento durante estos casi 5 años que he vivido en España. Las adoro.*

*A mi familia, por los ricos asados y los buenos momentos compartidos en mis visitas a Argentina.*

*A Debo, Ceci, Vicky y Eri, por estar presentes a pesar de estar lejos.*

*A mis amadas mascotas: Olivia, Agador, Megala, y también Melinda y Dana que ya no están. Son mis soles. Me hacen sonreír como nadie. Gracias mis pequeñ@s.*

*Por ultimo a las dos personas que mas amo en todo el universo. Mi mami y mi papi. Todo esto es solo posible gracias a ustedes, les debo todo. Son mis mejores amigos, mis personas favoritas, mis almas gemelas. Tenemos un lazo especial los 3. Ustedes me han dado la fuerza que he necesitado para lograr este objetivo y no bajar los brazos nunca. Vos mami, con tu inigualable fortaleza y cariño. Vos papi, con tu chispa cordobesa única, y tu gran bondad y generosidad. Son mi vida, los amo. Gracias.*

¡¡Gracias a tod@s, los llevo en mi corazón!!



Este trabajo ha sido realizado dentro de los siguientes proyectos de investigación: AGL2011-23954, BIO2011-30503-C02-02 y BIO2014-53530-R del Ministerio de Economía y Competitividad.



# TABLE OF CONTENTS

<b>RESUMEN</b> .....	<b>3</b>
<b>SUMMARY</b> .....	<b>9</b>
<b>INTRODUCTION</b> .....	<b>13</b>
Generalities of bacterial biofilms.....	13
How a biofilm is formed? .....	15
Living inside the biofilm.....	18
Beneficial and detrimental biofilms.....	19
Pathogenesis of <i>Staphylococcus aureus</i> .....	20
The extracellular matrix.....	22
The extracellular matrix of <i>Staphylococcus aureus</i> .....	23
PIA/PNAG exopolysaccharide.....	23
Extracellular DNA.....	25
Proteins.....	25
Secreted, non-covalently attached surface proteins.....	28
Autolysin.....	28
Functional amyloids.....	28
Cytoplasmic proteins.....	30
LPXTG cell wall-anchored proteins (CWA).....	30
Microbial surface components recognizing adhesive matrix molecules (MSCRAMMs).....	33
SasG.....	34
SasC.....	35
SraP.....	36
Protein A.....	37
Biofilm-associated protein (Bap).....	37
Structural features of Bap protein.....	38
Role of Bap in biofilm formation.....	41
Role of Bap in pathogenesis.....	41
Regulation of Bap protein expression.....	43
Bap-related proteins.....	46
Structural and functional parallelism between SasG, Aap and Bap.....	49
<b>OBJETIVES</b> .....	<b>53</b>
<b>MATERIALS AND METHODS</b> .....	<b>57</b>
Oligonucleotides, plasmids, bacterial strains and culture conditions.....	57
DNA manipulations.....	57
Electrocompetent <i>Staphylococcus</i> cells.....	57
Generation of mutant strains.....	58
Generation of Bap-ClfA chimeric proteins.....	58
Generation of bap transcriptional and post-transcriptional fusions.....	60
Construction of plasmids for Bap expression in C-DAG system.....	61
Construction of chimeric Bap_B proteins fused to different tags: SpyTag and SNAP-tag® .....	62
Chromosomal labeling of Bap with SNAP-tag® .....	62
Expression and purification of Bap_B recombinant proteins from <i>S. aureus</i> and <i>S. saprophyticus</i> .....	63

Expression and purification of GFP and GFPSpyCatcher recombinant protein.....	64
Production of anti-Bap antibodies.....	65
Biofilm formation and biofilm dispersion assays.....	65
Bacterial clumping assays.....	67
Exogenous complementation.....	68
Microscopy analysis.....	68
Labeling of Bap/SNAP-tag fusion proteins.....	69
Labeling of Bap/SpyTag fusion protein.....	70
Immunoblot analysis.....	71
Identification of aggregative peptides.....	72
Formation of rBap_B aggregates and reversion assay.....	73
EGCG inhibition assay.....	73
Attenuated Total Reflectance - Fourier Transform Infrared spectroscopy (ATR-FTIR) .....	74
Circular dichroism (CD) .....	74
Thermal denaturation.....	75
Tryptophan intrinsic fluorescence.....	75
Static light scattering.....	75
Dynamic light scattering.....	76
Gel filtration chromatography.....	76
Analytical ultracentrifugation (AUC) .....	76
Nuclear magnetic resonance (NMR) .....	77
Thioflavin T binding assay.....	77
Congo Red binding assay.....	77
ProteoStat binding assay.....	78
Bis-ANS assay.....	78
Proteinase-K digestion.....	78
Preparation and aggregation of Bap_B short peptides.....	79
Cell adhesion assay.....	79
Experimental infection.....	79
Statistical analysis.....	80
Sequence analysis programs.....	80
<b>RESULTS.....</b>	<b>89</b>
Analysis of the distribution of Bap on the bacterial surface and its role in the multicellular behavior of <i>S. aureus</i> .....	89
Analysis of Bap regulation and expression.....	92
Bap forms aggregates under acidic solution conditions.....	94
The N-terminal region of Bap forms aggregates.....	96
Role of the N-terminal region in biofilm development.....	103
Purified recombinant Bap_B protein adopts an amyloid conformation at acidic pH.....	108
Identification and characterization of short amyloid stretches in Bap_B	115
Bap protein forms amyloid-like fibrils.....	119
EGCG specific amyloid inhibitor hinders Bap aggregation.....	122
Bap_B amyloid aggregates induce multicellular behavior in Gram-positive bacteria.....	124
Amyloid-like Bap fibers have a role in the pathogenic process of <i>S. aureus</i>	126
Calcium inhibits the formation of Bap amyloid aggregates.....	129
Biophysical characterization of Bap in the presence of calcium.....	133
Effect of pH and calcium on preformed <i>S. aureus</i> biofilms.....	138



The N-terminal domain of Bap homologous proteins generates amyloid-like aggregates.....	140
Use of SNAP-tag® as a tool for visualize <i>in vivo</i> formation of Bap amyloid-dependent matrices.....	148
Use of SpyTag-SpyCatcher system for the biotechnological functionalization of Bap fibers.....	153
<b>DISCUSSION.....</b>	<b>159</b>
Bap protein induces biofilm formation by self-assembly into amyloid-like fibrils.....	159
Bap amyloids formation is regulated by two factors: pH and calcium.....	167
Importance of amyloid sequence stretches in Bap self-fibrillation process...	170
Interaction of Bap amyloid-like fibrils with the bacterial surface.....	172
Bap orthologous proteins display amyloidogenic features.....	173
Contextualization of Bap-mediated multicellular behavior in the physiological situation of mastitis.....	177
Possible biotechnological applications of Bap fibers.....	182
<b>CONCLUSIONS.....</b>	<b>189</b>
<b>CONCLUSIONES.....</b>	<b>193</b>
<b>REFERENCES.....</b>	<b>197</b>



## ***RESUMEN***

---



## RESUMEN

La mayoría de los microorganismos son capaces de vivir en comunidades sésiles, siendo esta forma de crecimiento bastante más frecuente que la forma de vida planctónica. En estas comunidades microbianas, conocidas como biofilms, las células crecen adheridas a un sustrato y embebidas en una matriz exopolimérica que ellas mismas producen, y que confiere numerosas ventajas a la población: integridad estructural, protección ante factores externos, y control de la absorción de nutrientes. La composición de esta matriz extracelular es sumamente compleja, variando entre diferentes especies bacterianas y siendo muy susceptible a los cambios que puedan ocurrir en el ambiente circundante. Aproximadamente el 97% de la matriz es agua; el resto es una mezcla de nutrientes, metabolitos, productos de la lisis celular y polímeros secretados (polisacáridos, lípidos, DNA, proteínas).

*Staphylococcus aureus*, una bacteria comensal y patógena causante de numerosas infecciones agudas y crónicas tanto en animales como en humanos, tiene la capacidad de desarrollar biofilms sobre una gran diversidad de superficies vivas e inertes. Esto representa para la bacteria un importante factor de virulencia que aumenta su persistencia y patogenicidad. Por ello, la sociedad científica ha dedicado grandes esfuerzos a lo largo de las últimas décadas en descifrar la composición de la matriz extracelular estafilocócica, las características estructurales de sus elementos, así como las vías de regulación y los procesos moleculares que controlan su composición. Estudios recientes han puesto de manifiesto que las proteínas son uno de los componentes mayoritarios de la matriz extracelular de *S. aureus*, sin embargo, actualmente poco se sabe acerca de los aspectos relacionados con su organización espacial en la matriz del

biofilm y de las interacciones moleculares con otros componentes de la matriz extracelular o de la célula huésped.

En el presente trabajo, hemos estudiado los mecanismos moleculares mediante los cuales la proteína Bap (Biofilm associated protein) es capaz de inducir la interacción intercelular en *S. aureus*. Bap es una proteína de alto peso molecular que se encuentra anclada covalentemente a la superficie bacteriana mediante un mecanismo dependiente de la enzima sortasa. Hemos determinado que la proteína Bap interconecta células de *S. aureus* a través de un proceso de auto-ensamblaje que da lugar a agregados de tipo amiloide en respuesta a determinadas condiciones ambientales. Mas específicamente, nuestros resultados indican que Bap sufre un procesamiento en el que se liberan fragmentos que contienen la región N-terminal. Esta región tiene una conformación de tipo glóbulo fundido (molten-globule) que cambia a una estructura rica en láminas  $\beta$  cuando el pH se acidifica. El estado glóbulo fundido de los fragmentos N-terminales de Bap se caracteriza por poseer una estructura terciaria poco organizada. Sin embargo, cuando se organiza en laminas  $\beta$  tiene tendencia a polimerizar para formar fibras de tipo amiloide. La transición de Bap desde glóbulo fundido a lamina- $\beta$  no ocurre en presencia de calcio. La unión del calcio a los dominios EF-hand presentes en la región N-terminal de Bap estabiliza la conformación de glóbulo fundido impidiendo la transición a lamina  $\beta$  y el subsecuente ensamblaje de las fibrillas amiloides. Estos resultados indican que Bap juega una doble función en el proceso de formación del biofilm, primero como sensor de condiciones ambientales externas, y segundo como modulo para la construcción de un andamiaje proteico que sustente la matriz del biofilm en determinadas situaciones ambientales. Este comportamiento multicelular dependiente de pH está conservado en

proteínas Bap presentes en otros estafilococos coagulasa negativos. La existencia de proteínas homólogas a Bap en otras bacterias sugiere que este mecanismo de agregación amiloide como estrategia para formar la matriz del biofilm, está conservado en bacterias.

---

Secciones de esta Tesis Doctoral han sido publicadas en:

- [A. Taglialegna](#), S. Navarro, S. Ventura, J. Garnett, S. Matthews, J. R. Penades, I. Lasa and J. Valle (2016). Staphylococcal Bap proteins build amyloid scaffold biofilm matrices in response to environmental signals. *PLoS Pathogens* *In press*.
- [A. Taglialegna](#), I. Lasa and J. Valle (2016). Amyloid structures as biofilm matrix scaffolds *J. Bacteriol* *In press*.





## ***SUMMARY***

---



## SUMMARY

Community-based life style is very common in the microbial world and it happens to be more prevalent than the planktonic mode of growth. In these microbial communities, known as biofilms, cells grow adhered to a substrate and encased in a self-produced exopolymeric matrix, which gives several benefits to the population: it provides structural integrity, protection against external factors and controls nutrient adsorption. The complex composition of this extracellular matrix varies among different bacterial species and is susceptible to changes in the surrounding environment. Around 97% of the matrix is actually water; the rest is a complex of nutrients, metabolites, products from cell lysis and secreted polymers (polysaccharides, DNA, lipids and proteins).

*Staphylococcus aureus*, a commensal as well as a major pathogen responsible for a wide range of serious acute and chronic diseases in humans and animals, has the capacity to reside in biofilms adhered to a plethora of alive and inert surfaces. For bacteria, this represents an important virulence factor that enhances their persistence and pathogenicity thus contributing to the success of the pathogen in both healthcare and community settings. For this reason, the scientific society have dedicated a lot of effort over the past few decades to elucidate the composition of staphylococcal extracellular matrix, the structural features of its elements and the regulatory pathways as well as the molecular processes that control its composition. Recent studies have revealed that proteins are one of the major components of the *S. aureus* extracellular matrix, although their spatial organization and molecular interactions within a biofilm remain in most cases largely unknown.

In the present work, we have studied the molecular mechanism by which Bap (Biofilm associated protein) mediates interbacterial interactions

during biofilm development in *S. aureus*. Bap is a high molecular weight multi-domain protein that is localized at the bacterial cell surface by a covalent sortase-dependent mechanism. We have determined that the protein connects staphylococcal cells through a self-assembly process resulting in the formation of amyloid-like aggregates that build up the biofilm matrix in response to environmental conditions. Specifically, our results indicate that Bap undergoes partial proteolytic cleavage during which fragments containing the N-terminal region are released. This region has a molten globule-like conformation that, when the pH becomes acidic, switch to a  $\beta$ -sheet-rich form. The molten globule-like state of Bap fragments is characterized by a not-well defined tertiary structure. However, when it organizes into  $\beta$ -sheets, it is capable of polymerize to form amyloid-like fibers. Calcium binding to the EF-hand motifs present in the N-terminal region of Bap stabilizes the molten globule conformation preventing  $\beta$ -sheet transition and the subsequent self-assembly into amyloid fibers. These findings define a dual function for Bap, first as a sensor of environmental external signals and second, as a scaffold protein that promotes biofilm development in defined settings. Since the pH-driven multicellular behavior mediated by Bap occurs in coagulase-negative staphylococci, and many other bacteria exploit Bap-like proteins to build a biofilm matrix, the mechanism of amyloid-like aggregation described in the present work may be widespread among bacteria.

---

Sections of this Doctoral Thesis have been published at:

- A. Taglialegna, S. Navarro, S. Ventura, J. Garnett, S. Matthews, J. R. Penades, I. Lasa and J. Valle (2016). Staphylococcal Bap proteins build amyloid scaffold biofilm matrices in response to environmental signals. *PLoS Pathogens* *In press*.

- A. Taglialegna, I. Lasa and J. Valle (2016). Amyloid structures as biofilm matrix scaffolds *J. Bacteriol* *In press*.

# ***INTRODUCTION***

---



## INTRODUCTION

- **Generalities of bacterial biofilms**

For most of the history of microbiology, microorganisms have primarily been characterized as planktonic, freely suspended cells and described on the basis of their growth characteristics in nutritionally rich culture media. It was not until the 1970s that scientific community began to appreciate that bacteria in the biofilm mode of existence constitute a major component of the bacterial biomass in many environments (Costerton, 1999). It is now well recognized that almost all microorganisms in nature, given the right conditions, have the ability to grow as part of a sessile, exopolymer-enshrouded community referred to as biofilms (Donlan, 2002; Borucki *et al.*, 2003; Jefferson, 2004; Uhlich *et al.*, 2006; Berk *et al.*, 2012) (Fig. 1). Furthermore, virtually any surface (biotic and abiotic) can be suitable for bacterial colonization and biofilm formation and in many circumstances the substrate might also be a nutrient source (i.e. cellulose) (Dunne, 2002; Hall-Stoodley and Stoodley, 2002).

Given the diversity of biofilms in nature, it is likely that interspecies interactions play important roles in determining the development, structure and function of these microbial communities. Metabolic cooperation can occur when metabolic by-products of one organism might serve to support the growth of another, and the adhesion of one species might provide ligands allowing the attachment of other species. Also, there might be intense competition for resources, which could limit species diversity within a biofilm (Le *et al.*, 2014). Although, less common, single-species biofilms can also form on medical devices or in the laboratory setting (Donlan, 2002). The enormous effect that microbial biofilms have on human health and industrial productivity has attracted the interest for the study of the mechanisms leading the formation of biofilms in many bacteria.

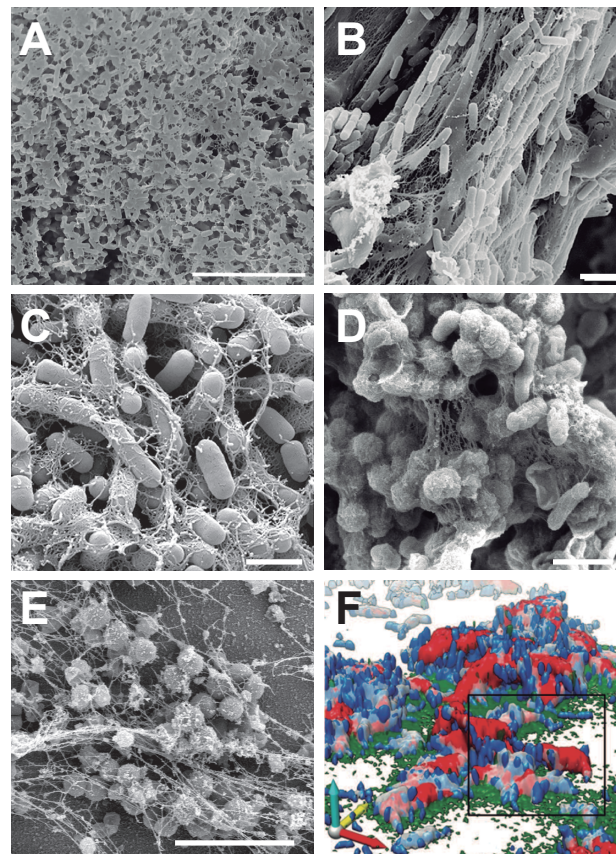


**Figure 1. Biofilms formed by gram-positive and gram-negative bacteria on different substrates.** SEM images of **A)** *Listeria monocytogenes* M39503A on PVC surface, bar=8,6  $\mu$  m (Borucki *et al.*, 2003); **B)** *Bacillus subtilis* from the pellicle at the air-liquid interphase, bar=2  $\mu$  m (Morikawa, 2006); **C)** *Escherichia coli* O157:H7 from the biofilm pellicle located below the medium-air interphase, bar=2  $\mu$  m (Uhlich *et al.*, 2006); **D)** biofilm pellicle produced by *Salmonella enteritidis* at the air-liquid interphase of LB medium, bar=2  $\mu$  m (Lasa, 2006); **E)** *S. aureus* V329 biofilm formed on a glass spatula after an overnight incubation in TSBglu, bar=5  $\mu$  m. **F)** Three-dimensional architecture of *Vibrio cholerae* biofilm. The colors represent distributions of cells (blue), and three different proteins of the bacteria (red, green and grey) (Berk *et al.*, 2012).



- **How a biofilm is formed?**

Biofilms are defined as microbially-derived sessile communities, typified by cells that are attached to a substratum, interface, or to each other, and embedded in a matrix of extracellular polymeric substances (Archer *et al.*, 2011). This is a highly dynamic and regulated process that begins when free-floating bacterial cells attach to a surface. This attachment is followed by growth into a mature, structurally complex biofilm and culminates in the dispersal of detached bacterial cells into the bulk fluid (Hall-Stoodley and Stoodley, 2002) (Fig. 2).

The first step of adhesion to a solid surface is dictated by a number of variables, including surface and bacterial cell wall composition and environmental factors. First, the organism must be brought into close proximity to the surface, driven either randomly by a stream of fluid flowing over a surface as occurs for non-motile bacteria, or in a directed fashion via chemotaxis, twitching (pili) or swimming (flagella) motility (O'Toole *et al.*, 2000; Hall-Stoodley and Stoodley, 2002). Once the organism reaches a surface, adhesion occurs depending on different forces between the microorganism and the substrate (electrostatic and hydrophobic interactions, steric hindrance, van der Waals forces and hydrodynamic forces) and the presence of bacterial surface molecules, such as adhesins or fimbriae (Dunne, 2002). Once irreversible attachment to the surface occurs, the process of biofilm maturation begins. In this stage, bacteria replicate and synthesize extracellular polymeric substances comprising polysaccharides and proteins that form the extracellular matrix and maintain bacteria interacting with each other. At this moment, channels and mushroom-shaped structures form to facilitate nutrient delivery and oxygen circulation to deeper layers of the biofilm (Le *et al.*, 2014). Finally, to conclude the cycle, some bacteria detach from the biofilm and initiate the colonization of new niches. Three different dispersal strategies can be

observed for biofilm bacteria: swarming dispersal, clumping dispersal and surface dispersal (Hall-Stoodley and Stoodley, 2005). Mechanic forces, surfactant molecules and enzymes that degrade biofilm matrix molecules such as nucleases and proteases also stimulate this process (Le *et al.*, 2014). All of these dynamic detachment events could succeed in dispersing biofilm bacteria to new surfaces or to a susceptible host (Hall-Stoodley and Stoodley, 2005) (Fig. 2).

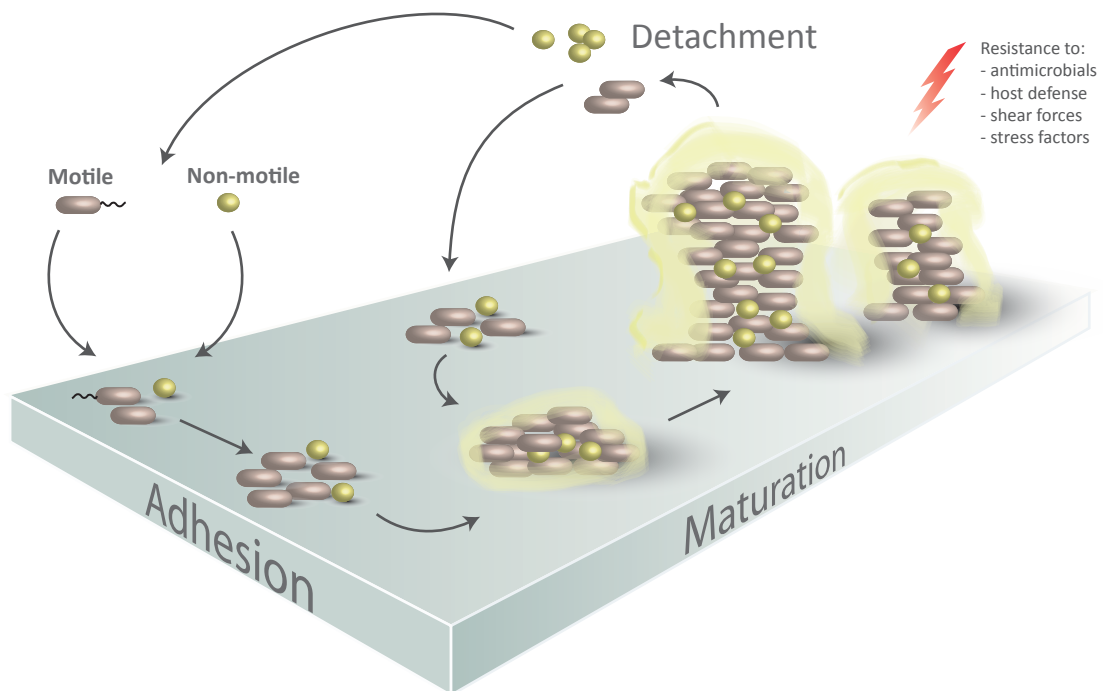


**Figure 2. Steps in biofilm formation.** First, motile and sessile bacteria reach a surface and irreversibly adhere to it. Cell-surface, cell-to-cell interactions and production of the biofilm exopolymeric matrix result in a mature biofilm architecture. Finally, some bacterial cells disperse from the biofilm to colonize nearby surfaces.

- **Living inside the biofilm**

Each bacterium within a biofilm lives in a customized microniche taking part of a complex microbial community that has a primitive circulatory (homeostasis) system and metabolic cooperativity (Costerton *et al.*, 1995). Thus, sessile cells in the biofilm exhibit an altered phenotype with regard to growth, gene expression and protein production compared to the planktonic cells of the same species.

Community-based mode of growth confers several advantages to microorganisms, some of which are named below. The extracellular matrix is capable of sequestering water and concentrating environmental nutrients such as carbon, nitrogen and phosphate. Accumulation of enzymes is also important for biofilm since enables the digestion of exogenous macromolecules for nutrient acquisition and the degradation of the extracellular polymeric substance, allowing the release of cells from biofilms. Organisms within biofilms can withstand nutrient deprivation, pH and osmolarity changes and the presence of oxygen radicals (Fux *et al.*, 2005; Archer *et al.*, 2011). Biofilms growing in natural and industrial environments are resistant to bacteriophage, amoebae, and to the chemically diverse biocides used to combat biofouling in industrial processes. Furthermore, biofilm-forming bacteria can withstand host immune responses, and they are much less susceptible to antibiotics than their nonattached planktonic counterparts (Dunne, 2002). This is not only due to the fact that a dormant phenotype established within the biofilm renders the organisms indifferent to biological activity, but also because the biofilm matrix acts as a barrier that prevents the perfusion of biocides, being an environment that can adversely affect the activity of the antimicrobials (Dunne, 2002).

- **Beneficial and detrimental biofilms**

The establishment of biofilms on diverse surfaces can have both a beneficial or a detrimental effect (Dunne, 2002). On the beneficial side, the use of biofilms has been probed to increase the productivity of agriculturally important leguminous plants (Espinosa-Urgel, 2004) and to act as efficient biocontrol agents through the formation of biofilms in the plant rizosphere (Chen *et al.*, 2013). Reactors with bacterial biofilms have been successfully used in wastewater treatment, reduction of corrosion of metal surfaces, degradation of harmful compounds from petroleum or other contaminants and the production of fermented products such as vinegar and acetic acid (Morikawa, 2006; Zuo, 2007). Besides, probiotic bacteria capable to form biofilms on the tooth surface, vagina and digestive tract are proposed as an alternative strategy to diminish colonization by bacterial pathogens (Kolenbrander, 2000).

On the harmful side, biofilms can cause filters obstruction and blockage of conducts in water distribution systems, corroding metal surfaces, and contaminating food processing equipment (Carpentier and Cerf, 1993; Dunne, 2002; Tournu and Van Dijck, 2012). In medicine, it has been recognized that biofilms readily colonize many body compartments, especially when the host defense is compromised. For instance, numerous bacterial species are capable of colonizing teeth surface causing caries, heart valves causing endocarditis, lungs of cystic fibrosis patients causing chronic bronchopneumonia, middle ear in patients with chronic and secretory otitis media, sinus in chronic rhinosinusitis, bones in chronic osteomyelitis (Høiby *et al.*, 2011). Also, biofilm development is associated with infections caused by implantable medical devices. Surface of implants provide a focal point for infecting pathogens. Immediately after exposure of a device to body fluids, macromolecular components (serum albumin, fibrinogen, collagen, and fibronectin) adsorb to form a conditioning film,

which will ultimately contribute to subsequent bacterial adhesion (Reid, 1999). Biofilm formation on devices as shunts, prostheses (voice, heart valve, knee, etc.), stents, implants (lens, breast, denture, etc.), endotracheal tubes, cardiac pacemakers and various types of catheters result in infections that are usually hard to eradicate by conventional antibiotic therapy. As a consequence, current treatment guidelines recommend the removal of infected devices, given their persistence in the face of antimicrobial therapy (Donlan, 2001).

- **Pathogenesis of *Staphylococcus aureus***

*Staphylococcus aureus* is a Gram-positive, ubiquitous bacterial species. It is a commensal as well as a major pathogen responsible for a wide range of serious acute and chronic diseases, both in humans and animals (Weidenmaier *et al.*, 2012). Approximately 30% of the human population is colonized with *S. aureus* being the anterior nares of the nose the most frequent carriage site (Tong *et al.*, 2015). Extra-nasal sites that typically harbor the organism include the skin, perineum, and pharynx. Other less frequent carriage sites include the gastrointestinal tract, vagina, and axillae (Wertheim *et al.*, 2005). The organism can be carried asymptotically for weeks or months on mucous membranes. Colonization is believed to precede infection, since it provides a reservoir from which bacteria can be introduced when host defenses are penetrated (Archer, 1998; Gordon and Lowy, 2008). Once the organism is inoculated from a site of carriage, the infection can spread locally or can gain access to the blood (Archer, 1998) causing a plethora of infections ranging from mild skin and wound infections to more serious infections such as septicaemia, endocarditis, osteomyelitis and toxic shock syndrome (Arvidson and Tegmark, 2001).

The success of the organism as a pathogen and its ability to cause such a wide range of infections are due to the combined action of extensive virulence factors comprising extracellular toxins, enzymes, and cell surface proteins (Archer, 1998). These virulence factors can promote *S. aureus* pathogenesis by (i) mediating adhesion of bacteria to cells and tissues through numerous surface proteins, (ii) promote tissue damage and spread by expression of proteases, lipases, nucleases, hyaluronate lyase, and (iii) protect the bacteria from the host immune system through the action of leukocidins, capsular polysaccharides, the protein A and small amphipathic peptides called “phenol soluble modulins” (PSMs) (Archer, 1998; Arvidson and Tegmark, 2001). Highly important is the presence of specific global regulatory systems, such as *agr* and *sarA*, that determine which virulence factors are produced at specific times during growth and in response to the local environment (Archer, 1998).

Due to its ubiquity and ability to survive outside the body, infections caused by *S. aureus* are highly prevalent both in the community and in hospital settings. *S. aureus* infections become particularly dangerous when they are caused by strains that are resistant to commonly used antibiotics. Due to the widespread use of the antibiotic methicillin in the 1960s, several strains exist that are resistant to a wide range of  $\beta$ -lactam antibiotics, known as methicillin-resistant *S. aureus* or MRSA (Kreiswirth *et al.*, 1993). MRSA infections are difficult to treat, with a mortality rate of 20%, and are the leading cause of death by a single infectious agent in the USA, being responsible for more deaths than HIV (Klebens *et al.*, 2007). Methicillin resistance is conferred by the *mecA* gene, which encodes a penicillin-binding protein (PBP2) with decreased affinity for  $\beta$ -lactam antibiotics. *mecA* is part of a mobile genetic element called the “staphylococcal cassette chromosome (SCC) *mec*” which is flanked by cassette chromosome

recombinase genes (*ccrA/ccrB* or *ccrC*) that allow intra- and interspecies horizontal transmission of *SCCmec* (Gordon and Lowy, 2008). The high prevalence of MRSA infections is a serious challenge faced in contemporary medical practice, therefore alternative therapies with new agents for the treatment of staphylococcal infections are needed. Vancomycin is currently the drug of choice for the treatment of MRSA, but is being compromised by the recent emergence of vancomycin-intermediate or -resistant *S. aureus* (VISA and VRSA) strains (Jones, 2008). The *S. aureus* infection rate has been correlated with an increase in the use of prosthetic and indwelling devices in modern medical practices (Gordon and Lowy, 2008). *S. aureus*, as well as other coagulase-negative staphylococci, displays a strong capacity to irreversibly attach to the surface of implanted medical devices and forms multilayered communities of bacteria that grow embedded in a self-produced extracellular matrix. The capacity to reside in biofilms enhances *S. aureus* persistence and pathogenicity thus contributing to the success of this bacterium as a human pathogen in both healthcare and community settings (Brady *et al.*, 2008; McCarthy *et al.*, 2015).

- **The extracellular matrix**

The formation and maintenance of biofilms critically depends upon the production of extracellular substances that, in conglomerate, constitute the extracellular matrix. The composition and architecture of this matrix is very complex and varies among different bacterial species or even within the same species, under different environmental conditions (Wimpenny *et al.*, 2000). However, in spite of its heterogeneous conformation, biofilm matrix displays some common features. Around 97% of the matrix is actually water; the rest is a complex of secreted polymers, absorbed nutrients and metabolites, products from cell lysis and even particulate material and detritus from the immediate surrounding environment. Thus, all



major classes of macromolecule – proteins, polysaccharides, DNA and RNA – can be present in addition to peptidoglycan, lipids, phospholipids and other cell components (Sutherland, 2001).

In the next section, I will focus on the description of the biofilm matrix of *S. aureus* (Fig. 3).

- **The extracellular matrix of *Staphylococcus aureus***

### **PIA/PNAG exopolysaccharide**

Extracellular polysaccharides are usually very important components of biofilm matrices. In staphylococci, one of the first and best characterized exopolysaccharide compound of the biofilm matrix was the polysaccharide intercellular adhesin (PIA) of *Staphylococcus epidermidis* (Mack *et al.*, 1996). Later, a PIA-related exopolysaccharide, whose chemical composition is poly- $\beta$  (1,6)-linked *N*-acetyl D-glucosamine (PNAG), was described in *S. aureus* (McKenney *et al.*, 1999; Cramton *et al.*, 1999). PIA and PNAG are structurally and immunologically identical and are both synthesized by the action of four homologous proteins (IcaA, IcaD, IcaB, and IcaC) encoded by genes organized in the *icaADBC* (intercellular adhesion) operon (Lasa, 2006; Arciola *et al.*, 2015). IcaA, C and D are located in the membrane fraction while IcaB is mainly present in the culture supernatant (Götz, 2002). IcaA contains four transmembrane helices and has *N*-acetylglucosaminyl-transferase activity with UDP-*N*-acetylglucosamine as a substrate. IcaA alone has only low transferase activity, but when it is co-expressed with IcaD it reaches full transferase activity. IcaD appears to be a chaperone that directs the correct folding and membrane insertion of IcaA and, in addition, it might act as a link between IcaA and IcaC. The *N*-acetylglucosamine oligomers produced by IcaAD reach a maximal length of only 20 residues;

for longer oligomers to be synthesized the *icaAD* genes need to be co-expressed with *icaC*. IcaC protein might also be involved in the export of the growing PIA/PNAG chain (Gerke *et al.*, 1998). The surface attached protein IcaB is responsible for deacetylation of the poly-*N*-acetylglucosamine molecule that introduces positive charges crucial for its biological function (Vuong *et al.*, 2004). The divergently transcribed *icaR* gene, which is located upstream of the *icaADBC* operon in both *S. epidermidis* and *S. aureus*, encodes a transcriptional repressor with a central role in the environmental regulation of *ica* operon expression. Modification of the bacterial environment by the addition of NaCl or ethanol to the growth medium can activate the *ica* operon via separate regulatory pathways in an *icaR*-dependent manner (O'Gara, 2007).

This glucosaminylglycan plays a fundamental function in mediating intercellular adhesion of bacterial cells. In addition to aggregation, this exopolysaccharide has important structural functions in the biofilm matrix architecture and is implicated in bacterial adhesion to biomaterial surfaces as well as evasion from host immune-response (Arciola *et al.*, 2015).

The *ica* locus is present not only in *S. epidermidis* and *S. aureus*, in which it is well conserved, but also in other *Staphylococcus* species like *S. auricularis*, *S. capitis*, *S. intermedius*, *S. lugdunensis* and *S. pasteurii* (Cramton *et al.*, 1999). Moreover, the same exocellular polysaccharide has been recently identified even in numerous other gram-negative bacterial species members such as *Escherichia coli*, *Yersinia pestis*, *Pseudomonas fluorescens*, *Bordetella spp.*, *Aggregatibacter actinomycetemcomitans* and *Actinobacillus pleuropneumoniae* (Arciola *et al.*, 2015). The extended distribution of this biofilm matrix component in several bacterial genera denotes the extremely important function that this polysaccharide plays in the biofilm formation process along with other matrix molecules described as follow.

## **Extracellular DNA**

There are numerous studies that describe an important role for extracellular DNA (eDNA) in the structure of biofilm matrix as a cell-to-cell interconnecting compound. Bacteria release DNA in order to favor exchange of genetic material, especially antibiotic resistance genes (Pamp and Gjermansen, 2007). There are experimental evidences that confirm the presence of eDNA in the biofilm matrices of many bacteria such as *Pseudomonas aeruginosa*, *Bacillus cereus*, *Listeria monocytogenes*, *S. epidermidis* and *S. aureus* (Allesen-Holm *et al.*, 2006; Rice *et al.*, 2007; Qin *et al.*, 2007; Mann *et al.*, 2009; Vilain *et al.*, 2009; Harmsen *et al.*, 2010). In these bacteria, eDNA is relevant during early stages of biofilm formation, and its release from bacterial cells and its permanency within the matrix appears to be a regulated process involving different factors. In the case of *S. aureus*, several gene products have been shown to affect the release of eDNA into the early biofilm matrix. The *cid* and *Irg* operons encode effectors and inhibitors of cell lysis, respectively, controlling DNA release during biofilm development. Mutations in both of these operons led to aberrant biofilm maturation, indicating that balanced expression of these genes is important in biofilm development (Mann *et al.*, 2009). Furthermore, staphylococcal thermonuclease is also important in biofilm development, since the eDNA produced as a result of lysis is countered by nuclease-mediated degradation (Mann *et al.*, 2009). Other mechanisms that liberate eDNA into the biofilm matrix include the autolysin Atl which hydrolyses staphylococcal cells, and phage genes that change from lysogenic to lytic form in the stressed environment of the biofilm (Archer *et al.*, 2011).

## **Proteins**

So far, it is clear that PIA/PNAG polysaccharide and extracellular DNA are key factors involved in the elaboration and maintenance of the

extracellular matrix of *S. aureus* (Fig. 3). However, proteins constitute another extremely crucial and extensively studied part of the biofilm in this microorganism; they can act at different stages of the biofilm formation process, and they can build the extracellular matrix by interacting with eDNA and polysaccharides, or, in most cases, through a completely polysaccharide-independent mechanism. In the next section, *S. aureus* proteins implicated in biofilm development will be described, with special emphasis on Bap protein.

Classification according to the cellular location and type of attachment to the staphylococcal surface divides proteins into two major groups: (i) those that are secreted outside the cell and can either attach non-covalently to the cell surface or remain embedded in extracellular matrix, and (ii) those that remain covalently anchored to the bacterial surface.

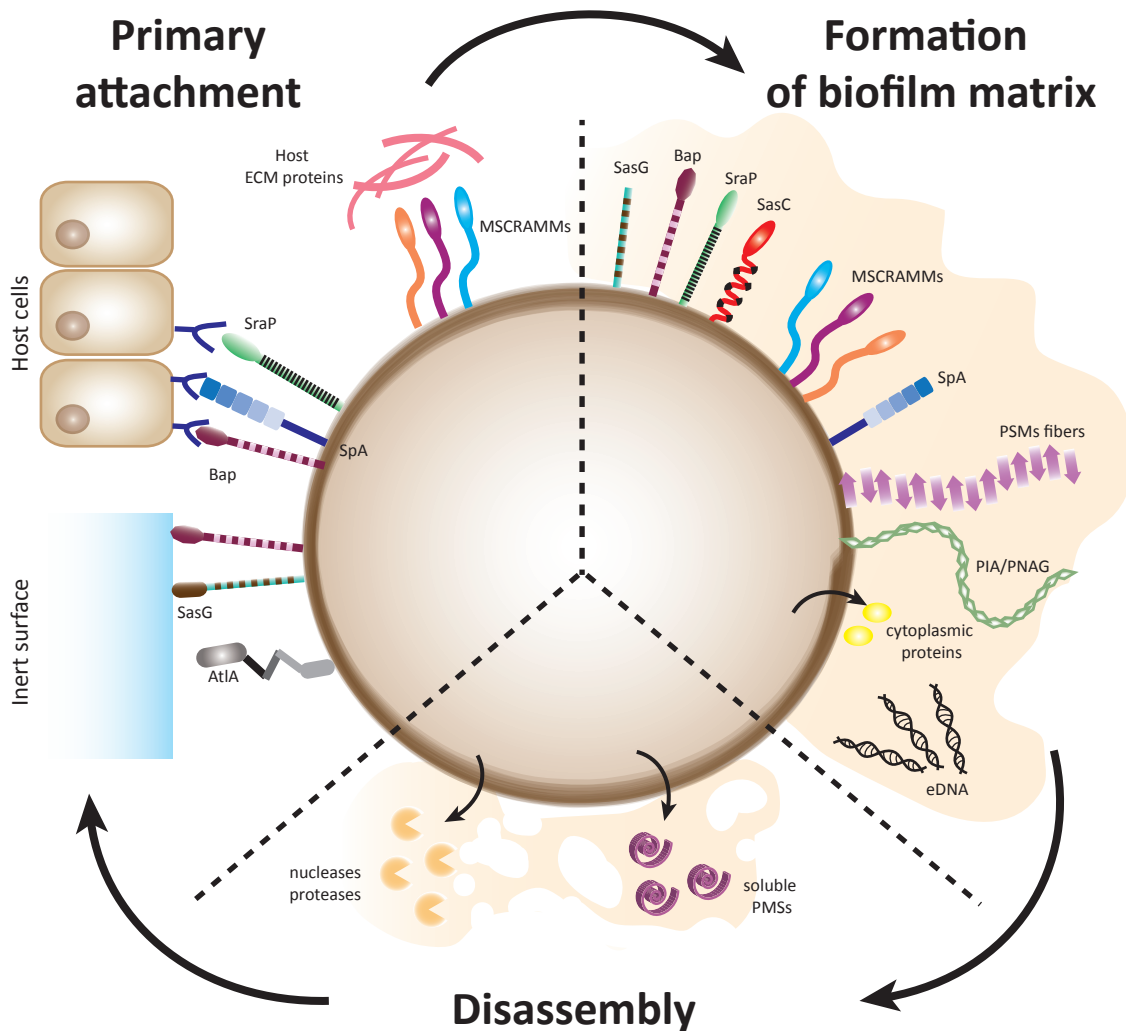


**Figure 3. Schematic diagram showing the contribution of surface proteins, polysaccharide and eDNA to *S. aureus* biofilm formation.** *S. aureus* can attach to an inert substrate or to epithelial host cells through an array of adhesins. During bacterial accumulation, several adhesins, amyloid fibers, PIA and eDNA participate in the formation of biofilm matrix. Next, enzymes and amphipathic molecules partially digest the matrix to aid staphylococcal cells disperse from the biofilm.

⇒ **Secreted, non-covalently attached surface proteins**

***Autolysins***

The autolysin Atl is the most predominant peptidoglycan hydrolase in staphylococci. AtlA of *S. aureus* (Oshida *et al.*, 1995), and AtlE of *S. epidermidis* (Heilmann *et al.*, 1997) are well-studied bifunctional enzymes, composed of an amidase and a glucosaminidase domain, and are involved in the cell wall turnover, cell division and separation and in the lysis of bacteria induced by the  $\beta$ -lactam antibiotics (Biswas *et al.*, 2006). Particularly, the structure of AtlA proprotein is composed of amidase (AM) and glucosaminidase (GL) domains separated by three direct repeats, R1, R2, and R3. Proteolytic cleavage of pro-Atl via an uncharacterized mechanism generates a 62-kDa peptide (amidase) and a 51-kDa peptide (glucosaminidase) (Houston *et al.*, 2011).

In addition to its role in cell division, several studies have described the importance of this adhesin in the initial stages of biofilm formation (Biswas *et al.*, 2006; Houston *et al.*, 2011; Bose *et al.*, 2012). An *atlA* mutant was deficient in primary attachment, whereas the wild type and the complemented mutant were not (Biswas *et al.*, 2006). Both AM and GL domains are essential for optimal biofilm development (Bose *et al.*, 2012). Thus, unprocessed wall-anchored Atl appears to promote primary attachment to surfaces whereas subsequent proteolytic cleavage of Atl leads to cell lysis, eDNA release, and cell accumulation that favors biofilm development (Houston *et al.*, 2011) (Fig. 3).

***Functional amyloids***

In *S. aureus*, the first and so far the only evidence of functional amyloids was reported by Schwartz and collaborators, who discovered that

*S. aureus* expresses fibers with amyloid-like properties that are composed of small peptides known as phenol soluble modulins (PSMs) (Schwartz *et al.*, 2012). PSMs can be classified according to their length:  $\alpha$ -PSMs can be 20-25 amino acids in length, and  $\beta$ -PSMs are about double that size (43-45 amino acids). *S. aureus* expresses four  $\alpha$ -PSM peptides encoded in the  $\alpha pms$  locus, two  $\beta$ -PSM peptides encoded in the  $\beta psm$  locus, and the  $\delta$ -toxin encoded within RNAlII, the effector molecule of the Agr system (Cheung *et al.*, 2014). These peptides are exported by an ATP-binding cassette (ABC) transporter with two separate membrane components (PmtB and PmtD) and two separate ATPases (PmtA and PmtC) (Chatterjee *et al.*, 2013). PSMs can be present either as soluble peptides or as polymerized amyloid structures. When soluble, PSMs adopt an amphipathic  $\alpha$ -helix that is able to stimulate chemotaxis of neutrophils, formation of pores in the membrane of competing microbes and host cells, and to act as surfactant molecules in the dispersal of biofilms. The soluble  $\alpha$ -helical peptides can switch, under still poorly understood environmental conditions, to  $\beta$ -sheet rich protein. In this conformation, the peptides aggregate and provide functional support to the biofilm community (Syed and Boles, 2014). Thus, PSMs are bifunctional peptides that can be stored as inert fibrils in a sessile biofilm matrix or as soluble peptides when environmental conditions call for biofilm disassembly and virulence (Schwartz *et al.*, 2012; Schwartz *et al.*, 2016) (Fig. 3).

Additionally, the signal peptide of the *S. aureus* quorum-sensing signal AgrD (N-AgrD) was shown to be present in *S. aureus* amyloid fibrils during biofilm growth. This peptide is capable of seeding amyloid polymerization of PSMs (Schwartz *et al.*, 2014).

### ***Cytoplasmic proteins***

Another group of proteins that participates in biofilm growth of *S. aureus* are cytoplasmic proteins, including enolase, transketolase, GAPDH, acetolactate synthase and lactate dehydrogenase, among others. These proteins are released during stationary phase, probably as a result of regulated autolysis, and reversibly associate to the staphylococcal surface in response to decreasing pH during biofilm formation (Foulston *et al.*, 2014). Some of these cytoplasmic proteins were found to be present in the exoproteome of both exopolysaccharide-based and protein-based biofilm matrices of *S. aureus* clinical strains (Gil *et al.*, 2014). These surface-aggregated cytoplasmic proteins appears to be an important component of the extracellular matrix that hold cells together in the biofilm, and this might be a frequent feature of biofilm formation in many *S. aureus* strains (Fig. 3). Also, the recycling of these cytoplasmic proteins as matrix components provides to *S. aureus* the advantage of not investing in the production of dedicated matrix proteins during biofilm formation, representing an efficient and versatile strategy for building multicellular communities (Foulston *et al.*, 2014).

### **⇒ LPXTG cell wall-anchored proteins (CWA)**

The surfaces of staphylococcal cells are decorated with a variety of CWA proteins that are anchored to peptidoglycan by the enzymatic activity of sortases (Foster *et al.*, 2014). The precise repertoire of CWA proteins varies among strains and can be altered by growth conditions. *S. aureus* can express up to 24 different CWA proteins whereas coagulase-negative staphylococci such as *S. epidermidis* and *S. lugdunensis* express a smaller number. Secretory signal sequences that are located at the amino terminal (N-terminal) region direct the translated proteins to the secretory (Sec) apparatus in the membrane and are cleaved during secretion. At their

30



carboxy terminal (C-terminal) region, each of these proteins has a characteristic sorting signal, which facilitates their covalent anchorage to peptidoglycan. The housekeeping Sortase A anchors the majority of CWA proteins, which have the LPXTG motif within their sorting signal. In contrast, Sortase B of *S. aureus* and *S. lugdunensis* anchors Isd proteins which have sorting signals with the motif NPQxN/P and are only expressed under iron-restricted conditions (Speziale *et al.*, 2014). The different groups of cell wall-anchored proteins present in *S. aureus* that are particularly involved in biofilm formation are classified and described in detail in the next section according to structural and functional considerations (Fig. 4).

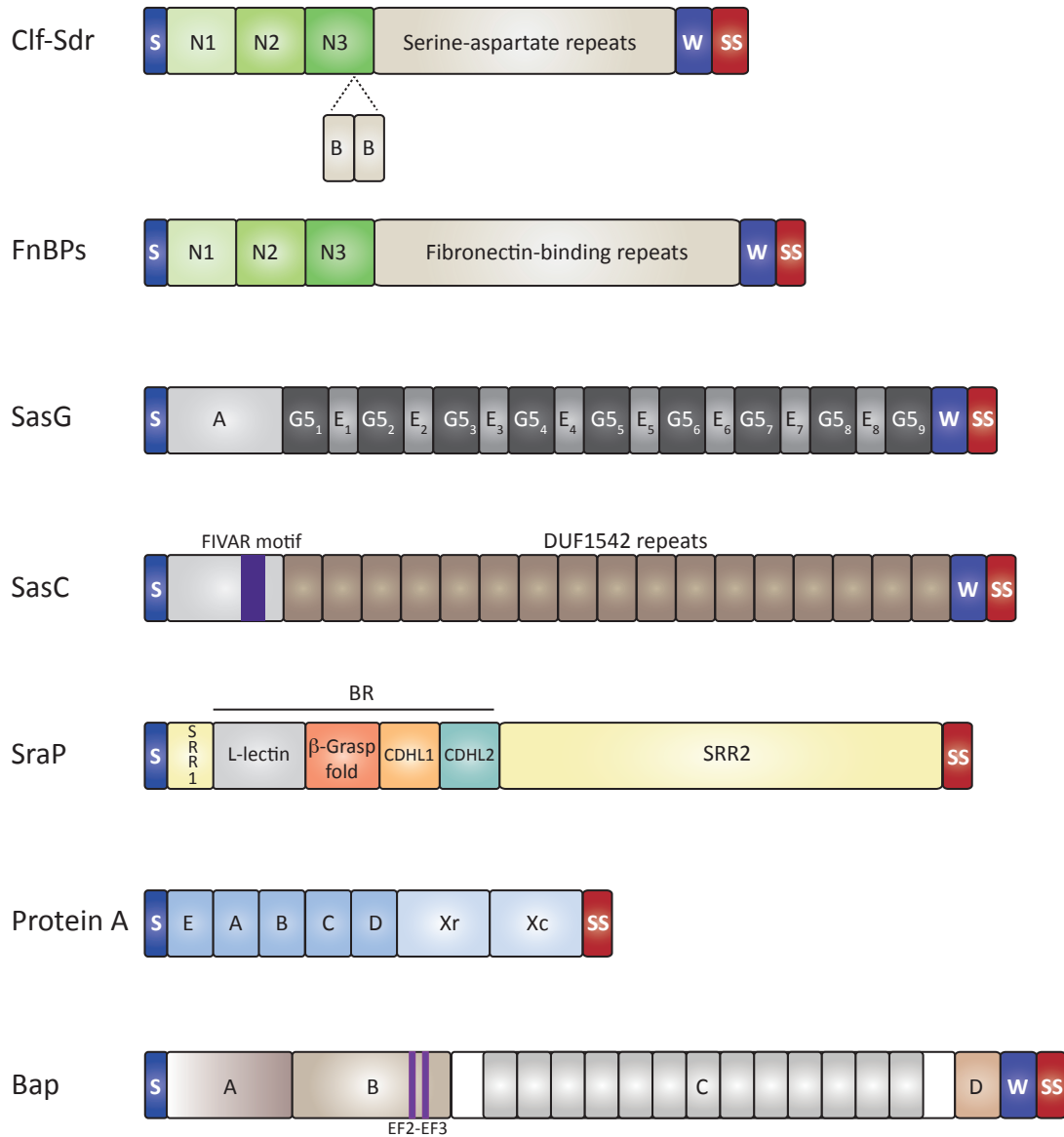


**Figure 4. Illustration of the major cell wall-anchored proteins of *S. aureus*.** The diagrams show the organization of the proteins into subdomains. Common features of CWA proteins are S, secretory signal peptide, W, wall-spanning region, and SS, the sorting signal. Structures were adapted from (Foster *et al.*, 2014) for Clf-Srd, FnBPs, SasG, SraP, and Protein A; from (Cucarella *et al.*, 2001) for Bap; and from (Schroeder *et al.*, 2009) for SasC.

### ***Microbial surface components recognizing adhesive matrix molecules (MSCRAMMs)***

The MSCRAMM family includes proteins that share structural similarities and a common mechanism for ligand binding. These proteins are characterized by an N-terminal region which contains at least two adjacent IgG-folded domains responsible for ligand binding (Foster *et al.*, 2014).

Among the most studied members of this family are Clumping factor A (ClfA), ClfB, serine-aspartate repeat protein C, D and E (SdrC, SdrD, SdrE), and Fibronectin-binding proteins A and B (FnBPA and FnBPB). The A region of these proteins is composed of three separately folded subdomains: N1, N2 and N3, these last two comprising the characteristic IgG-like folds responsible for binding to fibrinogen through a dock, lock and latch (DLL) mechanism. Following, there is a R region composed of serine-aspartate repeats (SD region) in the case of Clf-Sdr subfamily, or tandem repeats of fibronectin-binding domain in the case of FnBPs. The Sdr proteins have two additional B repeats located between the A region and the SD region that act as rigid rods to project the A domain further from the cell surface (Speziale *et al.*, 2014; Foster *et al.*, 2014) (Fig. 4).

Due to their capacity to bind host matrix molecules, MSCRAMM proteins are involved in the primary attachment to host tissues and synthetic surfaces coated with plasma proteins, such as fibronectin, fibrinogen, vitronectin, and collagen. Several MSCRAMM proteins can also promote biofilm accumulation (Fig. 3). ClfB plays a significant role in biofilm formation under  $\text{Ca}^{2+}$ -depleted conditions (Abraham and Jefferson, 2012). FnBPs are also able to promote biofilm formation under certain environmental conditions (Vergara-Irigaray *et al.*, 2009). In fact, it was recently described that FnBPA mediates specific cell-cell adhesion via multiple, low affinity homophilic bonds in the presence of  $\text{Zn}^{2+}$  ions (Herman-Bausier *et al.*, 2015). The required region for intermolecular interactions and biofilm

formation involves residues 166 to 498 of the A domain (Geoghegan *et al.*, 2013). Low-affinity binding between FnBPA molecules would enable dynamic cell behavior important for primary accumulation events, followed by more firm cell-cell adhesion determined by subsequent higher-affinity binding (Herman-Bausier *et al.*, 2015). Of the Sdr subfamily, SdrC was shown to promote bacterial intercellular interactions and subsequent biofilm formation *in vitro* through self-association mediated by N2 subdomain. These homophilic interactions are inhibited by  $Mn^{2+}$  (Barbu *et al.*, 2014).

### **SasG**

SasG has a domain organization that is typical for LPXTG protein family. At its N-terminus it contains a secretion signal and an A region, followed by a stretch of tandemly arrayed B repeats, each one composed by a G5 domain (~80 residues) followed by an approximately 50-residues sequence called E, that would act as a structural cap required for stability of the G5 domain. The B-repeat region is followed by a proline rich region and an LPKTG cell wall anchor sequence (Fig. 4). A similar domain arrangement exists in the *S. epidermidis* homologue Aap (Geoghegan *et al.*, 2010; Gruszka *et al.*, 2012).

SasG was shown to participate in the accumulation phase of *ica*-independent biofilms. The process is dependent on physiological concentrations of  $Zn^{2+}$ , and involves partial processing of the protein. More in detail, during the first stages of growth the full-length SasG protein is covalently attached to the cell wall and a limited cleavage of SasG within the B region occurs. SasG seems to be spontaneously processed at labile peptide bonds because protease inhibitor cocktails did not inhibit the cleavage (Geoghegan *et al.*, 2010). SasG fragments of different lengths are released into the supernatant, and some fragments reattach to exposed B domains on the cell surface in a non-covalent manner that is dependent on

Zn<sup>2+</sup>. The cleaved and exposed SasG B domains on neighboring cells interact with each other leading to cell accumulation and biofilm formation (Geoghegan *et al.*, 2010). The structural basis for this homophilic interaction was recently studied, revealing that the B-repeats self-assemble in an antiparallel fashion by coordinating Zn<sup>2+</sup> *in trans*. The interacting B-repeat regions wrap around one another. At least, five tandem B-repeats are required for each chain to circumnavigate the other completely which explains why five repeats are needed to support biofilm formation (Corrigan *et al.*, 2007; Conrady *et al.*, 2013). A very recent report determined that Zn<sup>2+</sup> activates intercellular adhesion not only by promoting SasG homophilic bonds, but also by inducing the collapse of the cell surface constituents, triggering the projection of highly elongated SasG structures beyond other surface components, and enabling homophilic binding between opposing cells (Formosa-Dague *et al.*, 2016).

In *S. epidermidis*, Aap-dependent biofilm formation occurs in a similar manner, but the cleavage is within the A region (Corrigan *et al.*, 2007; Conrady *et al.*, 2008). Before being processed, the Aap N-terminal A domain is involved in mediating primary attachment (Conlon *et al.*, 2014). Owing to strong structural similarities, SasG and Aap are capable of forming zinc-dependent homophilic bonds, thus promoting interspecies interactions in mixed biofilms (Formosa-Dague *et al.*, 2016). Furthermore, Aap B-repeats possess heterophilic binding activity, as reflected by specific interactions with newly described Sbp (Small basic protein), that would serve as a necessary factor during Aap mediated bacterial aggregation (Decker *et al.*, 2015).

### **SasC**

SasC represents another *S. aureus* CWA protein that is involved in cell-cell aggregation and biofilm formation. It is a 240 kDa protein that has

an N-terminal region containing a FIVAR motif, followed by 17 direct repeated sequences of 72 amino acids (aa) each separated by a stretch of 5 aa, which are homologous to a domain of unknown function (DUF1542) (Fig. 4). The FIVAR motif and the DUF1542 domains are also present within the cell surface protein Ebh from *S. aureus* and the homologous Embp from *S. epidermidis*. Finally, at the C-terminus SasC contains the typical LPXTG anchor-motif. Expression of full-length SasC or its N-terminal domain, mediates the formation of bacterial aggregates, increase attachment to polystyrene, and enhances biofilm formation (Schroeder *et al.*, 2009).

### **SraP**

*S. aureus* encodes a 2,271-residues protein termed serine-rich adhesin for binding to platelets (SraP), which is involved in the pathogenesis of infective endocarditis. This protein is a member of the serine-rich repeat glycoproteins (SRRPs), a family of adhesins encoded by gram-positive bacteria that mediate attachment to a variety of host cells or bacteria themselves. In the case of SraP of *S. aureus*, it consists of a signal peptide at the N-terminus, a short SRR region (SRR1), a ligand-binding region (BR) followed by a much longer SRR region (SRR2), and finally a C-terminal LPXTG motif anchoring to the cell wall (Speziale *et al.*, 2014; Yang *et al.*, 2014) (Fig. 4). Particularly, the BR region forms a rigid rod-like structure organized into four discrete modules: a legume lectin-like module, a module with a  $\beta$ -grasp fold, and two tandem cadherin-like modules (CDHL1 and CDHL2) that create the rigid stem of BR. This ligand binding region is the responsible for mediating intraspecies interaction and promoting bacterial aggregation (Yang *et al.*, 2014). On the one hand, the L-lectin module mediates adhesion to host cells by recognizing Neu5Ac, usually the non-reducing terminal residue of glycoconjugates of extracellular receptors. On

the other hand, cadherin-like domains would be responsible for promoting biofilm formation through an homophilic interaction in which CDHL-2 from one subunit packs against the junction between CDHL-1 and CDHL-2 from the symmetric subunit, and *vice versa* (Yang *et al.*, 2014).

### **Protein A**

Protein A is a multifunctional CWA protein that is ubiquitous in *S. aureus*. At the N-terminus, protein A contains five homologous modules (known as EABCD), each of which consists of single separately folded three-helical bundles that can bind to several distinct ligands. Located between this region and the cell surface is region Xr, which is composed of octapeptide repeats that are highly variable in number, followed by a constant region Xc. After this, there is the LPXTG motif recognized by Sortase A for cell wall attachment (Foster *et al.*, 2014) (Fig. 4).

Protein A is primarily known for its ability to bind to the Fc region of IgGs and inhibit opsonophagocytosis. It can mediate attachment of *S. aureus* to Von Willebrand factor, a protein present at sites of damage to the endothelium, and therefore plays a role as an adhesin during the initiation of intravascular infections (Foster, 1998).

Regarding its role in biofilm development, the overproduction of protein A in a wild-type *S. aureus* strain showed it is responsible for cellular aggregation. Furthermore, aggregation and biofilm formation also occurred when soluble protein A was added to a bacterial growing culture demonstrating that this protein does not need to be necessarily covalently linked to the peptidoglycan to promote multicellular behavior (Merino *et al.*, 2009).

### **Biofilm associated protein (Bap)**

Bap protein, identified during a screening of a library of mutants

generated from *S. aureus* strain V329, was found to be the first *ica*-independent mechanism essential for biofilm formation (Cucarella *et al.*, 2001). Since it is the focus of the present thesis, in the next section I will summarize the current knowledge about Bap structure and function, as well as different Bap-related surface proteins.

### Structural features of Bap protein

Bap is a 2,276-amino acids surface protein with a multidomain architecture typical of cell wall-anchored proteins present in gram-positive bacteria (Fig. 4). The first 44 amino acids of the protein correspond to the characteristic gram-positive signal sequence for extracellular secretion (Latasa *et al.*, 2006). Following the putative signal peptide, the N-terminal region of Bap can be divided into two regions. Region A (aa 45 to 360) contains two short repeats of 32 aa (repeats A<sub>1</sub> and A<sub>2</sub>) separated by 26 aa. This region reveals no significant sequence similarity scores among GenBank sequences. Region B, the remaining part of the N-terminal domain (aa 361 to 818), contains two EF-hand calcium-binding motifs, EF2 (729-741) and EF3 (752-764), which exhibit high similarity (91% and 89% respectively) to the loop of the consensus EF-hand motif, differing from it at a single position. The proximity of EF2 and EF3 suggests that they might act coordinately as a pair of EF-hand domains (Cucarella *et al.*, 2001; Arrizubieta *et al.*, 2004). The central region of Bap (aa 819 to 2147) begins with a spacer region of 128 residues followed by 13 nearly identical 258-nt tandem repeat units encoding reiterations of an 86-aa sequence (C-repeats, aa 948 to 2139) (Fig. 5A-B). The C-repeat region accounts for 52% of the Bap protein and each repeat shows high sequence identity (Cucarella *et al.*, 2001). These repeats are predicted to fold into a seven-strand- $\beta$ -sandwich and likely belong to the HYR module (Latasa *et al.*, 2006). Although the



function of this region has not been discerned, it is hypothesized that it could have a structural role, maintaining the proper protein conformation on the cell surface (Latasa *et al.*, 2006). Curiously, the decreased number of repeats does not affect the protein functionality, even when only one repeat constitutes the core region (Cucarella *et al.*, 2004). The C-terminal region of Bap comprises the D region, the LPETG motif, and a hydrophobic transmembrane sequence. The D region (aa 2148 to 2208) consists of three short repeats of 18 aa each followed by an incomplete repeat comprising the first 7 aa of the D repeats (Cucarella *et al.*, 2001) (Fig. 5).

Analysis of sequences flanking *bap* gene revealed that Bap is carried by a transposon-like element, together with an ABC transporter operon and a transposase (*tnp*). The composite transposon is inserted in a pathogenicity island (SaPIbov2) that is mobile without the presence of a helper phage (Fig. 5A). Mobility of SaPIbov2 depends on the activity of the Staphylococcal integrase protein (Sip), a functional recombinase of the integrase family that promotes excision, circularization and site-specific integration into the *att<sub>B</sub>* site of the *S. aureus* chromosome (Ubeda *et al.*, 2003; Lasa and Penadés, 2006).



### Role of Bap in biofilm formation

Bap protein was first detected in *S. aureus* V329 strain isolated from a bovine mastitis. *In vitro* experiments have shown that Bap is involved in primary attachment to an abiotic surface, but also in intercellular adhesion and accumulation in multilayered clusters (Cucarella *et al.*, 2001; Cucarella *et al.*, 2004). Inactivation of the *icaADBC* operon in a *bap*-positive strain had no effect on biofilm formation capacity, confirming that expression of the Bap protein is sufficient to promote a PIA/PNAG-independent biofilm development (Cucarella *et al.*, 2001). It is of particular interest that the number of repeats within Bap is not related to the ability to form biofilms *in vitro*. Thus, the biofilm phenotype of a strain harboring a Bap protein with a single C-repeat is indistinguishable from the biofilm produced by the strain harboring the Bap protein with thirteen C-repeats (Cucarella *et al.*, 2004).

Additionally, the *bap*-mediated multicellular behavior is regulated by the presence or absence of calcium in the growth medium. Calcium binds with low affinity (when present at millimolar concentrations) to the EF-hand 2 and 3 motifs present in the region B of Bap, impeding bacterial clumping mediated by Bap. In contrast, mutations at the EF-hand motifs result in a strain that is completely insensitive to the presence of calcium in the culture media, confirming that the Ca<sup>2+</sup>-regulated process occurs indeed through binding of the cation to EF-hand domains (Arrizubieta *et al.*, 2004).

### Role of Bap in pathogenesis

The *bap* gene is present in *S. aureus* and coagulase-negative *Staphylococcus* isolates obtained from animal with mastitis, but has never been found in *S. aureus* human isolates, strongly suggesting that human and ruminant mastitis isolates are not clonally related and that specific host-dependent pathogenic factors may have evolved independently in both humans and ruminants (Cucarella *et al.*, 2001; Lasa and Penadés, 2006).

In lactating animals, *S. aureus* and other coagulase negative staphylococci frequently cause intramammary infections that usually evolve into a chronic mastitis. Previous results suggest that the capacity to form biofilm on the epithelium of the mammary gland could be related to the propensity of staphylococci to produce chronic infections (Baselga *et al.*, 1993; Baselga *et al.*, 1994; Cucarella *et al.*, 2004).

The presence of Bap on the bacterial surface was shown to improve staphylococcal colonization and persistence on the mammary glands of infected animals. Apparently, in the bovine mammary gland the presence of Bap may facilitate biofilm formation connected with the persistence of *S. aureus* (Cucarella *et al.*, 2004). Thus, biofilm formation constitutes a pathogenesis strategy that helps microorganisms to survive in the mammary gland and to persist in the farm.

In a previous study of the laboratory, it was shown that Bap enhances the adhesion but inhibits the entry of *S. aureus* into epithelial cells. It was demonstrated that Bap binds directly to Gp96, which is a major chaperon of the lumen of the endoplasmic reticulum and is also present on the surface of several epithelial cell lines (Valle *et al.*, 2012). This interaction has an inhibitory effect on the capacity of *S. aureus* to invade host cells (Fig. 6). More in detail, fibronectin-mediated binding between bacterial FnBPs and  $\alpha 5\beta 1$  integrins on the host cell surface is the principal mechanism of *S. aureus* invasion (Fraunholz and Sinha, 2012); direct binding of FnBPs to the human heat shock protein 60 (Hsp60) exposed on the cellular surface also contributes to FnBPs-internalization pathway (Dziewanowska *et al.*, 1999; Dziewanowska *et al.*, 2000). Accordingly, Bap-Gp96 interaction may cause a steric impairment that hinders the recognition of FnBPs to Hsp60 and fibronectin, thus avoiding entry to host cells (Valle *et al.*, 2012). Contrary to what happens with invasion, increased adhesion of Bap-positive strains was

independent on the presence of Gp96 suggesting that Bap interacts with another factor, not necessarily a protein, to promote the adhesion of bacteria to epithelial cells (Valle *et al.*, 2012) (Fig. 6). Bap-mediated biofilm development facilitates the formation of bacterial aggregates that survive attached to the epithelial cells of the mammary gland by impairing the bacterial internalization through the interaction with Gp96. In this situation, the Bap biofilm matrix promotes the establishment of long-term persistent infections and mediates immune evasion by masking surface antigens (Valle *et al.*, 2012).

It is important to highlight the fact that, while the number of C-repeats is irrelevant for biofilm phenotype, they play a fundamental role during infection. A short but still functional version of Bap in which twelve of the thirteen repeats are deleted, is able to interact with Gp96 but fails to block the infection capacity of the wild type bacteria (Valle *et al.*, 2012). Also, it was observed that the number of C-repeats varies throughout the course of the infection. These phase-switching differences in the number of C-repeats could also be related to an evasion from the immune response (Cucarella *et al.*, 2004).

#### Regulation of Bap protein expression

It has already been mentioned that biofilm formation is a highly controlled process that not only involves bacterial global regulators but also depends on a number of environmental cues. In *S. aureus*, many virulence factors involved in biofilm formation are controlled by the accessory gene regulator (Agr) and staphylococcal accessory regulator (SarA) (Götz, 2002). The *sarA* locus encodes a 14.5 kDa protein, SarA, that binds to the *agr* promoter to stimulate RNAlII transcription, resulting in the modulation of target genes downstream on the *agr* regulatory cascade (*agr*-dependent pathway). Additionally, SarA can interact directly with target gene promoters

to control gene expression (*agr*-independent pathway) (Valle *et al.*, 2003). Regarding Bap, it seems reasonable that the synthesis of such a large protein implicates a considerable metabolic effort and therefore has to be strictly regulated and coordinated with the production of other elements of the biofilm matrix (Latasa *et al.*, 2006). Experimental evidences show that SarA positively regulates the *bap* gene by an *agr*-independent mechanism (Fig. 6). SarA protein forms complexes with the *bap* promoter with fairly high affinity, as shown by gel shift and DNase I footprinting assays (Trotonda *et al.*, 2005).

Regulation of Bap not only occurs at a transcriptional level in a SarA-dependent manner, but also, once the protein is expressed, at a post-translational level through a Ca<sup>2+</sup>-binding mechanism. As previously described, binding of Calcium to the EF-hand motifs of Bap B renders the protein unable to mediate cell-cell interactions and biofilm formation (Arrizubieta *et al.*, 2004).

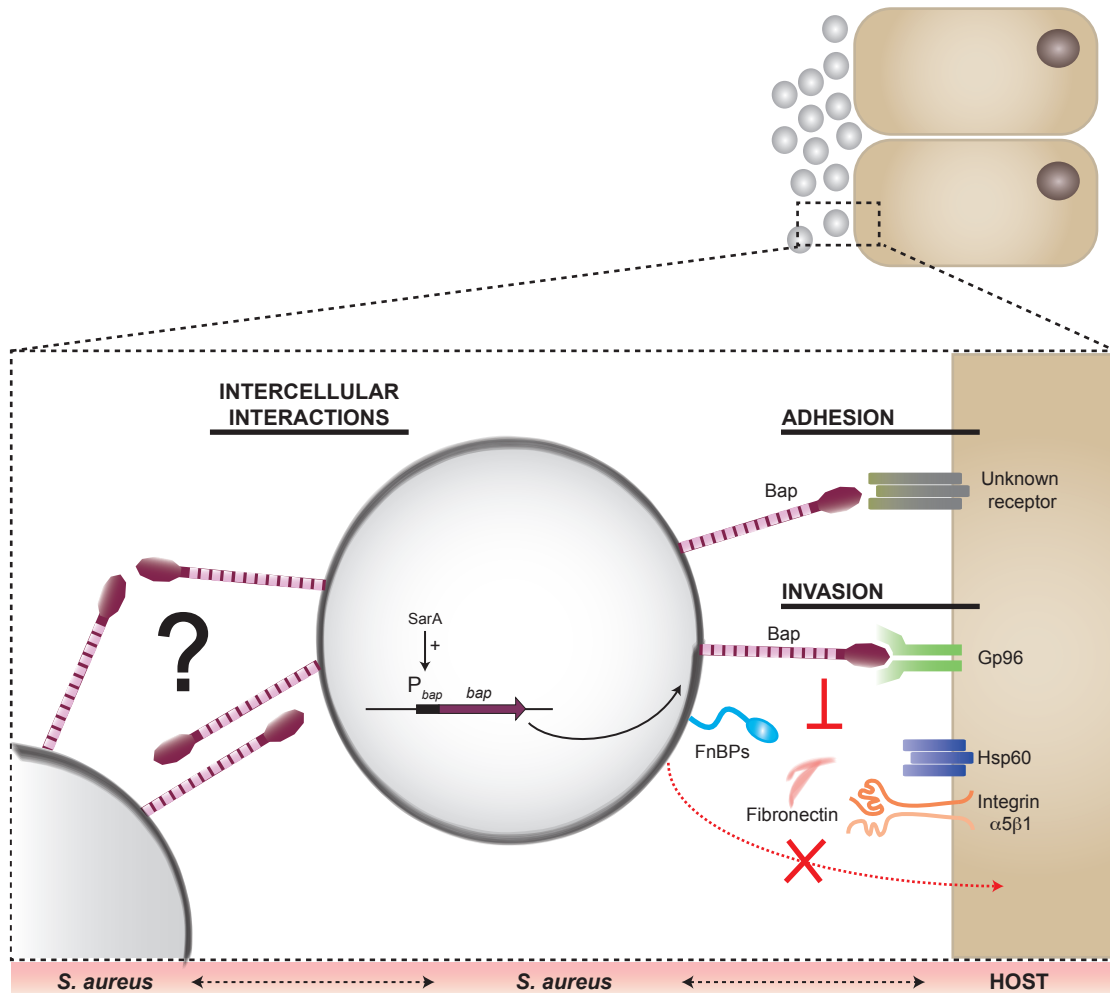


**Figure 6. Role of Bap in the pathogenesis and cell-to-cell interactions.** Bap promotes adhesion of staphylococcal cells to host cells through interaction with an unknown host receptor. On the contrary, interaction of Bap with Gp96 prevent *S. aureus* entrance into eukaryotic cells, by hindering contact of the FnBPs with fibronectin. Bap also promotes bacteria-bacteria interactions through a yet undetermined molecular mechanism.

### Bap-related proteins

Several coagulase-negative staphylococci (CNS), including *S. epidermidis*, *S. chromogenes*, *S. xylosus*, *S. hyicus* and *S. simulans* harbour orthologues of Bap. As occurs in *S. aureus*, the strains harbouring the Bap orthologues show strong biofilm formation capacity through an *ica*-independent mechanism (Tormo *et al.*, 2005).

Besides, Bap-related surface proteins involved in biofilm formation by diverse bacterial genera have been described (Fig. 7). These Bap-related proteins share several structural and functional features: (i) high molecular weight; (ii) the presence of a core domain of tandem repeats; (iii) anchoring to the cell surface; (iv) capacity to induce biofilm development; and (v) relevance during bacterial infectious processes (Lasa and Penadés, 2006).

One example of a Bap-related protein is **Esp** of *Enterococcus faecalis* (Toledo-Arana *et al.*, 2001). The amino terminal region of Esp shares 33% of identity with the region B of Bap while the C-repeats share 33% sequence identity with C-repeats of Bap (Latasa *et al.*, 2006). In regard to its functionality, there is a strong correlation between the presence of Esp and the capacity of the strain to promote primary attachment and biofilm formation in *E. faecalis* (Toledo-Arana *et al.*, 2001; Tendolkar *et al.*, 2004). Besides, Esp contributes to colonization and persistence of *E. faecalis* at the urinary tract (Shankar *et al.*, 2001).

Another example of a large cell-surface protein required for biofilm formation in *Salmonella enteritidis* is **BapA** (Latasa *et al.*, 2005). The central region of BapA contains 28 imperfect tandem repeats each of which has on average 29% identity with a C-repeat of Bap (Latasa *et al.*, 2006). BapA was shown to be essential but not sufficient for biofilm development in *S. enteritidis* and it has been proven that it is clearly implicated in virulence (Latasa *et al.*, 2005).

A protein homologous to Bap was described in *Acinetobacter*

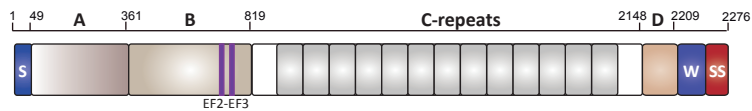


*baumannii* (Loehfelm *et al.*, 2008). In this case, the homology with Bap of *S. aureus* is limited to small stretches of amino acids of “A-C” repeats. Bap of *A. baumannii* is involved in maintaining the mature biofilm architecture (Loehfelm *et al.*, 2008) and it is also involved in bacterial attachment to eukaryotic cells *in vitro* (Brossard and Campagnari, 2012).

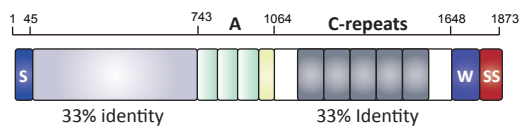
Several other Bap-related proteins involved in biofilm formation and interaction with the host have been described in different bacterial genera, including Bap of *Burkholderia cepacia* (Huber *et al.*, 2002), Lsp of *Lactobacillus reuteri* (Walter *et al.*, 2005) and LapA of *Pseudomonas putida* (Hinsa *et al.*, 2003). In addition, BlastP searches for Bap homologs in databases show the presence of more than 100 proteins with remarkable similarity (e-value lower than  $e^{-42}$ ), suggesting that the Bap family of proteins is widespread in bacteria.

Whereas the relevance of Bap-related proteins for biofilm development has been studied in great detail, the mechanism by which Bap homologous proteins contribute to biofilm development is still lagging behind, though their large size and the presence of a high number of repeats suggest that these proteins could mediate homophilic intercellular interactions.

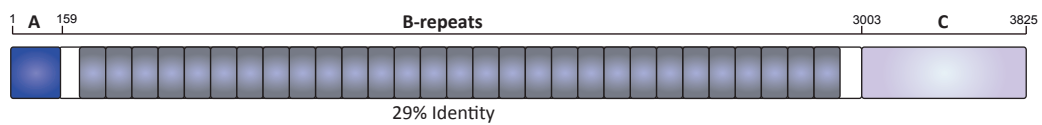
Bap *S. aureus*



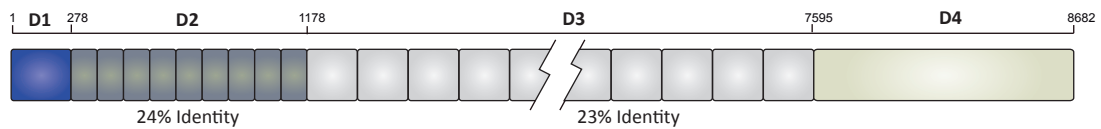
Esp *E. faecalis*



BapA *S. typhimurium*



LapA *P. fluorescens*



Bap *A. baumannii*

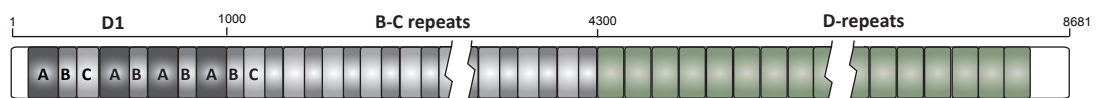


**Figure 7. Structural analysis of Bap-related proteins.** The different domains of Esp from *E. faecalis*, BapA from *S. enteritidis*, LapA from *P. aeruginosa*, and Bap from *A. baumannii* are shown, as well as percent identity to Bap from *S. aureus*.

- **Structural and functional parallelism between SasG, Aap and Bap.**

The functional and structural comparison of Bap, SasG, and its homolog in *S. epidermidis*, Aap, revealed that the three proteins share common features not only at a structural level, but also regarding aspects like interaction with host cells and participation in biofilm development.

First of all, these are high molecular weight proteins that are covalently anchored to the cell wall of staphylococcal cells through an LPXTG domain. They display a characteristic domain organization with a central repeats region (C-repeats in the case of Bap and B-repeats in the case of SasG and Aap). Aap and Bap show strain-dependent length polymorphisms resultant from a different number of the repeats present in their core region (Cucarella *et al.*, 2004; Rohde *et al.*, 2005).

Regarding the distribution of these proteins among different hosts, it was reported that most *S. aureus* clinical isolates from human are SasG positive (Sung *et al.*, 2008). It is also note-worthy that most isolates from animal species are SasG negative (Sung *et al.*, 2008). On the contrary, Bap has never been found in *S. aureus* human isolates, but it is specifically enriched in mastitis-derived isolates where Bap facilitates the persistence of the bacteria in lactating ewes mammary glands (Cucarella *et al.*, 2004; Tormo *et al.*, 2005).

In respect to the role of these surface proteins with host cells, Bap, SasG and Aap promote adhesion to the surface of mammary epithelial cells, nasal epithelial cells and corneocytes, respectively, through its binding with an unknown host receptor (Roche *et al.*, 2003; Macintosh *et al.*, 2009; Valle *et al.*, 2012). In addition, SasG and Bap masks the FnBPs-mediated binding of *S. aureus* to fibrinogen and fibronectin (Cucarella *et al.*, 2002; Corrigan *et al.*, 2007; Valle *et al.*, 2012). In both cases, the protein length, determined by the numbers of C- or B-repeats, is crucial for this process since shorter

versions of SasG (4 or less B-repeats) and Bap (1 C-repeat) hindered the blocking effect on fibrinogen binding (Corrigan *et al.*, 2007; Valle *et al.*, 2012).

In relation to biofilm formation, these three proteins share the ability to develop a completely PIA/PNAG-independent biofilm. SasG and Aap promote the accumulation phase of biofilm formation. For that, SasG and Aap must undergo a proteolysis process to allow the N-terminal domain to interact and promote biofilm accumulation (Rohde *et al.*, 2005; Geoghegan *et al.*, 2010). As I previously mentioned, in the case of SasG, the exposed B-repeats region establish a  $Zn^{2+}$ -dependent homophilic interaction to form an antiparallel twisted cable (Conrady *et al.*, 2008; Conrady *et al.*, 2013). Finally, it must be taken into account that the capacity of the three proteins to form biofilm is somehow influenced by the presence or absence of cations: SasG and Aap require  $Zn^{2+}$  to promote intercellular interactions (Conrady *et al.*, 2008; Geoghegan *et al.*, 2010), while Bap multicellular behavior is inhibited in the presence of  $Ca^{2+}$  (Arrizubieta *et al.*, 2004).

Summarizing, an expansion of the knowledge that explains how SasG and Aap promote cell-cell interactions and biofilm development is occurring. In contrast, the molecular mechanism underlying Bap-mediated biofilm development remains largely unknown. The present work intends to shed some light on Bap *modus operandi* and unravel the molecular basis behind Bap-dependent cell-cell interactions and biofilm development.

## ***OBJECTIVES***

---



## OBJECTIVES

We used the Bap protein of *S. aureus* as a model to explore how this protein promotes interbacterial interactions necessary for the establishment of a biofilm matrix.

The specific objectives of this thesis are:

1. Analysis of the expression and localization of Bap protein along the growth curve of *S. aureus*.
2. Characterization of the molecular mechanisms through which Bap mediates cell-cell interactions and biofilm development.
3. Analysis of the role of calcium in the functionality of Bap.
4. Analysis of Bap-mediated cell-cell interactions in other staphylococcal species.





## ***MATERIALS AND METHODS***

---



## MATERIALS AND METHODS

- **Oligonucleotides, plasmids, bacterial strains and culture conditions**

Bacterial strains, plasmids and oligonucleotides used in this study are listed in Table 1. *Staphylococcus spp.* strains were grown in Luria-Bertani broth (LB), trypticase soy broth (TSB) and B2 medium (1% casein hydrolysate, 2.5% yeast extract, 2.5% NaCl, 0.1% K<sub>2</sub>HPO<sub>4</sub>, and 0.5% glucose [wt/vol]). *Enterococcus faecalis*, *Listeria monocytogenes*, *Escherichia coli* and *Salmonella enteritidis* were grown in Luria-Bertani (LB) broth or in LB agar (Pronadisa). Media were supplemented when appropriate with 10 µl/ml or 1.5 µl/ml erythromycin, 100 µl/ml ampicillin, 0.25% or 0.5% wt/vol glucose, 1 µM CdCl<sub>2</sub>, 20 mM CaCl<sub>2</sub> and 1.25 mM EDTA.

- **DNA manipulations**

Routine DNA manipulations were performed using standard procedures (Sambrook *et al.*, 1989). Plasmid DNA was isolated from *E. coli* strains using a Qiagen plasmid miniprep kit (BioRad), according to the manufacturer's protocol. Plasmids were transformed into staphylococci and *E. coli* strains by electroporation, using a previously described procedure (Cucarella *et al.*, 2001). Restriction enzymes were supplied by Fermentas and were used according to manufacturer's recommendations. DNA polymerase was purchased from Thermo Scientific. Oligonucleotides were obtained from StabVida (Caparica - Portugal) (Table 3).

- **Electrocompetent *Staphylococcus* cells**

Staphylococcal electrocompetent cells were generated as previously described (Schenk and Laddaga, 1992). Briefly, bacteria were grown in 200

ml of B2 broth at 37 °C under shaking conditions (200 rpm) until the culture reached an OD<sub>600nm</sub> of 0.5. Culture was incubated for 15 min on ice and then it was centrifuged and the pellet was washed three times with sterile water. A final washing step was done with 30 ml of ice-cold 10% glycerol. The pellet was resuspended into 15 ml of ice-cold 10% glycerol and incubated for 15 min at 20 °C. Culture was centrifuged and bacterial pellet was resuspended into 200 µl of ice-cold 10% glycerol. Aliquots of 50 µl were stored at -80°C.

- **Generation of mutant strains**

To generate the deletion in the *aur*, *sspA*, *sspB* genes coding for proteases present in *S. aureus*, and a deletion in the *spa* gene coding for surface protein A, we used the pJP437, pJP438, pJP439 (Martí *et al.*, 2010) and pMAD*spaAD* (Merino *et al.*, 2009) plasmids (Table 2) which contained two fused fragments of 500 bp each that flanked the left and the right sequence of *aur*, *sspA*, *sspB* and *spa* genes, respectively. Plasmids were transformed in V329 or  $\Delta bap$  strains by electroporation. Homologous recombination experiments were performed as described (Valle *et al.*, 2003). V329  $\Delta aur$ ,  $\Delta sspA$  and  $\Delta sspBC$  (this last strain was also deleted in the cysteine protease inhibitor SspC, which is the last gene of the operon that codifies for SspA and SspB) strains were verified using primers ssp-20cN/ssp-17mS, ssp-24cN/ssp-21mS and aur-Fw/aur-11mE (Table 3). V329  $\Delta spa$  and  $\Delta bap\Delta spa$  strains were verified using primers spaF/spaE (Table 3).

- **Generation of Bap-ClfA chimeric proteins**

The signal peptide (SP) and the different N-terminal domains of the Bap protein were amplified from the *bap* gene (AB, B, B\_ΔEF and A) of *S.*

*aureus* V329 and V329  $\Delta$ EF (Arrizubieta *et al.*, 2004). To amplify Bap\_AB fragment we used primers Bapori-1mB and Bap-63cK (Table 3). To obtain Bap\_B and Bap\_B\_ $\Delta$ EF regions we first amplified the signal peptide sequence using primers Bapori-1mB and Bap-65c and second, the region B with primers Bap-66m and Bap-63cK. An overlapping PCR was performed with primers Bapori-1mB and Bap-63cK to get a single fragment. To obtain Bap\_A region, two fragments were amplified using primers Bapori-1mB and BapB1 (comprising signal peptide sequence), and BapB2 and BapB3K (comprising A domain). A second overlapping PCR was performed with primers Bapori-1mB and BapB3K in order to obtain a single fragment. To obtain Bap\_B region of *S. saprophyticus*, we first amplified the signal peptide of Bap from *S. aureus* V329 using primers Bapori-1mB and SPbap-sapro-Rv and second, the B-region from *S. saprophyticus* B20080011225 using primers bapB-sapro-Fw and Sapbap-KpnI-Rv. An overlapping PCR was performed with primers Bapori-1mB and Sapbap-KpnI-Rv to obtain a single fragment. To allow anchoring of amplified *bap* domains to the bacterial cell wall, the R region of clumping factor A gene (*clfA*) containing an LPDTG motif was amplified from *S. aureus* Newman strain using primer K-3xF-ClfA containing a flag tag and a recognition sequence for KpnI, and primer ClfA-7cE with a recognition sequence for EcoRI. The KpnI/EcoRI-restricted *R-clfA* was ligated with KpnI/EcoRI-restricted pCN51 vector (Charpentier *et al.*, 2004). The resulting construct was then digested with BamHI and KpnI to insert the previously amplified domains of *bap* gene. The final pCN51 plasmid constructs thus contained different parts of *bap* gene fused to a flag tag followed by the C-terminal R domain of *clfA* gene, expressed under the activity of a cadmium inducible promoter (Table 2). The entire ClfA fragment, used as a control for Bap chimeras, was developed by amplifying *clfA* gene from *S. aureus* Newman using primers

ClfA-9mB and ClfA-7cE. The final pCN51 constructs were transformed in *S. aureus*  $\Delta bap$  by electroporation.

To obtain Bap\_B chimeric protein with mutated amyloid peptides I and II ( $\Delta pepI_{II}$ ) we developed the following strategy: pCN51 vector containing *bap\_B* sequence fused to *3xflag* tag and *R-clfA* sequences was digested with BamHI/PacI enzymes and then ligated with BamHI/PacI-restricted *bap\_B* fragment containing mutations in both peptide I and II obtained by synthetic synthesis (GeneArt™ service, Thermo Fisher Scientific). In this fragment, amino acid sequences of the two amyloid peptides (peptide I: <sup>358</sup>TVGNIISNAG<sub>367</sub>, acagttgtaatatcatatctaacgctggc; peptide II: <sup>450</sup>GIFSYS<sub>455</sub>, ggtattttctcatatagt) were substituted by repeated sequences coding for serine and glycine residues (peptide I: <sup>358</sup>SGSGSGSGSG<sub>367</sub>, tctggatctggatctggatctggatctgga; peptide II: <sup>450</sup>SGSGSG<sub>455</sub>, tctggatctggatctgga). The final construct, pCN51 vector containing *bap\_B*  $\Delta pepI_{II}$  fused to *3xflag* and *R-clfA*, was verified using primers Pcad-Fw, pept1\_Bap\_check\_Rv, pept2\_Bap\_check\_Rv (Table 3) and transformed in  $\Delta bap$  strain by electroporation.

- **Generation of *bap* transcriptional and post-transcriptional fusions**

To obtain *S. aureus* V329  $P_{bap}$  strain, we amplified *bap* promoter using primers pBap-KpnI-Fw and pBap-EcoRI-Rv (Table 3). The PCR product was amplified with Phusion® High-Fidelity DNA Polymerase (Thermo Scientific), purified and cloned in pJET1.2/blunt vector (Thermo Scientific). Fragments were then ligated using KpnI and EcoRI enzymes in the vector pCN52, containing the reporter gene *gfpmut2* (Charpentier *et al.*, 2004). To perform *bap-gfp* post-transcriptional fusion at a chromosomal level, we first amplified by PCR two fragments (500 bp each) at the end of

*bap* gene that flanked the left (primers Bap-GFP-EcoR-A and Bap-GFP-BamHI-Sal-B, Table 3) and the right (primers Bap-GFP-BamHI-C and Bap-GFP-BglII-D, Table 3) sequences of the region targeted for *gfp* insertion. Fragments were fused by ligation into the shuttle vector pMAD (Arnaud *et al.*, 2004). The resulting plasmid was then digested with BamHI and Sall and ligated with BamHI/Sall-restricted *gfp*. The resulting plasmid was transformed into *S. aureus* V329 by electroporation and homologous recombination experiments were performed as described (Valle *et al.*, 2003).

- **Construction of plasmids for Bap expression in C-DAG system**

To obtain *E. coli* strains for curli-dependent amyloid generator (C-DAG) system, we PCR amplified from purified genomic DNA (i) region A of *bap* from *S. aureus* (primers CDAG BAP\_A-Fw and CDAG BAP\_A-Rv, Table 3) and (ii) region B of *bap* from several staphylococcal species: *S. aureus* (primers cdag-B-NotI-Fw and cdag-B-XhoI-Rv, Table 3), *S. saprophyticus* (primers BAPsapro-cdag-Fw and BAPsapro-cdag-Rv), *S. simiae* (primers BAPsimiae-cdag-Fw and BAPsimiae-cdag-Rv), *S. epidermidis* (primers epider-CDAG-Fw and epider-CDAG-Rv), *S. simulans* (primers simulans-CDAG-Fw and simulans-CDAG-Rv), and *S. xyloso* (primers xyloso-CDAG-Fw and xyloso-CDAG-Rv). The NotI/XhoI-restricted *bapA* and *bapB* fragments were ligated with NotI/XhoI-restricted pEXPORT<sub>XhoI</sub> plasmid (Table 2). This vector was obtained by replacing XbaI recognition sequence of the original pEXPORT plasmid (Sivanathan and Hochschild, 2013) for that of XhoI using QuikChange II XL Site-Directed Mutagenesis Kit (Agilent Technologies) and primers pVS72-XhoI-5 and pVS72-XhoI-3 (Table 3). The final pEXPORT constructs (Table 2) were transformed in *E. coli* VS39 strain. Induction of protein production and presence of amyloid-like material was assessed on solid medium containing

10 µg/ml Congo Red by evaluating colony-color phenotype, as previously described (Sivanathan and Hochschild, 2013).

- **Construction of chimeric Bap\_B proteins fused to different tags: SpyTag and SNAP-tag®**

To obtain  $\Delta bap$  strain expressing Region B of Bap fused to the two tags we developed the following strategies. SpyTag fragment (39 bp) (Schoene *et al.*, 2014) was obtained by incubating 10 µl of primers Spy\_tag\_fw and Spy\_tag\_rv (properly designed to contain the entire *spytag* sequence, Table 3) at 96 °C for 15 minutes. SNAP-tag sequence (543 bp) was PCR amplified from plasmid pSNAP-tag® (T7)-2 (New England BioLabs, Inc) using primers Fw\_snap\_kpnI and Rv\_snap\_kpnI. The two fragments were purified and cloned in pJET1.2/blunt (Thermo Scientific), and then ligated using KpnI enzyme with the KpnI-digested pCN51 vector containing the Bap\_B-ClfA chimera. The final pCN51 plasmid constructs thus contained B region of *bap* gene fused to SpyTag or SNAP-tag followed by the C-terminal R domain of *clfA* gene, expressed under the activity of a cadmium inducible promoter (Table 2).

- **Chromosomal labelling of Bap with SNAP-tag®**

To fuse the SNAP-tag sequence (181 amino acids) with the *bap* gene in the chromosome of *S. aureus* V329 (between amino acids 819 and 820), we amplified the following three fragments: (i) fragment AB corresponding to the last ~ 500 bp of the B region (primers Bap\_SNAP\_A\_EcoRI and Bap\_SNAP\_B, Table 3), (ii) fragment CD corresponding the first ~ 500 bp of the C core region (primers Bap\_SNAP\_C and Bap\_SNAP\_D\_BamHI), and (iii) fragment corresponding to the SNAP-tag sequence (543 bp; primers SNAPtag\_A and SNAPtag\_B). Overlapping PCR was performed to obtain a



single fragment using primers Bap\_SNAP\_A\_EcoRI and Bap\_SNAP\_D\_BamHI. This final *bapAB-snaptag-bapCD* fragment was purified and cloned in pJET1.2/blunt (Thermo Scientific), and then finally ligated using EcoRI and BamHI enzymes into the shuttle vector pMAD. The resulting plasmid was transformed into *S. aureus* V329 by electroporation and homologous recombination experiments were performed as previously described (Valle *et al.*, 2003).

- **Expression and purification of Bap\_B recombinant proteins from *S. aureus* and *S. saprophyticus***

Region B of Bap (amino acids 361-819) was PCR amplified from purified *S. aureus* V329 genomic DNA using Phusion<sup>®</sup> High-Fidelity DNA Polymerase (Thermo Scientific) and primers *bapB1-LIC-Fw* and *bapB1-LIC-Rv* (Table 3) designed for use in the Ligase Independent Cloning (LIC) system. The resulting 1377 bp fragment was cloned in pET46-Ek/LIC vector (Novagen). B-region of Bap from *S. saprophyticus* B20080011225 (amino acids 186-622) was PCR amplified from its purified genomic DNA using primers *bapB-sapro-LIC-Fw* and *bapB-sapro-LIC-Rv* (Table 3). The resulting 1311 bp fragment was cloned in pET46-Ek/LIC vector (Novagen). Both fusions resulted in BapB constructs containing an N-terminal hexahistidine tag (*rBap\_B* and *rBap\_B<sub>sapro</sub>*). Overnight cultures of *E. coli* BL21 DE3 containing BapB expression plasmids were diluted 1:100 and grown to an OD<sub>600nm</sub> of 0.6. Isopropyl β-D-thiogalactopyranoside (IPTG) was added to a final concentration of 0,1 mM and the cultures were shaken overnight (150 rpm) at 20 °C. After centrifugation (8000 rpm, 15 minutes), pellets were suspended in lysis buffer (1X Phosphate buffer, 20 mM imidazole, 0,2 mg/ml lysozyme, 20 μg/ml DNase, 1 mM MgCl<sub>2</sub>, 1 mM PMSF), sonicated and centrifuged (16000 rpm, 30 minutes). After

supernatants were filtered (0,45  $\mu\text{m}$ ), rBap\_B and rBap\_B<sub>sapro</sub> proteins were purified by Ni affinity chromatography using HisGraviTrap gravity-flow columns (GE Healthcare). To achieve the highest purity, size exclusion chromatography was applied with a HiLoad 16/600 Superdex 200 pg column (GE Healthcare). The concentration of the purified protein was determined by the Bincichoninic Acid (BCA) Protein Assay (Pierce, Thermo Scientific) using BSA as a standard. Detection of recombinant proteins in the corresponding elution fractions was performed by SDS-PAGE and Western Blot using monoclonal anti-polyHistidine-alkaline phosphatase antibody produced in mouse (Sigma).

- **Expression and purification of GFP and GFP-SpyCatcher recombinant proteins**

To obtain GFP expression plasmid, the *gfp* sequence was PCR amplified from pAD-GFP plasmid (Table 2) using Phusion<sup>®</sup> High-Fidelity DNA Polymerase (Thermo Scientific) and primers GFP\_Ek\_LIC\_Fw and GFP\_Ek\_LIC\_Rv (Table 3) designed for use in the LIC cloning system. The resulting 717 bp fragment was cloned in pET46-Ek/LIC vector (Novagen). To obtain GFP-SpyCatcher expression plasmid, *gfp* sequence fused to the *spycatcher* sequence was PCR amplified from pAU1108-GFPCatcher plasmid (Table 2) using Phusion<sup>®</sup> High-Fidelity DNA Polymerase (Thermo Scientific) and primers GFP\_Ek\_LIC\_Fw and GFP\_Catcher\_Ek\_LIC\_Rv (Table 3) designed for use in the LIC cloning system. The resulting 1095 bp fragment was cloned in pET46-Ek/LIC vector (Novagen). Both constructs resulted in recombinant GFP and GFP-SpyCatcher proteins containing an N-terminal hexahistidine tag (rGFP and rGFP-SpyCatcher).

Overnight cultures of *E. coli* BL21 Origami (DE3) containing GFP and GFP-Catcher expression plasmids (Table 1 and 2) were diluted 1:100 and

grown to an  $OD_{600nm}$  of 0.5 in LB supplemented with 100  $\mu$ g/ml ampicillin and 1% glucose, at 37 °C, 200 rpm. Isopropyl  $\beta$ -D-thiogalactopyranoside (IPTG) was added to a final concentration of 1 mM and the cultures were shaken (150 rpm) at 20 °C overnight. After centrifugation (8000 rpm, 15 minutes), pellets were suspended in BugBuster lysis buffer (Novagen) and centrifuged (16000 rpm, 30 minutes). Supernatants were filtered (0,45  $\mu$ m) and rGFP and rGFP-Catcher proteins were purified by Ni affinity chromatography using HisGraviTrap gravity-flow columns (GE Healthcare). The gradient elution method was performed to obtain the proteins of interest, using elution buffers with increasing concentrations of imidazole (100, 200, 300, 400 and 500 mM imidazole in 1X Phosphate buffer, pH 7.4). The concentration of purified proteins was determined by the Bincichoninic Acid (BCA) Protein Assay (Pierce, Thermo Scientific) using BSA as a standard. Detection of recombinant proteins in the corresponding elution fractions was performed by SDS-PAGE and Western Blot using monoclonal anti-polyHistidine-alkaline phosphatase antibody produced in mouse (Sigma).

- **Production of anti-BapB antibodies**

Rabbit polyclonal antibodies raised against purified rBap\_B protein were supplied by Abyntek Biopharma S.L. (Spain). Antibodies were subsequently immunoabsorbed and purified using NAb Spin Kit (Thermoscientific).

- **Biofilm formation and biofilm dispersion assays**

Biofilm formation assay in microtiter wells was performed as described (Heilmann *et al.*, 1996). Briefly, strains were grown overnight at 37 °C and then diluted 1:40 in LB, LB-glu or TSB-glu supplemented when

required with the corresponding antibiotic. Cell suspension was used to inoculate sterile 96-well polystyrene microtiter plates (Thermo Scientific). After 24 hours of incubation at 37 °C wells were gently rinsed two times with water, dried and stained with 0.1% of crystal violet for a few minutes. When desired, crystal violet adhered at the bottom of the wells was resuspended with 200 µl of a solution of ethanol:acetone (80:20 vol/vol) and quantified using a Multiskan EX microplate photometer (Thermo Scientific) with a 595 nm filter.

For inhibition assays, 20 mM CaCl<sub>2</sub> or increasing amounts of anti-Bap purified antibody were added to inoculated wells at the beginning of the biofilm assay, incubated, washed and stained as described above.

For biofilm disassembly assays, cells were grown in LB-glu at 37 °C on polystyrene microtiter plates. Once formed, adhered biofilm were treated with dispersant agents (0.4 µg/ml Dispersin B and 0.4 µg/ml DNaseI) for 2 hours at 37 °C. Alternatively, old LB-glu media were extracted and replaced for new LB, LB-glu, or LB-glu + 20 mM CaCl<sub>2</sub>, and incubated overnight at 37 °C. Finally, treated and non-treated biofilms adhered to polystyrene wells were macroscopically determined and quantified as previously described.

To analyze biofilm formation under flow conditions, we used 60 ml microfermenters (Pasteur Institute's laboratory of Fermentation) with a continuous flow of 40 ml/h of LB-glu and constant aeration with sterile pressed air (0.3 bar) (Ghigo, 2001). Medium was supplemented with 10 µg/ml erythromycin and 1 µM CdCl<sub>2</sub> when required. Pyrex glass spatula were submerged in microfermentators and used as a solid substrate for bacterial growth. Each microfermentator was inoculated with 10<sup>8</sup> bacteria from an overnight culture of the corresponding strain. Biofilm development was recorded with a FUJIFILM FinePix S5800 digital camera.

Colony morphology was analyzed using Congo red agar plates as previously described (Valle *et al.*, 2003). Congo red agar was prepared as follow: 30 g/l of trypticase soy (Pronadisa), 15 g/l of agar (Pronadisa), 0.8 g/l of Congo Red stain (Sigma) and 20 g/l of sucrose (VWR Chemicals). *S. aureus* strains were streaked on Congo red agar and were incubated overnight at 37 °C. Rough colonies indicate biofilm formation and smooth colonies indicate a deficiency in biofilm formation.

- **Bacterial clumping assays**

Aggregation phenotype in cell suspension was determined as described before (Valle *et al.*, 2003). Cells were grown overnight in the corresponding medium (LB or LB-glu) supplemented when required with antibiotics, 20 mM CaCl<sub>2</sub> or proteases inhibitors (2 U/ml α-macroglobulin, 2 mM cysteine protease inhibitor E64, and 10 μM PMSF) at 37 °C, shaking at 200 rpm and were examined macroscopically for the presence or absence of aggregates (intercellular adhesion).

For inhibition assays, cells were incubated overnight in 50 ml of TSB-glu, centrifuged and resuspended with the filtered supernatant (0,22 μm). 250 μl of anti-Bap purified antibody were added to 10 ml of the culture and the mixture was divided in three glass tubes. The same procedure was performed without anti-Bap antibodies. The optical density at 650 nm was measured every 30 minutes and pictures were taken with a FUJIFILM FinePix S5800 digital camera.

For bacterial clumping reversion assay, bacteria were grown overnight in LB-glu at 37 °C, 200 rpm. Cultures were subsequently centrifuged and LB-glu medium was replaced for LB. After 6 and 24 hours incubation at 37 °C, 200 rpm, bacterial aggregation at the bottom of the tube

was evaluated for each strain and pictures were taken with a FUJIFILM FinePix S5800 digital camera.

To quantify bacterial aggregation, the OD<sub>600nm</sub> at the top of the culture tubes (approximately 1 cm from the surface) was measured as an estimation of non-settled bacteria (planktonic cells) present in the culture after an overnight incubation at 37 °C, 200 rpm. Each experiment was independently repeated three times, and data were analyzed with the Mann-Whitney U test.

- **Exogenous complementation**

To test extracellular complementation, bacteria were grown in LB, LB-glu or LB-glu + 20 mM CaCl<sub>2</sub> mixed with 2 μM-purified region B of Bap shaking at 200 rpm at 37 °C. Bacterial aggregation phenotype in cell suspension was macroscopically determined and quantified as described in “Bacterial clumping assays”.

- **Microscopy analysis**

For immunofluorescence, cells were grown overnight in the corresponding tested conditions and fixed with 3% paraformaldehyde (Sigma) for 10 minutes at room temperature. 200 μl of fixed bacteria were added to coverslips and incubated for 30 minutes. After several washes with PBS, cells were saturated with PBS + 0.5% BSA, and finally stained with anti-Bap or anti-Flag (Sigma) antibodies diluted 1:1000. Alexa Fluor 488-conjugated goat anti-rabbit (Invitrogen) diluted 1:200 was used as a secondary antibody and DAPI diluted 1:200 was used to label nuclei. For ProteoStat staining of amyloid material *in vivo*, cells were grown overnight in LB and LB-glu, at 37 °C, in polystyrene 24-wells plates. Adhered biofilm was resuspended and fixed with 3% paraformaldehyde (Sigma) for 5 minutes. Bacteria were washed several times with 1X PBS, and then incubated for 30

minutes, at room temperature and in darkness with ProteoStat Mix buffer (1X Assay Buffer, 1  $\mu$ l ProteoStat<sup>®</sup>, 2  $\mu$ l Hoechst). Bacteria were washed twice with 1X PBS. All preparations were observed with an Axioskop 2 plus epifluorescence microscope (Zeiss) equipped with a HBO 50/AC camera (Zeiss) and images were acquired and analyzed with EZ-C1 software (Nikon).

Electron microscopy images were obtained at the Laboratory of Cellular Biology and Electron Microscopy of the Medicine Faculty at Tours (France). For Transmission electron microscopy (TEM), cells were grown overnight in the corresponding tested conditions, washed twice with PBS and then fixed with 2% paraformaldehyde (Sigma) for 1 hour at room temperature. Formvar/carbon-coated nickel grids were deposited on a drop of fixed sample during five minutes and rinsed three times with PBS. Negative staining was performed using 2% uranyl acetate (Agar Scientific, Stansted, UK). Observations were made with a JEM-1011 transmission electron microscope (JEOL). For immunogold labeling of Bap, grids coated with the sample were washed and incubated for 45 minutes on a drop of PBS containing 1:10 antibody against region B of Bap. After washing with PBS, grids were incubated 45 minutes with gold-conjugated (10 nm) goat-anti-rabbit secondary antibody (Aurion, Wageningen, Netherlands). Grids were stained with uranyl acetate as described above. For Scanning Electron Microscopy (SEM), samples were incubated with 2% osmium tetroxide for 1 hour. Observation was made under a Zeiss Ultra plus FEG-SEM scanning electron microscope (Oberkochen, Germany).

- **Labeling of Bap/SNAP-tag fusion protein**

*S. aureus*  $\Delta$ *bap* expressing Bap<sub>B</sub> and Bap<sub>B</sub><sup>SNAPtag</sup> were grown overnight in LB (pH>7) and LB-glu (pH<5), supplemented with 10  $\mu$ l/ml

erythromycin and 1  $\mu\text{M}$   $\text{CdCl}_2$ , at 37 °C, 200 rpm. Overnight cultures of *S. aureus* V329<sup>SNAPtag</sup> strain were diluted 1:100, grown in LB-glu (pH<5) and LB (pH>7) and samples were obtained at OD<sub>600nm</sub> of 0.6, 2, 5 and 8. For both strains, cells were harvested and washed with phosphate-buffered saline (PBS). 400  $\mu\text{l}$  of bacterial suspension was incubated with 1  $\mu\text{l}$  of SNAP-surface<sup>®</sup> Alexa fluor<sup>®</sup> 488 substrate (New England BioLabs, Inc) at 37 °C, 200 rpm for 30 minutes. After three washes with PBS, the samples were fixed with 3% paraformaldehyde for 10 minutes at room temperature. After several washes with PBS, cells were stained with 1:1000 diluted Hoechst (Thermo Scientific) to label nuclei. Preparations were observed with an Axioskop 2 plus epifluorescence microscope (Zeiss) equipped with a HBO 50/AC camera (Zeiss) and images were acquired and analyzed with EZ-C1 software (Nikon).

- **Labeling of Bap/SpyTag fusion protein**

*S. aureus*  $\Delta\text{bap}$  expressing Bap<sub>B</sub><sup>SpyTag</sup> was grown overnight in LB (pH>7) and LB-glu (pH<5), supplemented with 10  $\mu\text{l/ml}$  erythromycin and 1  $\mu\text{M}$   $\text{CdCl}_2$ , at 37 °C, 200 rpm. Cells were harvested and washed with PBS + 0.5% Tween. Bacteria were suspended in 200  $\mu\text{l}$  of PBS + 0.5% Tween + 1% BSA and incubated with 0,5 mg/ml of purified rGFP and rGFP-SpyCatcher at 4 °C for 1 hour. After three washes with PBS + 0.5% Tween, the samples were fixed with 3% paraformaldehyde for 10 minutes at room temperature. After several washes with PBS, Hoechst (Thermo Scientific) diluted 1:1000 was used to label nuclei. Preparations were observed with an Axioskop 2 plus epifluorescence microscope (Zeiss) equipped with a HBO 50/AC camera (Zeiss) and images were acquired and analyzed with EZ-C1 software (Nikon).



- **Immunoblot analysis**

Overnight cultures of *S. aureus* strains were diluted 1:100 and grown in LB-glu or LB supplemented with the corresponding antibiotic, 20 mM CaCl<sub>2</sub> and 1 μM CdCl<sub>2</sub> when necessary at 37 °C, 200 rpm. Samples were obtained at different point of the growth curve. Cells were harvested and washed in PBS. For surface protein extracts, cells were resuspended in 100 μl of PBS + 30% raffinose (Sigma), 5 μl of 1 mg/ml lysostaphin (Sigma) and 2 μl of 1 mg/ml DNase (Sigma). After 2 hours of incubation at 37 °C and 200 rpm, cells were centrifuged (8000 rpm, 30 minutes, 4 °C, slow deceleration). For total protein extracts, cells were resuspended in PBS, 5 μl of 1 mg/ml lysostaphin (Sigma) and 2 μl of 1 mg/ml DNase (Sigma), incubated 2 hours at 37 °C and centrifuged at 12.000 rpm for 10 minutes. Supernatants from surface protein and total protein extracts were recovered and analyzed by SDS-PAGE and Western blot, as detailed below. For analysis of supernatants from *S. aureus* V329 cultures, cells were grown overnight in LB, LB + 20 mM CaCl<sub>2</sub>, LB-glu, and LB-glu + 20 mM CaCl<sub>2</sub>, at 37 °C, 200 rpm. After centrifugation, the recovered supernatants were filtered (0,45 μm), concentrated with Amicon Ultra-15 centricons (Merck Millipore) and analyzed as follow. For SDS-PAGE, 1 volume of Laemmli buffer was added to the supernatants. The samples were boiled for 5 minutes. 10 μg of protein was used for SDS-PAGE analysis (7,5% or 12% separation gels; 5% stacking gel). Gels were stained with 0.25% Coomassie brilliant blue R250 (Sigma) as loading controls. For Native gels, supernatants were mix 1:2 with native sample buffer (BioRad). Proteins were separated in Criterion XT Tris-acetate gels and Tris/glycine running buffer (BioRad). For Western blot analysis, protein extracts were blotted onto Hybond-ECL nitrocellulose membranes (Amersham Biosciences). Anti-BapB, monoclonal anti-Flag<sup>®</sup> M2-Peroxidase (HRP) (Sigma) or anti-GFP (Living Color<sup>®</sup> A.v. Monoclonal Antibody (JL-8), Clontech) antibodies were diluted 1:20.000, 1:1000 and

1:10.000, respectively, with 0.1% PBS-Tween 5% skim-milk. Alkaline phosphatase-conjugated goat anti-rabbit Immunoglobulin G (Thermo Scientific) and alkaline phosphatase-conjugated goat anti-mouse Immunoglobulin G (Sigma) diluted 1:5000 in 0.1% PBS-Tween 5% skim-milk were used as secondary antibodies for Bap and GFP detection respectively, and the subsequent chemiluminescence reaction was recorded (Chemiluminescent Substrate Thermo Scientific).

- **Identification of aggregative peptides**

*S. aureus* V329 strain was grown in LB and LB-glu media, at 37 °C, 200 rpm. After an overnight incubation, cells were harvested, washed and finally resuspended in 100 ml of PBS buffer containing 30% raffinose (Sigma), 5 ml of lysostaphin 1 mg/ml (Sigma) and 2 ml of DNase 1mg/ml (Sigma). After 2 hours of incubation at 37° C, cells were centrifuged. Supernatants were mix 1:2 with native sample buffer (BioRad). Proteins were separated in Criterion XT Tris-acetate gels using Tris/glycine running buffer (BioRad). The material retained in the wells of the native gels was excised, washed three times in ddH<sub>2</sub>O, and digested in-gel with 250 ng of trypsin (Sequencing grade modified Trypsin-Promega) in 50 mM ammonium bicarbonate for 16 h at 37 °C, after a denaturation step with DTT (10 mM, 30 min, 40 °C) and an alkylation step with Iodoacetamide (25 mM, 30 min, room temperature). The resulting peptides were extracted with 1% formic acid, 50% acetonitrile and evaporated to dryness prior to LC-MSMS analysis. For each digested sample, a total volume of 5 µl of tryptic peptides was injected with a flow rate of 300 nl/min in a nanoLC Ultra1D plus (Eksigent). A trap column Acclaim PepMap100 (100 µm x 2 cm; C18, 2 µm, 100 Å) and an analytical column Acclaim PepMap RSLC (75 µm x 15 cm, C18, 5 µm, 100 Å) from Thermo Scientific were used following the next gradient: 0–1 min (5% B), 1-50 min (5–40% B), 50-51 min (40-98% B), 51-72

55 min (98% B), 55-56 min (5% B), 56-75 min (5% B). (Buffer B: 100% acetonitrile, 0.1% formic acid, Buffer A: 0.1% formic acid). MS analysis was performed on a Q-TRAP 5500 system (ABSciex) with a NanoSpray<sup>®</sup> III ion source (ABSciex) using Rolling Collision Energy in positive mode. MS/MS data acquisition was performed using Analyst 1.5.2 (AB Sciex) and submitted to Protein Pilot software (ABSciex) against UniprotKB/Swiss-Prot database (restricted to "*Staphylococcus*") and then against a specifically restricted database for BAP protein from *Staphylococcus aureus*, using the Paragon<sup>™</sup> Algorithm and the pre-established search parameters for 5500 QTRAP.

- **Formation of rBap\_B aggregates and reversion assay**

To determine the exact pH at which rBap\_B is capable to form aggregates, 2  $\mu$ M of the protein was incubated in phosphate-citrate buffer at pH ranging from 2.0 until 8.0. For aggregates reversion assay of 2  $\mu$ M assembled rBap\_B and rBap\_B<sub>sapro</sub> protein, the phosphate-citrate buffer at pH 4.5 was removed and exchanged for phosphate-citrate buffer at pH 7. After an overnight incubation at 37 °C and 200 rpm, dissolution of rBap\_B and rBap\_B<sub>sapro</sub> aggregates was macroscopically determined and pictures were taken with a FUJIFILM FinePix S5800 digital camera.

- **EGCG inhibition assay**

2  $\mu$ M purified rBap\_B protein was incubated overnight at 37 °C, 200 rpm in phosphate-citrate buffer at 4.5 in the absence or presence of 10 mM, 100  $\mu$ M and 10  $\mu$ M of (-)-epigallocatechine gallate (EGCG) (gently provided by Dr. Salvador Ventura). Formation of rBap\_B aggregates was macroscopically determined and pictures were taken with a FUJIFILM FinePix S5800 digital camera. Disassembly of *S. aureus* V329 and 15981

biofilms formed on polystyrene microtiter plates in the presence of 10, 20, and 200  $\mu\text{M}$  EGCG was determined and quantified as previously described.

- **Attenuated Total Reflectance-Fourier Transform Infrared spectroscopy (ATR-FTIR)**

ATR FTIR spectroscopy analyses of rBap\_B aggregates formed in phosphate-citrate buffer pH 4.5 were performed with a Bruker Tensor 27 FTIR Spectrometer (Bruker Optics Inc.) with a Golden Gate MKII ATR accessory. Spectrum acquisitions consisted of 16 independent scans, measured at a resolution of  $2\text{ cm}^{-1}$  within the  $1800\text{--}1500\text{ cm}^{-1}$  range. Spectra were acquired, background subtracted, baseline corrected and normalized using the OPUS MIR Tensor 27 software. Second derivatives of the spectra were used to determine the frequencies at which the different spectral components were located. All FTIR spectra were fitted to overlapping Gaussian curves using PeakFit package software (Systat Software) and the maximum and the area of each Gaussian were calculated.

- **Circular dichroism (CD)**

Far-UV CD spectra were measured in a Jasco-710 (Jasco, Japan) or in a Chirascan (Applied Photophysics) spectropolarimeter thermostated at  $25^\circ\text{C}$ . rBap\_B at concentrations ranging from 0.2 to 1.5 mg/ml was measured in 10 mM MOPS either with 1mM  $\text{CaCl}_2$ , 10 mM  $\text{CaCl}_2$  or 100 mM  $\text{CaCl}_2$ , or alternatively 10 mM NaCl or 100 mM NaCl and 10 mM EDTA at pH 7.0/7.5. For measurements at acidic pH, rBap\_B (6 mg/ml) in 10 mM  $\text{NaPO}_4$  pH 7.0, 50 mM  $(\text{NH}_4)_2\text{SO}_4$  was diluted 30-fold to 0.2 mg/ml into 100 mM  $\text{NaPO}_4$ , 10 mM EDTA at pH 4.4. Spectra were recorded from 260 to 190 nm, at 0.2 nm intervals, 1 nm bandwidth, and a scan speed of 50 nm/min. Twenty accumulations were averaged for each spectrum.

Deconvolution of the data were performed using the Dichroweb server (Whitmore and Wallace, 2004) implementing the CDSSTR algorithm with reference set 7 (Sreerama and Woody, 2000).

Near-UV CD spectra were recorded in a Jasco-710 spectropolarimeter (Jasco, Japan) thermostated at 25°C, from 260 to 320 nm with a 1 nm bandwidth, and a scan speed of 50 nm/min in 10 mM MOPS pH 7.0 with 1 mM CaCl<sub>2</sub>, 10 mM CaCl<sub>2</sub>, or 10 mM NaCl 10 mM EDTA.

- **Thermal denaturation**

Thermal denaturation was monitored in a Jasco FP-8200 fluorescence spectrophotometer (Jasco, Japan). Samples were excited at 280 nm and the emission was recorded at 350 nm, using slit widths of 5 nm for excitation and emission. The emission was registered each 0.25 K with a heating rate of 0.5 K/min.

- **Tryptophan intrinsic fluorescence**

Tryptophan intrinsic fluorescence of 1.5 mg/ml rBap\_B in 10 mM MOPS either with 100 mM CaCl<sub>2</sub> or 100 mM NaCl, 10 mM EDTA at pH 7.5, was measured at 25 °C on a Varian Cary Eclipse spectrofluorometer using an excitation wavelength of 280 nm and recording the emission from 300 to 400 nm. Five averaged spectra were acquired using slit widths of 5 nm for excitation and emission.

- **Static light scattering**

Static light scattering of 0.1 mg/ml rBap\_B and rBap\_B<sub>sapro</sub> in phosphate-citrate buffer at pH 4.5 and pH 7 was recorded using a Jasco FP-8200 spectrofluorometer (Jasco corporation, Japan). Five accumulative spectra were registered with excitation at 330 nm and emission between 320 and 340 nm. Slit widths of 5 nm for excitation and emission were used.

- **Dynamic light scattering**

Dynamic light scattering data of 1 mg/ml rBap\_B protein in phosphate-citrate buffer at pH 3, 4.4 and 7 were obtained with a DynaPro DLS reader (Wyatt Technology, Germany) using an 825 nm wavelength laser and analyzed with Dynamics V6 software. Hydrodynamic radius (nm), polydispersity percentage and diffusion coefficient ( $\text{cm}^2/\text{s}$ ) of each population observed at the different pH values were obtained.

- **Gel filtration chromatography**

The size exclusion chromatography experiment was performed using a HiLoad 16/600 Superdex 200 pg column (GE Healthcare) connected to an AKTAprime™ Plus chromatography system (GE Healthcare). A 500  $\mu\text{l}$  portion of rBap\_B was loaded onto the gel filtration column equilibrated in MOPS buffer (10 mM MOPS, 100 mM NaCl, pH 7.5) with 100 mM  $\text{CaCl}_2$  or 10 mM EDTA and eluted with one column volume (124 ml) at a flow rate of 1 ml/min. Recorded data were analyzed using PrimeView software (GE Healthcare).

- **Analytical Ultracentrifugation (AUC)**

All AUC experiments were carried out at 20 °C in 10 mM MOPS either with 100 mM  $\text{CaCl}_2$  or 100 mM NaCl, 10 mM EDTA at pH 7.5, on a Beckman XL-I analytical centrifuge using absorbance optics. Sedimentation velocity was performed for rBap\_B at three different concentrations (1, 2 and 3 mg/ml) at 48,000 rpm overnight and the data were analyzed using SedFit 14.7g (Schuck, 2000). Sedimentation equilibrium runs were performed for rBap\_B (loading concentrations of 1, 2 and 3 mg/ml) at speeds of 13,000 and 8,500 rpm and analyzed using HeteroAnalysis 1.1.44.

- **Nuclear magnetic resonance (NMR)**

One-dimensional proton NMR experiments were performed at 30 °C on 350  $\mu$ M rBap\_B in buffers containing 10 mM MOPS, 100 mM CaCl<sub>2</sub>, 10% D<sub>2</sub>O or 10 mM MOPS, 100 mM NaCl, 10 mM EDTA, 10% D<sub>2</sub>O. Spectra were processed within TopSpin (Bruker).

- **Thioflavin-T binding assay**

Thioflavin-T (ThT) binding was analyzed for 0.1 mg/ml aggregated rBap\_B and rBap\_B<sub>sapro</sub> in the presence of 25  $\mu$ M ThT, 25 °C, pH 4.5. ThT binding was also measured for rBap\_B at different concentrations (0.01, 0.018, 0.027 and 0.036 mg/ml) in the presence of 25  $\mu$ M ThT, 25 °C, at pH 4.5 and pH 7.0. Fluorescence emission spectra were recorded from 460 to 600 nm with an excitation wavelength of 440 nm, using a slit width of 5 nm for excitation and emission in a Jasco FP-8200 spectrophotometer (Jasco corporation, Japan). Each trace represents the average of 5 accumulated spectra. Aggregation kinetics of 0.01 mg/ml rBap\_B protein in phosphate-citrate buffer at pH 4.5, pH 4.5 + 100 mM CaCl<sub>2</sub> and pH 7.0 were recorded for 1000 s under agitation (800 rpm) at 25 °C, in the presence of 25  $\mu$ M ThT. The kinetic traces were measured exciting at 440 nm and emission was recorded at 475 nm. Slit widths of 5 nm were used for excitation and emission in a Jasco FP8200 spectrophotometer (Jasco corporation, Japan). ThT fluorescence spectra were recorded at the end of the experiment.

- **Congo Red binding assay**

Congo red (CR) interaction with 0.1 mg/ml aggregated rBap\_B and rBap\_B<sub>sapro</sub> at pH 4.5 was tested using a Cary-400 UV/Vis spectrophotometer at 25 °C. After 5 minutes of equilibration, the absorbance spectra were recorded from 400 to 700 nm. Each trace represents the average of 5 accumulated spectra.

- **ProteoStat binding assay**

Fluorescence emission of 0.1 mg/ml assembled rBap\_B and rBap\_B<sub>sapro</sub> at pH 4.5, stained with ProteoStat, was measured on a Jasco FP-8200 fluorescence spectrophotometer (Jasco corporation, Japan) at 25 °C. The samples were excited at 484 nm and the emission spectra were recorded between 500 and 650 nm. Slit widths of 5 nm were used for excitation and emission. The spectra were obtained from the average of 5 consecutive scans.

- **Bis-ANS binding assay**

Samples of 0.1 mg/ml rBap\_B and rBap\_B<sub>sapro</sub> soluble proteins (phosphate-citrate buffer at pH 7.0) or protein aggregates (phosphate-citrate buffer at pH 4.5), were prepared in solutions containing 10 µM of Bis-ANS and analyzed immediately on a Jasco FP-8200 fluorescence spectrophotometer (Jasco corporation, Japan) at 25 °C. The samples were excited at 370 nm and emission was measured between 400 and 600 nm with slit widths of 5 nm. The spectra were obtained from the average of 5 consecutive scans.

- **Proteinase-K digestion**

Proteolysis of 1 mg/ml rBap\_B was performed at 37 °C in the presence or absence of 50 mM CaCl<sub>2</sub>. The protein was incubated with 80 mg/ml Proteinase-K (Sigma) for 0, 15, 30, 45 minutes and the reaction was stopped by the addition of 5 mM PMSF. Degradation pattern was analyzed by SDS-PAGE (12%) followed by western immunoblotting with anti-Bap purified primary antibody (1:10.000) and alkaline phosphatase-conjugated goat anti-rabbit Immunoglobulin G (1:5000) (Thermo Scientific) as a secondary antibody.



- **Preparation and aggregation of Bap\_B short peptides**

The predicted TVGNIISNAG (peptide I) and GIFSYS (peptide II) peptides were obtained from CASLO ApS (Lyngby, Denmark) with high purity (98.29% and 99.88% respectively). Peptide stock solutions at 1 mM were prepared by dissolving into citrate buffer. Samples were immediately sonicated for 10 min to disassemble preformed nuclei and centrifuged (5 min at 16,100g) to deposit insoluble material. Peptide solutions were incubated at room temperature (25 °C) for four weeks and amyloid properties were evaluated as described above.

- **Cell adhesion assay**

Adherence and invasion experiments were performed as described previously (Dziewanowska *et al.*, 1999). Briefly, prior to use, wells were seeded with  $0.3 \times 10^6$  cells in 6-well tissue culture plates. Once cells were confluent ( $1.2 \times 10^6$ ) the culture medium was removed and cells were washed with DMEM plus 10% heat-inactivated fetal bovine serum. For adherence assays, overnight bacterial cultures were mixed vigorously and added to the monolayer cells in a multiplicity of infection of 10 in DMEM. Incubation was carried out 1 hour at 37 °C in 5% CO<sub>2</sub>. To remove non-adherent bacteria, cells were washed three times with sterile PBS. Eukaryotic cells were lysed with 0.1% Triton X-100. Before plating extracts were mixed vigorously by vortexing. The number of adherent bacteria were determined by serial dilution and plating. Experiments were performed in triplicate.

- **Experimental infection**

A mouse foreign body infection model was used to determine the role of Bap aggregates in the pathogenesis of *S. aureus*. Groups of 6 CD1 mice

were used. A 3-cm segment of intravenous catheter (24G1", B. Braun) was aseptically implanted into the subcutaneous interscapular space. Each group of six mice was inoculated with  $1 \times 10^7$  CFU of either *S. aureus* V329 or  $\Delta bap$  mutant previously grown overnight in LB-glu at 37 °C. Twelve animals were euthanatized by cervical dislocation on days 4 or 10 post-infection. The catheter was aseptically removed, placed in a sterile microcentrifuge tube containing 1 ml of PBS, and vortexed at high speed for 3 min. Samples were serially diluted and plated onto TSA plates for enumeration of viable staphylococci.

- **Statistical analysis**

The statistical analysis was performed with the GraphPad Prism 5 program. A nonparametric Mann-Whitney U test was used to assess significant differences in biofilm formation and bacterial aggregation capacity, as well as for analysis of cellular adhesion and experimental infection. The differences in bacterial aggregation after exogenous complementation with rBap\_B protein were determined using the unpaired Student's *t* test.

- **Sequence analysis programs**

The predicted amino acid sequence of region B of Bap from the different strains were analyzed with the PrositeScan program (Combet *et al.*, 2000) on the web server [http://npsa-pbil.ibcp.fr/cgi-bin/npsa\\_automat.pl?page=npsa\\_prosite.html](http://npsa-pbil.ibcp.fr/cgi-bin/npsa_automat.pl?page=npsa_prosite.html), in order to identify potential EF-hand like domains. The isoelectric point for each protein was calculated using the Compute pI/Mw tool of the ExPaSy server. Selection of 15 Bap B domain sequences from orthologous strains was performed with tBlastn

program and the multiple sequence alignment was performed with ClustalW2. To predict amyloidogenic regions within region B of Bap we used four different computational algorithms: AGGRESCAN (Conchillo-Solé *et al.*, 2007), PASTA (Walsh *et al.*, 2014), WALTZ (Oliveberg, 2010), and ZipperDB (Thompson *et al.*, 2006). RosettaDesign (Kuhlman and Baker, 2000) program was utilized to model the supramolecular steric-zipper structures potentially formed by the small peptides included in Bap B region.

**Table 1.** Strains used in this study

Strain	Relevant characteristic(s)	MIC <sup>a</sup>	Reference
<b><i>Staphylococcus aureus</i></b>			
V329	Expresses Bap; biofilm positive	01	(Cucarella <i>et al.</i> , 2001)
V329 P <sub>bap</sub>	V329 complemented with pCN52: P <sub>bap</sub>	281	This study
V329 <i>bap-gfp</i>	V329 with <i>bap</i> gene fused to <i>gfp</i> gene in the chromosome	842	This study
V329 $\Delta$ <i>spa</i>	V329 with deletion in <i>spa</i> gene	905	This study
V329 $\Delta$ <i>aur</i>	V329 with deletion in <i>aur</i> gene	578	This study
V329 $\Delta$ <i>sspA</i>	V329 with deletion in <i>sspA</i> gene	8	
V329 $\Delta$ <i>sspBC</i>	V329 with deletion in <i>sspB</i> and <i>sspC</i> gene	786	This study
V329 Bap <sup>SNAPtag</sup>	Bap-B region labelled with SNAP-tag	787	This study
V329 $\Delta$ EF	V329 mutated in its EF-hand 2 and 3 motifs	557	This study
$\Delta$ <i>bap</i>	V329 with deletion in <i>bap</i> gene.	175	(Arrizubieta <i>et al.</i> , 2004)
$\Delta$ <i>bap<math>\Delta</math><i>spa</i></i>	V329 with deletion in <i>bap</i> and <i>spa</i> genes	341	(Valle <i>et al.</i> , 2012)
$\Delta$ <i>bap</i> pBap_AB	$\Delta$ <i>bap</i> complemented with pBap_AB plasmid	907	This study
$\Delta$ <i>bap</i> pBap_B	$\Delta$ <i>bap</i> complemented with pBap_B plasmid	803	This study
$\Delta$ <i>bap</i> pBap_A	$\Delta$ <i>bap</i> complemented with pBap_A plasmid	804	This study
$\Delta$ <i>bap</i> pClfA	$\Delta$ <i>bap</i> complemented with pClfA plasmid	805	This study
$\Delta$ <i>bap</i> pBap_B_ $\Delta$ EF	$\Delta$ <i>bap</i> complemented with pBap_B_ $\Delta$ EF plasmid	937	This study
$\Delta$ <i>bap</i> pBap_B_ $\Delta$ <i>pepl-II</i>	$\Delta$ <i>bap</i> complemented with pBap_B_ $\Delta$ <i>pepl-II</i> plasmid	946	This study
$\Delta$ <i>bap</i> pBap_B <sub>sapro</sub>	$\Delta$ <i>bap</i> complemented with pBap_B <sub>sapro</sub> plasmid	785	This study
$\Delta$ <i>bap</i> pBap_B <sup>SpyTag</sup>	$\Delta$ <i>bap</i> complemented with pBap_B <sup>SpyTag</sup> plasmid	503	This study
$\Delta$ <i>bap</i> pBap_B <sup>SNAPtag</sup>	$\Delta$ <i>bap</i> complemented with pBap_B <sup>SNAPtag</sup> plasmid	647	This study
10833_ $\Delta$ <i>tagO_</i> $\Delta$ <i>ica</i>	10833 with deletion in <i>tagO</i> gene and <i>ica</i> operon	436	This study
10833_ $\Delta$ <i>tagO_</i> $\Delta$ <i>ica</i> pBap_B	10833 with deletion in <i>tagO</i> gene and <i>ica</i> operon complemented with pBap_B plasmid	412	(Vergara-Irigaray <i>et al.</i> , 2008)
Newman	Biofilm-negative strain.	789	This study
Newman pBap	Newman complemented with pBap plasmid	58	(Duthie and Lorenz, 1952)
Newman pBap_B	Newman complemented with pBap_B plasmid	724	(Cucarella <i>et al.</i> , 2002)
MW2	Biofilm-negative strain.	112	This study
MW2 pBap	MW2 complemented with pBap plasmid	566	(Baba <i>et al.</i> , 2002)
MW2 pBap_B	MW2 complemented with pBap_B plasmid	219	This study
132	MRSA clinical strain with the capacity to form proteinaceous biofilm in TSB-glucose and PIA-PNAG-dependent biofilm in TSB-NaCl	181	This study
132 <i>srtA</i> -	132 <i>srtA</i> :: <i>erm</i>	9	(Vergara-Irigaray <i>et al.</i> , 2009)
218			(Vergara-Irigaray <i>et al.</i> , 2009)
<b><i>Staphylococcus carnosus</i></b>			
TM300	Biofilm negative		(Rosenstein <i>et al.</i> , 2009)
TM300 pBap_B	<i>S. carnosus</i> TM300 complemented with pBap_B plasmid	255	This study
<b><i>Staphylococcus saprophyticus</i></b>			
B20080011225	Clinical strain	96	CUN <sup>b</sup>
<b><i>Staphylococcus simiae</i></b>			
CCM 7213	Squirrel monkey isolate	199	(Pantůček <i>et al.</i> , 2005)
<b><i>Staphylococcus epidermidis</i></b>			
C533	<i>bap</i> -positive strain	309	(Tormo <i>et al.</i> , 2005)
<b><i>Staphylococcus xylosus</i></b>			
C482	<i>bap</i> -positive strain	103	(Tormo <i>et al.</i> , 2005)
<b><i>Staphylococcus simulans</i></b>			
ATCC 1362	<i>bap</i> -positive strain	91	(Tormo <i>et al.</i> , 2005)

Continued on the following page

Table 1. Continued

Strain	Relevant characteristic(s)	MIC <sup>a</sup>	Reference
<b><i>Escherichia coli</i></b>			
XL1-Blue	Used for cloning assays	97	Stratagene
BL21 (DE3) pET46-ek/LIC: <i>bap<sub>B</sub></i>	BL21 (DE3) containing pET46-ek/LIC: <i>bap<sub>B</sub></i> plasmid	85	This study
BL21 (DE3) pET46-ek/LIC: <i>bap<sub>B</sub>sapro</i>	BL21 (DE3) containing pET46-ek/LIC: <i>bap<sub>B</sub></i> plasmid	713	This study
BL21 Origami (DE3) pET46-ek/LIC: <i>gfp</i>	BL21 (DE3) containing pET46-ek/LIC: <i>gfp</i> plasmid	529	This study
BL21 Origami (DE3) pET46-ek/LIC: <i>gfp-spyCatcher</i>	BL21 (DE3) containing pET46-ek/LIC: <i>gfp-spyCatcher</i> plasmid	530	This study
VS39	Δ( <i>csgABC</i> ) + pVS76 (produces CsgG)	156	(Sivanathan and Hochschild, 2013)
VS39 Bap_ <i>B<sub>aur</sub></i>	VS39 complemented with pEXPORT <sub>XhoI</sub> : <i>bap<sub>B<sub>aur</sub></sub></i>	380	This study
VS39 Bap_ <i>A<sub>aur</sub></i>	VS39 complemented with pEXPORT <sub>XhoI</sub> : <i>bap<sub>A<sub>aur</sub></sub></i>	384	This study
VS39 Bap_ <i>B<sub>sapro</sub></i>	VS39 complemented with pEXPORT <sub>XhoI</sub> : <i>bap<sub>B<sub>sapro</sub></sub></i>	467	This study
VS39 Bap_ <i>B<sub>simiae</sub></i>	VS39 complemented with pEXPORT <sub>XhoI</sub> : <i>bap<sub>B<sub>simiae</sub></sub></i>	468	This study
VS39 Bap_ <i>B<sub>epid</sub></i>	VS39 complemented with pEXPORT <sub>XhoI</sub> : <i>bap<sub>B<sub>epid</sub></sub></i>	610	This study
VS39 Bap_ <i>B<sub>xylo</sub></i>	VS39 complemented with pEXPORT <sub>XhoI</sub> : <i>bap<sub>B<sub>xylo</sub></sub></i>	613	This study
VS39 Bap_ <i>B<sub>simul</sub></i>	VS39 complemented with pEXPORT <sub>XhoI</sub> : <i>bap<sub>B<sub>simul</sub></sub></i>	612	This study
<b><i>Listeria monocytogenes</i></b>			
EGD	Biofilm negative.	2	(Mackaness, 1964)
<b><i>Enterococcus faecalis</i></b>			
23	Esp-negative. Biofilm negative.	31	(Toledo-Arana <i>et al.</i> , 2001)
<b><i>Salmonella enteritidis</i></b>			
3934	Wild-type clinical isolate	4	(Solano <i>et al.</i> , 1998)

<sup>a</sup>Microbial Biofilm Laboratory strain<sup>b</sup>CUN, Clínica Universitaria de Navarra (Pamplona, Spain)

**Table 2.** Plasmids used in this study.

Plasmids	Relevant characteristic(s)	Source or reference
pJET1.2/blunt	Cloning vector	Thermo Scientific
pCN51	<i>E. coli</i> - <i>S. aureus</i> shuttle vector with a cadmium inducible promoter	(Charpentier <i>et al.</i> , 2004)
pBap_AB	pCN51 plasmid expressing A and B domains of Bap from <i>S. aureus</i> fused to 3xflag, followed by R region of ClfA	This study
pBap_B	pCN51 plasmid expressing B domain of Bap from <i>S. aureus</i> fused to 3xflag, followed by R region of ClfA	This study
pBap_A	pCN51 plasmid expressing A domain of Bap from <i>S. aureus</i> fused to 3xflag, followed by R region of ClfA	This study
pClfA	pCN51 plasmid expressing the entire <i>clfA</i> gene	This study
pBapB_Δpepl-II	pCN51 plasmid expressing B domain of Bap from <i>S. aureus</i> with amyloidogenic peptides I and II mutated, fused to 3xflag, followed by R region of ClfA	This study
pBap_B_ΔEF	pCN51 plasmid expressing B domain of Bap from <i>S. aureus</i> mutated in EF-hand motifs 2 and 3, fused to 3xflag, followed by R region of ClfA	This study
pBap_B <sub>sapro</sub>	pCN51 plasmid expressing B domain of Bap from <i>S. saprophyticus</i> fused to 3xflag, followed by R region of ClfA	This study
pBap_B <sup>SNAPtag</sup>	pCN51 plasmid expressing B domain of Bap from <i>S. aureus</i> fused to SNAP-tag, followed by R region of ClfA	This study
pBap_B <sup>Spy1ag</sup>	pCN51 plasmid expressing B domain of Bap from <i>S. aureus</i> fused to SpyTag peptide, followed by R region of ClfA	This study
pCN52	<i>E. coli</i> - <i>S. aureus</i> promoterless shuttle vector for promoter- <i>gfp</i> fusions	(Charpentier <i>et al.</i> , 2004)
pCN52:P <sub>bap</sub>	pCN52 expressing GFP under de control of <i>bap</i> promoter	This study
pET46-ek/LIC	Expression vector	Novagen
pET46-ek/LIC: <i>bap_B</i>	pET46-ek/LIC plasmid expressing recombinant N-terminal His <sub>6</sub> -tagged B region of Bap from <i>S. aureus</i>	This study
pET46-ek/LIC: <i>bap_B</i> <sub>sapro</sub>	pET46-ek/LIC plasmid expressing recombinant N-terminal His <sub>6</sub> -tagged B region of Bap from <i>S. saprophyticus</i>	This study
pET46-ek/LIC: <i>gfp</i>	pET46-ek/LIC plasmid expressing recombinant N-terminal His <sub>6</sub> -tagged GFP protein	This study
pET46-ek/LIC: <i>gfp-spyCatcher</i>	pET46-ek/LIC plasmid expressing recombinant N-terminal His <sub>6</sub> -tagged GFP-SpyCatcher protein	This study
pMAD	<i>E. coli</i> - <i>S. aureus</i> shuttle vector with a thermosensitive origin of replication for Gram-positive bacteria. The vector contains the <i>bgaB</i> gene encoding a β-galactosidase under the control of a constitutive promoter as reporter of plasmid presence. Ap <sup>R</sup> , Em <sup>R</sup>	(Arnaud <i>et al.</i> , 2004)
pMAD <i>spaAD</i>	pMAD plasmid containing the mutant allele for deletion of <i>spa</i> gene	(Merino <i>et al.</i> , 2009)
pMAD <i>bapAB-gfp-bapCD</i>	pMAD plasmid containing the mutant allele for insertion of <i>gfp</i> gene at the end of <i>bap</i> gene	This study
pMAD <i>bapAB-snaptag-bapCD</i>	pMAD plasmid containing the mutant allele for insertion of <i>snaptag</i> sequence between B and C regions of <i>bap</i> gene	This study
pJP437	pMAD derivatives used to generate the Δ <i>sspA</i> mutants	(Martí <i>et al.</i> , 2010)
pJP438	pMAD derivatives used to generate the Δ <i>sspBC</i> mutants	(Martí <i>et al.</i> , 2010)
pJP439	pMAD derivatives used to generate the Δ <i>aur</i> mutants	(Martí <i>et al.</i> , 2010)
pEXPORT	Expression vector for C-DAG system (NotI-XbaI restriction sites for insertion of gene of interest)	(Sivanathan and Hochschild, 2013)
pEXPORT <sub>XhoI</sub>	Expression vector for C-DAG system (NotI-XhoI restriction sites for insertion of gene of interest)	This study
pEXPORT <sub>XhoI</sub> : <i>bap_Aaur</i>	pEXPORT plasmid expressing CsgA signal peptide fused to A domain of Bap from <i>S. aureus</i>	This study
pEXPORT <sub>XhoI</sub> : <i>bap_Baur</i>	pEXPORT plasmid expressing CsgA signal peptide fused to B domain of Bap from <i>S. aureus</i>	This study
pEXPORT <sub>XhoI</sub> : <i>bap_Bsapro</i>	pEXPORT plasmid expressing CsgA signal peptide fused to B domain of Bap from <i>S. saprophyticus</i>	This study
pEXPORT <sub>XhoI</sub> : <i>bap_Bsimi</i>	pEXPORT plasmid expressing CsgA signal peptide fused to B domain of Bap from <i>S. simiae</i>	This study
pEXPORT <sub>XhoI</sub> : <i>bap_Bepid</i>	pEXPORT plasmid expressing CsgA signal peptide fused to B domain of Bap from <i>S. epidermidis</i>	This study
pEXPORT <sub>XhoI</sub> : <i>bap_Bxylo</i>	pEXPORT plasmid expressing CsgA signal peptide fused to B domain of Bap from <i>S. xylo</i>	This study
pEXPORT <sub>XhoI</sub> : <i>bap_Bsimu</i>	pEXPORT plasmid expressing CsgA signal peptide fused to B domain of Bap from <i>S. simulans</i>	This study
pSNAP-tag@(T7)-2	Expression vector encoding the SNAP-tag protein	New England Biolabs
pAD-cGFP	GFP expression under the control of constitutive promoter <i>PhyPer</i>	(Balestrino <i>et al.</i> , 2010)
pAU1108-GFPcatcher	Expression vector encoding <i>gfp-spycatcher</i> sequence under de expression of <i>Ptac</i> promoter	This study

**Table 3.** Oligonucleotides used in this study.

Oligonucleotide	Sequence
<b>Design of Bap-ClfA quimeric proteins</b>	
Bapori-1mB	<u>GGATCC</u> TTTTTTTTGAGGTGAGTAAATATGGG
bap-63cK	<u>GGTACC</u> GGTGCCTTCTGGTGAATTTGG
bap-65c	GGCTCTTTAATTGAATTAGATGAAGCACTATTTTGTACTTCCGC
bap-66m	GCGGAAGTACAAAATAGTGCTTCATCTAATTCAATTAAGAGCC
bap-B1	GCCATCAGTATCTTCGTTTTTCAGCAATAATTGGATCTAAT
bap-B2	ATTAGATCCAATTATTGCTGAAAACGAAGATACTGATGGC
bap-B3K	<u>GGTACC</u> ATTTACAGTTGCTGTACC
K-3xF-clfA	<u>GGTACC</u> gactacaagaccatgacgggtattataaagatcatgacatcgactacaaggatgacgatgacaagGAAATTGAA CCAATTCCAGAGGAT
clfA-7cE	<u>GAATTC</u> TTACACCCCTATTTTTTCGCC
clfA-9mB	<u>GGATCC</u> TTTTTAAAAAGAGGGAATAAAATGAATATG
SPbap-sapro-Rv	TTGTCAGAATAATCCAATGCTTCGCTAATGCTTCACCTTTGTC
bapB-sapro-Fw	GACAAAGGTGAAGCATTAGACGAAGCATTGGATTATTCTGACAA
Sapbap-KpnI-Rv	<u>GGTACC</u> TGATTTATGAAATTCAAAGTTATCT
Pcad-Fw,	CTAGCTTTATATTCTTTAGTGT
pept1_Bap_check_Rv	AGATCCAGATCCAGAATCGTCCAATTCTAT
pept2_Bap_check_Rv	AGATCCAGATCCAGAGTTCTTCATGATTTGT
<b>Production of recombinant proteins</b>	
bapB1-LIC-Fw	<b>GACGACGACAAG</b> ATGCAAAAATCTTTAGGTTACACAGATAAATTATAC
bapB1-LIC-Rv	<b>GAGGAGAAGCCCGGTTA</b> AATTTACAGTTGCTGTACCAACTGTTGTAC
bapB-sapro-LIC-Fw	<b>GACGACGACAAG</b> ATGGAAGCATTGGATTATTCTGACAA
bapB-sapro-LIC-Rv	<b>GAGGAGAAGCCCGGTTA</b> TAAATTTACTTTACCAATTACTGTAGTATC
GFP_Ek_LIC_Fw	<b>GACGACGACAAG</b> ATGAGTAAAGGAGAAGAAGCTTTTC
GFP_Ek_LIC_Rv	<b>GAGGAGAAGCCCGGTTA</b> TTTGTATAGTTTCATCCATGCC
GFP_Catcher_Ek_LIC_Rv	<b>GAGGAGAAGCCCGGTTA</b> ATATGAGCGTCACCTTTAG
<b>Transcriptional and post-transcriptional fusions for <i>bap</i> gene</b>	
Bap-GFP-EcoRI-A	<u>GAATTC</u> CCAATACGACTATAATCG
Bap-GFP-BamHI-Sal-B	<u>GGATCC</u> CCCGGGGTCGACCAATAATTTAAACATTTATTTTT
Bap-GFP-BamHI-C	<u>GGATCC</u> TAAATAAGTACAGGGCTCTC
Bap-GFP-BglII-D	<u>AGATCT</u> CCGAAATGTTGGCCGTATT
pBap- KpnI Fw	<u>GGTACC</u> GCA AAG AAT ACT TTA AAA GG
pBap-EcoRI-Rv	<u>GAATTC</u> TTT TTA CAA TTT TAT GAC GC
<b>Construction of plasmids for C-DAG system</b>	
pVS72-XhoI-5	CCAAGCTTGCATGCCTGCAGGTCGACCTCGAGTTAGTGATGATGGTGATGGTGATCGTTA
pVS72-XhoI-3	TAACGATCACCATCACCATCATCACTAACTCGAGGTCGACCTCGAGGCATGCAAGCTTGG
cdag_B_NotI_Fw	<u>GCGGCCGC</u> ACAAAAATCTTTAGGTTACACAGATAAATTATAC
cadg_B_XhoI_Rv	<u>CTCGAG</u> TTAGTGATGATGGTGATGGTGATTTACAGTTGCTGTACCAACTGTTGTAC
CDAG BAP_A-Fw	<u>GCGGCCGC</u> ATCAGAAAAATCCAATGACACTGCT
CDAG BAP_A-Rv	<u>CTCGAG</u> TTAGTGATGATGGTGATGGTGTTCTAATTCAGATTCTTCATTTTTATCAGT
BAPsapro_cdag_Fw	<u>GCGGCCGC</u> AGAAAGCATTGGATTATTCTGACAA
BAPsapro_cdag_rv	<u>CTCGAG</u> TTAGTGATGATGGTGATGGTGTAATTTACTTTACCAATTACTGTAGTATC
BAPsimiae_cdag_Fw	<u>GCGGCCGC</u> ACAAAAATCATTAGGTTATTCAAGTAACT
BAPsimiae_cdag_Rv	<u>CTCGAG</u> TTAGTGATGATGGTGATGGTGATTAACAGCTGATGTACCTATCA
epider_CDAG_Fw	<u>GCGGCCGC</u> ACAAAAATCTTTAGGTTACACAGAT
epider_CDAG_Rv	<u>CTCGAG</u> TTAGTGATGGTGATGGTGATGATTTACAGTTGTTGTACCAACT
xylofus_CDAG_Fw	<u>GCGGCCGC</u> AGAAAAATCATTAGGTTACTTAGATAATT
xylofus_CDAG_Rv	<u>CTCGAG</u> TTAGTGATGGTGATGGTGATGGTTAACTGTAGATGTTCCAATCA
simulans_CDAG_Fw	<u>GCGGCCGC</u> AAAAATCTTTAGGTTACACAGATGA
simulans_CDAG_Rv	<u>CTCGAG</u> TTAGTGATGGTGATGGTGATGCTCTGCATTAATTACTTTAGCT
<b>Bap tagging with SNAPtag and SpyTag</b>	
Bap_SNAP_A_EcoRI	<u>GAATTC</u> GAAACTGTAGGCGTTAGAGT
Bap_SNAP_B	ATTTTCGCAATCTTTGTCCATATTTACAGTTGCTGTACCAAC
Bap_SNAP_C	CTGGGTAACCCGGGCTCTGGGATCAGATGGTACATTCTCAGTGT
Bap_SNAP_D_BamHI	<u>GGATCC</u> TGTATTTACTTCACTAATGTTGG
SNAPtag_A	TTGGTACAGCAACTGTAATATGACAAAGATTGCGAAATGA
SNAPtag_B	ACACTGAGAATGTACCATCTGATCCCAGACCCGGTTTACCCAG
Spy_tag_fw	GGGCCAGCCGGTACCGCCACATCGTGATGGTGGACGCCCTACAAGCCGACGAAG
Spy_tag_rv	GGGCCAGCCGGTACCCTTCGTCGGCTTGTAGGCGTCCACCATCAGATGTGGGC
Fw_snap_KpnI	GGGGTACCATGGACAAAGATTGCGAAATG
Rv_snap_KpnI	<u>GGTACC</u> TCCAGACCCGGTTACCCAG
<b>Deletion of <i>spa</i> gene</b>	
spa-E	GATGATGTATACAATGTATTTTC
spa-F	TGCGTCTCGATTTAATTGG
<b>Deletion of protease genes</b>	
ssp-20cN	TTGAACTTGATCTTCTTGTATCGC
ssp-17mS	ATTACCGCTCAACCTGAAGGC
ssp-24cN	GGTGAAGACCAATCCCTCGC
ssp-21mS	ACGAATGGTCATTATGCACCC
aur-Fw	CTTCATGTTACAATAGTGCTAAAC
aur-11mE	ACAAAGGAAGCTGATAGCGG

<sup>a</sup>Restriction sites of enzymes are underlined.

<sup>b</sup>3xflag sequence is in small letters.

<sup>c</sup>LIC tails are in bold letters.





## ***RESULTS***

---



## RESULTS

- **Analysis of the distribution of Bap on the bacterial surface and its role in the multicellular behavior of *S. aureus***

As previously mentioned in the introduction, Bap is a surface protein that participates in intercellular adhesion and bacterial accumulation steps during biofilm formation process (Cucarella *et al.*, 2001; Arrizubieta *et al.*, 2004). However, the distribution of the protein on the bacterial surface has not been determined. There are evidences showing that signal peptides determine the destination of surface proteins in the bacterial envelope (DeDent *et al.*, 2008). Signal peptides containing the YSIRK/GS motif direct surface proteins secretion and anchorage close to the cell division site where peptidoglycan synthesis is actively occurring. Following cell division, the proteins become distributed across the cell surface in a ring-like manner. In contrast, proteins without this motif are directed to peripheral secretion sites at the cell pole where they remain located in discrete assembly sites (DeDent *et al.*, 2008). We first analyzed the presence of the YSIRK/GS motif in the signal peptide of Bap. Amino acid sequences of signal peptides from staphylococcal surface proteins with ring-like distribution (clumping factor A, protein A, fibronectin-binding protein B, serine-aspartate repeat protein C and D) were aligned with the amino acid sequence of the Bap signal peptide. Results revealed the presence of an YSIRK/GS motif in the signal peptide sequence of Bap (Fig. 8A). Next, we performed immunofluorescence microscopy to visualize Bap on the surface of *S. aureus* V329 by labeling the protein with anti-Bap polyclonal antibodies. We used V329 and  $\Delta bap$  strains deleted in their *spa* gene (V329  $\Delta spa$  and  $\Delta bap\Delta spa$ ) to avoid unspecific labeling of protein A through its union to the Fc fraction of immunoglobulins. In agreement with the presence of the YSIRK/GS motif, Bap showed a ring-like distribution on the surface of

the bacteria (Fig. 8B). The  $\Delta bap\Delta spa$  mutant cells showed no immunolabeling, confirming antibodies specificity (Fig. 8B). These results confirm that Bap localizes on the bacterial surface as a ring surrounding each cell.

Aggregation kinetics showed that V329 strain aggregated over time, while cells of *bap* mutant remained suspended in the culture medium (Fig. 8C). To further confirm that Bap specifically mediates this aggregation, we evaluated the capacity of anti-Bap antibodies to interfere with Bap-mediated bacterial aggregation. We reasoned that anti-Bap antibodies could sterically interfere with the capacity of the protein to induce cell-cell interactions and biofilm formation. To test this hypothesis, we performed aggregation and biofilm formation assays of *S. aureus* V329 strain in the presence of a polyclonal antibody raised against Bap (Fig. 8C and D). The *S. aureus* 132 strain was included as a control in the study, as its biofilm formation capacity depends on the production of the fibronectin binding proteins (Vergara-Irigaray *et al.*, 2009). We found that aggregation and biofilm formation capacity of the V329 strain was completely inhibited in a dose-dependent manner by anti-Bap antibody (Fig. 8E). Taken together, these results indicate that the interaction of antibodies with Bap sterically blocks the capacity of the protein to mediate biofilm development; this finding provides further evidence of the requirement for Bap in the biofilm development process.

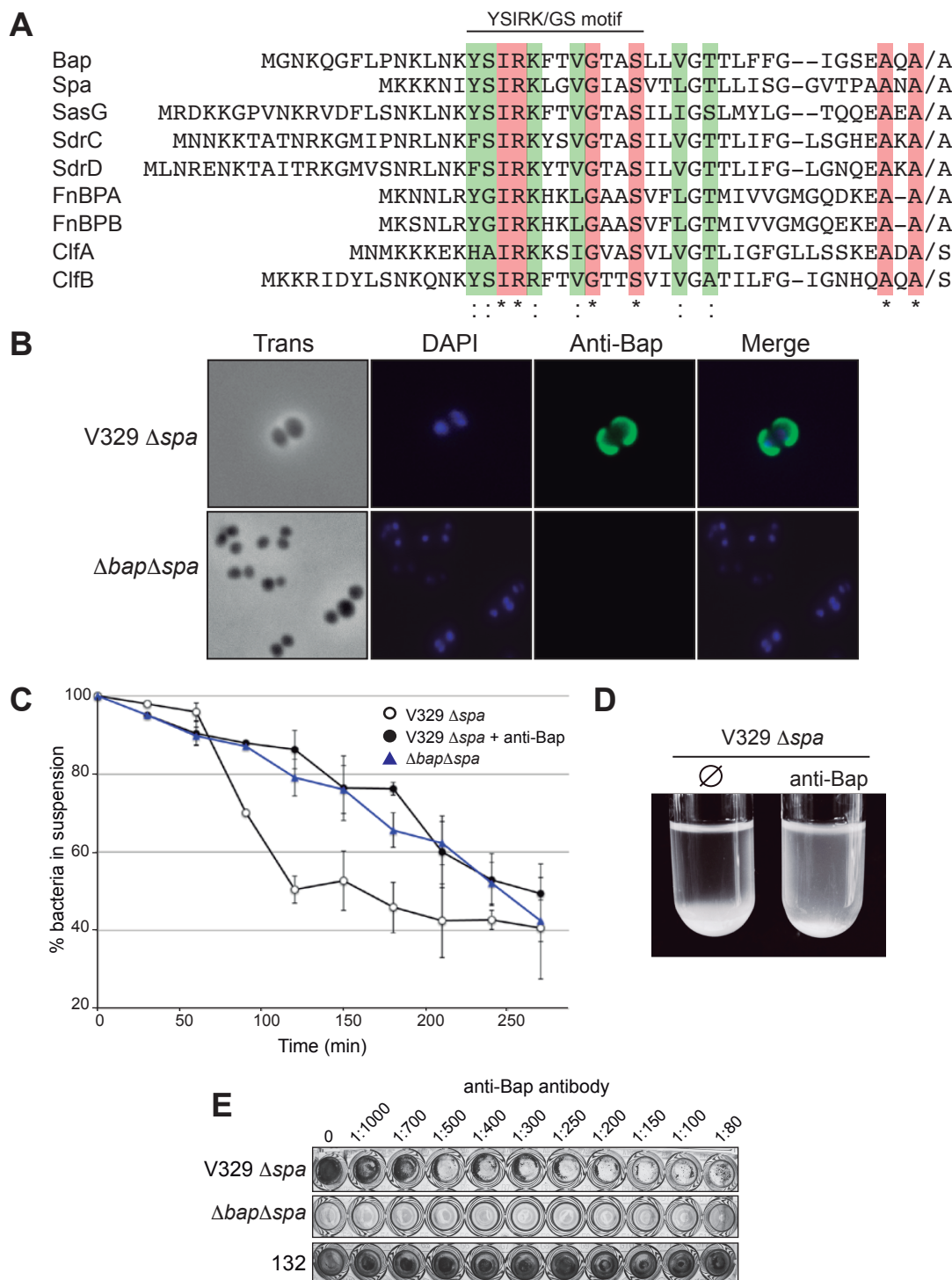


**Figure 8. Bap promotes cell-to-cell interactions.** **A**) Signal peptides of *S. aureus* surface proteins containing the YSIRK/GS motif were aligned at their predicted signal peptidase cleavage sites (A/X). Identical residues are marked in red and summarized as \*, conserved residues are marked in green or summarized with a colon (:). **B**) Immunofluorescence showing surface localization of Bap. Bacteria were fixed and labeled with anti-Bap antibodies and DAPI. **C**) Bacterial aggregation kinetics of *S. aureus* V329  $\Delta spa$ ,  $\Delta bap \Delta spa$  and V329  $\Delta spa$  plus 10  $\mu$ l of anti-Bap antibody. **D**) Bacterial clumping at the bottom of the tube of *S. aureus* V329 in the absence ( $\emptyset$ ) or presence of anti-Bap antibodies. **E**) Biofilm formation in polystyrene microtiter plates of *S. aureus* V329  $\Delta spa$ ,  $\Delta bap \Delta spa$  and 132 strains in the presence of decreasing dilutions of anti-Bap antibody.

- **Analysis of Bap regulation and expression**

To have a better understanding of how Bap is mediating cell-to-cell interaction during biofilm formation in *S. aureus*, we decided to monitor the expression of the protein in rich liquid medium (LB-glu) along the growth curve. Western immunoblotting revealed that Bap was expressed at early stages of growth but its expression decreased when the bacteria entered the stationary phase ( $OD_{600nm} \sim 4-5$ ) (Fig. 9A), suggesting a possible regulation of protein expression by an unknown factor. To deepen in the regulatory mechanisms determining Bap expression, we successively constructed two *S. aureus* V329 strains: (i) *S. aureus* V329  $P_{bap}$ , harboring a transcriptional fusion between *bap* promoter and *gfpmut2* expressed in plasmid pCN52 (Charpentier *et al.*, 2004), and (ii) *S. aureus* V329 *bap-gfp*, harboring a post-transcriptional fusion of *bap* RNA with *gfp* RNA in the chromosome. Both strains show identical replication time to the wild type V329 (Fig. 9D). We next determined Bap and GFP expression levels by western blot. The results revealed that GFP expression was constant all along the growth curve (Fig. 9B and C). Accordingly, analysis of GFP expression using fluorescence microscopy revealed the presence of GFP during all stages of growth (Fig. 9E). These results indicate that the decreased accumulation of the Bap protein at stationary phase was not due to a transcriptional repression of *bap* gene expression.

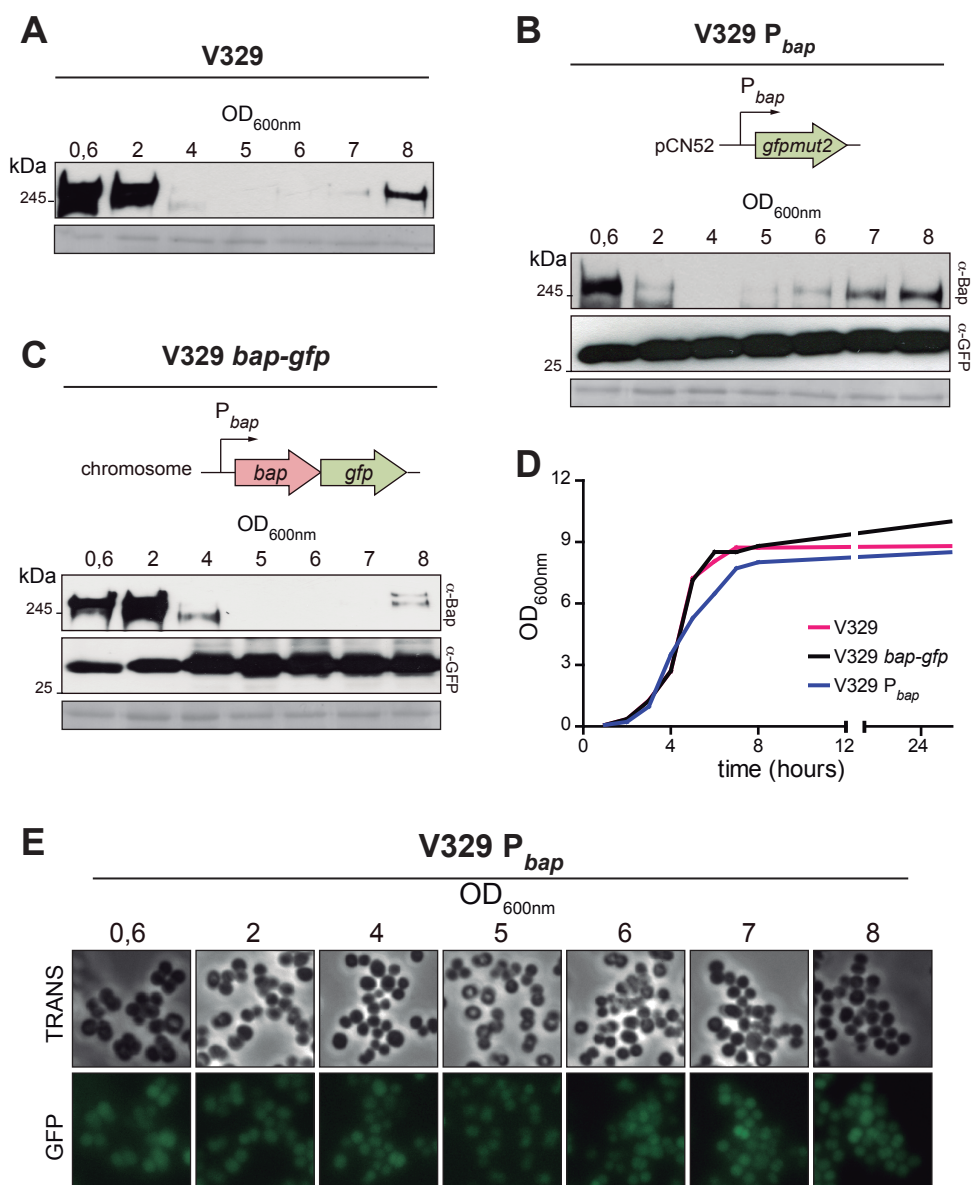


**Figure 9. Bap is constitutively expressed during *S. aureus* growth. A)** Bap expression of *S. aureus* V329 at different points of the growth curve. Bap and GFP expression of *S. aureus* V329 P<sub>bap</sub> (**B**) and *S. aureus* V329 *bap-gfp* (**C**) at different points of the growth curve. Cell wall extracts and total protein extracts were separated on 7,5% and 12% acrylamide gels and probed with anti-Bap (α-Bap) or anti-GFP (α-GFP) antibodies for Bap and GFP detection, respectively. **D**) Parallel growth of *S. aureus* V329, V329 P<sub>bap</sub> and V329 *bap-gfp* strains in LB-glu, at 37 °C, 200 rpm. **E**) GFP fluorescence micrographs of *S. aureus* V329 P<sub>bap</sub> cells confirming constitutive activity of *bap* promoter at different stages of bacterial growth.

- **Bap forms aggregates under acidic solution conditions**

We next hypothesized that the decreased accumulation of Bap at stationary phase might be linked to changes in the oligomerization state of the protein. To test this, we monitored the expression of Bap in rich liquid medium (LB-glu) along the growth curve using native and denaturing gel electrophoresis. Western immunoblotting of SDS-PAGE gels confirmed once again the presence of Bap until the population entered stationary phase ( $OD_{600nm} \sim 5$ ). From that point, the levels of Bap decreased significantly under denaturing conditions whereas a band of high molecular weight appeared in the native gels suggesting that Bap forms aggregates when bacteria enter stationary growth phase (Fig. 10A).

In media containing glucose, *S. aureus* growth is accompanied by a decrease in the pH due to the accumulation of acidic byproducts from sugar fermentation. Thus, we wondered whether Bap aggregation and Bap-mediated biofilm development were related and occurred in response to changes in the medium pH. To investigate this hypothesis, bacteria were grown in LB-glu, where pH levels dropped below 5 when bacteria reached stationary phase ( $OD_{600nm} \sim 5$ ) and in LB without glucose, where the pH remained neutral all along the growth curve (Fig. 10B). Western immunoblotting revealed that Bap failed to form protein aggregates when bacteria were grown in LB (Fig. 10C). Moreover, results showed a strong correlation between Bap protein aggregates and Bap-mediated biofilm formation since bacteria grown in LB-glu (pH<5) formed bacterial clumps at the bottom of the tube and a strong biofilm in microtiter plates, whereas in LB medium (neutral pH) Bap failed to promote bacterial clumping and biofilm development (Fig. 10D and E).

Together, these results suggest that acidification of the growth media promotes Bap aggregation and biofilm development.



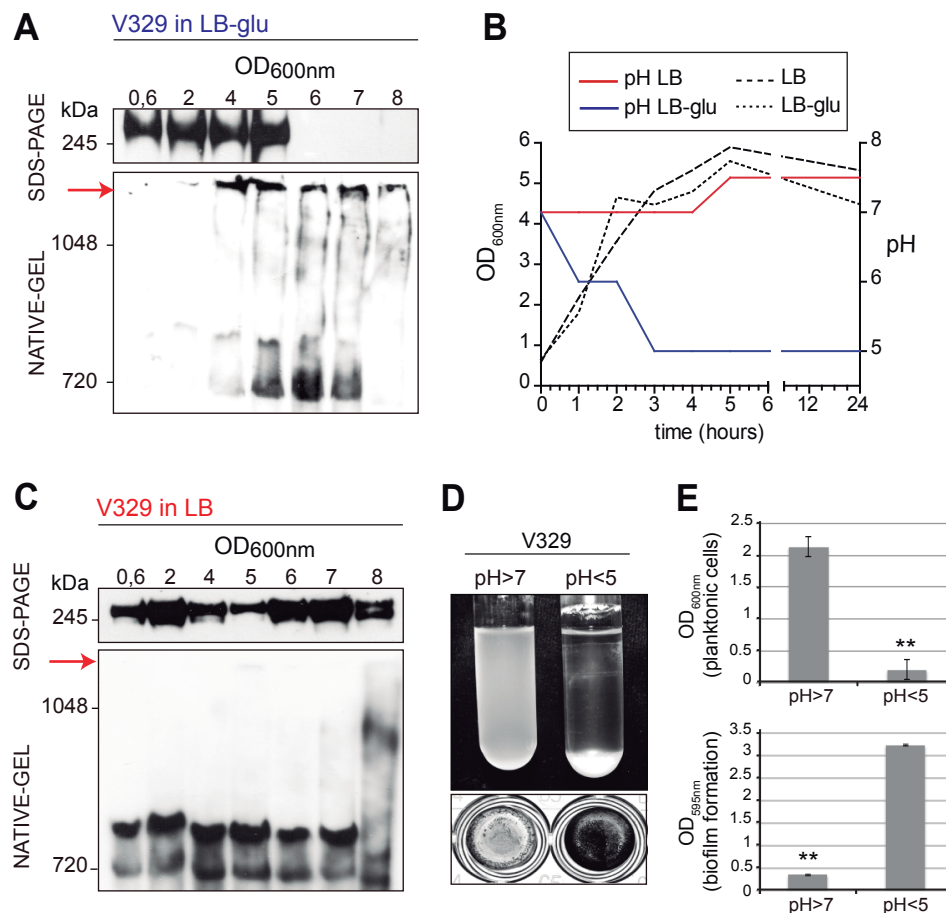


**Figure 10. Culture pH determines Bap-mediated aggregation.** Cell wall extracts taken at different points of the growth curve from *S. aureus* V329 grown in LB-glu (**A**) or LB (**C**) were separated on 7.5% acrylamide gels (upper panels) or Criterion XT Tris-acetate gels with Tris/glycine running buffer (lower panels) and probed with anti-Bap antibodies. Bap-related insoluble aggregates are indicated by a red arrow. **B**) Growth curve of *S. aureus* V329 cultured in LB-glu (dotted line) or LB (dashed line). pH changes in the supernatant of LB-glu (blue line) or LB (red line) culture along staphylococcal growth. **D**) Bacterial clumping and biofilm formation of *S. aureus* V329 in LB (pH>7) and LB-glu (pH<5). For bacterial clumping, bacteria were cultured overnight, at 37 °C, 200 rpm. For biofilm formation, *S. aureus* V329 was cultured overnight at 37°C in polystyrene microtiter plates under static conditions. **E**) Quantification of bacterial aggregation (upper graphic) and biofilm formation (lower graphic). Autoaggregation assays were performed by measuring the OD<sub>600nm</sub> at the top of the culture tubes (1 cm from the surface) as an indication of non-settled cells after an overnight incubation at 37 °C, 200 rpm. Static biofilm formation on polystyrene microtiter plates was quantified by solubilizing crystal violet-stained cells with ethanol-acetone (80:20 v/v) and determining the absorbance at 595nm. Data represent the means from three independent experiments. Error bars represent SD (\*\*,  $P<0.01$ ). Statistical analysis was performed using the Mann-Whitney test.

- **The N-terminal region of Bap forms aggregates**

Next, we focused our study on how these Bap aggregates are formed and the mechanism by which they mediate biofilm formation. We reasoned that Bap aggregates should contain mainly the Bap protein in the case that Bap is engaged in homophilic interactions during biofilm development. In contrast, Bap aggregates should contain also additional proteins in the case that Bap mediates heterophilic interactions with other surface proteins. To distinguish between these possibilities, we determined the protein content of the Bap aggregates by recovering the insoluble aggregated material retained within the wells of the stacking native gel and analyzing their identity by mass spectrometry (MS). MS analysis identified peptides that corresponded mostly to the Bap protein, strongly suggesting that this polypeptide is the main constituent of the aggregates (Table 4). Apart from Bap and a few ribosomal and metabolic proteins, the vast majority of the identified peptides corresponded to proteins that were also detected by MS analysis from preparations of *S. aureus* grown in LB medium, where no presence of Bap was observed (Table 4). To discard the possibility that additional non proteinaceous matrix molecules such as PNAG or eDNA could be involved in the formation of the Bap aggregates, we performed dispersion assays of biofilms formed by *S. aureus* V329 on polystyrene plates, using two disaggregation molecules: dispersin B (DspB), an enzyme of *Aggregatibacter actinomycetemcomitans* that is able to hydrolyze  $\beta$ -(1-6) glycosidic linkages (Kaplan *et al.*, 2004), and DNaseI. The results revealed that the biofilm formed by *S. aureus* V329 was not affected by treatments with dispersin B and DNaseI (Fig. 11A and B). As expected, dispersin B completely disrupted the PNAG-dependent biofilm formed by wild type *S. aureus* strain 15981 (Fig. 11A), used as a control for dispersion assays. Furthermore, Bap protein aggregates were still detected by immunoblotting

when purified cell wall extracts of *S. aureus* V329 were treated with the two degrading agents for 2 h at 37°C (Fig. 11C), strongly suggesting that Bap aggregates do not contain exopolysaccharides or DNA.

MS analysis also showed that the identified Bap peptides covered almost completely the N-terminal sequence of mature Bap (amino acids 49 to 819) and surprisingly no peptides matching other regions were identified (Fig. 12A), suggesting that Bap must suffer a proteolytic processing and only the resulting N-terminal region has the capacity to form the aggregates.

To further investigate the relationship between Bap proteolytic cleavage and aggregation, we analyzed by western blot the degradation pattern of Bap both in cell wall extracts and culture supernatants of bacteria grown in LB and LB-glu, using specific antibodies recognizing the N-terminal region of Bap. Results revealed that Bap was proteolytically processed in both media, as shown by Bap degradation pattern of cell wall extracts in LB and LB-glu (Fig. 12C). However, small bands recognized by anti-Bap antibodies raised against B domain were only detected in supernatants of bacteria grown in LB medium and not in bacteria grown in LB-glu (Fig. 12D), probably because the fragments containing the N-terminal region of Bap are sequestered to form the insoluble aggregates observed in native gels (Fig. 12B).

With the aim to identify the precise mechanism by which Bap is processed, we generated *S. aureus* V329 derivatives deficient in the three most important proteases: *S. aureus*  $\Delta aur$  lacking the metalloprotease aureolysis, *S. aureus*  $\Delta sspA$  lacking the serine protease SspA and *S. aureus*  $\Delta sspBC$  lacking the cysteine protease SspB and its specific inhibitor SspC (Martí *et al.*, 2010). None of the mutants lost their capacity to aggregate or produce biofilm (Fig. 13A and B, left panels), and Bap cleavage patterns were similar to the wild type strain (Fig. 13C, left panel).

## Results

---

Next, we evaluated Bap degradation pattern in the presence of protease inhibitors, such as  $\alpha_2$ -macroglobulin, E64 and PMSF. The results revealed that none of the inhibitors was able to prevent Bap proteolytic processing (Fig. 13A-C, right panels). At this point, we can only conclude that the N-terminal region of Bap undergoes a proteolytic cleavage that occurs either by spontaneous autoproteolysis, by the activity of a protease different from the ones tested here or by the action of more than one protease.

**Table 4.** Summary of the proteins identified by proteomics from aggregates of *S. aureus* V329 in LB-glu and LB.

Putative Protein	NCBI GI n°	LB-glu			LB		
		Total score	% coverage	Peptides (>95%)	Total score	% coverage	Peptides (>95%)
<b>Biofilm-associated protein</b>	<b>31616158</b>	<b>89,13</b>	<b>53,3</b>	<b>53</b>	--	--	--
Bifunctional autolysin precursor	151221134	50,48	53,6	26	41,98	62	20
Hypothetical protein	151220813	33,77	70,2	28	45,82	78,3	33
branched-chain alpha-keto acid dehydrogenase subunit E2	151221173	31,49	64,7	18	24,37	54,9	14
Dihydrolipoamide dehydrogenase	151221174	29,13	68,6	22	22,48	68,2	13
ABC transporter, amino acid binding protein	151222525	26,25	75,7	15	11,96	69,1	8
50s ribosomal protein L2	151222361	21,97	69,7	12	1,27	37,6	1
Penicillin binding protein 2	151221573	20,29	44,3	12	24,9	68,8	13
Pyruvate kinase	151221804	18,53	58,5	11	--	--	--
Molybdate binding protein	151222391	18,31	65,8	9	10,89	74,2	8
Elongation factor Tu	151220722	17,33	64,7	9	8,82	61,9	6
peptidyl-propyl cis/trans-isomerase	151221945	15,72	66,6	9	14,85	74,4	9
ABC transporter substrate-binding protein	151220994	15,2	67,4	7	22,25	70,7	14
Pyruvate dehydrogenase E1	151221172	13,41	46,8	7	12,71	71,1	7
Hypothetical protein	151220899	12,99	52,9	7	5,95	93,9	3
malate:quinone oxidoreductase	151222716	12,38	37,4	8	2,46	34,4	1
Glyceraldehyde-3-phosphate dehydrogenase	151220953	12,15	67	7	2,1	56,9	1
Signal peptidase IB	151221048	12,01	67,5	7	10,74	63,4	5
Immunoglobulin-binding protein (Sbi)	151222529	10,96	69	4	9,88	57,1	5
50s ribosomal protein L15	151222345	10,38	82,2	5	--	--	--
phosphopyruvate hydratase	151220957	10,09	48,6	5	--	--	--
50s ribosomal protein L21	151221761	9,59	96,1	6	3,72	68,6	2
N-acetylmuramoyl-L-alanine amidase	151222755	8,76	54,9	4	--	--	--
Hypothetical protein	151221023	8,5	32,8	4	--	--	--
Bifunctional preprotein translocase subunit SecD/SecF	151221751	8	30,6	4	1,96	30,2	1
Universal stress protein	151221816	7,95	62,1	4	7,44	76,5	5
Hypothetical protein	151220965	7,43	59,5	4	5,73	50	3
Secretory antigen precursor SsaA	151222411	7,01	34,8	7	0,37	3,7	1
Hypothetical protein	151220889	6,47	52,7	4	--	--	--
30s ribosomal protein S13	151222340	6,17	53,7	3	1,96	79,3	1
30s ribosomal protein S9	151222331	6,1	59,2	4	--	--	--
L-lactate dehydrogenase	151220388	5,64	20,2	3	--	--	--
elongation factor G	151220721	5,57	25,5	4	--	--	--
30S ribosomal protein S4	151221825	5,5	41	3	2,61	39,5	2
30S ribosomal protein S2	151221378	5,48	33,3	3	2	60,4	2
50S ribosomal protein L17	151222337	5,43	63,9	3	--	--	--
50S ribosomal protein L20	151221784	5,35	83,1	4	2,99	83,1	2
Hypothetical protein	151221170	5,08	52,4	2	2	50,5	2
50S ribosomal protein L19	151221363	5,06	76,7	3	1,09	50	1
Cell envelope-related transcriptional attenuator	151222423	4,53	26,7	3	2,12	37,8	2
Hypothetical protein	151221647	4,5	54,4	3	2,29	53,9	2
Immunodominant antigen B	151222749	4,41	57,7	3	11,24	66,9	8
pyruvate dehydrogenase E1 component, alpha subunit	151221171	4,38	49,2	2	4,69	49,2	2
acetolactate synthase	151222323	4,31	31,4	3	--	--	--
ABC transporter iron compound-binding protein	151222143	4,24	55,8	2	4,05	58,1	2
30S ribosomal protein S7	151220720	4,24	41,7	2	2,21	78,2	2
Hypothetical protein	151222466	4,21	36,7	2	2,92	40,5	2
mannosyl-glycoprotein endo-beta-N-acetylglucosamidase	151221879	4,18	33,1	2	1,64	53,9	1
Immunodominant antigen A	151222681	4,02	32,6	3	2,05	21,5	1
30S ribosomal protein S10	151222365	4	72,6	2	2,04	51	1
ferrichrome ABC transporter lipoprotein	151222290	4	24,2	2	8,63	55,7	4
50S ribosomal protein L16	151222357	4	46,5	2	2,44	58,3	2
Hypothetical protein	151220576	3,96	31,1	2	7,97	78,4	5
30S ribosomal protein S8	151222350	3,84	60,6	3	1,37	64,4	1
50S ribosomal protein L5	151222352	3,76	52	3	--	--	--
50S ribosomal protein L4	151222363	3,72	36,2	3	--	--	--
quinol oxidase polypeptide II QoxA	151221142	3,45	49,7	3	16,6	62	9
50S ribosomal protein L29	151222356	3,34	43,8	2	--	--	--
50S ribosomal protein L14	151222354	3,28	32,8	2	--	--	--
alcohol dehydrogenase	151220789	3	17	2	--	--	--

Common proteins identified in both LB and LB-glu conditions are highlighted in yellow.

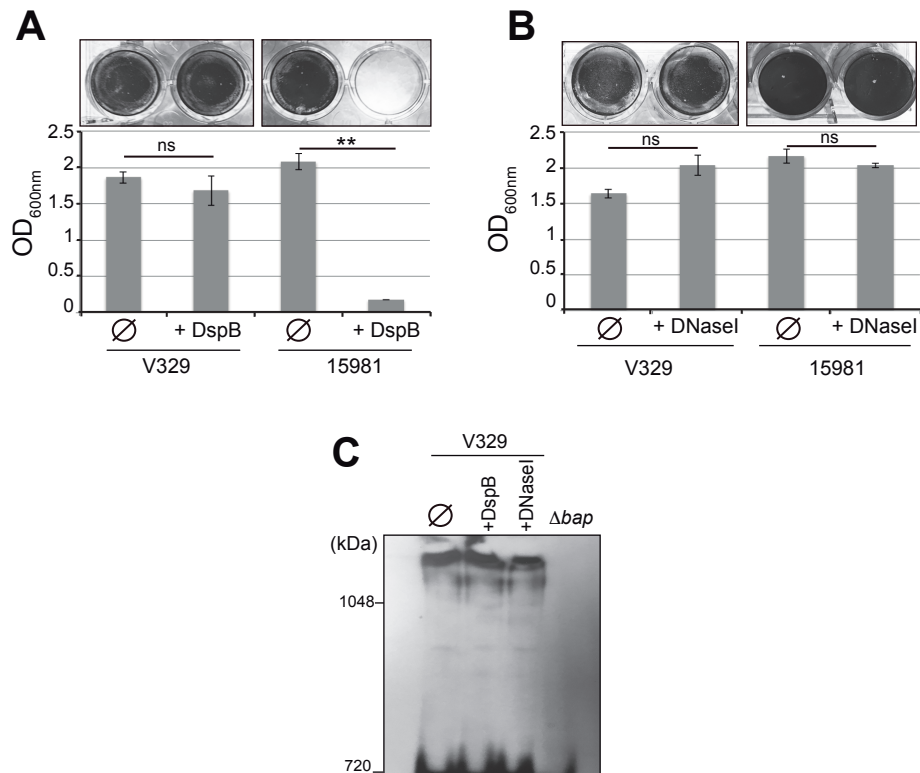


**Figure 11. Role of biofilm matrix molecules in Bap mediated aggregation and biofilm phenotype.** For detachment experiments, biofilms formed by *S. aureus* V329 and 15981 strains grown in LB-glu for 24 h, were treated with 0,4  $\mu$ g/ml dispersin B (DspB) (**A**) or 0,4  $\mu$ g/ml DNaseI (**B**) for 2 h at 37°C. The quantification of adhered biofilm was performed by the solubilization of crystal violet-stained cells with ethanol-acetone (80:20 v/v) and determination of the absorbance at 595nm. Data represent the means from three independent experiments. Error bars represent SD (\*\*,  $P < 0.01$ ; ns, no statistical differences). ∅: no treatment. Statistical analysis was performed using the Mann-Whitney test. **C**) Purified Bap aggregates from cell wall extracts were treated with 0,4  $\mu$ g/ml dispersin B (DspB) or 0,4  $\mu$ g/ml DNaseI for 2 h at 37°C. After treatment, samples were separated in Criterion XT Tris-acetate gels with Tris/glycine running buffer and probed with anti-Bap antibodies. ∅: untreated V329 cell wall extracts.

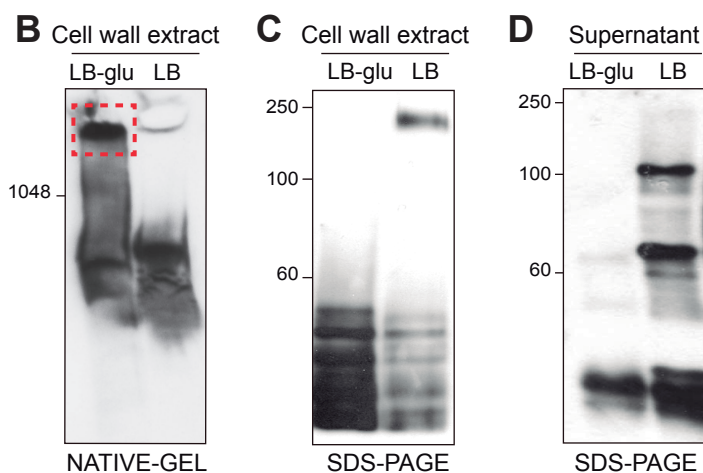
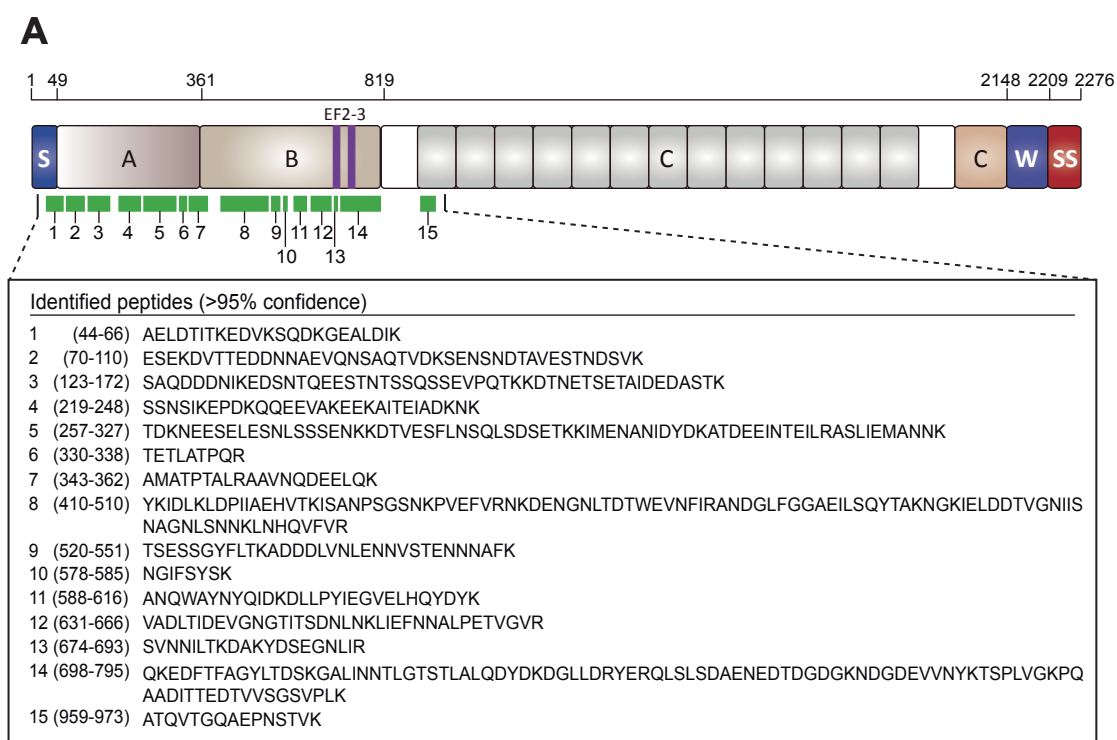


**Figure 12. Proteolytic cleavage of Bap protein allows the formation of Bap-aggregates.**  
**A)** Proteomic analysis of Bap protein aggregates. The structural organization of Bap is shown. S, signal peptide; A, region A; B, region B; C, repeats region; D, region of serine-aspartate (SD) repeats; W, wall-spanning region; SS, sorting signal; EF2-3, EF-hand calcium binding motifs 2 and 3. Green lines correspond to peptides obtained by MS analysis from the Bap insoluble aggregates. In the table, amino acid sequences and positions of identified peptides are shown.  
**B)** Insoluble material (from cell wall extracts) retained in the native gel pocket that was subjected to MS analysis. Samples were separated in Criterion XT Tris-acetate gels with Tris/glycine running buffer and probed with anti-Bap antibodies. Cell wall extracts **(C)** or culture supernatants **(D)** from *S. aureus* V329 grown overnight in LB-glu or LB were separated on 7.5% acrylamide gels and probed with anti-BapB antibodies.

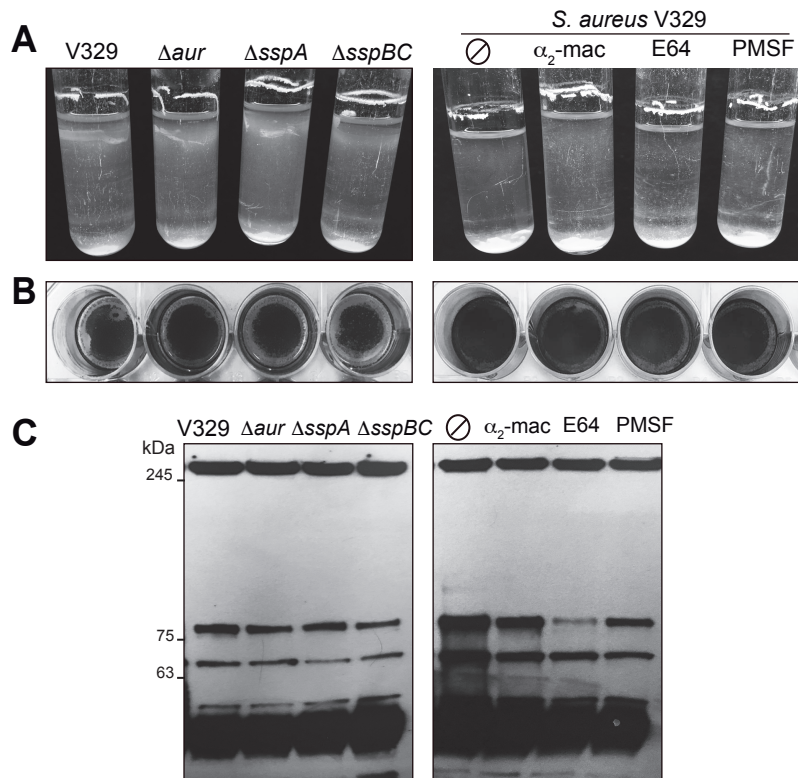


**Figure 13. Analysis of proteases responsible for Bap cleavage.** *S. aureus* V329 wild type strain, *S. aureus* V329  $\Delta aur$ ,  $\Delta sspA$  and  $\Delta sspBC$  mutant strains, and *S. aureus* V329 cultured in the presence of protease inhibitors  $\alpha_2$ -macroglobulin ( $\alpha_2$ -mac), cysteine protease inhibitor (E64), phenylmethylsulfonyl fluoride (PMSF) were grown in LB-glu and evaluated for bacterial clumping (**A**) and biofilm formation in microtiter plates (**B**) after an overnight incubation at 37 °C.  $\emptyset$ : no addition of protease inhibitor. **C**) Western immunoblotting of cell wall proteins extracted from exponential cultures were separated on 7.5% acrylamide gels and probed with anti-BapB antibodies.



- **Role of the N-terminal region in biofilm development**

The finding that Bap aggregates contained exclusively the N-terminal region of Bap leads us to consider that this region may be sufficient to promote biofilm development. To assess this hypothesis, we generated chimeric proteins comprising different regions of Bap tagged with the 3xFlag amino acid sequence and linked to the R domain of the clumping factor A (R-ClfA) containing the LPDTG motif (Fig. 14A). Variants of Bap comprising domain A (Bap\_A, amino acids 49 to 361), domain B (Bap\_B, amino acids 362 to 819), or domain A and B (Bap\_AB, amino acids 49 to 819) were cloned in pCN51 vector under the control of the  $P_{cad-cadC}$  promoter and expressed in *S. aureus*  $\Delta bap$  mutant. The expression of the whole Bap or the chimeric Bap proteins on the bacterial cell wall was verified by western-blot and immunofluorescence, showing similar expression levels (Fig. 14B) and a proper surface localization of all chimeras (Fig. 14C). *S. aureus*  $\Delta bap$  producing Bap\_AB or Bap\_B formed huge bacterial clumps (Fig. 15A and B) and robust biofilms on polystyrene plates under static conditions (Fig. 15C and D) and on a glass surface under flow culture conditions (Fig. 15E). In contrast, no cell clusters and biofilm development were found in  $\Delta bap$  pBap\_A and pClfA strains.

The observation that domain B of Bap was sufficient to induce biofilm phenotype made us wonder whether  $\Delta bap$  Bap\_B functionality was affected by pH. Similarly to the Bap protein, Bap\_B formed high molecular weight aggregates when a culture of  $\Delta bap$  strain expressing Bap\_B reached stationary phase (Fig. 16A). Accordingly, this strain formed biofilm when grown in LB-glu (pH<5) but not in LB (pH>7) (Fig. 16B and C). Next, we explored whether Bap\_B was sufficient to confer cell-to-cell interaction and biofilm formation capacity to naturally *bap* deficient strains: *S. aureus* MW2, *S. aureus* Newman and *S. carnosus* TM300. As shown in Figure 16D and E,

expression of Bap\_B in these strains conferred a strong biofilm phenotype and a robust capacity to form bacterial clumps at the bottom of the tube after an overnight incubation in LB-glu. Finally, we complemented a *S. aureus* strain lacking the genes responsible for the synthesis of PNAG (*icaADBC* operon) and teichoic acids (*tagO* gene, encoding the first enzyme involved in the wall teichoic acids biosynthetic pathway) with pBap\_B plasmid (Vergara-Irigaray *et al.*, 2008). The *S. aureus* 10833\_Δ*tagO*\_Δ*ica* strain expressing Bap\_B chimeric protein gained the ability to form biofilm (Fig. 16F) discarding the participation of PNAG and teichoic acids in the multicellular behavior and aggregation capacity promoted by Bap.

Taking together, these results indicate that the B domain of Bap (amino acids 362 to 819) is sufficient and necessary to bestow multicellular behavior under acidic culture conditions, similarly to the entire Bap protein.

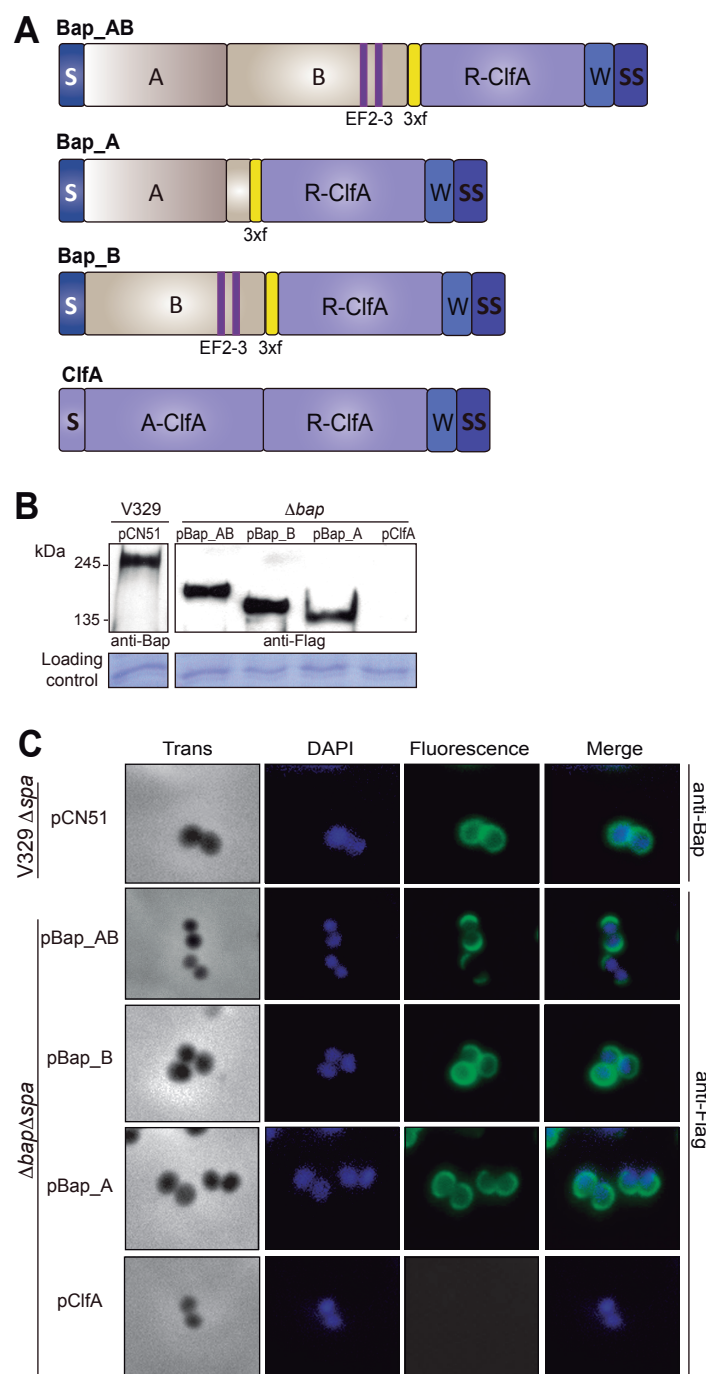


**Figure 14. Bap-CifA chimeric proteins are similarly expressed at the bacterial surface of *S. aureus*.** **A)** Structural organization of Bap chimeric proteins. EF2-3, EF-hand calcium binding motifs 2 and 3; 3xf, 3xFlag tag; R-CifA, clumping factor R domain; A-CifA, clumping factor A domain; W, wall-spanning region; SS, sorting signal. **B)** Western blot analysis showing similar expression levels of Bap chimeras. Cell wall extracts from *S. aureus* V329 and  $\Delta bap$  complemented with plasmids pCN51, pBap\_AB, pBap\_B, pBap\_A and pCifA grown until  $OD_{600nm}=4$ , were separated on 7.5% acrylamide gel and probed with anti-Bap or anti-Flag antibodies. Size markers (in kDa) are indicated. **C)** Immunofluorescence showing surface localization of chimeras. Bacteria were fixed and labeled with anti-Bap or anti-Flag antibodies and DAPI. For this experiment we used V329 and  $\Delta bap$  strains mutated in their *spa* gene (V329  $\Delta spa$  and  $\Delta bap \Delta spa$ ) to avoid unspecific labeling.

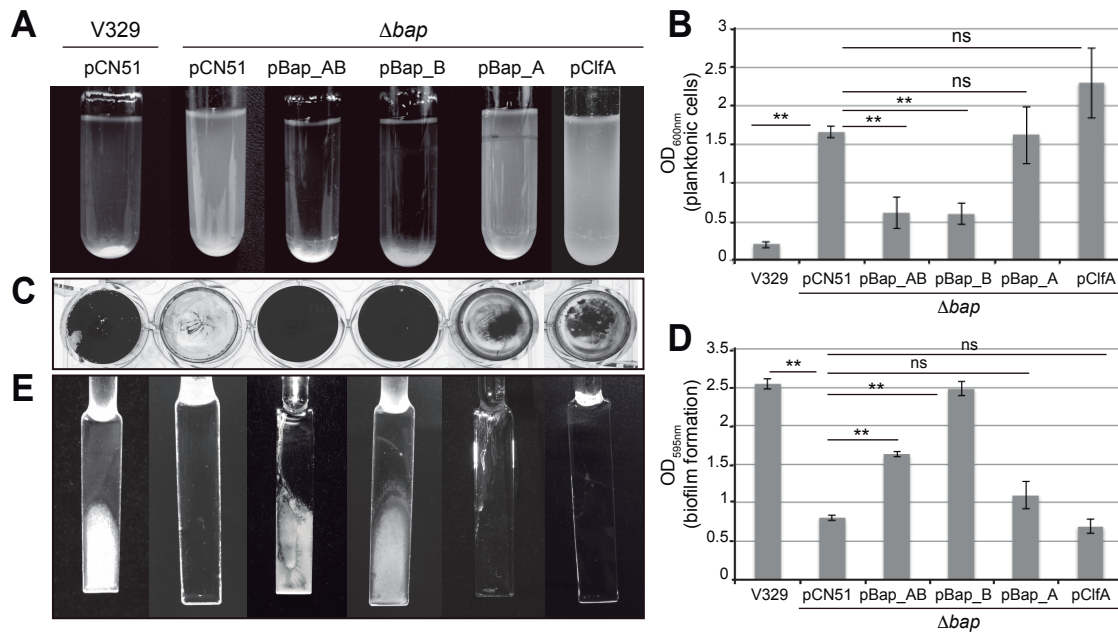


**Figure 15. Region B of Bap is sufficient to promote biofilm development.** Phenotypes of V329 and  $\Delta bap$  complemented with pBap\_AB, pBap\_B, pBap\_A, pCifA plasmids and pCN51 empty vector. **A)** Bacterial clumping of overnight cultures grown at 37°C, 200 rpm. **B)** Quantification of bacterial aggregation phenotype was performed by measuring the OD<sub>600nm</sub> at the top of the culture tubes (1 cm from the surface) as an indication of non-settled cells after an overnight incubation at 37 °C, 200 rpm. **C)** Biofilm formation in polystyrene microtiter plates under static conditions and after an overnight incubation at 37 °C. **D)** Quantification of static biofilm formation on polystyrene microtiter plates was performed by solubilizing crystal violet-stained cells with ethanol-acetone (80:20 v/v) and determining the corresponding absorbance at 595 nm. Data represent the means from three independent experiments. Error bars represent SD (\*\*,  $P < 0.01$ ; ns, no statistical differences). Statistical analysis was performed using the Mann–Whitney test. **E)** Biofilm formed on glass slides under flow culture conditions using microfermentors. For assays performed with *S. aureus*  $\Delta bap$  expressing the chimeric proteins of Bap, media were all supplemented with 1  $\mu$ M of CdCl<sub>2</sub>.

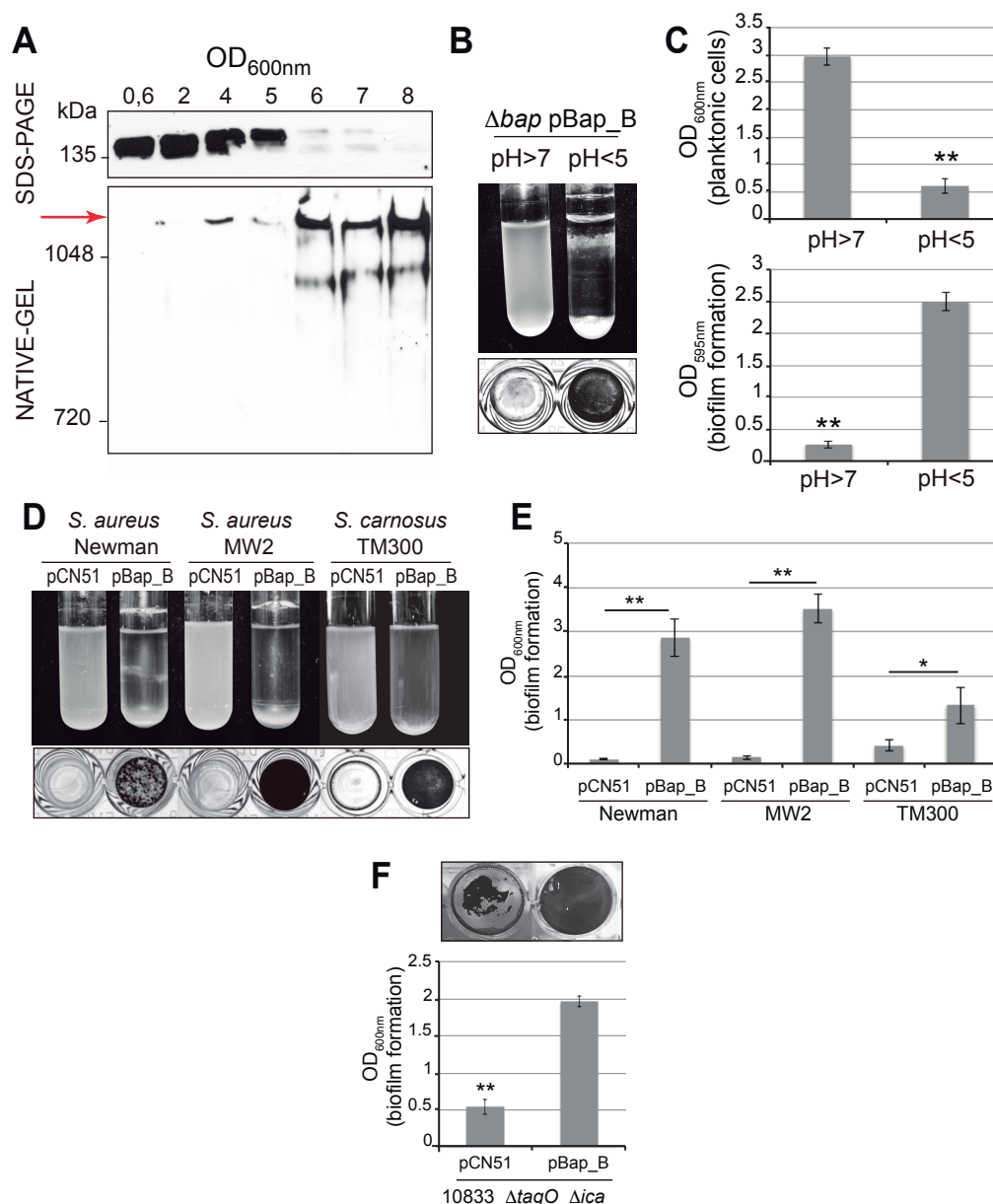


**Figure 16. Region B of Bap promotes biofilm formation in a pH-dependent manner. A)** Western immunoblotting results demonstrate that Bap\_B chimeric protein is sufficient to induce formation of insoluble aggregates (red arrow). Cell wall extracts from  $\Delta bap$  pBap\_B strain grown in LB-glu were separated on 7.5% acrylamide gels (upper panel) or Criterion XT Tris-acetate gels with Tris/glycine running buffer (lower panel) and probed with anti-Bap antibodies. **B)** Bacterial clumping and biofilm formation of *S. aureus*  $\Delta bap$  mutant expressing Bap\_B chimeric protein grown overnight in LB (pH>7) and LB-glu (pH<5), at 37 °C. **C)** Quantification of bacterial clumping (upper graphic) and biofilm formation (lower graphic) of *S. aureus*  $\Delta bap$  complemented with pBap\_B. **D)** Bacterial clumping and biofilm formation of *S. aureus* Newman, *S. aureus* MW2 and *S. carnosus* TM300 complemented with pBap\_B plasmid or with pCN51 empty plasmid. Bacteria were cultured overnight in LB-glu, at 37°C. **E)** Quantification of biofilm formation of *S. aureus* Newman, *S. aureus* MW2 and *S. carnosus* TM300 complemented with pBap\_B. **F)** Biofilm formed by *S. aureus* 10833\_ΔtagO\_Δica expressing Bap\_B chimeric protein. In all graphics, data represent the mean values from three independent experiments. Error bars represent SD (\*,  $P < 0.05$ ; \*\*,  $P < 0.01$ ). Statistical analysis was performed using the Mann–Whitney test.

- **Purified recombinant Bap\_B protein adopts an amyloid conformation at acidic pH**

To get insight about the molecular mechanisms by which the N-terminal region of Bap mediates cell-to-cell interactions, we used a purified recombinant protein comprising exclusively the B region of Bap fused to a histidine tag at its N-terminal region (rBap\_B). Purified rBap\_B formed a visible ring of biomass adhered to the wells of the tube when incubated at pH ranging from 3.6 until 5 but not at higher or lower pH values (Fig. 17A). Interestingly, this process was reversible and rBap\_B aggregates completely dissociated when the protein was subsequently incubated at neutral pH (Fig. 17B). To validate the functionality of rBap\_B, we analyzed its capacity to induce bacterial clumping phenotype in *S. aureus*  $\Delta bap$ . Exogenous addition of rBap\_B peptide (2  $\mu$ M) induced bacterial aggregation only when *S. aureus*  $\Delta bap$  was grown under acidic culture conditions (LB-glu) (Fig. 17C). Next we performed a biophysical characterization of the rBap\_B domain conformation at neutral and acidic pH. First, we determined the relative size of the aggregates by dynamic light scattering (DLS). Graphic in figure 18A illustrates the size characterization (hydrodynamic radius R) of rBap\_B in solution at three different pH values. In the table, the correlation between the diffusion coefficient (D) of each population and its corresponding radius is shown. rBap\_B protein (peak 2) displayed at pH 4.4 the highest hydrodynamic radius and the lowest D value as expected for aggregated particles that move slower than smaller particles, with a polydispersity percentage below 15% indicating monodispersed samples. At neutral pH the obtained peak had a D value that once substituted in the Svedberg equation, together with the sedimentation coefficient, buffer density and partial specific volume, corresponded to the monomer of the protein (Fig. 18A). A fast assembly of rBap\_B at pH 4.5 into aggregates was

also evident from the strong increase in light scattering relative to the signal obtained at pH 7.0 (Fig. 18B). These early assemblies displayed a strong binding to the dye bis-ANS, evidencing the presence of hydrophobic patches exposed to solvent, which potentially might recruit rBap\_B monomers into the aggregates and/or contact other cellular molecules through non-polar interactions (Fig. 18C). Lastly, Far-UV circular dichroism spectra (CD) of rBap\_B showed a moderate increase in  $\beta$ -sheet structure (+5%) when the pH was acidified, at the expense of the predominant non-ordered secondary structure (Fig. 18D).

To analyze more in depth these  $\beta$ -sheet-rich rBap\_B aggregates formed at acidic pH, we examined the amide I region of the Attenuated Total Reflectance–Fourier Transform Infrared spectroscopy (ATR-FTIR) spectrum ( $1700\text{--}1600\text{ cm}^{-1}$ ) of rBap\_B ring assemblies. This region corresponds to the absorption of the carbonyl peptide bond group of the protein main chain and is a sensitive marker of the protein secondary structure. Deconvolution of the FTIR-absorbance spectra allowed us to assign the individual secondary structure elements and their relative contribution to the main absorbance signal. The FTIR spectrum of rBap\_B aggregates was dominated by  $\beta$ -sheet/ $\beta$ -turn components, contributing more than 80% to the signal. In particular, the strong bands at  $1628$  and  $1694\text{ cm}^{-1}$  were consistent with the presence of amyloid-like intermolecular  $\beta$ -sheet structure (Fig. 19A). To assess whether the prevalent intermolecular  $\beta$ -sheet formed in rBap\_B aggregates had an amyloid-like nature, we evaluated the binding of the aggregates to the amyloid diagnostic dyes Thioflavin-T (ThT), Congo Red (CR) and ProteoStat. The presence of rBap\_B aggregates induced a 25-fold increase in ThT fluorescence emission maximum (Fig. 19B). Interestingly, when fresh rBap\_B was incubated at pH 4.5 for 5 min it already bound to ThT in a concentration dependent manner, indicating a fast assembly of

rBap\_B into ThT positive structures (Fig. 19C). In contrast, no change in ThT fluorescence was observed when the protein was incubated at pH 7.0, independently of the protein concentration assayed (Fig. 19D). In agreement with an amyloid conformation the absorbance of CR and its spectrum maximum red-shifted in the presence of rBap\_B ring-shaped aggregates (Fig. 19E). The absorbance of ProteoStat, a novel fluorescent dye able to specifically stain amyloid aggregates *in vivo* (Navarro and Ventura, 2014), showed a 20-fold increase in its fluorescence maximum at 550 nm (Fig. 19F).

Finally, visualization of the aggregates formed by purified rBap\_B at pH 4.5 using TEM showed the presence of isolated fibers and fibers entangled in larger electrodense aggregates (Fig. 20A). Similar fibers were detected in the surface of *S. aureus*  $\Delta bap$  when bacteria were grown in the presence of exogenously added rBap\_B under acidic conditions (Fig. 20C). It is important to notice that fibers were not detected when *S. aureus*  $\Delta bap$  was grown in the presence of rBap\_B at pH 7 (Fig. 20D).

Altogether, these data strongly suggest that the intermolecular  $\beta$ -sheet structures formed upon aggregation of rBap\_B at pH 4.5 possess an amyloid-like conformation.



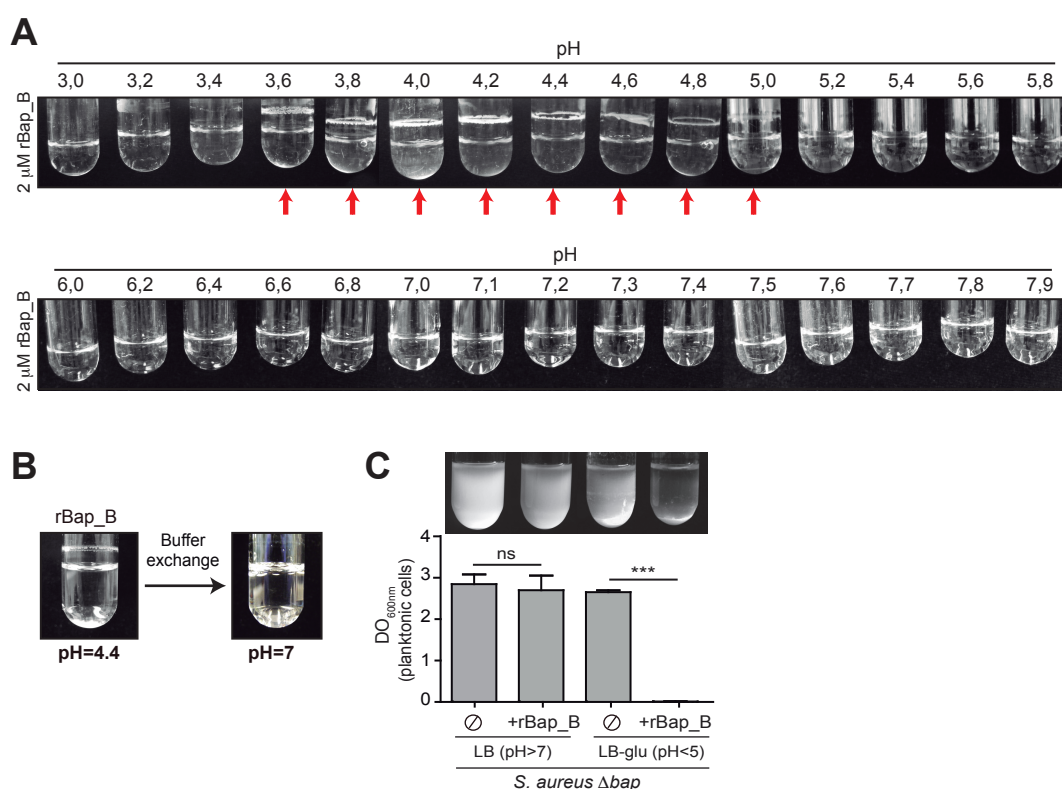


**Figure 17. rBap\_B forms reversible aggregates under acidic conditions. A)** 2  $\mu$ M of purified rBap\_B protein was incubated in phosphate-citrate buffer at different pH values. Aggregates were only visible when pH fluctuated from 3.6 until 5 (indicated by a red arrow). **B)** Reversion assay showing complete disassembly of Bap aggregates both at the bottom and on the top of the tube, after performing phosphate-citrate buffer exchange from pH=4.4 to pH=7. **C)** Bacterial clumping of *S. aureus*  $\Delta bap$  grown in LB (pH>7) or LB-glu (pH<5) incubated with 2  $\mu$ M purified rBap\_B protein.  $\emptyset$ , no addition of rBap\_B. Cells were incubated for 24 h with agitation at 37 °C. Data represent the mean values from three independent experiments. Error bars represent SD (\*\*\*,  $P<0.001$ ; ns, no statistical differences). Statistical analysis was performed using the unpaired Student *t* test .

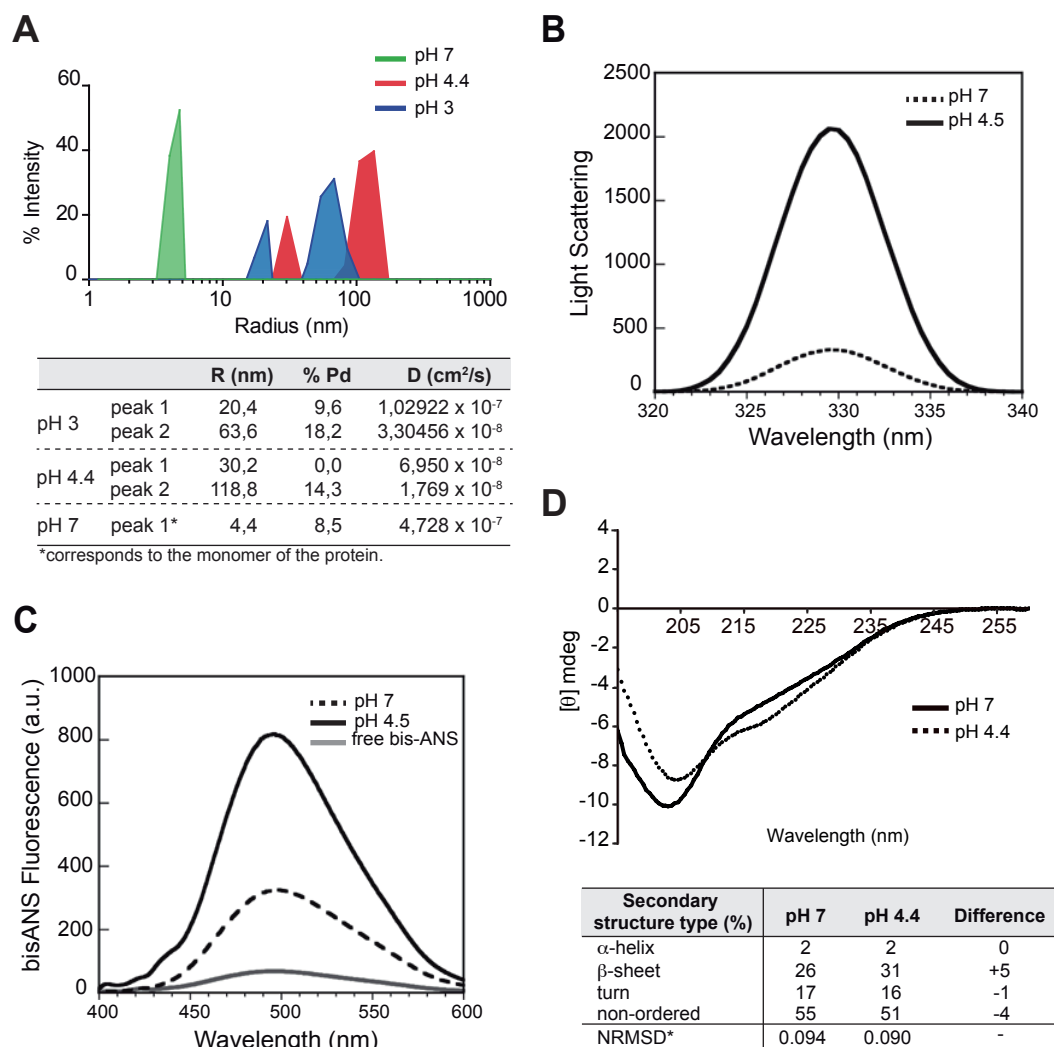


**Figure 18. rBap\_B aggregation propensity and secondary conformation at different pH.**

**A)** Hydrodynamic radius (R) of rBap\_B in solution at pH 7 (green), 4.4 (red) and 3 (blue) analyzed by dynamic light scattering. The table shows the diffusion coefficient (D) of each population, its corresponding radius (R), and polydispersity percentages (% Pd). **B)** Static light scattering of 0.1 mg/ml rBap\_B at pH 4.5 (solid line) and pH 7 (dashed line). **C)** Bis-ANS fluorescence of 0.1 mg/ml rBap\_B at pH 4.5 (solid line) and pH 7 (dashed line). Free bis-ANS is represented in grey. **D)** Far-UV CD spectra of 0.2 mg/ml rBap\_B at pH 7 (solid line) and pH 4.4 (dotted line). The table shows secondary structure composition of rBap\_B at pH 7 and 4.4. Data were analyzed with Dichroweb implementing the CDSSTR algorithm. \*NRMSD =  $[\sum(\theta_{\text{exp}} - \theta_{\text{cal}})^2 / \sum(\theta_{\text{exp}})^2]^{1/2}$  where  $\theta_{\text{exp}}$  and  $\theta_{\text{cal}}$  are the experimental and calculated ellipticity values at a particular wavelength, respectively.

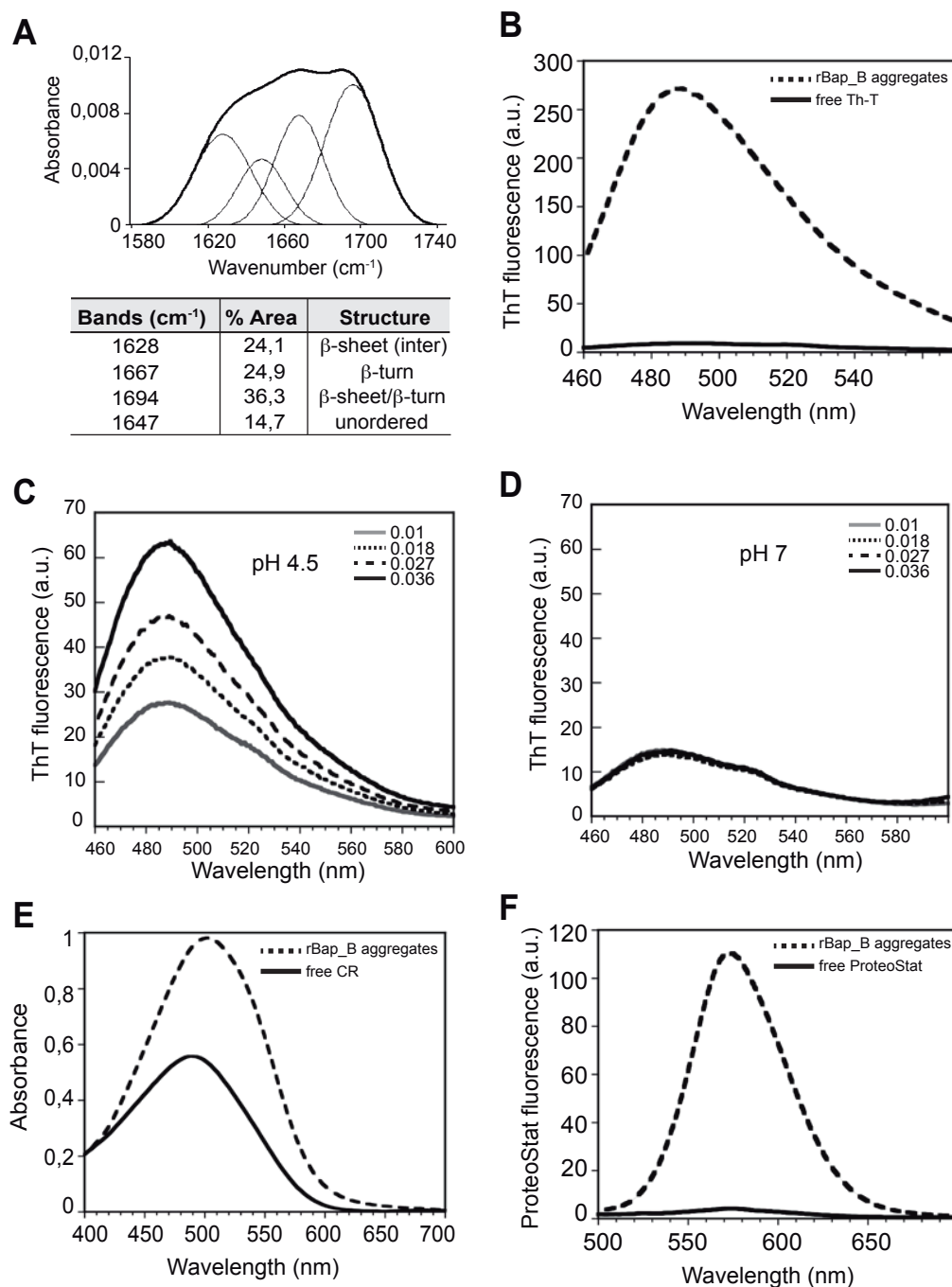


**Figure 19. rBap\_B aggregates display amyloid-like features.** **A)** ATR-FTIR spectrum in the Amide I region of rBap\_B ring-shaped aggregates formed after 24h in phosphate-citrate buffer pH 4.5 (thick curve). Deconvolution of the ATR-FTIR absorbance spectra into its main secondary structure contributions is shown (thin curves). Percentage of each secondary structure is detailed in the bottom table. **B)** Increase in ThT emission fluorescence upon binding to 0.1 mg/ml rBap\_B ring-shaped aggregates at pH 4.5 (dashed line). Free ThT emission spectrum is represented in solid line. Increase in ThT fluorescence emission upon binding to rBap\_B at pH 4.5 (**C**) and pH 7 (**D**). Data for Bap protein at 0.01, 0.018, 0.027 and 0.036 mg/ml are represented as grey, dotted, dashed and continuous lines, respectively. **E)** Shift in CR absorbance spectrum upon binding to 0.1 mg/ml rBap\_B from ringed-aggregates (dashed line). Free CR absorbance spectrum is represented in solid line. **F)** Increase in ProteoStat emission fluorescence upon binding to 0.1 mg/ml rBap\_B ringed-aggregates (dashed line). Free Proteostat emission spectrum is represented in solid line.

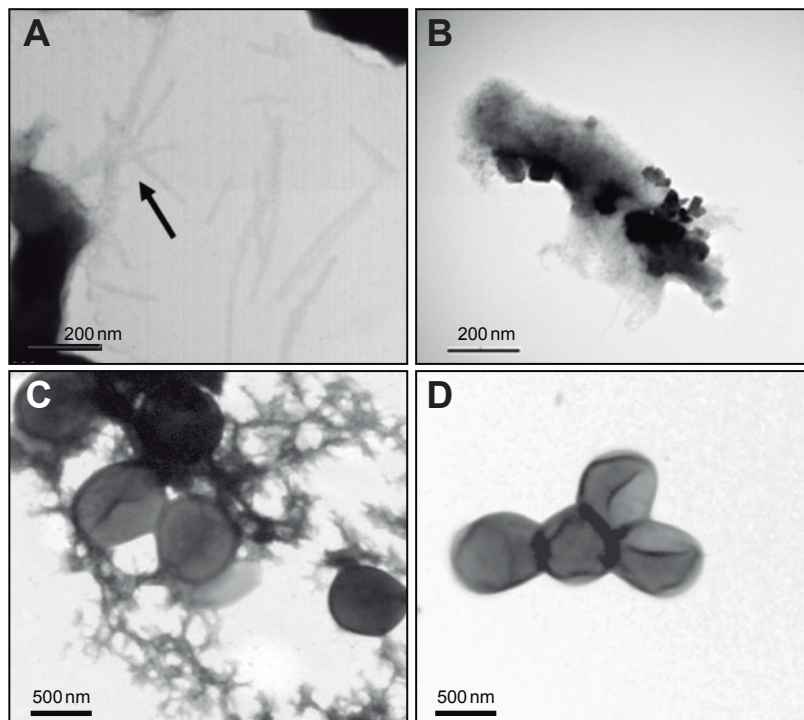


**Figure 20. rBap\_B forms amyloid-like fibers.** Negatively stained fibers formed by purified rBap\_B protein. Protein was incubated 24 h in phosphate-citrate buffer pH 4.5 (**A**) and at pH 7 (**B**). Electron micrographs of *S. aureus*  $\Delta bap$  cells grown overnight incubated with 2  $\mu$ M purified rBap\_B protein in LB-glu (pH<5) (**C**) and in LB (pH>7) (**D**).

- **Identification and characterization of short amyloid stretches in Bap\_B**

Not all the sequence is equally important for the ability of a protein to form amyloid-like aggregates, but instead there are short sequence fragments that promote and guide the formation of amyloid-like structures, becoming embedded in the inner core of the cross- $\beta$  structure (Ventura *et al.*, 2004; Ivanova *et al.*, 2004; Castillo *et al.*, 2011). We used AGGREGSCAN (Conchillo-Solé *et al.*, 2007), PASTA (Walsh *et al.*, 2014), WALTZ (Oliveberg, 2010) and ZipperDB (Thompson *et al.*, 2006) computational algorithms to predict amyloidogenic regions in the complete series of Bap\_B peptides previously identified by MS in the biofilm where Bap aggregates formed at acidic pH.

The predictions converged to indicate two Bap\_B short sequence stretches as potentially amyloidogenic: TVGNIISNAG named as peptide I (aa 487 to 496), and GIFSYS named as peptide II (aa 579 to 584) (Fig. 21A). We synthesized the two peptides and incubated them at 10  $\mu$ M at pH 4.5. Both peptide solutions formed an evident gel (Fig. 21B), a property shared by many amyloidogenic peptides (Woodard *et al.*, 2014) as well as biofilm matrices (Cogan and Keener, 2004). Analysis of the structure of the two gels by transmission electron microscopy (TEM) indicated that they are constituted by fibrils with a typical amyloid morphology (Fig. 21D), which bind to ThT with high affinity (Fig. 21C). These data converge to indicate that region B of Bap contains at least two short regions with high amyloidogenic propensity. Analysis of these peptides using the RosettaDesign program (Kuhlman and Baker, 2000) implemented in ZipperDB (Goldschmidt *et al.*, 2010) rendered average interaction energies of -25.0 and -25.9 kcal/mol for peptide I and peptide II and shape complementarities between strands of 0.87 and 0.81, respectively. These parameters are compatible with these peptides being able to form steric-

zippers that might lead N-terminal Bap amyloid assembly. Modeling of the supramolecular steric-zipper structure potentially formed by peptide II (GIFSYS) is illustrated, to show how it might facilitate Bap\_B self-interactions (Fig. 21E).

In order to see if these peptides are critical for biofilm formation we constructed a Bap\_B chimeric protein with mutated amyloid peptides I and II (Bap\_B\_Δ*pepI-II*). Amino acid sequences of the two amyloidogenic stretches (peptide I: <sub>358</sub>TVGNIISNAG<sub>367</sub>,; peptide II: <sub>450</sub>GIFSYS<sub>455</sub>) were substituted by repeated sequences coding for serine and glycine residues, to provide entropy and solubility to the mutated sequences that could potentially counteract aggregation (peptide I: <sub>358</sub>SGSGSGSGSG<sub>367</sub>, peptide II: <sub>450</sub>SGSGSG<sub>455</sub>) (Fig. 22A). *S. aureus* Δ*bap* expressing the Bap\_B chimeric protein with mutated amyloid peptides formed cell clumps (Fig. 22B) and biofilm (Fig. 22C) when grown in LB-glu (pH<5) but not in LB (pH>7) media.

Overall, these results demonstrate the existence of short sequence stretches with amyloidogenic properties in the N-terminal region of Bap. The finding that the mutation of these peptides is not critical for inducing bacterial clumping and biofilm formation strongly suggest that additional short amino acid stretches with amyloidogenic tendencies would be responsible for the assembly of N-terminal Bap fragments into aggregated structures at acidic pH.

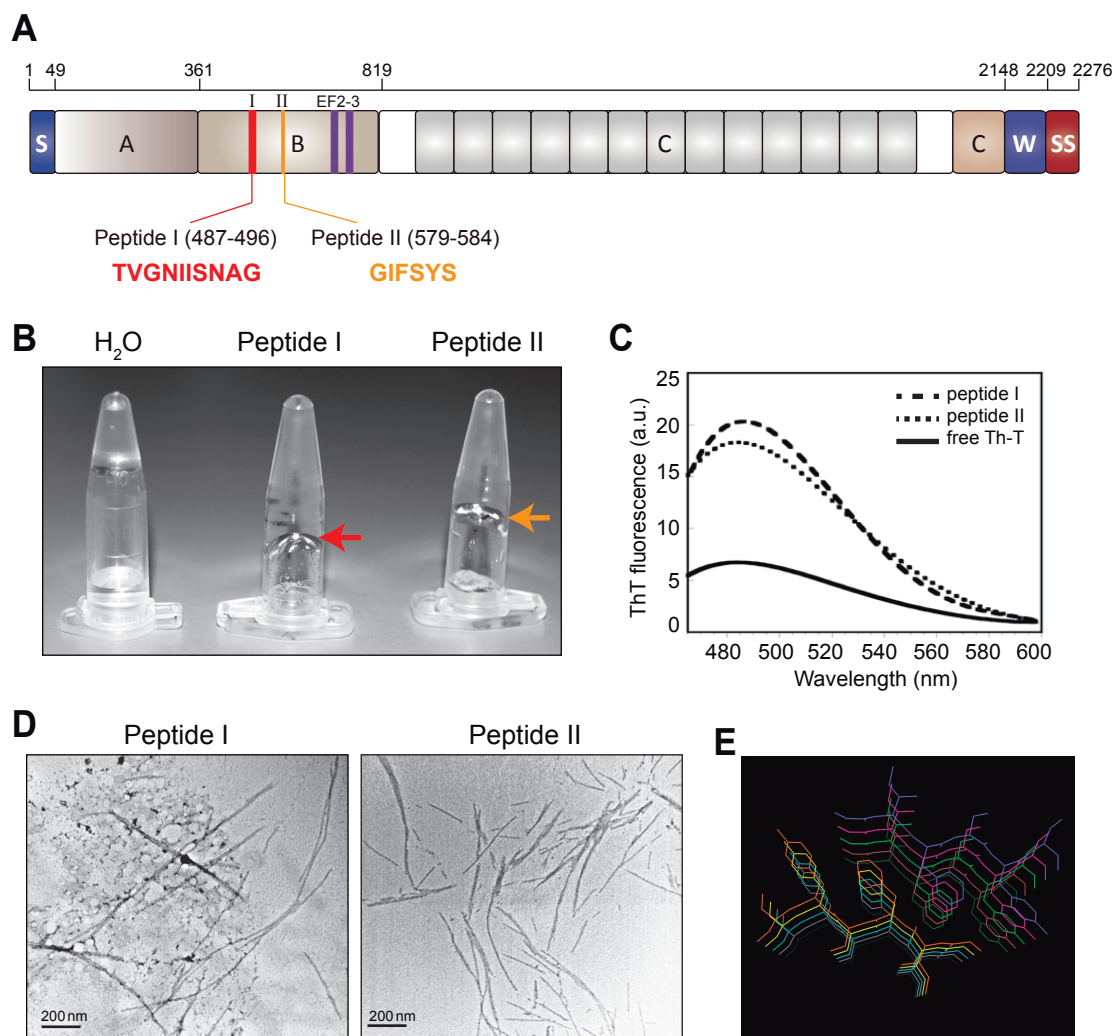


**Figure 21. Two short sequence stretches of Bap\_B domain show amyloid features.** **A)** Structural organization of Bap comprising the position and sequence of the two identified amyloidogenic peptides. S, signal peptide; A, region A; B, region B; C, repeats region; D, region of serine-aspartate (SD) repeats; W, wall-spanning region; SS, sorting signal; EF2-3, EF-hand calcium binding motif 2 and 3; I, peptide I (residues 487 to 496); II, peptide II (residues 579 to 584). **B)** Gel matrix formed by Bap\_B amyloidogenic peptide I (red arrow), and II (orange arrow) upon incubation at pH 4.5 for four weeks. **C)** ThT fluorescence emission spectra upon binding to 10  $\mu$ M amyloid peptide I (dashed line), and peptide II (dotted line). Free ThT fluorescence emission spectrum is represented in solid line. **D)** Electron micrographs of negatively stained fibers formed by amyloid Bap\_B peptide I and amyloid Bap\_B peptide II. **E)** Modeling of the supramolecular steric-zipper structures potentially formed by peptide II using the Rosetta Design program.

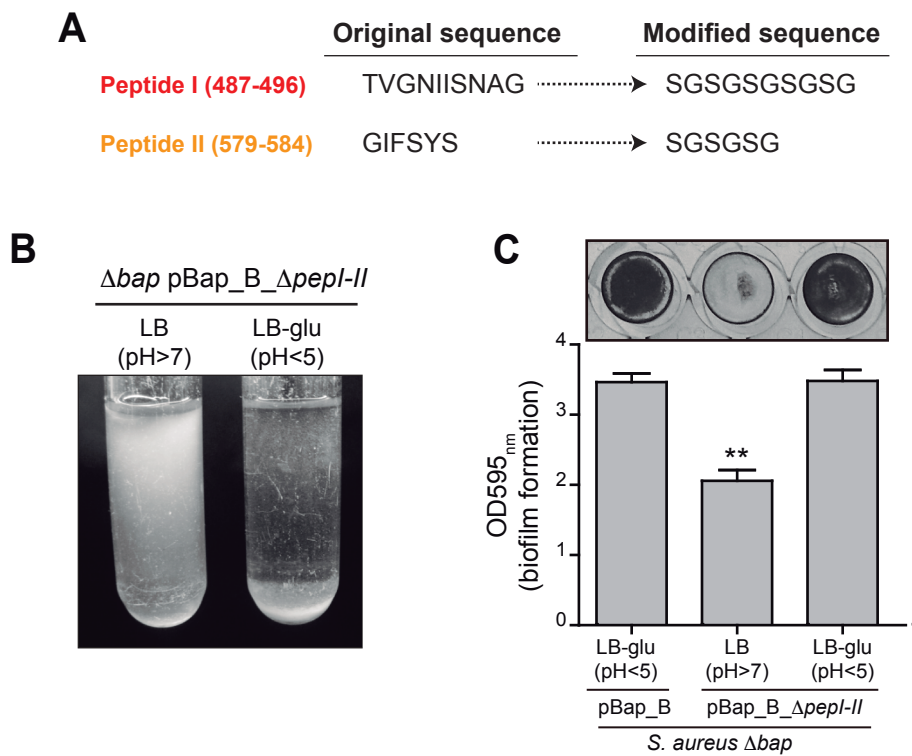


**Figure 22. Role of amyloidogenic peptides I and II in *S. aureus* multicellular behaviour. A)** The original sequences of peptides I and II were modified by replacing them with polar and flexible sequences rich in Serine-Glycine repeats. **B)** Bacterial clumping of *S. aureus Δbap* expressing Bap\_B chimeric protein with mutated amyloidogenic peptides I and II, grown in LB (pH>7) and LB-glu (pH<5), at 37 °C, 200 rpm. **C)** Biofilm formation of *S. aureus Δbap* expressing Bap\_B and Bap\_Δ*pepI-II* chimeric proteins after an overnight incubation at 37 °C on polystyrene microtiter plates. Cells were grown in LB and LB-glu. The quantification of adhered biofilm was performed by the solubilization of crystal violet-stained cells with ethanol-acetone (80:20 v/v) and determination of the absorbance at 595nm. Data represent the means from five independent experiments. Error bars represent SD (\*\*,  $P<0.01$ ). Statistical analysis was performed using the Mann-Whitney test.



- **Bap protein forms amyloid-like fibers**

We next analyzed by transmission electron microscopy the presence of fibers in wild type *S. aureus* V329 grown under biofilm forming conditions. Consistent with the capacity of rBap\_B domain to produce amyloidogenic fibers, the analysis revealed the presence of fibers in the biofilm formed by *S. aureus* V329 strain (Fig. 23A and B) that specifically reacted with gold-labeled anti-Bap antibody (Fig. 23C and D). As expected, no fibers were detected in  $\Delta bap$  deficient strain. We also analyzed by scanning electron microscopy (SEM) the biofilm formed by *S. aureus* V329 on a glass spatula when incubated in LB-glu, at 37 °C and under flow-growing conditions. The bacteria appeared to be encased in a matrix composed by fibers formed by Bap (Fig. 23E and F). Finally, we showed the presence of amyloid-like material in the extracellular matrix of *S. aureus* V329 grown in LB-glu medium by staining the biofilm with the amyloid specific staining dye, ProteoStat (Fig. 24A). Bacterial aggregates stained red even in the presence of dispersin B (DspB) and DNaseI (Fig. 24A). Interestingly, the insoluble aggregated material from *S. aureus* V329 that remains in the wells of native gels stained with ProteoStat while similar preparation from  $\Delta bap$  strain did not (Fig. 24B).

These results indicate the existence of fibers that stain with dyes specific of amyloid fibers in the biofilms produced by Bap.

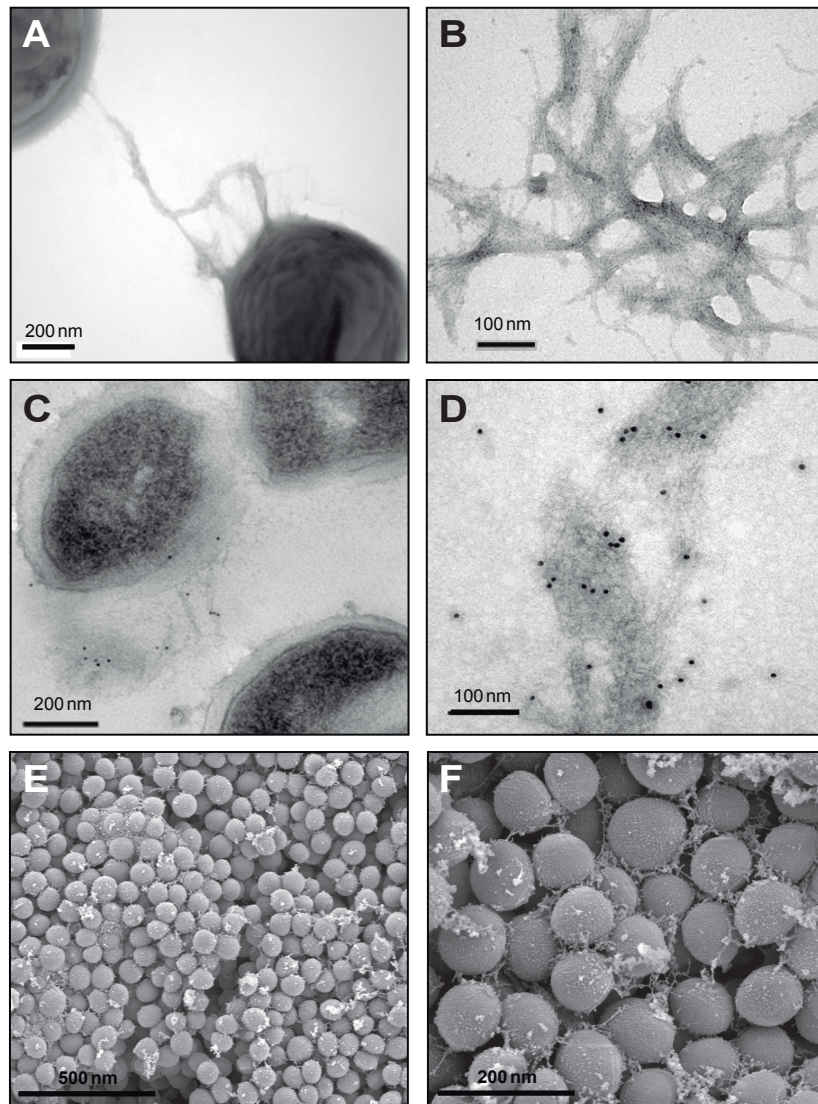


**Figure 23. Bap forms amyloid-like fibers.** **A)** Transmission electron micrograph of negatively stained *S. aureus* V329 cells grown in LB-glu (pH<5) for 24 h, at 37 °C, 200 rpm. Negatively stained fibers are shown at higher magnification in **(B)**. **C)** Transmission electron micrograph of immunogold labeled samples from *S. aureus* V329 cells grown in LB-glu (pH<5) for 24 h using anti-Bap B antibodies. Immunogold probed fibers are shown at higher magnification in **(D)**. **E)** Scanning electron micrograph of *S. aureus* V329 cells forming a biofilm on a glass slide after 24 hs incubation in LB-glu (pH<5), under flow culture conditions. *S. aureus* V329 cells and biofilm matrix are shown at higher magnification in **(F)**.

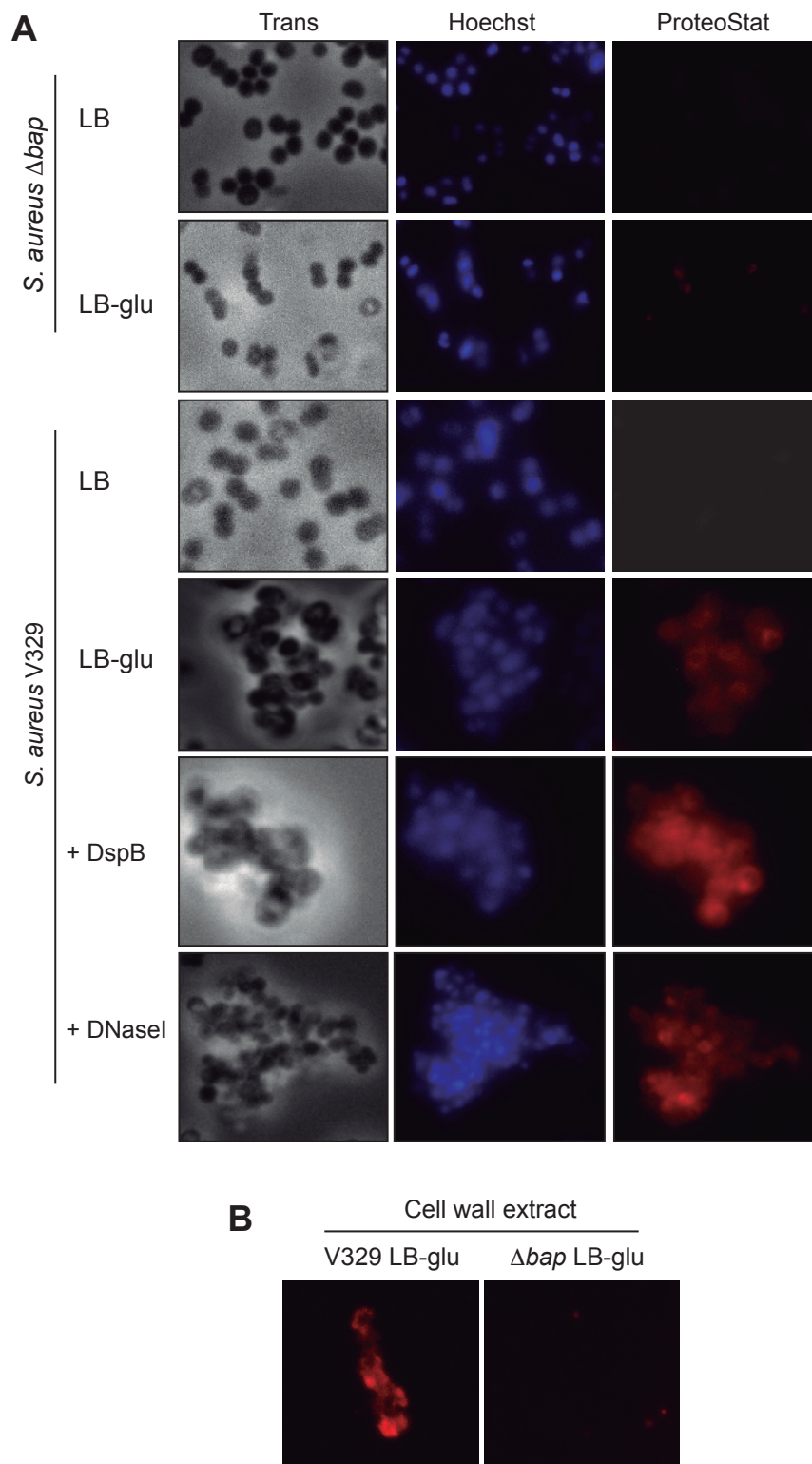


**Figure 24. Amyloid-like material is present in the extracellular matrix of *S. aureus* V329 biofilms. A)** Biofilms from *S. aureus* V329 and  $\Delta bap$  strains grown in LB and LB-glu, and treated or not with 0.4  $\mu\text{g/ml}$  Dispersin B or 0.4  $\mu\text{g/ml}$  DNase I, were stained with ProteoStat for 30 min. Representative fluorescence microscopic images are shown. **B)** Insoluble material retained in the native gel pocket from *S. aureus* V329 and  $\Delta bap$  strains cultured in LB-glu were extracted from the gel and stained with ProteoStat.

- **EGCG specific amyloid inhibitor hinders Bap aggregation**

The compound (-)-epigallocatechine gallate (EGCG) is a polyphenol found in large amounts in green tea. It has anti-amyloidogenic properties and modulates the misfolding of disease proteins and prions (Bieschke *et al.*, 2010). In particular EGCG efficiently inhibits the assembly into  $\beta$ -sheet-rich amyloids of  $\alpha$ -synuclein and amyloid- $\beta$  by binding to the natively unfolded polypeptides (Ehrnhoefer *et al.*, 2008). Thus, we asked whether this compound could inhibit Bap aggregation. To address this question, we incubated 2  $\mu$ M rBap\_B in phosphate-citrate buffer at pH 4.5 in the absence or presence of different concentrations of EGCG. At all concentration tested (1 mM, 100  $\mu$ M and 10  $\mu$ M EGCG) there was no formation of rBap\_B aggregates (Fig. 25A). In contrast, purified rBap\_B formed the typical protein aggregate at pH 4.5 when no EGCG was added (Fig. 25A, red arrow). We also tested the capacity of this compound to inhibit Bap-based biofilms. As a control, we used *S. aureus* 15981 strain that forms a PNAG-dependent biofilm. As observed in figure 25B, after 3 hours incubation at 37 °C, the epigallocatechine gallate significantly disassembled biofilm formed by *S. aureus* V329 strain, but not the biofilm produced by *S. aureus* 15981 ( $P < 0.001$ ,  $n = 5$ ).

These results demonstrate that EGCG polyphenol is capable to inhibit Bap self-aggregation and Bap-dependent biofilm formation, providing another evidence of the amyloidogenic nature of Bap assemblies.

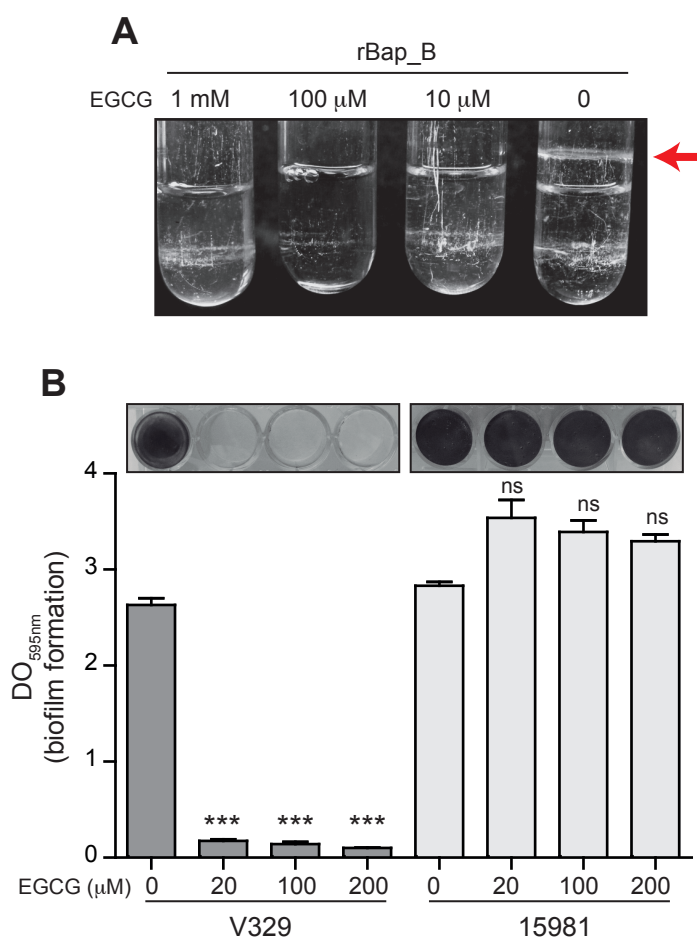


**Figure 25. EGCG interferes with Bap aggregation and biofilm disassembly at acidic pH.** **A)** 2  $\mu$ M of rBap\_B was incubated overnight in the absence or presence of 1 mM, 100  $\mu$ M and 10  $\mu$ M of epigallocatechin gallate (EGCG) in phosphate-citrate buffer pH 4.5, at 37 °C, 200 rpm. The red arrow indicates the presence of rBap\_B aggregates. **B)** Disassembly of *S. aureus* V329 biofilm formed in LB-glu at 37 °C in the absence or presence of 20, 100 and 200  $\mu$ M EGCG, after 3 h at 37 °C. *S. aureus* 15981 was used as a control and showed no significant differences of biofilm levels in the presence or absence of EGCG. Data represent the means from five independent experiments. Error bars represent SD (\*\*\*,  $P < 0.001$ ; ns, no statistical differences). Statistical analysis was performed using the Mann-Whitney test.

- **Bap\_B amyloid aggregates induce multicellular behavior in Gram-positive bacteria**

We had previously assessed that neither PIA/PNAG exopolysaccharide nor cell wall teichoic acids were necessary for biofilm formation mediated by Bap (Fig. 16F). To investigate whether Bap fibers interact with another surface protein, we exogenously complemented with rBap\_B the *S. aureus* 132 *srtA* strain, which is deficient in proteins covalently anchored to the cell-wall, (Vergara-Irigaray *et al.*, 2009). The Sortase A enzyme is responsible for anchoring surface proteins to the peptidoglycan. The results showed that addition of rBap\_B peptide (2  $\mu$ M) induced cell-to-cell aggregation of the Sortase-deficient *S. aureus* 132 strain (Fig 26A).

Next, we wondered whether exogenously supplied rBap\_B could induce cellular clumping in other gram-positive and gram-negative bacterial genera. For this purpose, we incubated *Listeria monocytogenes* EGD, *Enterococcus faecalis* 23, *Salmonella enteritidis* 3934 and *Escherichia coli* VS39 in the presence of 2  $\mu$ M rBap\_B in LB-glu medium at 37 °C, 200 rpm. As shown in Fig. 26A, rBap\_B induced aggregation of *L. monocytogenes* EGD and *E. faecalis* 23. In contrast, rBap\_B was unable to induce aggregation of *S. enteritidis* and *E. coli*, even when the media was acidified to pH 4.5 (Fig. 26B). Altogether, these data suggest that Bap is capable of inducing bacterial aggregation through the formation of fibrillar amyloid-like structures in gram-positive bacteria. Also, these results imply that Bap aggregates interact with a common component present on the surface of gram-positive bacteria.

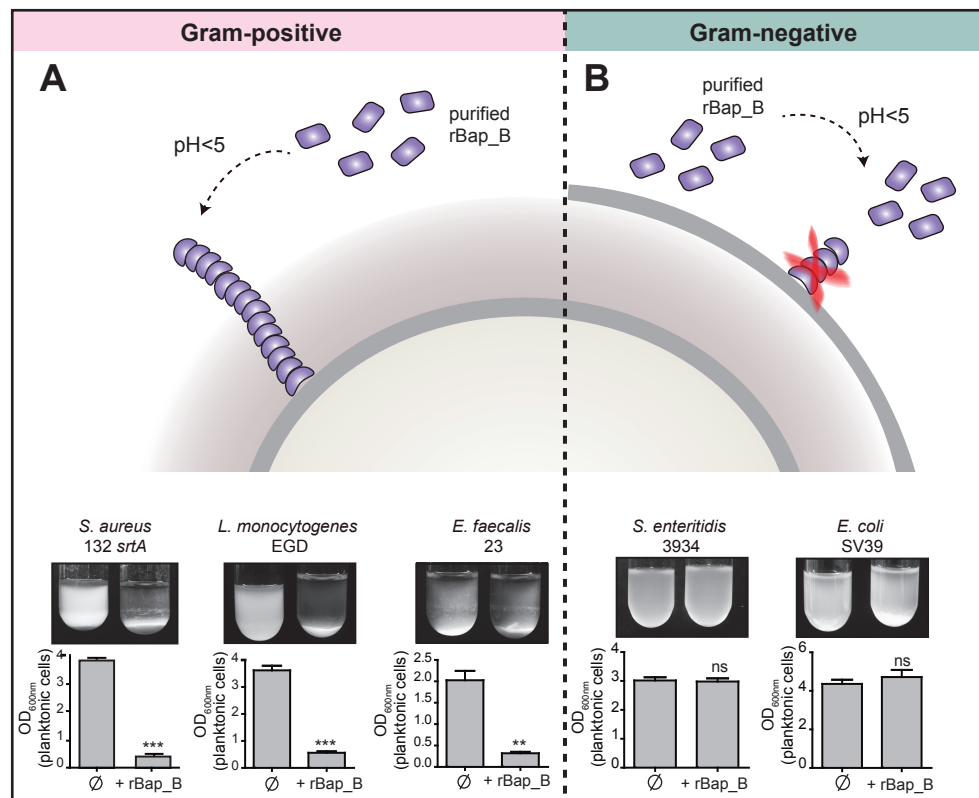


**Figure 26. Exogenous complementation of gram-positive and gram-negative bacteria with rBap\_B purified protein.** Schematic illustration showing possible fibers formation on the bacterial surface of gram-positive (A) and gram-negative (B) bacteria after complementation with purified rBap\_B. Bacterial clumping of *S. aureus* 132 *srtA* mutant, *L. monocytogenes* EGD and *E. faecalis* 23 (A, lower panel), and *S. enteritidis* 3924 and *E. coli* SV39 (B, lower panel) after an overnight incubation at 37 °C, 200 rpm, in the presence of 2 μM rBap\_B protein. Data represent the means from three independent experiments. Error bars represent SD (\*\*,  $P < 0.01$ ; \*\*\*,  $P < 0.001$ ; ns, no statistical differences). Statistical analysis was performed using the unpaired Student *t* test.

- **Amyloid-like Bap fibers have a role in the pathogenic process of *S. aureus*.**

*S. aureus* V329 adhesion to host cells is favored under amyloid-forming conditions.

A previous study from our group determined that Bap-mediated matrix promoted bacterial adhesion to different epithelial cell lines (Valle *et al.*, 2012). To test whether Bap fibrillar aggregates could play a role in host-pathogen interaction, we analyzed the capacity of *S. aureus* V329 strain and  $\Delta bap$  mutant grown in LB-glu (amyloid) and LB (non-amyloid) conditions, to adhere to a bovine mammary epithelial cell line (MAC-T). The results revealed that V329 strain adhered more efficiently ( $P < 0.01$ ) when bacteria were grown in LB-glu than in LB media whereas  $\Delta bap$  mutant strain showed similar adhesion values when grown in either media (Fig. 27A). These results suggest that Bap is capable to promote adhesion to host cells more efficiently in the fiber conformation.

Amyloid-like Bap fibers promote colonization and persistence in a mouse foreign body infection model

To evaluate the biological relevance of Bap amyloids during infection, we compared the colonization ability of *S. aureus* V329 wild type and  $\Delta bap$  mutant strains using a catheter biofilm infection model. If the presence of Bap favors biofilm development in this specific environment, *S. aureus* V329 wild type strain would have higher capacity to colonize a subcutaneous foreign catheter than the  $\Delta bap$  strain. A 3-cm segment of an intravenous catheter was aseptically implanted in the subscapular space of mice, and animals were infected with equal numbers of *S. aureus* V329 and the corresponding *bap*-deficient strain. Enumeration of *S. aureus* cells attached



---

to the catheters 4 days after infection showed no significant differences between *S. aureus* V329 wild type and the  $\Delta bap$  mutant strains (Fig. 27B). However, at day 10 post-infection, the number of Bap-positive colonies recovered from the catheters was significantly higher than Bap-negative colonies ( $P < 0.05$ ) (Fig. 27B). These data indicate that Bap can significantly contribute to the development of biofilm-associated infections caused by *S. aureus*.

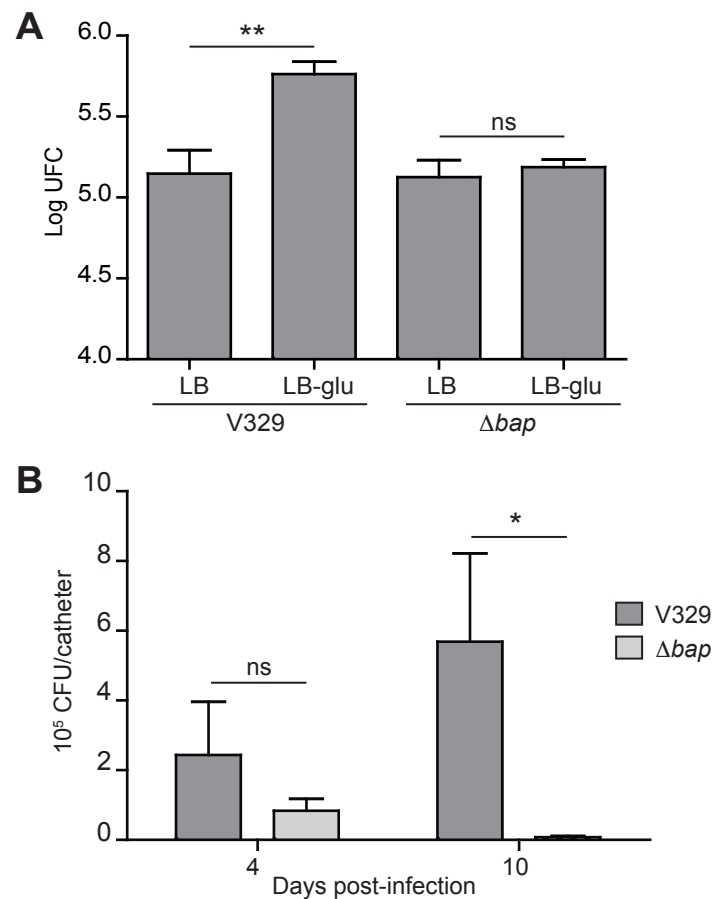


**Figure 27. Biological relevance of Bap-amyloid fibers. A)** Effect of Bap fibers formation in *S. aureus* adherence to epithelial cells. After 1 h of infection, bacterial adhesion of *S. aureus* V329 wild type and  $\Delta bap$  mutant to the bovine mammary gland epithelial cells MAC-T was measured by CFU counts. Data represent the means from three independent experiments. Error bars represent SD (\*\*,  $P < 0.01$ ; ns, no statistical differences). Statistical analysis was performed using the Mann–Whitney test. **B)** *In vivo* biofilm formation of *S. aureus* V329 wild type and  $\Delta bap$  mutant using a catheter infection model. Catheters were infected with equal numbers of the strains, bacteria were recovered from implanted catheters and counted after 4 or 10 days post- infection. Data represent the means from three independent experiments. Error bars represent SD (\*,  $P < 0.01$ ; ns, no statistical differences). Statistical analysis was performed using the Mann–Whitney test (\*,  $P < 0.05$ ).

- **Calcium inhibits the formation of Bap amyloid aggregates.**

Bap-mediated multicellular behavior is inhibited in the presence of millimolar concentrations of calcium bound to the EF-hand domains present in the region B of Bap (Arrizubieta *et al.*, 2004). The question arises as how calcium and pH environmental signals reconcile to regulate Bap mediated biofilm formation. To address this question, we investigated the aggregation kinetics of Bap when *S. aureus* V329 grew in LB-glu supplemented with 20 mM of CaCl<sub>2</sub>. Interestingly, the presence of calcium inhibited aggregation of the Bap protein (Fig. 28A), as well as biofilm formation and bacterial clumping (Fig. 28C) despite acidification of the growth media. In contrast, the presence of calcium in the media did not affect protein aggregation and multicellular behavior of bacteria producing Bap with mutations at the EF-hand calcium binding motifs ( $\Delta$ EF) (Fig. 28A and C). Consistent with these data *S. aureus*  $\Delta$ bap producing the Bap\_B chimeric protein displayed the same aggregation pattern and biofilm phenotype (Fig. 28B and D) as the entire Bap protein in the presence of CaCl<sub>2</sub>, while its respective  $\Delta$ bap pBap\_B\_ $\Delta$ EF was totally insensitive to the Ca<sup>2+</sup> present in the medium (Fig. 28B and D). It is worthy to note that a band corresponding to Bap\_B aggregates is present in native gels for  $\Delta$ bap pBap\_B strain in the presence of CaCl<sub>2</sub>. We attribute this to the fact that plasmid expression level of the chimera is higher compared to chromosomal levels of Bap; therefore, 20 mM CaCl<sub>2</sub> might not be enough to completely saturate the chimeric protein. This inhibitory effect of calcium on Bap aggregation and biofilm formation may interfere with: (i) the initial proteolytic processing of full-length anchored Bap, or (ii) the self-assembly into amyloid structures of the N-terminal processed fragments. To distinguish between these two hypothesis, we first analyzed the anti-Bap protein pattern of supernatants obtained from *S. aureus* V329 cultures grown in LB with and without glucose (pH<5 and pH>7, respectively), in the presence or absence of 20 mM CaCl<sub>2</sub>. It is clear

that, independently on the acidification of the culture media, in the presence of calcium the protein is processed releasing fragments that remain floating into the media (Fig. 29A). Next, we evaluated the effect of  $\text{Ca}^{2+}$  on bacterial aggregation of  $\Delta bap$  strain induced by rBap\_B under acidic culture conditions. We observed that interbacterial interactions did not occur when  $\Delta bap$  mutant strain exogenously complemented with rBap\_B was incubated in the presence of calcium (Fig 29B). We further tested the effect of calcium on Bap amyloid formation by analyzing *in vitro* aggregation of rBap\_B into ThT positive amyloid-like structures in the presence of the cation. Results showed that calcium significantly inhibited the formation of amyloid-like aggregates as shown by aggregation kinetic curves and endpoint graphic (Fig. 29C and D).

In summary, all these results suggest that binding of calcium to Bap somehow affects the protein conformation in a way that interferes with a proper self-assembly of N-terminal digested fragments into amyloid fibrillar structures, even when the pH of the medium acidifies.

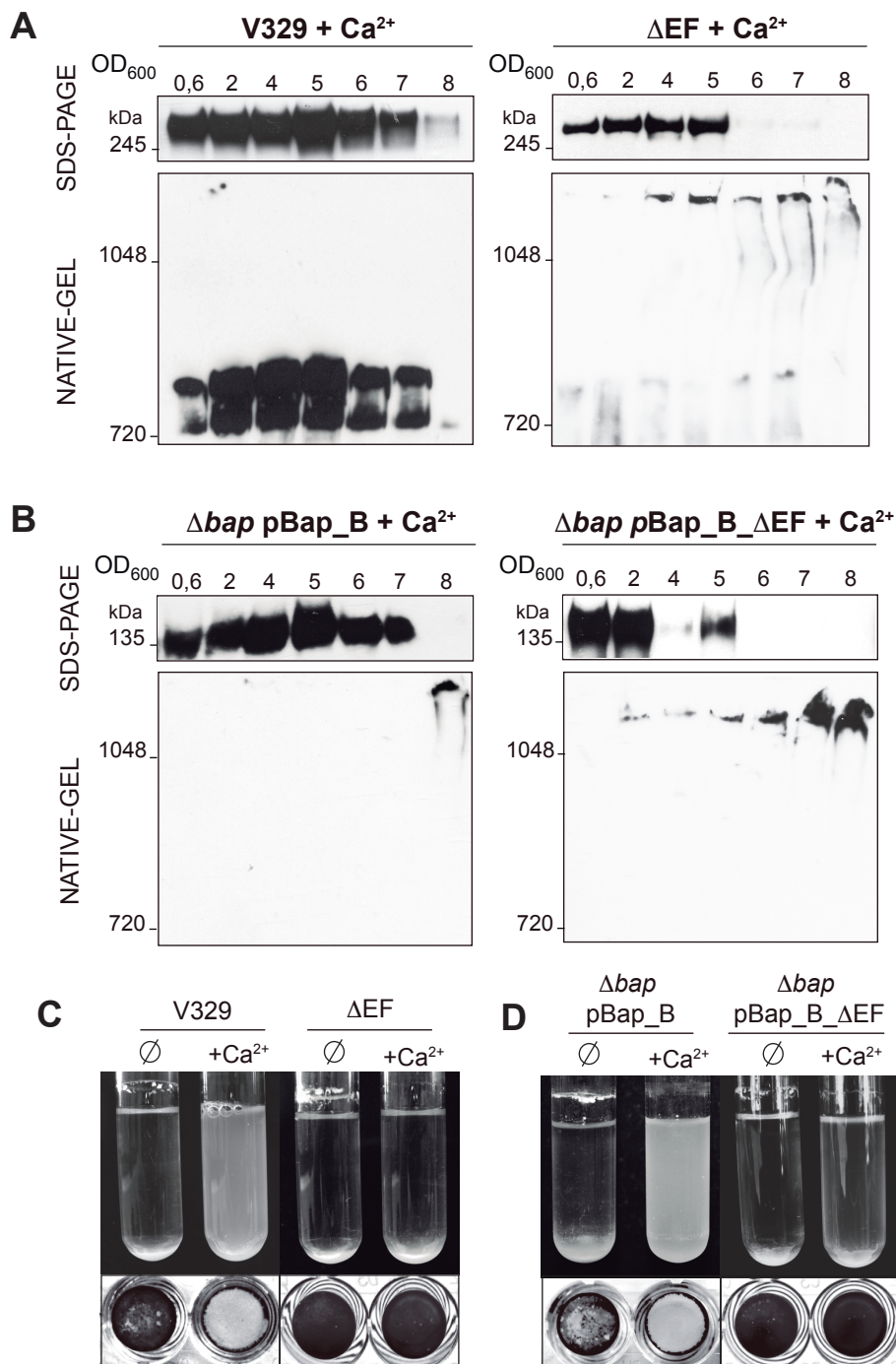


**Figure 28. Calcium inhibits Bap-mediated aggregative phenotype.** Immunoblot of cell wall extracts from **(A)** *S. aureus* V329 and *S. aureus* ΔEF and **(B)** Δ*bap* mutant expressing Bap\_B and Bap\_B\_ΔEF chimeric protein. Bacteria were grown in LB-glu supplemented with 20 mM CaCl<sub>2</sub>. Proteins were separated on 7.5% acrylamide gels (upper panel) or Criterion XT Tris-acetate gels with Tris/glycine running buffer (lower panel) and probed with anti-Bap antibodies. Size markers (in kDa) are indicated. Bacterial clumping and biofilm formation of **(C)** *S. aureus* V329 and ΔEF mutant and **(D)** Δ*bap* pBap\_B and Δ*bap* pBap\_B\_ΔEF grown in LB-glu supplemented (+Ca<sup>2+</sup>) or not (∅) with 20 mM CaCl<sub>2</sub>.

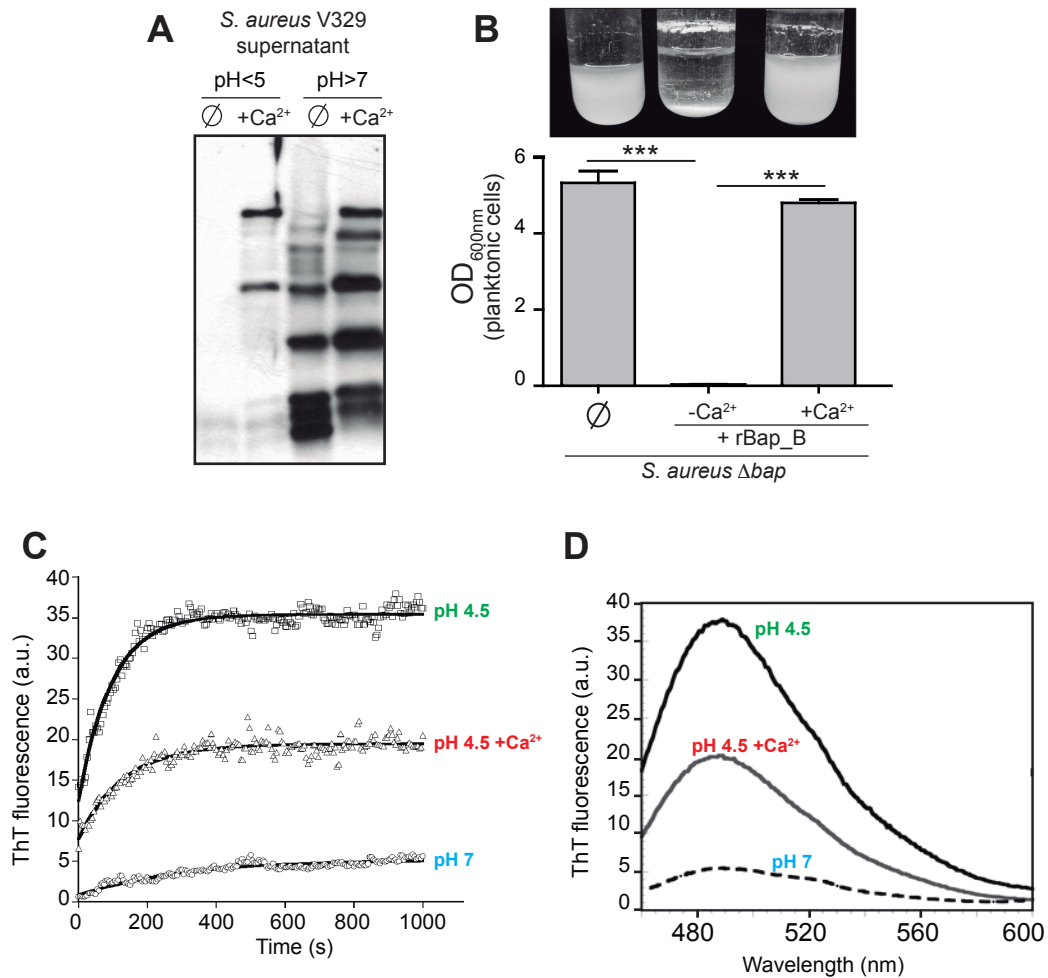


**Figure 29. Calcium affects the assembly of Bap N-terminal fragments into amyloid structures.** **A**) Immunoblotting of the supernatant fraction from overnight cultures of *S. aureus* V329 grown in LB (pH>7) and LB-glu (pH<5) in the presence (+Ca<sup>2+</sup>) or absence (∅) of 20 mM CaCl<sub>2</sub>. **B**) Bacterial clumping of *S. aureus*  $\Delta$ bap grown in LB-glu (pH<5) incubated with 2  $\mu$ M purified rBap\_B protein in the presence or absence of 20 mM CaCl<sub>2</sub>. ∅, no addition of rBap\_B. Cells were incubated for 24 h, at 37 °C, 200 rpm. Data represent the means from three independent experiments. Error bars represent SD (\*\*\*,  $P < 0.001$ ). Statistical analysis was performed using the Mann-Whitney test. **C**) rBap\_B aggregation kinetics were monitored by following the changes in relative ThT fluorescence emission intensity. rBap\_B at pH 4.5, at pH 4.5 + 100 mM CaCl<sub>2</sub>, and at pH 7 is represented. **D**) End point ThT emission fluorescence upon binding to rBap\_B at pH 4.5 (solid line), pH 4.5 + 100 mM CaCl<sub>2</sub> (grey line) and at pH 7 (dashed line).

- **Biophysical characterization of Bap in the presence of calcium**

We used several biophysical approaches to determine whether the inhibitory effect of calcium in Bap-amyloid aggregation is due to a change in protein structure upon binding to the cation. First, it is important to clarify that fast aggregation of rBap\_B at pH 4.5 even at low protein concentration (0.01 mg/ml) makes difficult the characterization of the conformational properties of the soluble monomers at this pH. To solve this problem, we analyzed the biophysical properties of the Bap\_B domain in the presence of calcium at neutral pH. Analysis of the far-UV CD spectra of rBap\_B revealed that 1 and 10 mM CaCl<sub>2</sub> are sufficient to induce a concentration dependent increase in the ellipticity (Fig. 30A). Deconvolution of the spectra in the absence and presence of 1 mM Ca<sup>2+</sup> indicated that the protein displays very similar secondary structure content in these conditions. The spectrum is dominated in both cases by disordered conformations, although a small reduction in the overall  $\beta$ -sheet content could be observed in the presence of the Ca<sup>2+</sup> (the 10 mM CaCl<sub>2</sub> spectrum could not be deconvoluted due to the strong increase in HT voltage below 200 nm in this condition). We next decided to monitor by near-UV CD and intrinsic fluorescence the overall tertiary structure of rBap\_B in the presence or absence of Ca<sup>2+</sup>. Despite no significant impact of Ca<sup>2+</sup> on the environment of rBap\_B aromatic residues could be observed by near-UV CD (Fig. 30B), the cation promoted a detectable increase in intrinsic fluorescence emission (Fig. 30C), suggesting rearrangements in the tertiary context of the protein. To confirm the existence of a change in the aromatic residues environment, we performed thermal denaturation in the absence and in the presence of 1 and 10 mM CaCl<sub>2</sub>. Results indicated that the temperature at which the protein loses half of its intrinsic fluorescence augmented in the presence of increasing concentrations of calcium (1 and 10 mM), suggesting that the cation exerts a global stabilizing effect on Bap conformation (Fig. 30D). The following

experiments support this idea. Sedimentation velocity analysis revealed that rBap\_B, which according to sedimentation equilibrium is a monomer both in the presence or absence of  $\text{Ca}^{2+}$  (Fig. 31A), exhibited a significantly higher sedimentation coefficient ( $s(20,w) \sim 3.3$  versus  $\sim 3.0$ ) when  $\text{Ca}^{2+}$  was present (Fig. 31B). Additionally, rBap\_B protein showed a frictional ratio  $f/f_0 = 1.39$ , compatible with a slightly elongated protein, while in the absence of the cation the protein showed a frictional ratio of 1.66 indicating a more elongated and moderately asymmetric protein shape (Fig. 31B). Size exclusion chromatography analysis supported this by revealing that rBap\_B is eluted with retard in the presence of calcium (Fig. 31C). Additionally, when we performed 1D-NMR of rBap\_B in the presence or absence of  $\text{Ca}^{2+}$ , we observed an increase in the number of peaks corresponding to the methyl (0.5 ppm) and amide (8.5 ppm) regions of the spectrum (Fig. 31D). The broader line-widths observed in these regions in the absence of  $\text{Ca}^{2+}$  are in concordance with a molten globule that is semi stable and fluctuates between several conformations. The sharpening of the peaks when  $\text{Ca}^{2+}$  is present would then be indicative of protein ordering into a more stable state with a smaller hydrodynamic radius (Fig. 31D). Finally, analysis of Bap accessibility to proteolytic degradation in the presence of calcium showed that rBap\_B was readily hydrolyzed by proteinase K in the absence of calcium, whereas it was protected from proteinase K activity when the cation was present (Fig. 31E). Together all these results are consistent with the idea that Bap protein adopts a molten globule-like state in the absence of calcium prior to amyloid formation that is stabilized upon calcium binding thus impeding amyloid assembly due to tertiary rearrangements of Bap conformation.



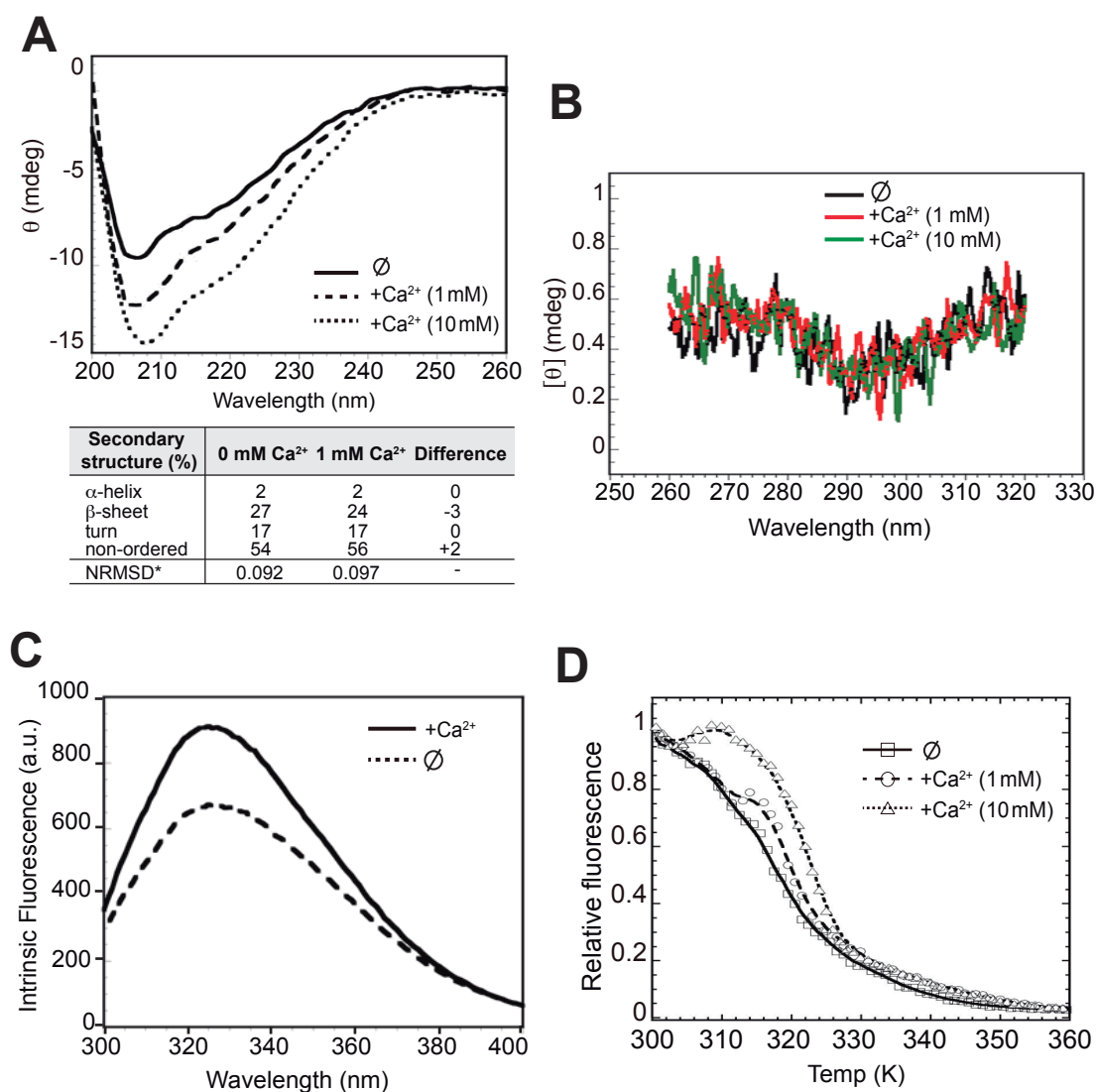


**Figure 30. Effect of calcium on rBap\_B structure.** **A)** Far-UV CD spectra of 0.2 mg/ml rBap\_B at pH 7 in the absence (solid line) or presence of 1 mM (dashed line) and 10 mM (dotted line) CaCl<sub>2</sub>. The table shows secondary structure composition of rBap\_B in those conditions. Data were analyzed with Dichroweb implementing the CDSSTR algorithm. \*NRMSD =  $[\sum(\theta_{\text{exp}} - \theta_{\text{cal}})^2 / \sum(\theta_{\text{exp}})^2]^{1/2}$  where  $\theta_{\text{exp}}$  and  $\theta_{\text{cal}}$  are the experimental and calculated ellipticity values at a particular wavelength, respectively. **B)** Near-UV CD spectra of 0.2 mg/ml rBap\_B in the absence (black) or presence of 1 mM (red) and 10 mM (green) CaCl<sub>2</sub>. **C)** Intrinsic fluorescence of 1.5 mg/ml rBap\_B at pH 7 in the presence (solid line) or absence (dashed line) of 100 mM CaCl<sub>2</sub>. **D)** Thermal melting curves of 0.2 mg/ml rBap\_B in the absence (squares) or presence of 1 mM (circles) and 10 mM (triangles) CaCl<sub>2</sub>.

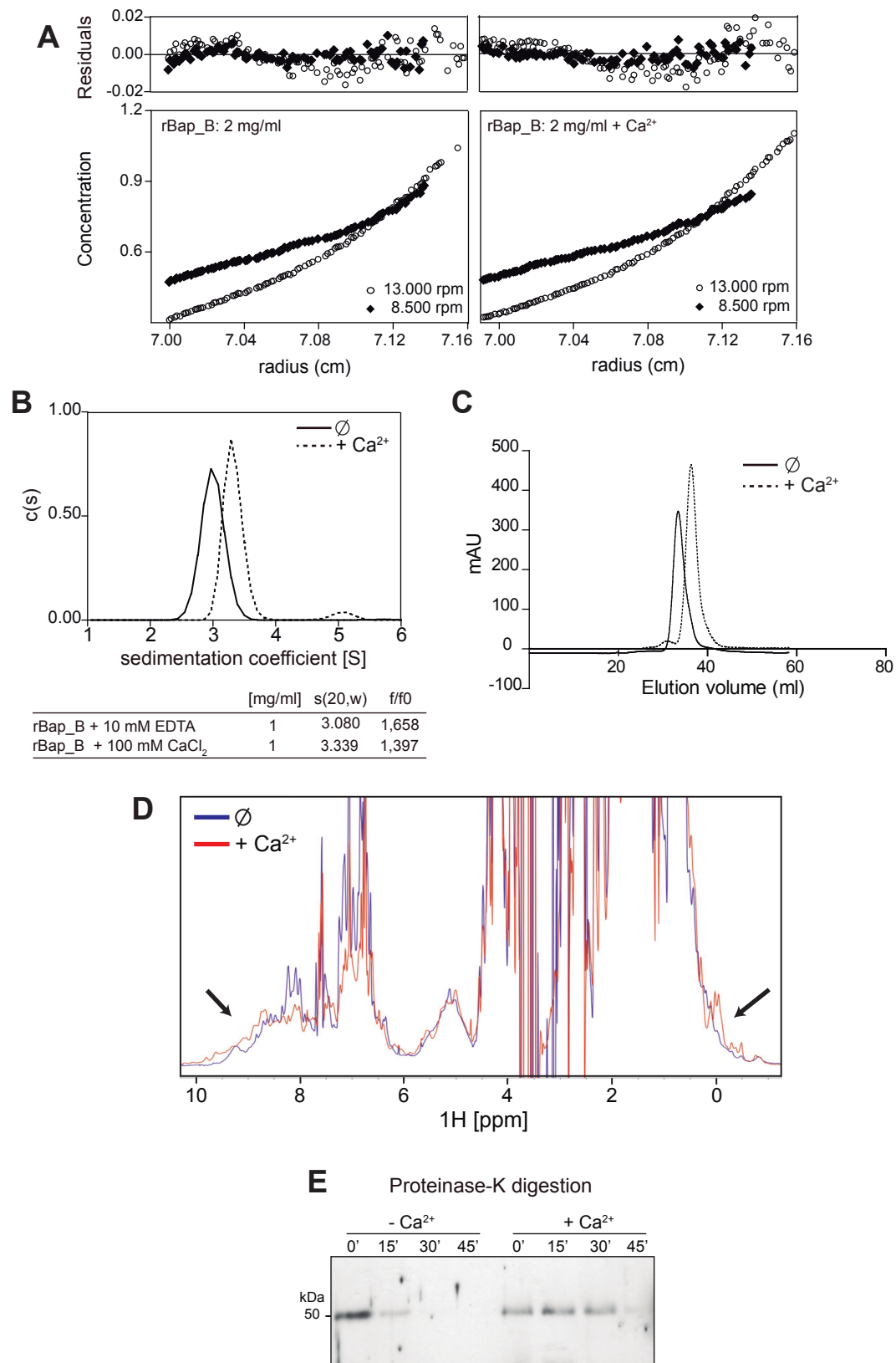


Figure 31. Legend is detailed in the next page

**Figure 31. Effect of calcium on rBap\_B stabilization.** **A)** Sedimentation equilibrium analysis of 2 mg/ml rBap\_B at pH 7 confirmed a monomeric state of the protein both in the presence (right panel) or absence (left panel) of 100 mM CaCl<sub>2</sub>. Dotted lines show global fits. Residuals are shown above. **B)** Sedimentation velocity analyses of 1 mg/ml rBap\_B in the presence 100 mM CaCl<sub>2</sub> (dashed line) revealed a specific retard in the sedimentation velocity. The continuous line represents cation-free rBap\_B. The corresponding sedimentation coefficients and frictional ratios are shown in the table below the graphic. **C)** Size exclusion chromatography of rBap\_B. Chromatograms showing the protein eluted from a HiLoad 16/600 Superdex 200 pg column in buffers in the presence (dashed line) and absence (solid line) of 100 mM CaCl<sub>2</sub>. **D)** 1D <sup>1</sup>H nuclear magnetic resonance (NMR) spectrum of 350 μM rBap\_B in the presence of 100 mM CaCl<sub>2</sub> (red) overlaid on that for 350 μM rBap\_B without added calcium (blue). The methyl region of the NMR spectrum includes high-field proton resonances observed at low chemical shifts (<0.5 ppm), which indicate the presence of characteristic clusters of aromatic and methyl groups in the core of a structured protein. In addition, the envelope of peaks resonating at high chemical shift (>8.5 ppm) correspond to highly ordered backbone amides present in secondary structure elements. The increase in the number of peaks within the fingerprint methyl and amide regions (black arrows) in the presence of calcium indicate binding and induced structure in the rBap\_B domain. **E)** Time course of rBap\_B proteinase-K digestion. Immunoblot patterns using anti-Bap antibodies are shown for the protein in the presence (+Ca<sup>2+</sup>) and absence (-Ca<sup>2+</sup>) of 50 mM CaCl<sub>2</sub> at 0, 15, 30 and 45 min after proteinase-K addition.

- **Effect of pH and calcium on preformed *S. aureus* biofilms**

So far, it remains clear that both pH and calcium are key determinants of biofilm development of *S. aureus* V329. However, the question remains whether a change in pH or addition of calcium to the medium is able to disrupt an already formed biofilm. To answer this question *S. aureus* V329 and  $\Delta bap$  strains were grown in LB-glu (pH<5), and after an overnight incubation the medium was replaced by LB (pH>7) to evaluate the possible disassembly of bacterial clumps. The results revealed that pH switched from acid to neutral disaggregated bacterial clumps (Fig. 32A). Using the same reasoning, we evaluated the influence of pH and calcium on the detachment of biofilms formed on polystyrene plates. Firstly, *S. aureus* V329 was grown in LB-glu in microtiter plates, and after an overnight incubation at 37 °C, the medium was replaced by LB-glu (pH<5, as control), LB (pH>7), and LB-glu + 20 mM CaCl<sub>2</sub> (pH<5). After 6 hours, we observed that LB completely disrupted the biofilm, while the addition of calcium had no significant effect on biofilm detachment (Fig. 32B).

These results demonstrate that pH-dependent aggregation of Bap protein is reversible. In contrast, Ca<sup>2+</sup> is unable to depolymerize Bap amyloid fibers probably because Ca<sup>2+</sup> interferes with Bap amyloid formation prior to Bap assembly process.

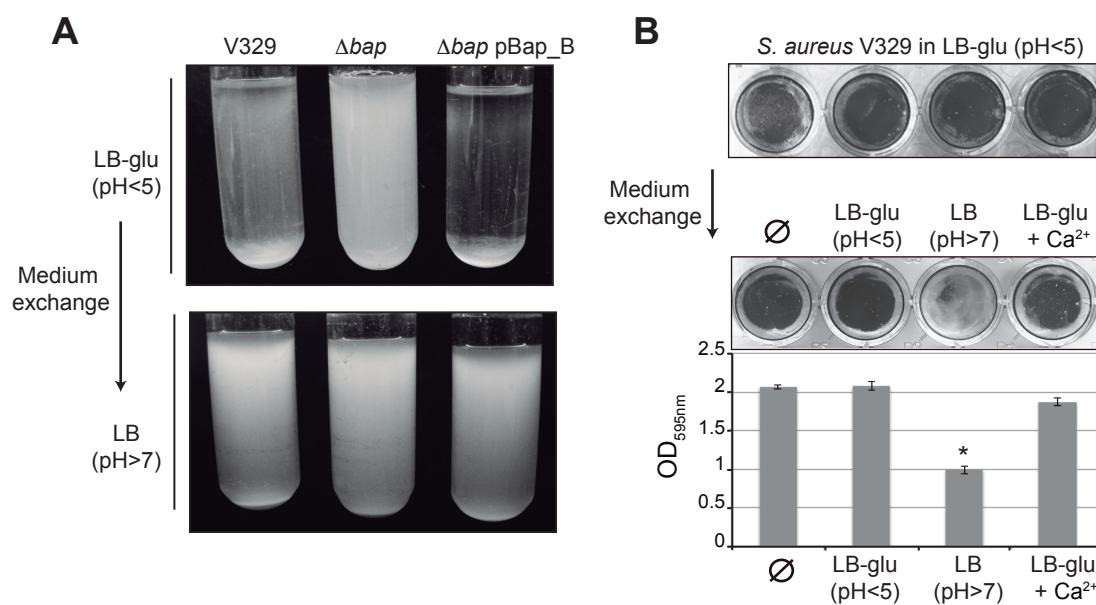


**Figure 32. Effect of pH and calcium addition on aggregated bacteria and pre-formed biofilms of *S. aureus*.** **A)** Reversibility of bacterial aggregates formed by *S. aureus* V329 and  $\Delta bap$  expressing Bap\_B chimeric protein cultured in LB-glu (pH<5) with agitation (upper panel). After an overnight incubation at 37 °C, the medium was replaced by LB (pH>7), and bacteria were incubated for 6 h (lower panel).  $\Delta bap$  strain was used as a control. **B)** Biofilm formation of *S. aureus* V329 cultured in LB-glu (pH<5). After an overnight incubation the medium was replaced by LB-glu (pH<5), LB (pH>7) and LB-glu + 20 mM CaCl<sub>2</sub>. Bacteria were incubated for 6 h, biofilms were quantified by solubilizing crystal violet-stained cells with ethanol-acetone and the absorbance at 595nm was determined. Data represent the means from three independent experiments. Error bars represent SD (\*,  $P<0.05$ ). Statistical analysis was performed using Mann-Whitney test.

- **The N-terminal domain of Bap homologous proteins generates amyloid-like aggregates**

Although orthologs of Bap exist in many coagulase negative staphylococci, homology in region B is variable (Tormo *et al.*, 2005). In Figure 33 we show a multiple alignment performed with ClustalW2 of region B of Bap proteins present in different bacteria and some relevant structural features of their Bap\_B regions in relation to Bap\_B of *S. aureus* are shown in Table 5.

We extended the analysis of the amyloid-forming propensity to Bap\_B domains of *S. saprophyticus*, *S. simiae*, *S. xylosus*, *S. epidermidis* and *S. simulans* (Table 5). For that, we used the curli-dependent amyloid generator system (C-DAG) that provides a simple cell-based method to test particular target proteins for their amyloid-forming propensity (Sivanathan and Hochschild, 2013). Briefly, C-DAG system has three fundamental components: (i) an *E. coli* strain that is deleted for the *csgA* and *csgB* genes responsible for curli synthesis (Table 1, Materials and Methods), (ii) a plasmid that directs the inducible synthesis of an epitope-tagged target protein fused to the CsgA signal sequence (CsgA<sub>ss</sub>), and (iii) a compatible plasmid that directs the inducible overproduction of CsgG needed to export the protein of interest outside the cell (Sivanathan and Hochschild, 2013). In our case, we fused Bap\_A and Bap\_B of *S. aureus*, and the Bap\_B domains from each selected orthologous staphylococcal strain to the CsgA signal peptide (Fig. 34A). The presence of extracellular amyloid aggregates was detected by analyzing the capacity of the strains to bind Congo red dye (CR). Interestingly, all the Bap\_B orthologs expressed in C-DAG system were able to bind CR, whereas Bap\_A domain of *S. aureus* did not (Fig. 34B). These data suggest that Bap orthologs would share the tendency to form amyloid aggregates.

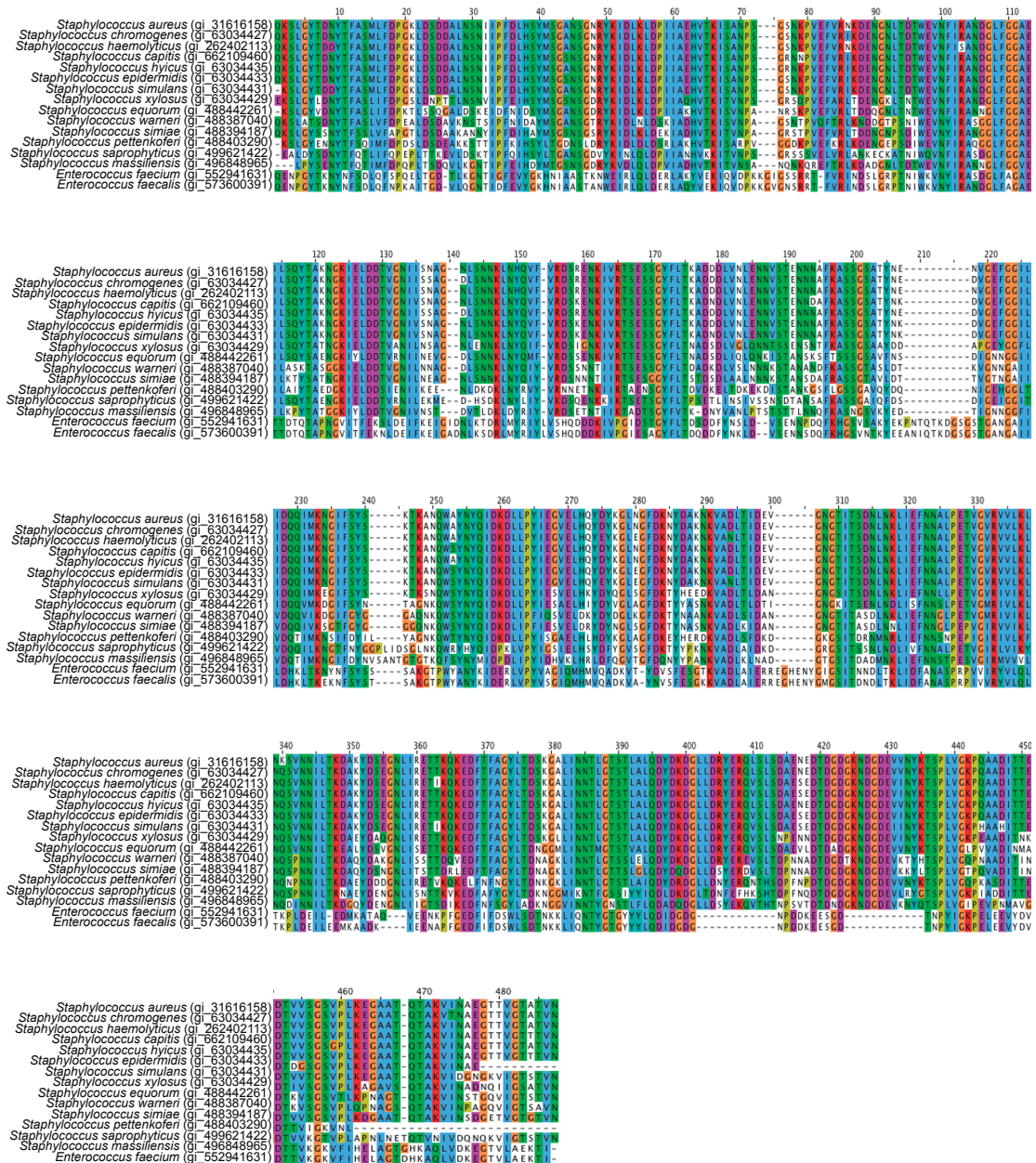


**Figure 33. Protein sequence alignment of Bap orthologs.** The alignment between regions B of Bap from 16 strains was generated using ClustalW2 multiple sequence alignment tool through Jalview program. GenBank accession numbers are shown in brackets for each strain.

**Table 5.** Sequence comparison of the B region of Bap between different staphylococcal species.

	Protein identity (%)	Protein similarity (%)	Theoretical pI <sup>a</sup>	EF-hand motifs <sup>b</sup>		
				aa	sequence	similarity
<i>S. aureus</i>	100	–	4.61	729-741 752-764	DYDKDGLLDREYr DTDGDGKnDGDEV	89 % 91 %
<i>S. epidermidis</i>	97	99	4.56	729-741 752-764	DYDKDGLLDREYr DTDGDGKnDGDEV	91 % 98 %
<i>S. simulans</i>	95	98	4.65	729-741 752-764	DYDKDGLLDREYr DTDGDGKnDGDEI	91 % 89 %
<i>S. xylosus</i>	80	91	4.52	725-737 748-760	DYDKDGLLDREYr DTDGDGKnDGDEV	91 % 89 %
<i>S. simiae</i>	68	80	4.43	612-624 651-663 743-755 766-778	DKDlIpFIESVEL DANGNGTITASDL DYDQDGLLDSYEr DTDGDGKnDGDEV	80 % Identity 91 % 89 %
<i>S. saprophyticus</i>	58	74	4.74	557-569 580-592	DLDKDGLIDNFEF DTDGDGKnDGDEV	89 % 89 %

<sup>a</sup>Theoretical pI corresponds to the estimated isoelectric point calculated using Compute pI/Mw tool of ExPaSy server.

<sup>b</sup>EF- hand motifs corresponds to the predicted EF-hand-like calcium binding domains calculated using PROSCAN (PROSITE database). Residues that do not conform the EF- hand loop consensus sequence are in lowercase letters.



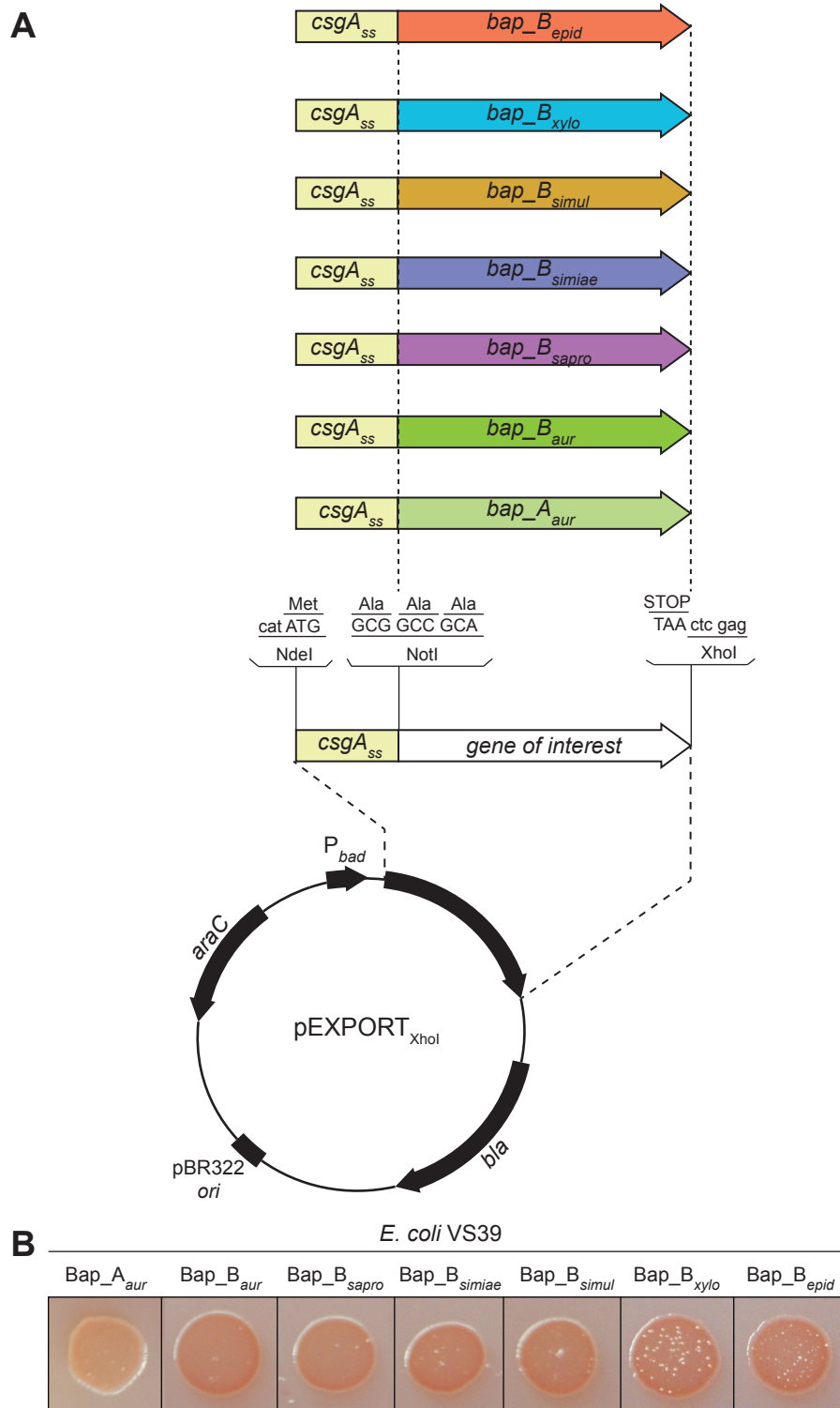


**Figure 34. Amyloidogenic behavior of Bap\_B orthologous proteins. A)** pEXPORT<sub>XhoI</sub> plasmid map with relevant features, containing *bap\_A* and *bap\_B* genes from *S. aureus*, as well as the different *bap\_B* orthologs from *S. saprophyticus*, *S. simiae*, *S. simulans*, *S. xylo*sus and *S. epidermidis* as the genes of interest. All restriction sites shown are unique. Adapted from (Sivanathan *et al.*, 2013). **B)** Variation in colony color phenotype of *E. coli* VS39 cells exporting the Bap\_B orthologous proteins grown on agar supplemented with CR. Bap\_B<sub>simiae</sub>: Bap\_B from *S. simiae*, Bap\_B<sub>simul</sub>: Bap\_B from *S. simulans*, Bap\_B<sub>xylo</sub>: Bap\_B from *S. xylo*sus, Bap\_B<sub>epid</sub>: Bap\_B from *S. epidermidis*. As negative control Bap\_A from *S. aureus* was used (Bap\_A<sub>aur</sub>).

Then, we selected Bap\_B of *S. saprophyticus* (Bap\_B<sub>sapro</sub>) for further analysis because it shares an intermediate percentage of identity with Bap\_B of *S. aureus* (58% identity over the entire length of the B domain). The chimeric protein containing Bap\_B<sub>sapro</sub> linked to R-ClfA (Fig. 35A) was correctly expressed and localized on the cell surface of *S. aureus*  $\Delta$ bap as determined by Western blotting (Fig. 35B) and immunofluorescence microscopy (Fig. 35C). *S. aureus*  $\Delta$ bap pBap\_B<sub>sapro</sub> formed bacterial clumps at the bottom of the tube under acidic culture conditions but not under basic conditions (Fig. 35D and E). In agreement with the presence of EF-hand domains,  $\Delta$ bap pBap\_B<sub>sapro</sub> was sensitive to the presence of calcium in the media (Fig. 35E). Together these results indicate that Bap\_B domain of *S. saprophyticus*, similarly to Bap\_B domain of *S. aureus*, mediates multicellular behavior under acidic culture conditions. Next, we purified the recombinant Bap\_B domain of *S. saprophyticus* (rBap\_B<sub>sapro</sub>) to evaluate its conformational properties in relation to pH changes. As previously shown for rBap\_B, purified rBap\_B<sub>sapro</sub> formed protein aggregates in acidic phosphate-citrate buffer (pH 4.5) that reversibly disassembled after changing the buffer to a neutral phosphate buffer (Fig. 36A). Biophysical characterization of the rings formed by rBap\_B<sub>sapro</sub> at pH 4.5 indicated that they have a clear amyloid-like nature, displaying strong binding to ThT (Fig. 36B), CR (Fig. 36C) and ProteoStat (Fig. 36D). rBap\_B<sub>sapro</sub> self-assembled very fast into aggregates displaying exposed hydrophobic clusters at pH 4.5, whereas it remained soluble at pH 7.0, as revealed by bis-ANS binding (Fig. 36F) and light scattering (Fig. 36G). Additionally, when fresh rBap\_B<sub>sapro</sub> was incubated at pH 4.5 for 24 h, the presence of fibrillar structures became apparent (Fig. 36E).

All together, these data indicate that Bap orthologs share the capacity to form amyloid-like aggregates as a molecular mechanism to induce multicellular behavior.

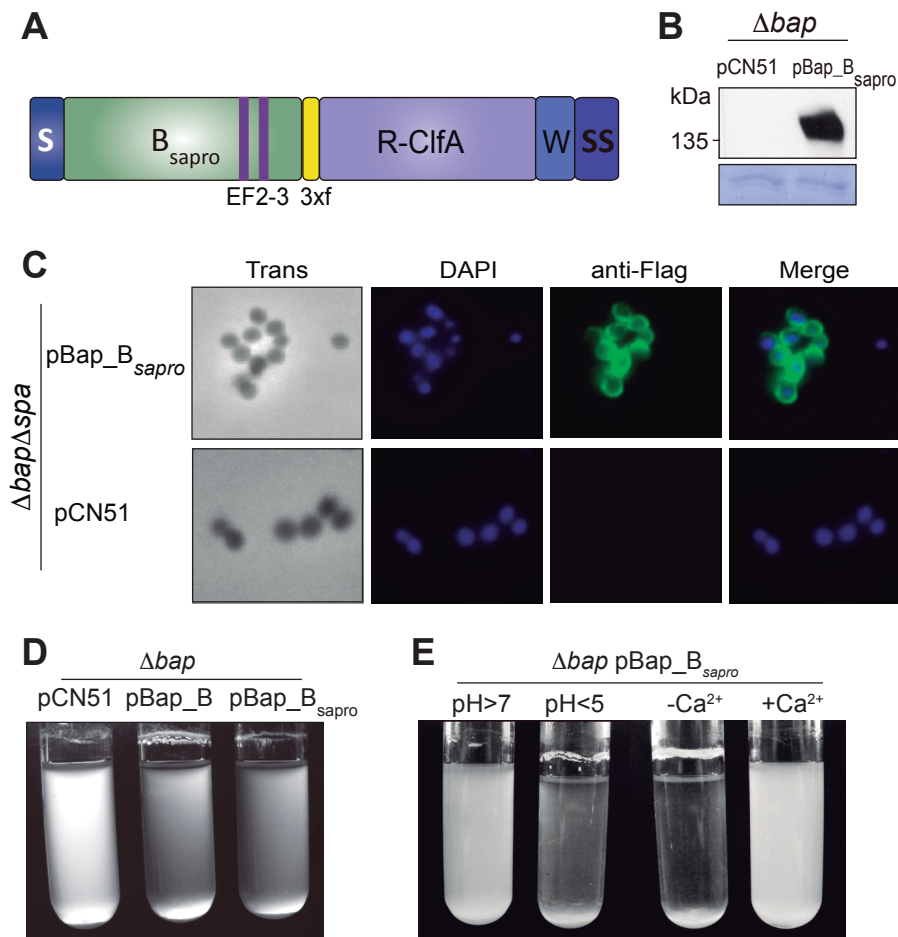


**Figure 35. Bap\_B domain of *S. saprophyticus* induces multicellular behavior.** **A)** Structural organization of Bap\_B chimeric protein of *S. saprophyticus*. EF2-3, EF-hand calcium binding motifs 2 and 3; 3xf, 3xFlag tag; R-ClfA, clumping factor R domain; A-ClfA, clumping factor A domain; W, wall-spanning domain; SS, sorting signal. **B)** Western blot analysis showing pBap\_B<sub>sapro</sub> expression. Cell wall extracts from *S. aureus*  $\Delta bap$  complemented with the pCN51 empty plasmid and plasmid expressing Bap\_B<sub>sapro</sub> chimeric protein (pBap\_B<sub>sapro</sub>), grown until OD<sub>600nm</sub>=4, were separated on 7.5% acrylamide gel and probed with anti-Flag antibodies. Size marker (in kDa) is indicated. **C)** Immunofluorescence showing surface localization of Bap\_B<sub>sapro</sub> chimera. Bacteria were fixed and labeled with anti-Flag antibodies and DAPI.  $\Delta bap\Delta spa$  strains were used in order to avoid unspecific antibody labeling. **D)** Bacterial clumping of *S. aureus*  $\Delta bap$  pBap\_B<sub>sapro</sub> strain. As a control, Bap\_B chimeric protein of *S. aureus* was used ( $\Delta bap$  pBap\_B). **E)** Bacterial clumping of *S. aureus*  $\Delta bap$  expressing Bap\_B<sub>sapro</sub> cultured in LB (pH>7) and LB-glu (pH<5) and in LB-glu supplemented or not with 20 mM CaCl<sub>2</sub>.

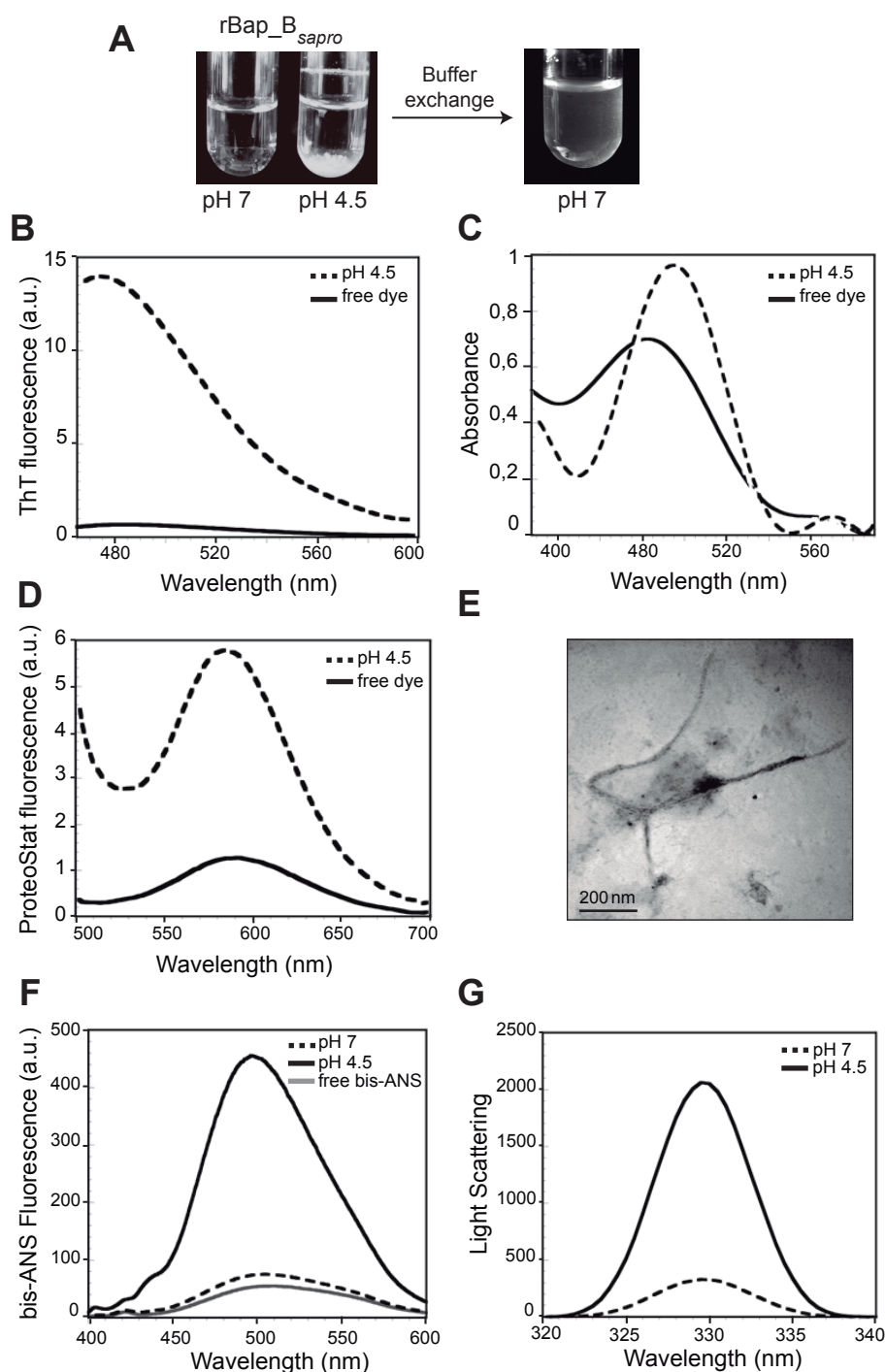


**Figure 36. rBap\_B of *S. saprophyticus* adopts an amyloid-like conformation at acidic pH.**

**A)** rBap\_B<sub>sapro</sub> forms aggregates at pH 4.5. Reversion assay shows complete disassembly after phosphate-citrate buffer is exchanged from pH 4.5 to pH 7. **B)** Increase in ThT emission fluorescence upon binding to 0.1 mg/ml rBap\_B<sub>sapro</sub> ring-shaped aggregates (dashed line). Free ThT emission spectrum is represented (solid line). **C)** Shift in CR absorbance spectrum upon binding to 0.1 mg/ml rBap\_B<sub>sapro</sub> aggregates (dashed line). Free CR absorbance spectrum is represented in solid line. **D)** Increase in ProteoStat emission fluorescence upon binding to 0.1 mg/ml rBap\_B<sub>sapro</sub> ring aggregates (dashed line). Free ProteoStat emission spectrum is represented (solid line). **E)** Transmission electron micrograph of negatively stained aggregates formed by rBap\_B<sub>sapro</sub>. Bis-ANS fluorescence (**F**) and static light scattering (**G**) of 0.1 mg/ml rBap\_B<sub>sapro</sub> at pH 4.5 (solid line) and pH 7 (dashed line). Free bis-ANS is represented in grey.

- **Use of SNAP-tag<sup>®</sup> as a tool for visualize *in vivo* formation of Bap amyloid-dependent matrices**

In an effort to visualize and fluorescently distinguish between the two major *S. aureus* V329 phenotypes discussed in the present work, Bap amyloid-forming and amyloid-non forming cells, we decided to use the SNAP-tag site-specific labeling approach instead of antibody-based imaging. SNAP-tag<sup>®</sup> is an engineered peptide of the human repair protein O<sub>6</sub>-alkylguanine-DNA alkyltransferase (hAGT) that covalently reacts with O<sub>6</sub>-benzylguanine (BG) substrate modified with a synthetic label (e.g. fluorophores, quantum dots, affinity ligands, and gold nanoparticles) (Keppler *et al.*, 2002; Keppler *et al.*, 2004). This strategy allows a fast, flexible, direct and specific covalent labeling for studying protein dynamics in fixed and living cells of both intracellular or membrane proteins (Corrêa, 2014).

We constructed a chimeric protein, named Bap\_B<sup>SNAPtag</sup>, in which the B region of Bap was fused at its C-terminal end with the SNAP-tag protein (Fig. 37A). *S. aureus*  $\Delta bap$  mutant strain expressing pBap\_B<sup>SNAPtag</sup> retained the capacity to generate bacterial clumps at the bottom of the tube after an overnight incubation in LB-glu (pH<5) but not in a medium where the pH remained neutral (Fig. 37B). In contrast to Bap\_B,  $\Delta bap$  mutant expressing Bap\_B<sup>SNAPtag</sup> was insensitive to the presence of 20 mM CaCl<sub>2</sub> (Fig. 37B). Probably, the close proximity of EF-hand motifs to the Bap/SNAP-tag fusion site caused a conformational change of their typical  $\alpha$ -helical structure affecting their union to Ca<sup>2+</sup>. Next, we labeled Bap\_B<sup>SNAPtag</sup> expressed by a  $\Delta bap$  mutant grown in LB (pH>7) and LB-glu (pH<5) after an overnight incubation at 37 °C, 200 rpm. Labeling of SNAP-tag was performed by adding SNAP-Surface<sup>®</sup> Alexa Fluor<sup>®</sup> 488 cell-impermeable substrate to the cells. SNAP-tag reacted with the substrate resulting in the covalent

attachment of the fluorescent label to the active site cysteine (Fig. 37C). As shown in Figure 37D, labeling was successfully accomplished. The sample corresponding to bacteria grown at neutral pH displayed the characteristic well-defined surface localization of Bap, while for those bacteria grown in a medium with acidic pH (pH<5), a diffuse labeling of Bap<sub>B</sub><sup>SNAPtag</sup> was observed (Fig. 37D).  $\Delta bap$  mutant containing pBap<sub>B</sub> without SNAP-tag exhibited no labeling (Fig. 37D). These results are in agreement with the presence of Bap<sub>B</sub> fibers as scaffolds of the biofilm matrix in acidic pH media.

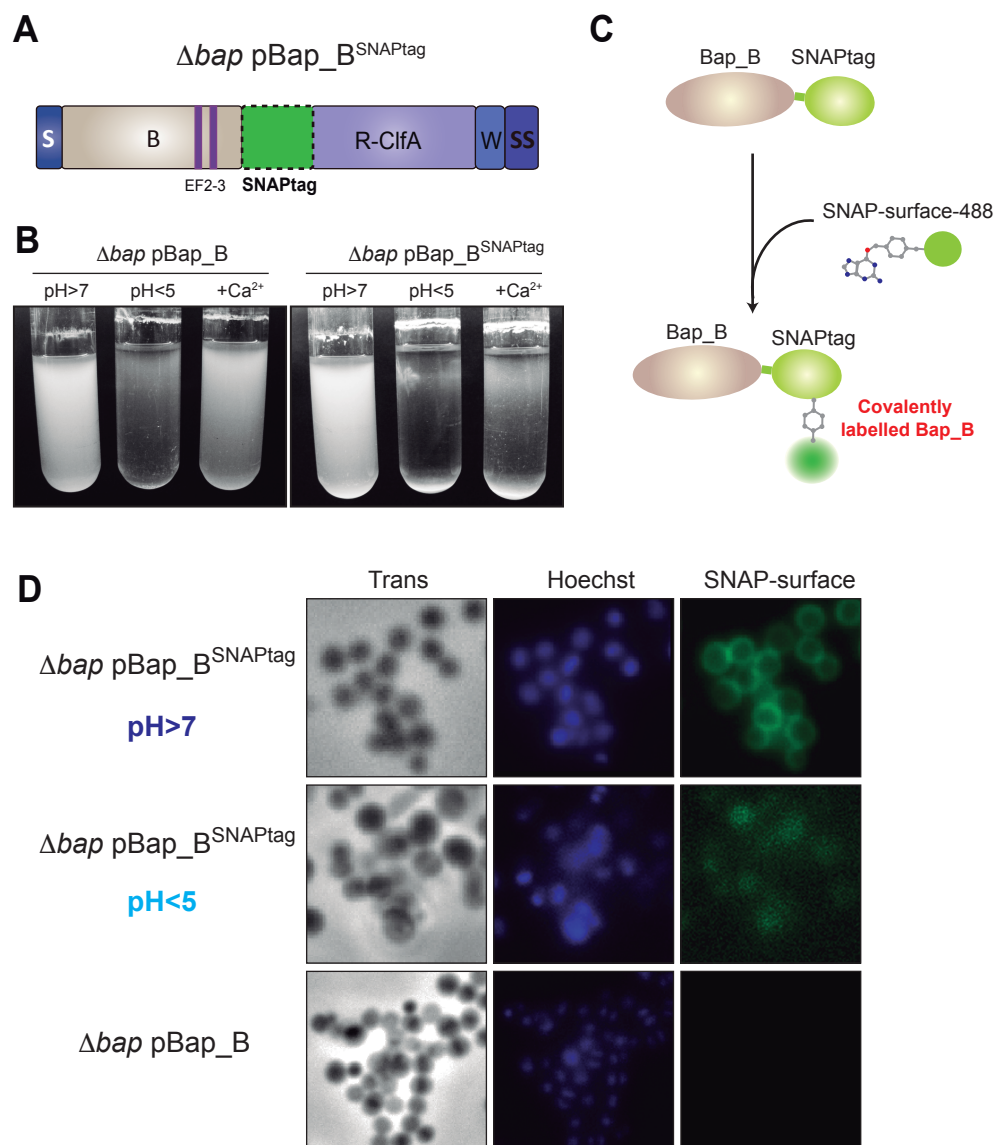


**Figure 37. SNAP-tag is an efficient tool for Bap detection. A)** Structural organization of Bap\_B chimeric protein fused to SNAP-tag. EF2-3, EF-hand calcium binding motifs 2 and 3; R-CifA, clumping factor R domain; A-CifA, clumping factor A domain; W, wall-spanning region; SS, sorting signal. **B)** Bacterial clumping of *S. aureus*  $\Delta bap$  expressing Bap\_B and Bap\_B<sup>SNAPtag</sup> chimeric proteins. Cells were cultured in LB (pH>7), LB-glu (pH<5) and in LB-glu supplemented with 20 mM CaCl<sub>2</sub> (+Ca<sup>2+</sup>). **C)** Schematic representation of Bap/SNAP-tag labeling mechanism. When SNAP-surface 488 is added, a covalent bond is formed between the substrate and the SNAP-tagged Bap, resulting in fluorescent probing. **D)** Immunofluorescence showing localization of Bap in *S. aureus*  $\Delta bap$  mutant expressing Bap\_B<sup>SNAPtag</sup> grown overnight in LB (pH>7) and LB-glu (pH<5) media at 37 °C, 200 rpm. Cells were labeled with SNAP-surface 488 substrate and Hoechst. *S. aureus*  $\Delta bap$  pBap\_B was used as a control.



We took this one step further through the fusion of SNAP-tag with the B region of chromosomally expressed Bap protein (Fig. 38A). *S. aureus* V329 strain expressing full-length Bap containing the SNAP-tag at the end of its B region (V329 Bap<sup>SNAPtag</sup>) was able to induce bacterial clumping under acidic but not under basic culture conditions, identically to the wild type strain (Fig. 38B). In agreement with results obtained for  $\Delta bap$  pBap\_B<sup>SNAPtag</sup>, V329 Bap<sup>SNAPtag</sup> strain was insensitive to the presence of Ca<sup>2+</sup> in the growth media (Fig. 38B). Next, V329 Bap<sup>SNAPtag</sup> was grown in LB with and without glucose and Bap/SNAP-tag fusion protein was labeled from samples taken at different points of the growth curve, to visualize the evolution of Bap amyloid formation. Samples grown in LB without glucose (pH>7, no fibers formation) showed a clear labeling of Bap on the surface of staphylococcal cells whereas samples grown in LB with glucose (pH<5) showed two different labeling patterns depending on the growth phase. A well-defined surface labeling of Bap protein was observed in bacteria at exponential phase. In contrast, when bacteria entered stationary phase, they displayed a more dispersed labeling with green background, probably corresponding to Bap fibers formation (Fig. 38C).

Taken together these results suggest that Bap diffused away along the growth curve from the bacterial surface to the intercellular space in the biofilm matrix.

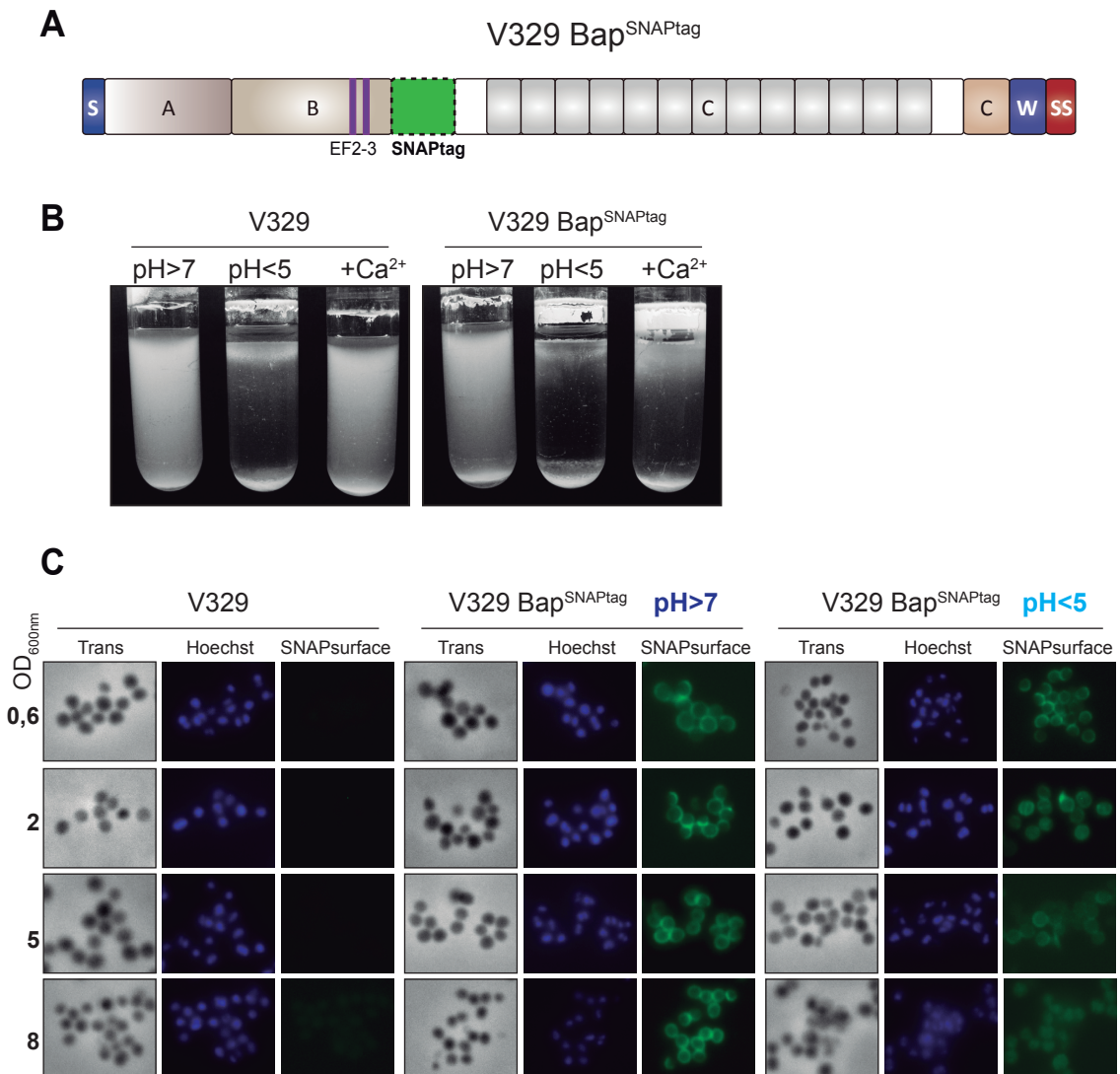


**Figure 38. SNAP-tag fused to the N-terminal region of Bap allows labeling of Bap amyloid-based matrices.** **A)** Structural organization of full length Bap fused to SNAP-tag. EF2-3, EF-hand calcium binding motifs 2 and 3; R-ClfA, clumping factor R domain; A-ClfA, clumping factor A domain; W, wall-spanning region; SS, sorting signal. **B)** Bacterial clumping of *S. aureus* V329 (used as a control) and V329 Bap<sup>SNAPtag</sup> after an overnight incubation in LB (pH>7), LB-glu (pH<5) and in LB-glu supplemented with 20 mM CaCl<sub>2</sub> (+Ca<sup>2+</sup>). **C)** Immunofluorescence showing localization of Bap at different points of *S. aureus* V329 Bap<sup>SNAPtag</sup> growth (OD<sub>600nm</sub> = 0.6, 2, 5 and 8) when incubated in LB (pH>7) and LB-glu (pH<5) at 37 °C, 200 rpm. *S. aureus* V329 was used as a control for specific probing. Cells were labeled with SNAP-surface 488 substrate and Hoechst.

- **Use of SpyTag-SpyCatcher system for the biotechnological functionalization of Bap fibers**

Amyloids are highly organized fibrillar structures that hold great potential to be used as nanomaterials for various technological and biological applications (Mankar *et al.*, 2011). We wanted to evaluate the power of Bap as a potential functionalized self-polymerized protein, based on its ability to withstand the union to different tags. We already proved that Bap maintains its functionality when tagged with 3xFLAG (Fig. 14 and 15), His<sub>6</sub> for rBap\_B (Fig. 17) and lastly with SNAP-tag (Fig. 37 and 38). We next tested a new and innovative peptide, the SpyTag, which shows some interesting advantages over the above named tags. This 13 amino acids peptide was obtained from the second immunoglobulin-like collagen adhesin domain (CnaB2) of the fibronectin binding protein FbaB of *Streptococcus pyogenes* (Zakeri *et al.*, 2012). CnaB2 confers to the protein exceptional stability by forming an intramolecular isopeptide bond between Lys and Asp residues (Zakeri *et al.*, 2012). The splitting of this domain and the engineering of the fragments, allowed the development of the peptide SpyTag (containing the reactive Asp), that forms a rapid, robust and highly stable covalent bond with its protein partner, the SpyCatcher (138 amino acids, 15 kDa), that derives from the rest of the protein and comprises the Lys residue (Zakeri *et al.*, 2012). The linkage of SpyTag-SpyCatcher is efficient at different pH and temperature ranges, at different buffer solutions, and the presence of several detergents does not affect the reaction, so that it can be used under a wide range of conditions (Zakeri *et al.*, 2012).

We designed a chimeric protein, named Bap\_B<sup>SpyTag</sup>, in which the SpyTag peptide was fused at the C-terminus of B region of Bap (Fig. 39A). As expected, the tagged chimera was functional exhibiting capacity for bacterial clumping at acidic but not at neutral pH (Fig. 39B), as previously observed for non-tagged and SNAP-tagged Bap\_B chimeras. The presence

of 20 mM CaCl<sub>2</sub> did not affect *S. aureus*  $\Delta bap$  pBap\_B<sup>SpyTag</sup> multicellular behavior, as occurred with Bap\_B<sup>SNAPtag</sup> chimeric protein.

*S. aureus*  $\Delta bap$  mutant expressing Bap\_B<sup>SpyTag</sup> was grown overnight in LB media in the presence and absence of glucose. In order to detect proper covalent linkage between Bap\_B<sup>SpyTag</sup> and the SpyCatcher partner protein, cells were incubated with 0,5 mg/ml of purified recombinant SpyCatcher fused to the reporter fluorescent protein GFP (rGFP-SpyCatcher) (Fig. 39C), and GFP fluorescence was measured.  $\Delta bap$  pBap\_B<sup>SpyTag</sup> incubated with purified rGFP was used as a control. As illustrated in Figure 39D, at neutral pH  $\Delta bap$  pBap\_B<sup>SpyTag</sup> showed a clear distribution of the chimera at the bacterial surface since no amyloid fibers were formed, while at pH<5 the protein displayed a more dispersed labeling, indicative of Bap amyloid matrix formation.

Altogether these results point out the potential utility of Bap amyloid-like fibers as nanomaterials for biotechnological applications that can be strictly controlled by changing pH conditions (Fig. 39E).

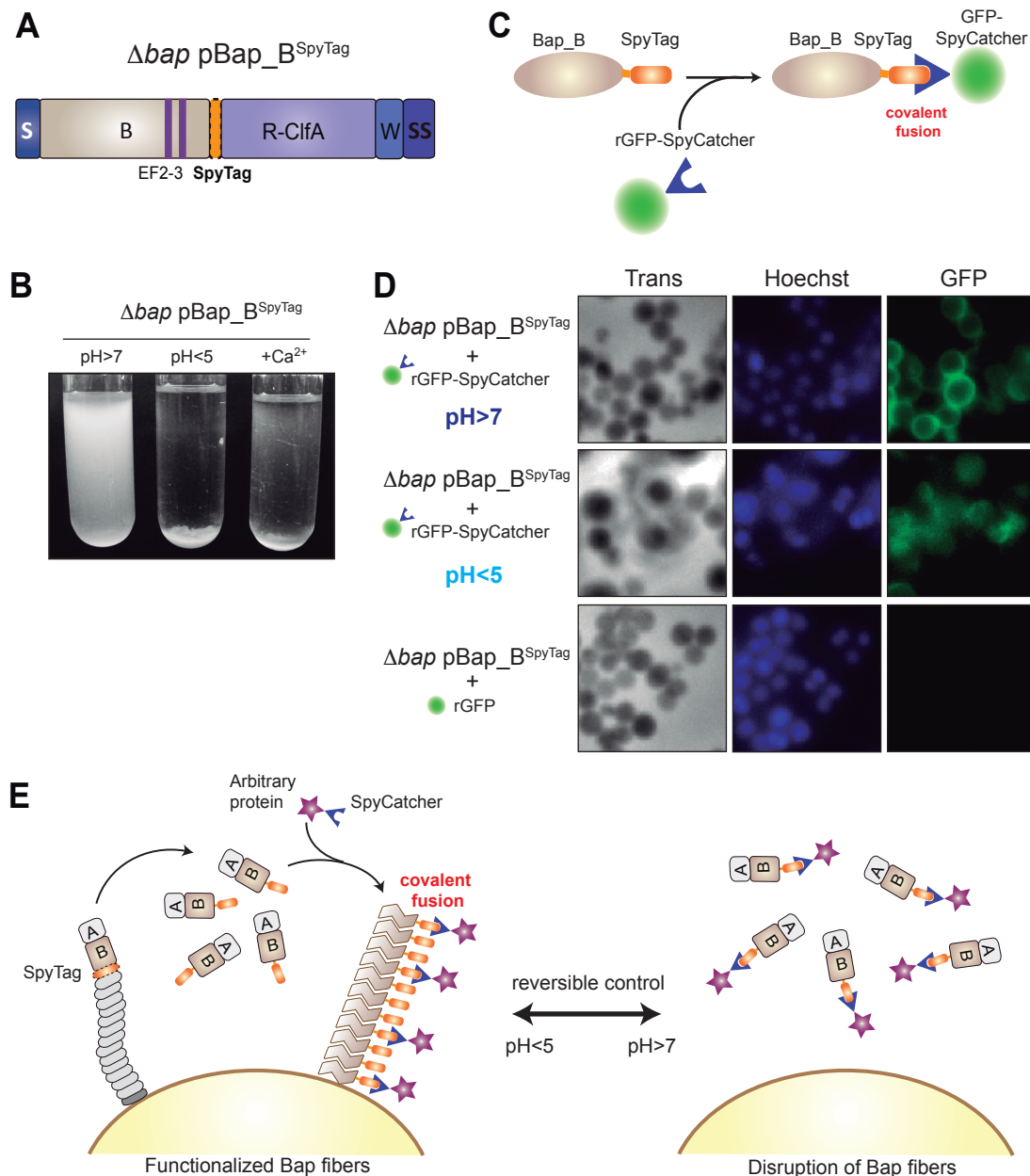


**Figure 39. SpyTag-SpyCatcher system can be used to generate programmable multifunctional biofilms based on Bap amyloid-like fibers.** **A)** Structural organization of Bap\_B chimeric protein fused to SpyTag peptide. EF2-3, EF-hand calcium binding motifs 2 and 3; R-ClfA, clumping factor R domain; A-ClfA, clumping factor A domain; W, wall-spanning region; SS, sorting signal. **B)** Bacterial clumping of *S. aureus*  $\Delta bap$  pBap\_B<sup>SpyTag</sup> cultured in LB (pH>7), LB-glu (pH<5) and in LB-glu supplemented with 20 mM CaCl<sub>2</sub> (+Ca<sup>2+</sup>). **C)** Schematic representation of Bap/SpyTag probing mechanism. When the protein partner SpyCatcher fused to GFP is added, a covalent bond is formed between Bap/SpyTag-SpyCatcher/GFP, resulting in fluorescent labeling of Bap. **D)** Immunofluorescence showing localization of Bap in *S. aureus*  $\Delta bap$  mutant expressing Bap\_B<sup>SpyTag</sup> grown overnight in LB (pH>7) and LB-glu (pH<5) at 37 °C, 200 rpm. Cells were probed with purified rGFP-SpyCatcher and purified rGFP alone (used as a control) followed by nucleic-acid stain Hoechst. **E)** SpyCatcher fused to an arbitrary protein of interest can be used to program the Spy-tagged Bap-fibers matrices with artificial functions (left). Since Bap-fibers formation is a reversible process highly dependent on pH, this property can be used to control the formation or disruption of programmed biofilms (right).



## ***DISCUSSION***

---





## DISCUSSION

- **Bap protein induces biofilm formation by self-assembly into amyloid like fibrils.**

There is a growing recognition that proteins play an important role building the biofilm matrix scaffold. To fulfill this function these proteins need to provide stable intercellular connections and at least in some cases, also mediate adhesion to the surface. In the present work, we have shown that the amino-terminal region of Bap forms extracellular amyloid-like fibers that assist in building the biofilm matrix of *S. aureus*. Bap is a surface protein that is displayed as a ring surrounding the surface of each cell and shares structural and functional properties with other staphylococcal surface proteins such as SasG and Aap, implicated in cell-to-cell accumulation and adhesion to epithelial cells (Cucarella *et al.*, 2002; Roche *et al.*, 2003; Rohde *et al.*, 2005; Macintosh *et al.*, 2009; Geoghegan *et al.*, 2010; Valle *et al.*, 2012). All three proteins undergo a limited proteolytic cleavage of the N-terminal domain that induces biofilm formation (Rohde *et al.*, 2005; Geoghegan *et al.*, 2010). The mechanism underlying this processing is different among the three proteins. SasG is known to suffer spontaneous cleavage at labile bonds in its B domain, since protease inhibitors added to the growth medium, as well as strains deficient in each known extracellular and membrane-bound proteases, had no effect on the pattern of SasG processing (Geoghegan *et al.*, 2010). In the case of Aap, endogenous and also exogenous host-derived proteases are the responsible for protein cleavage, and addition of  $\alpha_2$ -macroglobulin to the growth medium specifically led to the loss of cell clumping and biofilm formation of *S. epidermidis* (Rohde *et al.*, 2005). We failed to identify a staphylococcal protease that could be responsible for Bap cleavage, since protease mutants ( $\Delta aur$ ,  $\Delta sspA$  and  $\Delta sspBC$ ) and protease inhibitors ( $\alpha_2$ -

macroglobulin, E64 and PMSF) did not change the proteolytic pattern of Bap (Fig. 13). It is likely that similarly to SasG, Bap would suffer spontaneous cleavage at its N-terminus. However, we cannot exclude the possibility that a protease different from the ones tested here (for example, membrane-bound HtrA<sub>1</sub>/HtrA<sub>2</sub> proteases), or more than one protease simultaneously could be responsible for Bap cleavage.

In the case of SasG and Aap, the N-terminal domain is removed, allowing the C-terminal region containing the G5 domains to promote zinc-dependent self-association of opposing molecules (Rohde *et al.*, 2005; Conrady *et al.*, 2008; Geoghegan *et al.*, 2010; Conrady *et al.*, 2013). In contrast, it is the N-terminal region of Bap that is released to the extracellular media and self-assembles into amyloid-like fibers, whilst the C-terminal repeats region remains anchored to the membrane. Several pieces of experimental evidence support the amyloid-like properties of the Bap<sub>B</sub> domain aggregates. First, far-UV CD spectra reveal a modest switch in secondary structure of Bap from disordered to  $\beta$ -sheet, as the pH becomes more acid (Fig. 18D). Second, the FTIR spectrum of Bap aggregates is dominated by  $\beta$ -sheet/ $\beta$ -turn secondary structure (Fig. 19A). Third, rBap<sub>B</sub> binds to the amyloid diagnostic dyes Thioflavin-T, Congo Red and ProteoStat (Fig. 19B-F) and forms aggregates with fibrillar morphology when observed by electron microscopy (Fig. 20). Finally, rBap<sub>B</sub> contains canonical short-sequence stretches with significant amyloidogenic potential, which form fibrillar hydrogels by themselves (Fig. 21).

Genuine bacterial functional amyloids utilize sophisticated machineries that direct the polymerization of amyloid fibers outside the cell. For instance, curli (*csgACB-csgDEFG*) in *Escherichia coli* and its homologue Tafi in *Salmonella enterica*, Fap (*fapA-F*) in *Pseudomonas*, Chaplins (*chpA-H*) in *Streptomyces coelicolor* and TasA fibers (*tapA-sipW-*

*tasA*) in *Bacillus* are formed upon expression of the amyloid subunit together with accessory proteins involved in secretion, nucleation, and regulation of assembly of the final amyloid fiber (De Jong *et al.*, 2009; Romero *et al.*, 2010; Dueholm *et al.*, 2010; Romero *et al.*, 2011; Romero *et al.*, 2014). The curli biogenesis machinery is one of the best-characterized examples. It is encoded within two operons (*csgACB-csgDEFG*) that include a master transcriptional regulator of biofilm extracellular matrix components called CsgD. Encoded in the same operon there are two chaperone-like proteins (CsgE and CsgF) that coordinate with CsgG to form a unique secretion system that transports curli subunits to the cell surface. Once there, the major fiber subunit called CsgA is anchored to the cell and nucleated into a  $\beta$ -rich amyloid polymer by the CsgB protein (Hufnagel *et al.*, 2013; Van Gerven *et al.*, 2015) (Fig. 40B). Another complex system with strong structural and functional similarities to curli is encoded by the six-genes *fapA-F* operon in several *Pseudomonas* species (Dueholm *et al.*, 2010; Dueholm *et al.*, 2013b). FapC, together with small amounts of FapB and FapE, are the components of the final amyloid fibrils (Dueholm *et al.*, 2010; Dueholm *et al.*, 2013b). As for CsgB in curli, FapB would act as a fibrillation nucleator of FapC. FapF is predicted to be a  $\beta$ -barrel membrane pore present in the outer membrane to mediate the export of the fiber subunits. FapD and FapA periplasmic proteins may act as a protease and as a potential chaperon, respectively, for amyloid monomers affecting the ration of FapB and FapC in the final fibrils (Dueholm *et al.*, 2013b) (Fig. 40B). One of the best-studied amyloid system in gram-positives, TasA fibers, also requires for assembly the action of two other proteins (operon *tapA-sipW-tasA*): SipW, a peptidase required for the processing and secretion of TasA, and TapA that will mediate nucleation and polymerization of the final fibril. (Romero *et al.*, 2011; Romero and Kolter, 2014; Romero *et*

*al.*, 2014) (Fig. 40A).

Bap appears to follow a more simplistic model of amyloid auto-aggregation, which does not require the expression of accessory proteins (Fig. 40C). Bap relies only on itself and, ultimately, on the Sec translocon system that exports the protein outside de cell, in order to mediate fibrillar polymerization and thus biofilm development. The ABC transporter accompanying *bap* gene in the pathogenicity island is not essential for the secretion of Bap since heterologous complementation of the *S. aureus* Newman strain with *bap* in the absence of the ABC transporter bestowed biofilm formation capacity. Thirdly, in contrast to what occurs in curli or Fap systems, Bap would not require a chaperon to prevent toxic premature assembly inside the cytoplasm, since the Bap amyloid-like subunits are formed as a results of full Bap processing and pH acidification, once the protein is properly exported outside the cell and anchored to the bacterial envelope. Thus, the single Bap protein is sufficient to carry out numerous functions to buildup the extracellular matrix.

Bap is a large protein of around 250 kDa, and according to our results it is expressed all along *S. aureus* growth. So, why such a big protein needs to be constitutively expressed and only a fragment used to build amyloid-like fibrillar structures? We can hypothesize that Bap might play different roles along the growth curve depending on the environmental conditions. Initially, Bap is secreted and mostly covalently anchored to the cell wall in a ring-shaped manner. At this point, the protein would participate in primary attachment to biotic and abiotic surfaces (Cucarella *et al.*, 2001; Valle *et al.*, 2012). Then, the N-terminal domain is released to the media where it remains soluble at neutral pH. If the pH of the environment decreases, the N-terminal domain of Bap would transition from its partially ordered native state to an aggregation-prone conformation that would facilitate polymerization into amyloidogenic fibrillar structures. The presence

of calcium drastically influences the multicellular behavior promoted by Bap. From a biophysical perspective, the binding of calcium to the EF-hand domains of the protein stabilizes its initial molten-globule-like state, likely sequestering the functional N-terminal fragments released from Bap cleavage, and consequently impairing their self-assembly into amyloid structures (Fig. 41).

Expression of amyloid fibers in bacteria usually requires tight regulation to avoid toxicity. Therefore, each system has a regulator dedicated to strictly control the expression of amyloid components at an appropriate time during bacterial growth and under specific environmental conditions. CsgD controls the transcription of the curli structural genes, *csgBAC* (Romling *et al.*, 2000; Simm *et al.*, 2004), and its activity is in turn controlled by a variety of regulatory systems that respond to environmental signals including osmolarity, pH, temperature and nutrient availability (Prigent-Combaret *et al.*, 2001; Jubelin *et al.*, 2005). The formation of TasA amyloid fibers involves the participation of a master regulator, SinR, which directly represses the expression of *tapA-sipW-tasA* operon, and SinI, which antagonizes the repressive activity of SinR when conditions are propitious for biofilm development (Kearns *et al.*, 2005; Branda *et al.*, 2006). A further level of control of amyloid assembly in *B. subtilis* might be given by the bifunctional signal peptidase, SipW, particularly by its C-terminal tail that antagonize with the activity of SinR repressor through an unknown mechanism, leading to induction of the biofilm matrix genes (Terra *et al.*, 2012). In *S. aureus*, PSMs expression is regulated by direct binding of the AgrA response regulator of the accessory gene regulator (Agr) system, to *psm* loci (Janzon *et al.*, 1989; R Wang *et al.*, 2007; Queck *et al.*, 2008). In contrast to the previous examples, Bap expression does not depend on a dedicated regulatory factor; the protein is constitutively expressed along the growth of *S. aureus* and shows different levels of post-translational control

that strictly define whether fibers formation will occur or not: (i) a proper protein processing that liberates the N-terminus of the protein, (ii) the pH and (iii) the presence or absence of calcium in the media.

Besides Bap, other less complex models of auto-aggregative cell-surface proteins with amyloid propensities, have been identified in different bacterial genera. Antigen I/II (also called P1 adhesin) is a cell-surface localized adhesin with a highly extended fibrillar structure produced by the cariogenic pathogen *Streptococcus mutans*. The protein contains two globular domains composed of  $\beta$ -sheet secondary structure that might be the responsible for amyloid fibers formation (Troffer-Charlier *et al.*, 2002; Larson *et al.*, 2010; Larson *et al.*, 2011; Oli *et al.*, 2012) (Fig. 40C). The  $\alpha$ -module of Ag43 autotransporter of *E. coli* (Ag43 $\alpha$ ) promotes bacterial auto-aggregation and biofilm formation, adopting a parallel right-handed  $\beta$ -helix conformation with numerous  $\beta$ -strands located in parallel orientation that resemble the amyloid structure established for curli (Klemm *et al.*, 2004; Otzen, 2012) (Fig. 40D). Despite showing some amyloidogenic propensities (Knudsen *et al.*, 2008) this structure cannot be considered a typical amyloid since it remains anchored to the cell surface and it is unable to polymerize into fibers.

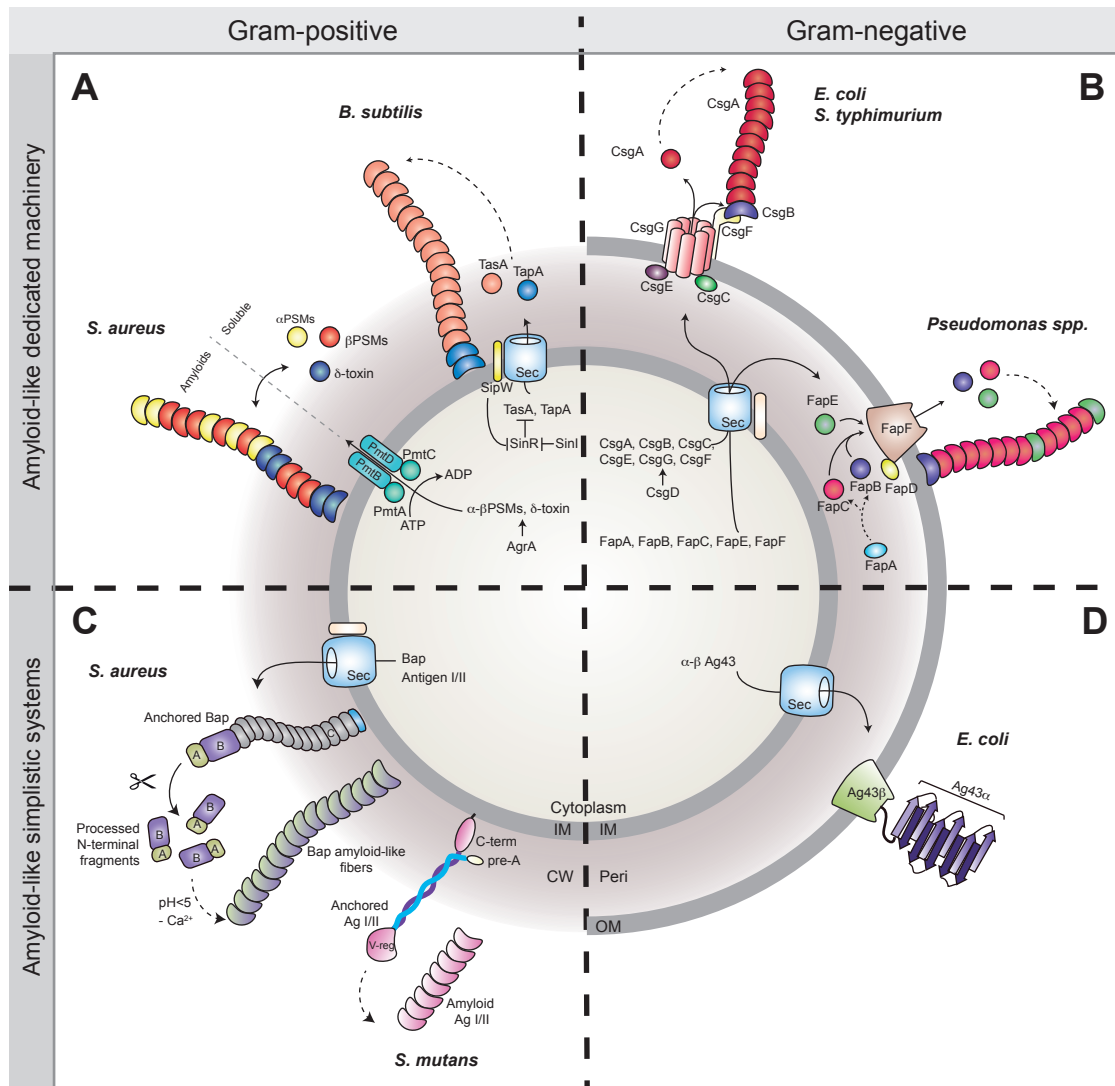


**Figure 40. Dedicated or simplistic amyloid-like fibers formation systems in gram-positive and gram-negative bacteria. A)** Sec export system secretes the products of *tapA-sipW-tasA* operon through the inner membrane (IM) of *B. subtilis*. SipW acts as a signal peptidase cleaving the signal peptide from TasA and TapA. TapA allows the anchorage of fibres to the cell wall (CW), and TasA is the major component of the fibers. In *S. aureus*  $\alpha$ -PSM,  $\beta$ -PSMs and  $\delta$ -toxin monomers are transported outside the cell through an ATP-dependent ABC transporter (PmtB and PmtD) transmembrane proteins, linked to ATPases PmtA and PmtC. PSMs can be present as soluble monomers, or, when required, forming amyloid-like fibers. **B)** All Fap and Csg proteins (except for CsgD) are expelled via Sec across the inner membrane. In the case of curli, the major fiber subunit CsgA and the nucleator CsgB are secreted across the outer membrane (OM) through CsgG channel, and once on the cell surface they start to polymerize into amyloidogenic fibers. Accessory proteins CsgC and CsgE regulate export by CsgG, and CsgF assist the nucleation of CsgA. In *Pseudomonas*, Fap B, FapC and FapE are further secreted across the outer membrane through FapF where FapB nucleates fiber assembly of FapC and, in minor proportion, FapE. FapA likely control FapB and FapC secretion, and FapD would act as a protease of Fap proteins. **C)** Once is anchored to the cell wall, Bap of *S. aureus* is processed by proteases present in the medium, liberating the N-terminal fragments that will ultimately self-assemble into amyloid-like fibrillar structures upon acidification of the media and in the absence of calcium. In *S. mutans*, non-attached P1 adhesin (Agl/II) would presumably form amyloidogenic fibers through its  $\beta$ -sheet rich V-region and C-terminal domain. **D)** The autotransporter Ag43 present in *E. coli*, though not considered a real amyloid, represents a very simplistic model of amyloid folding due to the high  $\beta$ -helix with  $\beta$ -strand conformation adopted by Ag43 $\alpha$  subunit at the bacterial envelope.

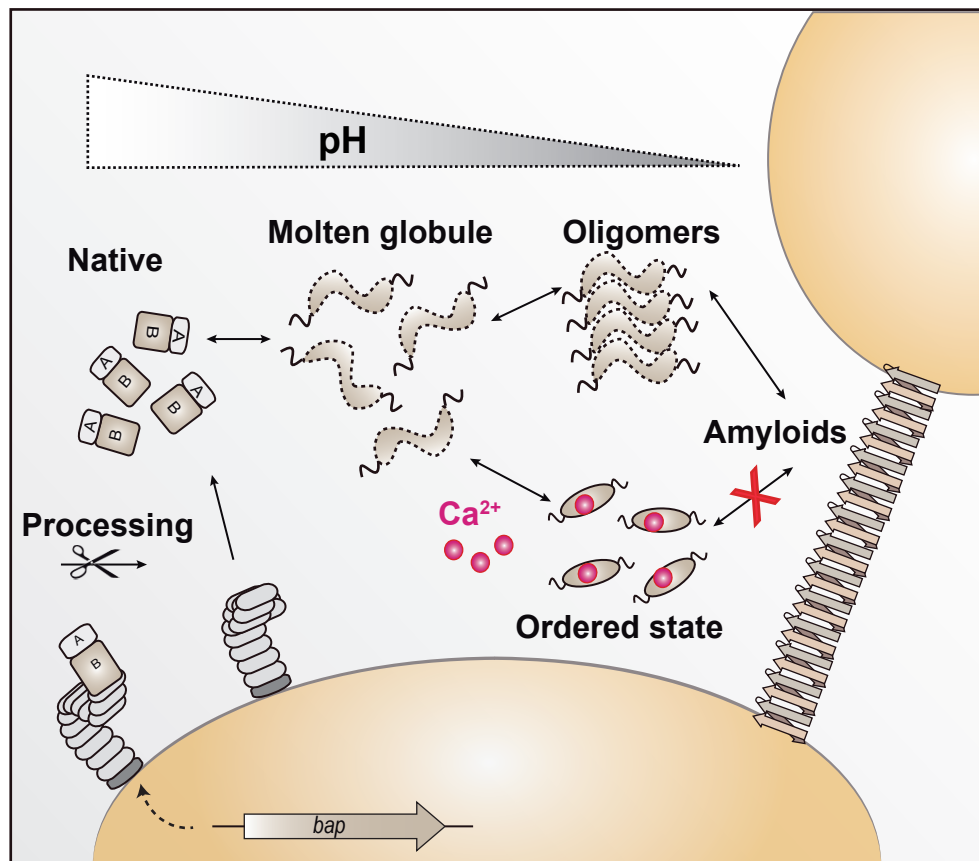


**Figure 41. Summary illustrating the effect of pH and calcium in Bap-mediated multicellular behavior.** Once located on the bacterial surface, Bap is processed liberating N-terminal fragments that adopt a molten globule-like transient state. In acidic environments, Bap N-terminal fragments start to self-assemble and ultimately form amyloid fibers that mediate cell-to-cell contacts and biofilm formation through the interaction with the bacterial cell surface by a still unknown mechanism. On the contrary, and in spite of medium acidification, the presence of calcium divalent cations bound to Bap stabilizes the molten globule-like state of the protein. Consequently, Bap is unable to self-assemble into amyloid fibers and does not mediate biofilm formation.



- **Bap amyloids formation is regulated by two factors: pH and calcium.**

Amyloid structures are especially well suited for assembling the biofilm matrix scaffold, as polymerization can occur in the extracellular media in the absence of energy and can be influenced by several environmental factors.

Medium pH can impact protein assembly because it affects the properties of proteins and their behavior in a particular solution by determining the charge distribution on the protein surface. As shown by our results, pH has a profound effect on Bap conformation: when pH becomes mildly acid, region B of Bap undergoes a conformational change towards the amyloidogenic state inducing its polymerization into fibrillar structures which will ultimately mediate staphylococcal biofilm formation. The pH at which Bap shows aggregation activity (pH~5, early stationary phase) is very close to the isoelectric point (pI~4.61), where lack of a net charge facilitates interactions between protein molecules, making protein self-assembly more likely. Indeed, a large number of globular and non-globular proteins, including the pathogenic amyloid- $\beta$  peptide and  $\alpha$ -synuclein have been shown to display maximum amyloid propensity when they approach their pI, indicating that the solubility of a polypeptide chain is a major factor determining its conversion to the amyloid state (Schmittschmitt and Scholtz, 2003). As another example, TasA oligomers purified in its native state *in vivo* from *B. subtilis* are stable at basic solution conditions, where the pH stays above TasA isoelectric point (pI~5) (Chai *et al.*, 2013). Exposure of such oligomers to acidic solution conditions induce a conformational change from  $\alpha$ -helix to  $\beta$ -sheet secondary structure and their assembly into fibrous aggregates (Chai *et al.*, 2013).

The ability to fluctuate between soluble and amyloid-like states has been shown to underlie several key physiological events such as the cellular response to DNA breakage (Altmeyer *et al.*, 2015), the integrity of the cytoskeleton (Li *et al.*, 2014) and processing bodies and stress granules formation (Kato *et al.*, 2012). An example in bacteria is the amyloid formation process of Microcin E492 (Mcc) produced by *Klebsiella pneumoniae*. To maintain homeostasis of the microbial ecosystem, Mcc aggregates and disaggregates upon small changes in pH, NaCl concentration and dilution (Shahnawaz and Soto, 2012). In this regard, we proved that Bap assembly can be reversed when pH is restored to neutrality, showing that Bap is able to withstand pH fluctuations, adapting its function by switching from aggregated to soluble forms (and *vice versa*) and thus determine the destiny of a formed biofilm, as shown by our disaggregation experiments (Fig. 11). In *S. aureus* this mechanism may have a relevant physiological effect in several host niches colonized by the bacteria that display mildly acidic conditions (e.g., skin, anterior nares, vagina, urinary tract and mouth) (Weinrick *et al.*, 2004; Wollenberg *et al.*, 2014), or in infectious processes, in which local acidosis usually arises from the accumulation of acidic products as a result of an inflammatory response (Lardner, 2001) and bacterial metabolism. In a similar way, Foulston *et al.* (Foulston *et al.*, 2014) demonstrated that many cytoplasmic proteins reversibly associate with the cell surface in response to pH, acting as biofilm scaffold matrix proteins in *S. aureus*. Also, phenol soluble modulins (PSMs) switch from soluble to amyloid fibrillar state to regulates the disassembly activity of PSMs monomers in the microenvironment of biofilms (Schwartz *et al.*, 2012).

The capacity to aggregate often depends on changes in protein folding caused by binding to metal ions, as occurs in eukaryotes for several proteins involved in amyloidogenic disorders (Leal *et al.*, 2012). This is the

case of S100A6, an amyloid protein largely expressed in patients with Amyotrophic Lateral Sclerosis (ALS) disease. When S100A6 binds calcium, it suffers a remodeling of the surface electrostatics and hydrophobic patch exposure at the aggregation hotspots inhibiting protein self-assembly into amyloid fibrils (Botelho *et al.*, 2012). In the case of bacteria,  $\text{Ca}^{2+}$  bound to  $\alpha$ -haemolysin secreted by pathogenic *E. coli*, makes the protein more compact, stabilizing its structure and making it less prone to oligomerization (Sánchez-Magraner *et al.*, 2010). We have shown that Bap adopts a molten globule-like state in the absence of calcium. The molten globule is defined as a partially unfolded intermediate state between the native and the completely denatured protein conformation. The establishment of this precursor is important for the aggregation process, since hydrophobic patches are more exposed and have higher flexibility compared to the folded state. Completely folded or unfolded proteins, in contrast, do not aggregate easily since the hydrophobic side chains are either mostly buried out of contact with water or randomly scattered (W Wang and Roberts, 2010). In the presence of calcium, altered charge-charge intramolecular interactions upon ion binding to the N-terminal fragments of Bap do not modify their secondary structure but clearly cause tertiary rearrangements that increase the stability of the molten globule-like state of the protein in solution and thus decrease its aggregation behavior. This hinders the polymerization of Bap fibers *in vitro* and *in vivo*, subsequently preventing cellular interactions and biofilm formation. This effect of calcium on Bap functionality might serve to explain how changes in  $\text{Ca}^{2+}$  levels during the stages of the lactation cycle affect intramammary infections caused by *S. aureus*. Bap displays low binding affinity to calcium, thus medium-to-high millimolar concentrations of the cation are required to saturate  $\text{Ca}^{2+}$ -binding sites in the protein. Normally, the concentration of free  $\text{Ca}^{2+}$  in mammalian

blood is strictly maintained between 1.1-1.3 mM (Brown *et al.*, 1995; Maurer *et al.*, 1996). However, the total  $\text{Ca}^{2+}$  concentration in milk is higher, around 1.2 mg/liter (~30 mM), being one third of this total amount free in serum (~11 mM) (Fox and McSweeney, 1998). Thus,  $\text{Ca}^{2+}$  levels present in the milk during the lactation period are sufficient to inhibit Bap-mediated biofilm development, while the low  $\text{Ca}^{2+}$ -concentration conditions that occurs in the udder during the dry period allows the formation of Bap-mediated biofilms and the establishment of long-term persistent infections on the mammary gland epithelium (Arrizubieta *et al.*, 2004) (Fig. 43).

- **Importance of amyloid sequence stretches in Bap self-fibrillation process**

The amyloid fibril formation is not just a general property of the polypeptide backbone depending on external factors, but it is strongly modulated by amino acid side chains (Esteras-Chopo *et al.*, 2005). The propensity of a given protein to aggregate and form amyloid fibrils under certain conditions may, to a large extent, be determined by the properties of short specific regions of its sequence, called “amyloid stretches” (Ventura *et al.*, 2004).

As demonstrated in this work, Bap is capable to polymerize without the involvement of a nucleator-dedicated protein. Concordantly, we identified two potential “hotspots” with strong amyloidogenic features similar to amyloid stretched identified in other proteins (Ventura *et al.*, 2004; Ivanova *et al.*, 2004; Esteras-Chopo *et al.*, 2005; Giraldo, 2007) (Fig. 19), that likely initiate Bap assembly into amyloids. Usually amyloid formation kinetic follows a sigmoidal shape where a lag phase indicates the assembly of monomers into oligomeric structures required for fiber polymerization (Epstein and Chapman, 2008). However, when monitoring rBap\_B

aggregation kinetics we observed no presence of a lag phase (Fig. 29C). This reflects a very fast nucleation process triggered by the formation of aggregation nuclei from soluble Bap monomers. In this context, the two identified amyloid short stretches (peptide I<sub>487</sub>TVGNIISNAG<sub>496</sub> and peptide II<sub>579</sub>GIFSYS<sub>584</sub>), presumably with other amyloidogenic “hot-spots” present in Bap N-terminal sequence, could be key mediators of the auto-aggregation process: their exposure and accessibility in the soluble Bap N-terminal fragments would favor intermolecular interactions that trigger the self-assembly reaction and pull the rest of the protein into the fibrillar aggregate. The identification of the exact sequence stretches of Bap relevant for biofilm formation *in vivo* will require additional studies. The presence of multiple amyloid stretches appears to be a common feature of bacterial amyloids: curli protein CsgA of *E. coli* contains two amyloidogenic domains that are critical for amyloid fibrils formation *in vivo* (X Wang *et al.*, 2007; Wang *et al.*, 2008), and ChpH produced by *Streptomyces coelicolor* has two amyloid domains both important for amyloid fibers assembly (Sawyer *et al.*, 2012).

Recently, a few interesting works have demonstrated a close association between functional amyloid fibers and extracellular DNA in a biofilm environment. More specifically, eDNA favors the assembly of CsgA and forms highly stable complexes with curli in *Salmonella typhimurium* biofilms (Gallo *et al.*, 2015). In *S. aureus*, the presence of eDNA is necessary to nucleate the polymerization of PSMs monomers, resulting in the formation of stable nucleic acid-amyloids complexes (Schwartz *et al.*, 2016). So, these evidences suggest that other molecules present in the biofilm matrix may support the polymerization step during amyloidogenesis, making us wonder if a similar mechanism could also assist self-assembly of Bap fibers.

- **Interaction of Bap amyloid-like fibrils with the bacterial surface.**

One of the questions that remains open from this study is how Bap amyloid fibers are anchored to the cell surface and how do they interact with bacterial surface to induce cell-to-cell aggregation? Different mechanisms have been described in other bacteria. *Streptomyces coelicolor* produces amyloid fibers that are made up of eight different chaplins (ChpA-H), three of which (large chaplins, ChpA-C) are covalently linked to the cell wall through the action of a sortase (Claessen, 2003; Claessen *et al.*, 2006). It has been proposed that chaplins ChpA-C contribute to anchoring the fibers to the cell surface (De Jong *et al.*, 2009). In *B. subtilis*, TasA fibers formation is assisted by TapA, which functions as a dual protein by anchoring the amyloid fibers to the cell wall as well as nucleating fiber polymerization. TapA localizes to the cell wall where it is necessary to support TasA fiber formation and attachment. Interestingly, TapA functionality does not depend on the two sortases present in *B. subtilis*, YhcS and YwpE, since a double mutant shows similar biofilm formation capacity compared to wild type strain. Thus, the mechanism of TapA linkage to the cell wall remains still unknown (Romero *et al.*, 2011). Also, pili produced by *Mycobacterium tuberculosis* are assembled in a sortase-independent manner since this bacterium lacks any identifiable sortase-encoding gene (Paterson and Mitchell, 2004). In our case, one would expect that Bap amyloid fibers might interact with the C-terminal domain of Bap that remains covalently anchored to the cell wall by a sortase-dependent mechanism. However, the finding that extracellular addition of rBap\_B to *bap* deficient *S. aureus* strains (Fig. 17C), *S. aureus* 132 *srtA* mutant and also to *L. monocytogenes* and *E. faecalis* (Fig. 26A) promoted intercellular adhesion makes this possibility unlikely. Surprisingly, the interbacterial aggregation did not occurred when rBap\_B was added to two gram-negative strains (Fig. 26B). Cell envelope of

gram-negative bacteria is more rigid and negatively charged compared to the surface of gram-positive bacteria (Sonohara *et al.*, 1995). Possibly, these differences have an impact on the intermolecular non-covalent interactions (Van der Waals and interionic forces) between Bap and the elements present in the envelope such as peptidoglycan or surface attached molecules (polysaccharides, lipids, proteins). Further clarification is obviously required.

- **Bap orthologous proteins display amyloidogenic features.**

Curli homologs have been previously identified in *Salmonella* (named Tafi, for thin aggregative fimbriae) as well as in other genera of the *Enterobacteriaceae* family, mainly *Citrobacter* and *Enterobacter* (Zogaj *et al.*, 2003). Recently, homologs were found in some families within at least four phyla: *Proteobacteria*, *Bacteroidetes* and a single *Firmicutes* and *Thermodesulfobacteria* strain (Dueholm *et al.*, 2012). The Fap amyloid system is conserved in several pathogenic and environmental *Pseudomonas* strains (Dueholm *et al.*, 2010; Dueholm *et al.*, 2013a) and genomic studies identified homologous Fap system also within species belonging to the *Beta-*, *Gamma-* and *Deltaproteobacteria* (Dueholm *et al.*, 2013a). Moreover, TasA expression is not limited to *B. subtilis*. A specific genomic region that contains two independent genomic factors that are both necessary for biofilm development through the assembly of TasA amyloid fibers was recently found in *Bacillus cereus* (Caro-Astorga *et al.*, 2014)

Similarly, Bap orthologous proteins were found in several coagulase negative staphylococci (CNS) able to induce biofilm formation and usually associated with chronic mastitis infections (Tormo *et al.*, 2005). In the present work, we established that Bap orthologs act through similar molecular mechanisms described for Bap from *S. aureus* to mediate biofilm development. By using the C-DAG system described by Sivanathan *et al.*

(Sivanathan and Hochschild, 2013), we showed that several Bap orthologs displayed amyloidogenic propensities (Fig. 36). Moreover, a more detailed biophysical analysis of the Bap protein present in the human pathogen *S. saprophyticus* demonstrated its amyloidogenic behavior. *S. saprophyticus* is a notable uropathogen of uncomplicated urinary tract infections (Kuroda *et al.*, 2005). The pH of the urinary tract varies between 4.5 and 7 (Weinrick *et al.*, 2004), representing an environment in which Bap, through the formation of amyloid-like aggregates and together with urease, UafA (Kuroda *et al.*, 2005) and other virulence factors (Park *et al.*, 2010) could play an important role in the survival and uropathogenesis of *S. saprophyticus*.

Considering the predicted theoretical isoelectric points of the Bap orthologous proteins (Table 5) and medium-to-high percentage of identity with Bap, it is tempting to predict that they will all have high tendency to aggregate at acidic pH, meaning that, just like Bap\_B from *S. aureus* and *S. saprophyticus*, a pH-driven amyloidogenic fibrillization process would likely be the responsible for bacterial clumping and biofilm formation in those strains.

Except for *S. saprophyticus* and *S. simiae*, the rest of CNS strains used in this study were mostly isolated from mastitis of lactating dairy cows (cultured from milk samples), a physiological situation in which the presence of calcium can actually play a relevant role in regulating the functionality of Bap. The diversity of yet unknown factors that could affect Bap amyloid behavior among different bacterial species and under variable environmental conditions is worthy of further study.

As previously stated, amyloidogenic stretches found in Bap seems to be important for the fibrillation process. The presence of these “hotspots” in Bap orthologs could be an additional evidence of the amyloidogenic behavior of these proteins (Fig. 42). However, the absence of the same sequences stretches in orthologs with medium-to-low sequence identity to



Bap, as in the case of *S. saprophyticus*, should not be interpreted as a lack of amyloid behavior of these proteins, since the ability to form amyloid fibrils is considered to be an inherent property of the polypeptide chain, rather than the special property of any given sequence element. Thus, as observed for *S. aureus*, other potential amyloid short spots apart from the ones identified in this work, would trigger fibrillation of Bap in CNS strains.

Lastly, surface proteins homologous to Bap and involved in biofilm development are present in *Salmonella enterica* (Latasa *et al.*, 2005), *Pseudomonas fluorescens* (Hinsa *et al.*, 2003), *Enterococcus faecalis* (Toledo-Arana *et al.*, 2001) and *Burkholderia cepacia* (Huber *et al.*, 2002). It would be interesting to analyze, from a structural and biological point of view, the mechanisms by which these other Bap-like proteins promote or contribute to biofilm formation.

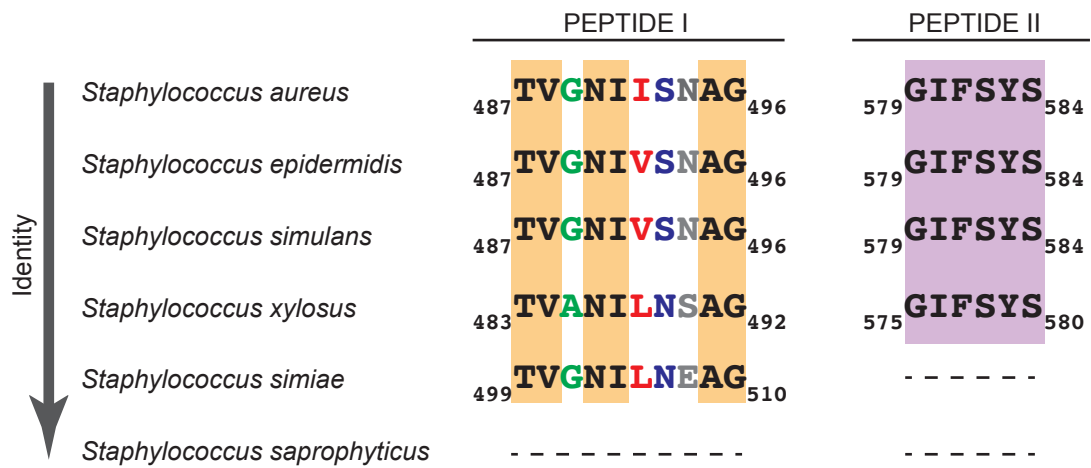


**Figure 42. Conservation of amyloidogenic peptides I and II present in Bap of *S. aureus* among Bap orthologous strains.** Strains are ordered according to decreasing identity percentage (grey arrow, see also Table 5 in Results section). Numbers indicate amino acidic positions. Conserved residues are shown in orange for peptide I and in violet for peptide II. Variable residues are shown in different colored letters (green, red, blue and grey) according to different residue positions.

- **Contextualization of Bap-mediated multicellular behavior in the physiological situation of mastitis.**

*S. aureus* is the major etiological agent of bovine mastitis, which is one of the most complex and costly diseases of the dairy industry (Harmon, 1994). Clinical infections are accompanied by local symptoms in the udder, systemic signs and alterations in milk, while subclinical infections are those for which no visible changes occur in the appearance of the milk or the udder, but milk production decreases, its composition is altered and bacteria are present in the secretion (Harmon, 1994). To establish an infection, *S. aureus* produces several virulence factors (surface-associated factors, degradative enzymes, staphylococcal enterotoxins). Biofilm formation has to be also considered very important in virulence, since it contribute to the persistence of the infection in the mammary gland (Veh *et al.*, 2015).

Early studies of Bap and its role in *S. aureus* pathogenesis established that Bap-positive strains display enhanced adherence but decreased invasion of bacteria to the mammary epithelium, with biofilm formation and the subsequent establishment of long-term persistent infections. In this scenario, antibiotic treatment is less effective and bacteria within the biofilm mediate immune evasion by masking surface antigens (Cucarella *et al.*, 2001; Cucarella *et al.*, 2002; Cucarella *et al.*, 2004; Valle *et al.*, 2012). According to this and based on the results obtained in the present study, we tried to fit Bap molecular model of fibers formation and biofilm development within the physiological situation of mastitis. During lactation period, *S. aureus* Bap-positive bacteria, presumably together with other potential contaminants like *Streptococcus agalactiae*, initiate the infection either by colonization of the teat canal with bacteria derived from infected epidermis or by an influx of contaminated milk entering the gland, a problem due to deficient management practices. Bacteria adapt and multiply in the milk, gaining access to the upper part of the gland (Cucarella *et al.*,

2004). Once there, *S. aureus* would adhere to the alveolar epithelium through cell wall anchored-Bap interaction with host receptors (Valle *et al.*, 2012), where the presence and number of C-repeats, though not being necessary for biofilm formation, would be relevant in the host-pathogen interaction (Tormo *et al.*, 2005; Valle *et al.*, 2012). According to our results, Bap N-terminal fragments are released by proteolysis, but the presence of millimolar concentrations of calcium in milk would inhibit the formation of amyloid-like Bap fibers. At this moment, bacteria would be mostly planktonic, with possible horizontal spread (Fig. 43A). However, fluctuations in the calcium concentration occur in the mammary gland environment: increased permeability of blood vessels and concomitant altered ionic chemical balances lowers local  $\text{Ca}^{2+}$  levels in the inflamed tissue (Radostits *et al.*, 2006).  $\text{Ca}^{2+}$  variations can occur also between lactation and dry period. During this latter phase of the mammary cycle, microcolonies attached to the epithelium start to form. The pH within these microenvironments would become mildly acidic as a consequence of bacterial metabolism, allowing N-terminal Bap domains to self-assemble into amyloid-like fibrillar structures that hold bacterial cells together and improve adhesion to epithelial cells. Thus, a chronic infection would be established in the animal, providing a bacterial reservoir (Fig. 43B).

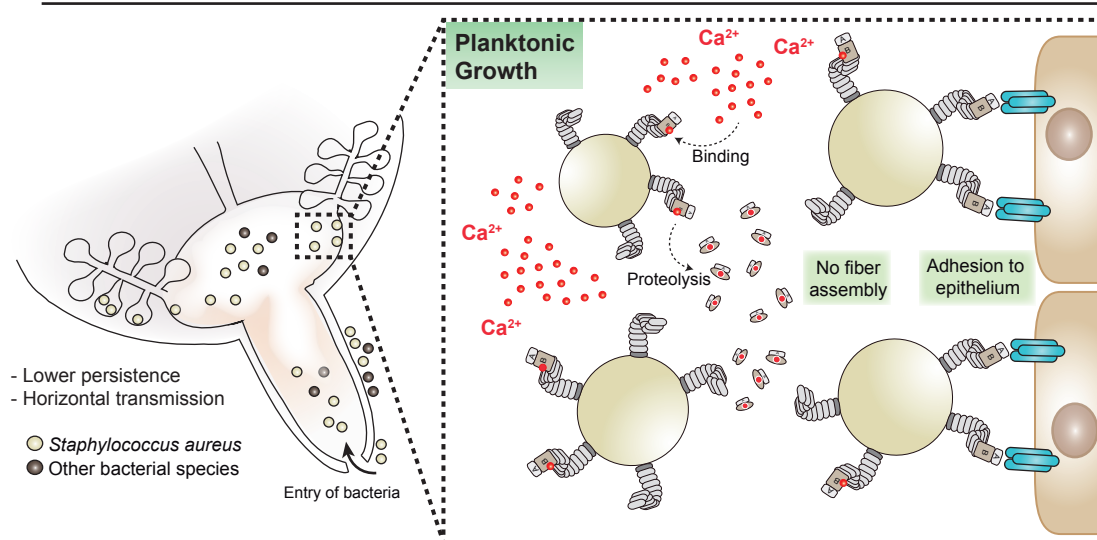
Antibiotic therapy to control chronic bovine mastitis is usually administer during dry period and is frequently chosen without taking into account the role of biofilm formation on resistance (Cucarella *et al.*, 2004). As high concentrations of many known antibiotics are required to kill biofilm bacteria there is a need to find more efficient antimicrobials to fight these infections. In this work we show that (-)-epi-gallocatechine gallate (EGCG) inhibits formation of Bap aggregates and disassemble Bap-mediated biofilm *in vitro*. This polyphenol is a potent remodeling agent of mature amyloid fibrils and inhibits fibrillation of human aberrant amyloids (Ehrnhoefer *et al.*,

2008; Bieschke *et al.*, 2010). It was shown that EGCG had also an inhibitory effect on *Streptococcus mutans* biofilm formation, and prevented amyloid fibrillation *in vitro* of *S. mutans* extracellular proteins (Oli *et al.*, 2012). The inhibitory activity of EGCG on *S. aureus* Bap-mediated biofilm formation suggest the potential role of this agent as an alternative strategy for controlling chronic mastitis.

Several compounds that interfere with the biogenesis of well-studied bacterial amyloid fibers like curli and TasA are starting to emerge. The first molecule to show inhibitory properties against biofilm amyloid fibrils was the ring-fused 2-pyridone called FN075, which is an analogue of BipC10 pilicide compound. FN075 proved to significantly reduce the polymerization of the main curli subunit CsgA and the biogenesis of curli and type 1 pili in uropathogenic *E. coli* (Cegelski *et al.*, 2009). This double curlicide-pilicide property of FN075 is important from a therapeutic point of view because *E. coli* can use both structures, pili or curli, to promote surface attachment and subsequent biofilm formation (Cegelski *et al.*, 2009). Authors further tested FN075 in a mouse urinary tract infection model to evaluate inhibitory activity *in vivo*. Pretreatment with FN075 of uropathogenic *E. coli* grown under pili-forming but not curli-forming conditions, significantly attenuated virulence demonstrating the importance of inhibiting pili formation to decrease infection (Cegelski *et al.*, 2009). However, direct treatment to validate its protective role in animal infection models remains to be done. Romero and collaborators (Romero *et al.*, 2013) used a simple screening method based on the alteration of *B. subtilis* wrinkly biofilm phenotype to search for possible anti-biofilm compounds. They successfully identified that AA-861, a benzoquinone derivative with anti-inflammatory activity and parthenolide, a sesquiterpene lactone with anti-inflammatory and anti-cancer activities, inhibited TasA polymerization into amyloid-like fibers *in vitro* (Romero *et al.*, 2013). Interestingly, AA-861 was more efficient to inhibit TasA

polymerization whereas parthenolide was more potent destroying pre-formed biofilms *in vivo* indicating that these molecules can work additively to inhibit biofilm formation (Romero *et al.*, 2013). In a recent report, Rifapentine, an antibiotic that targets RNA polymerase and is often used to treat tuberculosis, was shown to inhibit curli-dependent biofilm formation on different surfaces at a concentration that did not alter bacterial growth (Maher *et al.*, 2015). Lastly, it has been recently reported that the periplasmic protein CsgC is highly effective inhibiting human  $\alpha$ -synuclein and CsgA amyloid formation, while it does not affect polymerization of A $\beta$ <sub>42</sub> (Evans *et al.*, 2015; Klein and Hultgren, 2015). Further large-scale screenings are necessary to identify more molecules with inhibitory activities against amyloid proteins that could serve to control bacterial infections.

## A LACTATION



## B DRY PERIOD

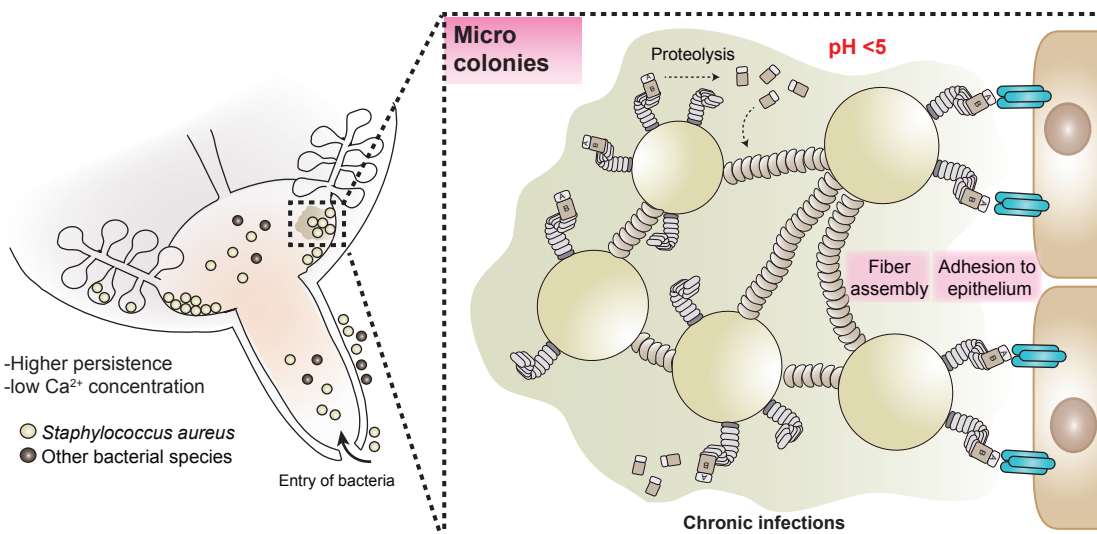


**Figure 43. Bap fibers model in the context of subclinical bovine mastitis. A)** During lactation, bacteria may enter the teat canal and arrive to the gland cistern where they proliferate and adhere to ductural and alveolar epithelium through the interaction of cell wall anchored Bap protein with host receptors. Calcium present at high concentration in the milk produced by the gland binds to Bap N-terminal fragments, which cannot self-assemble into fibrils due to conformational stabilization. The bacteria mostly growth planktonically, with possible horizontal spread to the offspring. **B)** In the dry period of lactation cycle, *S. aureus* adhered to the mammary epithelium are exposed to lower concentrations of calcium; microcolonies start to develop, in which pH decreases as a consequence of bacterial metabolism. Thus, Bap N-terminal fragments are now able to form amyloid-like fibrillar structures to maintain bacteria interacting with each other. Persistent infections take place under this condition, hindering their eradication with antibiotic treatment.

- **Possible biotechnological applications of Bap fibers**

The self-assembly properties of numerous amyloidogenic motifs, together with their observed polymorphism, makes them attractive natural building blocks for the design of new nanostructures and nanomaterials (Cherny and Gazit, 2008).

Amyloids are highly stable structures that can lead to the formation of complex networks of filaments, gels and films, which can be functionalized for specific applications; they display structural plasticity with the possibility of reverse its formation under certain conditions (Mankar *et al.*, 2011).

Recently, two elegant works have utilized the properties of bacterial curli fibers and engineered artificial cellular consortia such as biofilm, for biotechnological applications. Chen and co-workers (Chen *et al.*, 2014) developed an externally controllable and autonomous patterning of amyloid fibrils assembly by *E. coli* cells. The proposed system constitutes a versatile scaffold that is able to synthesize gold nanowires, nanorods and nanoparticles, composing switchable conductive biofilms. The other work describes a Biofilm-Integrated Nanofiber Display (BIND) system through which is possible to precisely genetically program the *E. coli* biofilm extracellular material by fusing functional peptide domains to the CsgA protein. This technique is compatible with a wide range of peptide domains of various lengths and secondary structures since they maintain their function after secretion and assembly, conferring artificial functions to the biofilm as a whole (Nguyen *et al.*, 2014) (Fig. 44A). Based on this work, Botyanszki *et al* (Botyanszki *et al.*, 2015) exploited the curli system of *E. coli* to create a biocatalytic biofilm in which a network of functional nanofiber are capable of covalently and site-specifically immobilize an industrially relevant enzyme, the  $\alpha$ -amylase.

In a similar way, we pretended to test the potential of Bap fibers as a



biofunctional material. We fused the protein with different peptide tags. Our results suggest that chimeric Bap-peptide constructs maintain their function after assembly, as demonstrated by aggregation phenotype and fluorescence microscopy of engineered *S. aureus* strains. Particularly, functionality of tagged Bap proteins was influenced by pH fluctuations in the media (pH>7 and pH<5), as observed for wild type Bap, indicating that pH could be used to voluntarily control the formation or disruption of programmed biofilms (Fig. 44B). This recycling behavior of amyloid fibrils may be exploited for specific applications such as drug delivery (Mankar *et al.*, 2011). For example, the property of reversible self-assembly has been used to formulate long-acting drugs where controlled release of peptide molecules occurs from the fibrils termini (Maji *et al.*, 2008).

When bacterial clumps composed of Bap<sup>SpyTag</sup> were incubated with rGFP-SpyCatcher, the reaction resulted in covalent attachment (Fig. 39B and D). Thus, other protein sequences instead of GFP could be fused to the SpyCatcher sequence, incorporating a vast range of functions to the *S. aureus* biofilm (Fig. 39E). However, it must be noticed that Bap fibers are likely less defined than curli, since fluorescence microscopy of Bap<sup>SpyTag</sup> or Bap<sup>SNAPtag</sup> fibers only detected a blurred labeling around cells under fibril-forming conditions. This feature of Bap fibers compared to other amyloids, instead of representing a handicap could be actually an advantage for some biotechnological purposes, as observed for amyloids with relatively low stability used as drug reservoirs due to high drug release capacity (Maji *et al.*, 2008).

Amyloid fibers can also be utilized for the development of scaffolds for tissue engineering applications (Mankar *et al.*, 2011). We show in this work that purified amyloidogenic stretches identified from Bap sequence (peptide I and II) formed macroscopically visible hydrogels composed of fibrous structures when observed by TEM (Fig. 21B). This property could

have several uses in biotechnology. It has been proposed that amyloid-based hydrogels, as determined for other self-assembling peptides (Kisiday *et al.*, 2002), may be an attractive platform for growing and maintaining stem cells *in vitro*, as well as direct their differentiation by the modulation of fibril diameter, alignment and nanotopography. Recent work also suggests that hydrogels formed from curly-amyloid fibrils of  $\alpha$ -synuclein can serve as a suitable nanomatrix for enzyme entrapment (Bhak *et al.*, 2010).

Bap system holds biotechnological potential, although deeper examinations, stability studies and optimization as well as precise control of physicochemical properties of Bap fibrillar assemblies is fundamental to come up with an efficient Bap-made technological nanomaterial.

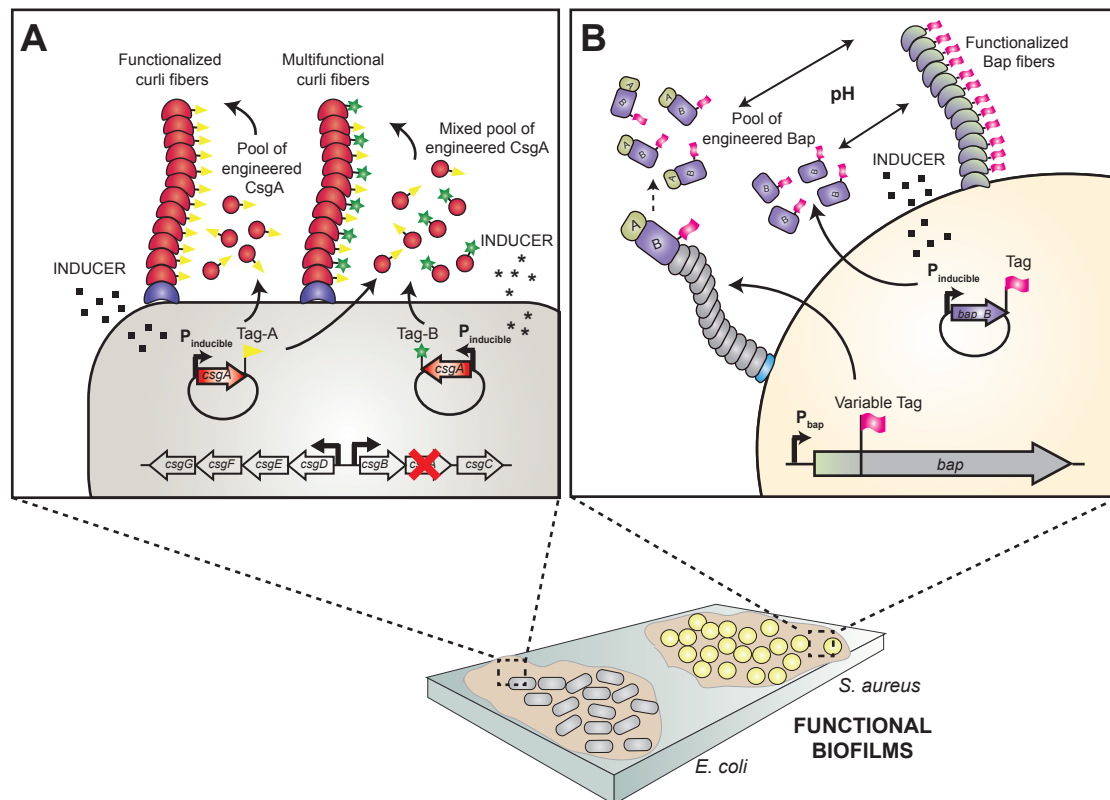


**Figure 44. Development of functionalized amyloid-dependent biofilms in gram-negative and gram-positive bacteria. A)** In *E. coli*, the major curli protein CsgA is engineered by fusing variable tags at its C-terminus. Once at the extracellular media, the fusion protein self-assembles into functional amyloid nanofibers. It is possible to obtain multifunctional biofilms by expressing engineered CsgA proteins under the control of different inducible promoters. The addition of measured concentrations of inducer molecules grants the expression and production of curli fibers containing precise multiple designed functions as a result of random extracellular self-assembly of CsgA monomers. **B)** In the case of *S. aureus*, variable tags fused to the C-terminal part of B domain of Bap could allow the formation of engineered Bap fibers. Since the B domain (amino acids 362 to 819) is sufficient to bestow multicellular behavior, it could be possible to express engineered Bap<sub>B</sub> proteins under the control of an inducible promoter. The property of Bap to reversibly form amyloids according to pH levels in the media could be used as an external way to control the formation or disruption of functionalized biofilms.



## ***CONCLUSIONS***

---



## CONCLUSIONS

1. Bap protein is constitutively expressed along the growth curve of *S. aureus* and following cell division it becomes distributed across the cell surface directed by the presence of a YSIRK/GS motif in the signal peptide.
2. After secretion, Bap undergoes a limited proteolytic processing. As a result, N-terminal fragments are released and self-assemble into amyloid-like fibrillar structures when the environment reaches mildly acidic pH values. The pH-dependent assembly of Bap into amyloid fibers is reversible.
3. Several evidences support the amyloid-like properties of aggregates formed by the B domain of Bap: far-UV CD spectra reveal a modest switch in secondary structure of Bap from disordered to  $\beta$ -sheet conformation, as the pH becomes more acid; the FTIR spectrum of Bap aggregates is dominated by  $\beta$ -sheet/ $\beta$ -turn secondary structure; rBap\_B recombinant protein forms aggregates that display fibrillar morphology when observed by electron microscopy and bind to the amyloid diagnostic dyes Thioflavin-T, Congo Red and ProteoStat; rBap\_B recombinant protein contains short-sequence stretches with significant amyloidogenic potential, which form fibrillar hydrogels by themselves; Bap aggregates and Bap-mediated biofilm are successfully disaggregated by the anti-amyloid compound epigallocatechine gallate (EGCG).

4. The molten globule-like state adopted by Bap N-terminal fragments is stabilized upon binding of  $\text{Ca}^{2+}$  to the EF-hand motifs present in the B domain, thus inhibiting the proper self-assembly into amyloid fibers.
5. The formation of Bap fibers is important in the host-pathogen interaction: *bap*-positive bacteria grown under amyloid-forming conditions show improved adhesion to host epithelial mammary gland cells, and higher capacity to develop biofilm-associated infections in implants.
6. Functional and biophysical analyses of the B domain of Bap from *S. saprophyticus* reveal that this protein forms amyloid-like structures *in vitro* in order to favor multicellular behaviour. The pH-driven mechanism of Bap amyloid-like aggregation described here may be widespread among staphylococci as a way to mediate biofilm formation.
7. *S. aureus* strains expressing chimeric Bap proteins fused to different peptide tags (His-tag, 3xflag-tag, SNAPtag, SpyTag) retain the capacity to induce bacterial aggregation and Bap fibers-based biofilm matrices under acidic conditions. This property could be used to develop functionalized biofilms.



## ***CONCLUSIONES***

---



## CONCLUSIONES

1. La proteína Bap se expresa constitutivamente a lo largo de la curva de crecimiento de *S. aureus* y se localiza en la superficie celular dirigida por su péptido señal que contiene el motivo YSIRK/GS.
2. Tras ser secretada, Bap es parcialmente procesada. Fragmentos de la región N-terminal son liberados al medio y se autoensamblan en estructuras fibrilares de tipo amiloide cuando el pH del medio alcanza valores ácidos. El ensamblaje de fragmentos de Bap en fibras amiloides en función del pH es un proceso reversible.
3. Varias evidencias avalan las propiedades amiloidogénicas de los agregados formados por el dominio B de Bap: los espectros de dicroísmo circular en UV lejano muestran un modesto cambio en la estructura secundaria de Bap de conformación desordenada a una estructura de tipo lamina- $\beta$ , conforme el pH se acidifica; en el espectro de Espectroscopia Infrarroja con Transformada de Fourier predominan estructuras secundarias de tipo lamina- $\beta$  y giros- $\beta$ ; la proteína recombinante rBap\_B forma agregados con morfología fibrilar detectados por microscopía electrónica, que son capaces de unir colorantes específicos para amiloides como son la Tioflavina-T, el Rojo Congo y ProteoStat; la proteína recombinante rBap\_B contiene secuencias cortas con alto potencial amiloidogénico y que son capaces de formar hidrogeles por sí mismos; los agregados y el biofilm mediado por Bap son completamente disgregados por el compuesto anti-amiloide galato de epigallocatequina (EGCG).

4. El estado de glóbulo fundido que adoptan los fragmentos de la región N-terminal de Bap se estabiliza tras la unión de iones  $\text{Ca}^{2+}$  a los motivos EF-hand presentes en la región B de Bap, inhibiendo así el correcto ensamblaje de los mismos en fibras amiloides.
5. La formación de las fibras amiloides por la proteína Bap es importante en la interacción huésped-patógeno: las bacterias *bap*-positivas crecidas en condiciones propicias para la formación de amiloides muestran mayor adhesión a células epiteliales de glándula mamaria y mayor capacidad de desarrollar infecciones asociadas a la formación de biofilms en implantes.
6. El análisis funcional y biofísico del dominio B de Bap de *S. saprophyticus* muestra que esta proteína es capaz de mediar el comportamiento multicelular formando estructuras de tipo amiloide a pH ácido, *in vitro*. El mecanismo aquí descrito de agregación amiloide de Bap dependiente de pH podría estar extendido entre estafilococos para favorecer el desarrollo de biofilms.
7. Cepas de *S. aureus* que expresan proteínas quiméricas de Bap etiquetadas con diferentes péptidos (His-tag, 3xflag-tag, SNAPtag, SpyTag) mantienen la capacidad de inducir la agregación bacteriana y la formación de biofilms mediado por Bap a pH ácido. Esta propiedad podría ser utilizada para la obtención de biofilms funcionalizados.

## ***REFERENCES***

---



---

## REFERENCES

- Abraham, N.M., and Jefferson, K.K. (2012) *Staphylococcus aureus* clumping factor B mediates biofilm formation in the absence of calcium. *Microbiology* **158**: 1504–1512.
- Allesen-Holm, M., Barken, K.B., Yang, L., Klausen, M., Webb, J.S., Kjelleberg, S., *et al.* (2006) A characterization of DNA release in *Pseudomonas aeruginosa* cultures and biofilms. *Mol Microbiol* **59**: 1114–1128.
- Altmeyer, M., Neelsen, K.J., Teloni, F., Pozdnyakova, I., Pellegrino, S., Grøfte, M., *et al.* (2015) Liquid demixing of intrinsically disordered proteins is seeded by poly (ADP-ribose). *Nat Commun* **6**: 8088.
- Archer, G.L. (1998) *Staphylococcus aureus*: a well-armed pathogen. *Clin Infect Dis* **26**: 1179–1181.
- Archer, N.K., Mazaitis, M.J., Costerton, J.W., Leid, J.G., Powers, M.E., and Shirtliff, M.E. (2011) *Staphylococcus aureus* biofilms: properties, regulation, and roles in human disease. *Virulence* **2**: 445–459.
- Arciola, C.R., Campoccia, D., Ravaioli, S., and Montanaro, L. (2015) Polysaccharide intercellular adhesin in biofilm: structural and regulatory aspects. *Front Cell Infect Microbiol* **5**: 7.
- Arnaud, M., Chastanet, A., and Débarbouillé, M. (2004) New vector for efficient allelic replacement in naturally nontransformable, low-GC-content, gram-positive bacteria. *Appl Environ Microbiol* **70**: 6887–6891.
- Arrizubieta, M.J., Toledo-Arana, A., Amorena, B., Penadés, J.R., and Lasa, I. (2004) Calcium inhibits Bap-dependent multicellular behavior in *Staphylococcus aureus*. *J Bacteriol* **186**: 7490–7498.
- Arvidson, S., and Tegmark, K. (2001) Regulation of virulence determinants in *Staphylococcus aureus*. *Int J Med Microbiol* **291**: 159–170.
- Baba, T., Takeuchi, F., Kuroda, M., Yuzawa, H., Aoki, K.-I., Oguchi, A., *et al.* (2002) Genome and virulence determinants of high virulence community-acquired MRSA. *Lancet* **359**: 1819–1827.
- Balestrino, D., Hamon, M.A., Dortet, L., Nahori, M.A., Pizarro-Cerda, J., Alignani, D., *et al.* (2010) Single-cell techniques using chromosomally tagged fluorescent bacteria to study *Listeria monocytogenes* infection processes. *Appl Environ Microbiol* **76**: 3625–3636.

## References

---

- Barbu, E.M., Mackenzie, C., Foster, T.J., and Höök, M. (2014) SdrC induces staphylococcal biofilm formation through a homophilic interaction. *Mol Microbiol* **94**: 172–185.
- Baselga, R., Albizu, I., and Amorena, B. (1994) *Staphylococcus aureus* capsule and slime as virulence factors in ruminant mastitis. A review. *Vet Microbiol* **39**: 195–204.
- Baselga, R., Albizu, I., La Cruz, De, M., Del Cacho, E., Barberan, M., and Amorena, B. (1993) Phase variation of slime production in *Staphylococcus aureus*: implications in colonization and virulence. *Infect Immun* **61**: 4857–4862.
- Berk, V., Fong, J.C.N., Dempsey, G.T., Develioglu, O.N., Zhuang, X., Liphardt, J., *et al.* (2012) Molecular architecture and assembly principles of *Vibrio cholerae* biofilms. *Science* **337**: 236–239.
- Bhak, G., Lee, S., Park, J.W., Cho, S., and Paik, S.R. (2010) Amyloid hydrogel derived from curly protein fibrils of alpha-synuclein. *Biomaterials* **31**: 5986–5995.
- Bieschke, J., Russ, J., Friedrich, R.P., Ehrnhoefer, D.E., Wobst, H., Neugebauer, K., and Wanker, E.E. (2010) EGCG remodels mature alpha-synuclein and amyloid-beta fibrils and reduces cellular toxicity. *Proc Natl Acad Sci USA* **107**: 7710–7715.
- Biswas, R., Voggu, L., Simon, U.K., Hentschel, P., Thumm, G., and Götz, F. (2006) Activity of the major staphylococcal autolysin Atl. *FEMS Microbiol Lett* **259**: 260–268.
- Borucki, M.K., Peppin, J.D., White, D., Loge, F., and Call, D.R. (2003) Variation in biofilm formation among strains of *Listeria monocytogenes*. *Appl Environ Microbiol* **69**: 7336–7342.
- Bose, J.L., Lehman, M.K., Fey, P.D., and Bayles, K.W. (2012) Contribution of the *Staphylococcus aureus* Atl AM and GL murein hydrolase activities in cell division, autolysis, and biofilm formation. *PLoS ONE* **7**: e42244.
- Botelho, H.M., Leal, S.S., Cardoso, I., Yanamandra, K., Morozova-Roche, L.A., Fritz, G., and Gomes, C.M. (2012) S100A6 amyloid fibril formation is calcium-modulated and enhances superoxide dismutase-1 (SOD1) aggregation. *J Biol Chem* **287**: 42233–42242.
- Botyanszki, Z., Tay, P.K.R., Nguyen, P.Q., Nussbaumer, M.G., and Joshi, N.S. (2015) Engineered catalytic biofilms: site-specific enzyme immobilization onto *E. coli* curli nanofibers. *Biotechnol Bioeng* **112**: 2016–2024.



- Brady, R.A., Leid, J.G., Calhoun, J.H., Costerton, J.W., and Shirtliff, M.E. (2008) Osteomyelitis and the role of biofilms in chronic infection. *FEMS Immunol Med Microbiol* **52**: 13–22.
- Branda, S.S., Chu, F., Kearns, D.B., Losick, R., and Kolter, R. (2006) A major protein component of the *Bacillus subtilis* biofilm matrix. *Mol Microbiol* **59**: 1229–1238.
- Brossard, K.A., and Campagnari, A.A. (2012) The *Acinetobacter baumannii* biofilm-associated protein plays a role in adherence to human epithelial cells. *Infect Immun* **80**: 228–233.
- Brown, E.M., Vassilev, P.M., and Hebert, S.C. (1995) Calcium ions as extracellular messengers. *Cell* **83**: 679–682.
- Caro-Astorga, J., Pérez-García, A., De Vicente, A., and Romero, D. (2014) A genomic region involved in the formation of adhesin fibers in *Bacillus cereus* biofilms. *Front Microbiol* **5**: 745.
- Carpentier, B., and Cerf, O. (1993) Biofilms and their consequences, with particular reference to hygiene in the food industry. *J Appl Bacteriol* **75**: 499–511.
- Castillo, V., Graña-Montes, R., Sabate, R., and Ventura, S. (2011) Prediction of the aggregation propensity of proteins from the primary sequence: aggregation properties of proteomes. *Biotechnol J* **6**: 674–685.
- Cegelski, L., Pinkner, J.S., Hammer, N.D., Cusumano, C.K., Hung, C.S., Chorell, E., *et al.* (2009) Small-molecule inhibitors target *Escherichia coli* amyloid biogenesis and biofilm formation. *Nat Chem Biol* **5**: 913–919.
- Chai, L., Romero, D., Kayatekin, C., Akabayov, B., Vlamakis, H., Losick, R., and Kolter, R. (2013) Isolation, characterization, and aggregation of a structured bacterial matrix precursor. *J Biol Chem* **288**: 17559–17568.
- Charpentier, E., Anton, A.I., Barry, P., Alfonso, B., Fang, Y., and Novick, R.P. (2004) Novel cassette-based shuttle vector system for gram-positive bacteria. *Appl Environ Microbiol* **70**: 6076–6085.
- Chatterjee, S.S., Joo, H.-S., Duong, A.C., Dieringer, T.D., Tan, V.Y., Song, Y., *et al.* (2013) Essential *Staphylococcus aureus* toxin export system. *Nat Med* **19**: 364–367.
- Chen, A.Y., Deng, Z., Billings, A.N., Seker, U.O.S., Lu, M.Y., Citorik,

- R.J., *et al.* (2014) Synthesis and patterning of tunable multiscale materials with engineered cells. *Nat Mater* **13**: 515–523.
- Chen, Y., Yan, F., Chai, Y., Liu, H., Kolter, R., Losick, R., and Guo, J.H. (2013) Biocontrol of tomato wilt disease by *Bacillus subtilis* isolates from natural environments depends on conserved genes mediating biofilm formation. *Environ Microbiol* **15**: 848–864.
  - Cherny, I., and Gazit, E. (2008) Amyloids: not only pathological agents but also ordered nanomaterials. *Angew Chem Int Ed Engl* **47**: 4062–4069.
  - Cheung, G.Y.C., Joo, H.-S., Chatterjee, S.S., and Otto, M. (2014) Phenol-soluble modulins - critical determinants of staphylococcal virulence. *FEMS Microbiol Rev* **38**: 698–719.
  - Claessen, D. (2003) A novel class of secreted hydrophobic proteins is involved in aerial hyphae formation in *Streptomyces coelicolor* by forming amyloid-like fibrils. *Gene Dev* **17**: 1714–1726.
  - Claessen, D., De Jong, W., Dijkhuizen, L., and Wösten, H.A.B. (2006) Regulation of *Streptomyces* development: reach for the sky! *Trends Microbiol* **14**: 313–319.
  - Cogan, N.G., and Keener, J.P. (2004) The role of the biofilm matrix in structural development. *Math Med Biol* **21**: 147–166.
  - Combet, C., Blanchet, C., and Geourjon, C. (2000) *NPS@: network protein sequence analysis*. *Trends Biochem Sci* **25**: 147–150.
  - Conchillo-Solé, O., de Groot, N.S., Avilés, F.X., Vendrell, J., Daura, X., and Ventura, S. (2007) AGGRESKAN: a server for the prediction and evaluation of “hot spots” of aggregation in polypeptides. *BMC Bioinformatics* **8**: 65.
  - Conlon, B.P., Geoghegan, J.A., Waters, E.M., McCarthy, H., Rowe, S.E., Davies, J.R., *et al.* (2014) Role for the A domain of unprocessed Accumulation-Associated Protein (Aap) in the attachment phase of the *Staphylococcus epidermidis* biofilm phenotype. *J Bacteriol* **196**: 4268–4275.
  - Conrady, D.G., Brescia, C.C., Horii, K., Weiss, A.A., Hassett, D.J., and Herr, A.B. (2008) A zinc-dependent adhesion module is responsible for intercellular adhesion in staphylococcal biofilms. *Proc Natl Acad Sci USA* **105**: 19456–19461.
  - Conrady, D.G., Wilson, J.J., and Herr, A.B. (2013) Structural basis for Zn<sup>2+</sup>-dependent intercellular adhesion in staphylococcal biofilms. *Proc*

*Natl Acad Sci USA* **110**: E202–E211.

- Corrêa, I.R. (2014) Live-cell reporters for fluorescence imaging. *Curr Opin Chem Biol* **20**: 36–45.
- Corrigan, R.M., Rigby, D., Handley, P., and Foster, T.J. (2007) The role of *Staphylococcus aureus* surface protein SasG in adherence and biofilm formation. *Microbiology* **153**: 2435–2446.
- Costerton, J.W. (1999) Bacterial Biofilms: A Common Cause of Persistent Infections. *Science* **284**: 1318–1322.
- Costerton, J.W., Lewandowski, Z., Caldwell, D.E., Korber, D.R., and Lappin-Scott, H.M. (1995) Microbial Biofilms. *Annu Rev Microbiol* **49**: 711–745.
- Cramton, S.E., Gerke, C., Schnell, N.F., Nichols, W.W., and Götz, F. (1999) The intercellular adhesion (*ica*) locus is present in *Staphylococcus aureus* and is required for biofilm formation. *Infect Immun* **67**: 5427–5433.
- Cucarella, C., Solano, C., Valle, J., Amorena, B., Lasa, I., and Penades, J.R. (2001) Bap, a *Staphylococcus aureus* surface protein involved in biofilm formation. *J Bacteriol* **183**: 2888–2896.
- Cucarella, C., Tormo, M.A., Knecht, E., Amorena, B., Lasa, Í., Foster, T.J., and Penadés, J.R. (2002) Expression of the biofilm-associated protein interferes with host protein receptors of *Staphylococcus aureus* and alters the infective process. *Infect Immun* **70**: 3180–3186.
- Cucarella, C., Tormo, M.A., Ubeda, C., Trotonda, M.P., Monzon, M., Peris, C., *et al.* (2004) Role of Biofilm-associated protein Bap in the pathogenesis of bovine *Staphylococcus aureus*. *Infect Immun* **72**: 2177–2185.
- De Jong, W., Wösten, H., and Dijkhuizen, L. (2009) Attachment of *Streptomyces coelicolor* is mediated by amyloid fimbriae that are anchored to the cell surface via cellulose. *Mol Microbiol* **73**: 1128–1140.
- Decker, R., Burdelski, C., Zobiak, M., Büttner, H., Franke, G., Christner, M., *et al.* (2015) An 18 kDa scaffold protein is critical for *Staphylococcus epidermidis* biofilm formation. *PLoS Pathog* **11**: e1004735.
- DeDent, A., Bae, T., Missiakas, D.M., and Schneewind, O. (2008) Signal peptides direct surface proteins to two distinct envelope locations of *Staphylococcus aureus*. *EMBO J* **27**: 2656–2668.

## References

---

- Donlan, R.M. (2001) Biofilms and device-associated infections. *Emerging Infect Dis* **7**: 277–281.
- Donlan, R.M. (2002) Biofilms: microbial life on surfaces. *Emerging Infect Dis* **8**: 881–890.
- Dueholm, M.S., Albertsen, M., Otzen, D., and Nielsen, P.H. (2012) Curli functional amyloid systems are phylogenetically widespread and display large diversity in operon and protein structure. *PLoS ONE* **7**: e51274.
- Dueholm, M.S., Otzen, D., and Nielsen, P.H. (2013a) Evolutionary insight into the functional amyloids of the pseudomonads. *PLoS ONE* **8**: e76630.
- Dueholm, M.S., Petersen, S.V., Sonderkaer, M., Larsen, P., Christiansen, G., Hein, K.L., *et al.* (2010) Functional amyloid in *Pseudomonas*. *Mol Microbiol* **77**: 1009–1020.
- Dueholm, M.S., Søndergaard, M.T., Nilsson, M., Christiansen, G., Stensballe, A., Overgaard, M.T., *et al.* (2013b) Expression of Fap amyloids in *Pseudomonas aeruginosa*, *P. fluorescens*, and *P. putida* results in aggregation and increased biofilm formation. *MicrobiologyOpen* **2**: 365–382.
- Dunne, W.M. (2002) Bacterial adhesion: seen any good biofilms lately? *Clin Microbiol Rev* **15**: 155–166.
- Duthie, E.S., and Lorenz, L.L. (1952) Staphylococcal coagulase: mode of action and antigenicity. *J Gen Microbiol* **6**: 95–107.
- Dziewanowska, K., Carson, A.R., Patti, J.M., Deobald, C.F., Bayles, K.W., and Bohach, G.A. (2000) Staphylococcal fibronectin binding protein interacts with heat shock protein 60 and integrins: role in internalization by epithelial cells. *Infect Immun* **68**: 6321–6328.
- Dziewanowska, K., Patti, J.M., Deobald, C.F., Bayles, K.W., Trumble, W.R., and Bohach, G.A. (1999) Fibronectin binding protein and host cell tyrosine kinase are required for internalization of *Staphylococcus aureus* by epithelial cells. *Infect Immun* **67**: 4673–4678.
- Ehrnhoefer, D.E., Bieschke, J., Boeddrich, A., Herbst, M., Masino, L., Lurz, R., *et al.* (2008) EGCG redirects amyloidogenic polypeptides into unstructured, off-pathway oligomers. *Nat Struct Mol Biol* **15**: 558–566.
- Epstein, E.A., and Chapman, M.R. (2008) Polymerizing the fibre between bacteria and host cells: the biogenesis of functional amyloid fibres. *Cell Microbiol* **10**: 1413–1420.

- Espinosa-Urgel, M. (2004) Plant-associated *Pseudomonas* populations: molecular biology, DNA dynamics, and gene transfer. *Plasmid* **52**: 139–150.
- Esteras-Chopo, A., Serrano, L., and López de la Paz, M. (2005) The amyloid stretch hypothesis: recruiting proteins toward the dark side. *Proc Natl Acad Sci USA* **102**: 16672–16677.
- Evans, M.L., Chorell, E., Taylor, J.D., Åden, J., Göthesson, A., Li, F., *et al.* (2015) The bacterial curli system possesses a potent and selective inhibitor of amyloid formation. *Mol Cell* **57**: 445–455.
- Formosa-Dague, C., Speziale, P., Foster, T.J., Geoghegan, J.A., and Dufrêne, Y.F. (2016) Zinc-dependent mechanical properties of *Staphylococcus aureus* biofilm-forming surface protein SasG. *Proc Natl Acad Sci USA* **113**: 410–415.
- Foster, T. (1998) Surface protein adhesins of *Staphylococcus aureus*. *Trends Microbiol* **6**: 484–488.
- Foster, T.J., Geoghegan, J.A., Ganesh, V.K., and Höök, M. (2014) Adhesion, invasion and evasion: the many functions of the surface proteins of *Staphylococcus aureus*. *Nat Rev Microbiol* **12**: 49–62.
- Foulston, L., Elsholz, A.K.W., Defrancesco, A.S., and Losick, R. (2014) The extracellular matrix of *Staphylococcus aureus* biofilms comprises cytoplasmic proteins that associate with the cell surface in response to decreasing pH. *mBio* **5**: e01667–14–e01667–14.
- Fox, P.F., and McSweeney, P. (1998) Dairy chemistry and biochemistry.
- Fraunholz, M., and Sinha, B. (2012) Intracellular *Staphylococcus aureus*: live-in and let die. *Front Cell Infect Microbiol* **2**: 43.
- Fux, C.A., Costerton, J.W., Stewart, P.S., and Stoodley, P. (2005) Survival strategies of infectious biofilms. *Trends Microbiol* **13**: 34–40.
- Gallo, P.M., Rapsinski, G.J., Wilson, R.P., Oppong, G.O., Sriram, U., Goulian, M., *et al.* (2015) Amyloid-DNA composites of bacterial biofilms stimulate autoimmunity. *Immunity* **42**: 1171–1184.
- Geoghegan, J.A., Corrigan, R.M., Gruszka, D.T., Speziale, P., O'Gara, J.P., Potts, J.R., and Foster, T.J. (2010) Role of surface protein SasG in biofilm formation by *Staphylococcus aureus*. *J Bacteriol* **192**: 5663–5673.

## References

---

- Geoghegan, J.A., Monk, I.R., O'Gara, J.P., and Foster, T.J. (2013) Subdomains N2N3 of fibronectin binding protein A mediate *Staphylococcus aureus* biofilm formation and adherence to fibrinogen using distinct mechanisms. *J Bacteriol* **195**: 2675–2683.
- Gerke, C., Kraft, A., Sussmuth, R., Schweitzer, O., and Götz, F. (1998) Characterization of the N-Acetylglucosaminyltransferase Activity Involved in the Biosynthesis of the *Staphylococcus epidermidis* Polysaccharide Intercellular Adhesin. *J Biol Chem* **273**: 18586–18593.
- Ghigo, J.M. (2001) Natural conjugative plasmids induce bacterial biofilm development. *Nature* **412**: 442–445.
- Gil, C., Solano, C., Burgui, S., Latasa, C., García, B., Toledo-Arana, A., *et al.* (2014) Biofilm matrix exoproteins induce a protective immune response against *Staphylococcus aureus* biofilm infection. *Infect Immun* **82**: 1017–1029.
- Giraldo, R. (2007) Defined DNA sequences promote the assembly of a bacterial protein into distinct amyloid nanostructures. *Proc Natl Acad Sci USA* **104**: 17388–17393.
- Goldschmidt, L., Teng, P.K., Riek, R., and Eisenberg, D. (2010) Identifying the amyloids, proteins capable of forming amyloid-like fibrils. *Proc Natl Acad Sci USA* **107**: 3487–3492.
- Gordon, R.J., and Lowy, F.D. (2008) Pathogenesis of methicillin-resistant *Staphylococcus aureus* infection. *Clin Infect Dis* **46**: S350–359.
- Götz, F. (2002) Staphylococcus and biofilms. *Mol Microbiol* **43**: 1367–1378.
- Gruszka, D.T., Wojdyla, J.A., Bingham, R.J., Turkenburg, J.P., Manfield, I.W., Steward, A., *et al.* (2012) Staphylococcal biofilm-forming protein has a contiguous rod-like structure. *Proc Natl Acad Sci USA* **109**: E1011–1018.
- Hall-Stoodley, L., and Stoodley, P. (2002) Developmental regulation of microbial biofilms. *Curr Opin Biotechnol* **13**: 228–233.
- Hall-Stoodley, L., and Stoodley, P. (2005) Biofilm formation and dispersal and the transmission of human pathogens. *Trends Microbiol* **13**: 7–10.
- Harmon, R.J. (1994) Physiology of mastitis and factors affecting somatic cell counts. *J Dairy Sci* **77**: 2103–2112.

- Harmsen, M., Lappann, M., Knøchel, S., and Molin, S. (2010) Role of extracellular DNA during biofilm formation by *Listeria monocytogenes*. *Appl Environ Microbiol* **76**: 2271–2279.
- Heilmann, C., Hussain, M., Peters, G., and Götz, F. (1997) Evidence for autolysin-mediated primary attachment of *Staphylococcus epidermidis* to a polystyrene surface. *Mol Microbiol* **24**: 1013–1024.
- Heilmann, C., Schweitzer, O., Gerke, C., Vanittanakom, N., Mack, D., and Götz, F. (1996) Molecular basis of intercellular adhesion in the biofilm-forming *Staphylococcus epidermidis*. *Mol Microbiol* **20**: 1083–1091.
- Herman-Bausier, P., El-Kirat-Chatel, S., Foster, T.J., Geoghegan, J.A., and Dufrêne, Y.F. (2015) *Staphylococcus aureus* Fibronectin-Binding Protein A mediates cell-cell adhesion through low-affinity homophilic bonds. *mBio* **6**: e00413–15.
- Hinsä, S.M., Espinosa-Urgel, M., Ramos, J.L., and O'Toole, G.A. (2003) Transition from reversible to irreversible attachment during biofilm formation by *Pseudomonas fluorescens* WCS365 requires an ABC transporter and a large secreted protein. *Mol Microbiol* **49**: 905–918.
- Houston, P., Rowe, S.E., Pozzi, C., Waters, E.M., and O'Gara, J.P. (2011) Essential role for the major autolysin in the fibronectin-binding protein-mediated *Staphylococcus aureus* biofilm phenotype. *Infect Immun* **79**: 1153–1165.
- Huber, B., Riedel, K., Köthe, M., Givskov, M., Molin, S., and Eberl, L. (2002) Genetic analysis of functions involved in the late stages of biofilm development in *Burkholderia cepacia* H111. *Mol Microbiol* **46**: 411–426.
- Hufnagel, D.A., Tükel, Ç., and Chapman, M.R. (2013) Disease to dirt: the biology of microbial amyloids. *PLoS Pathog* **9**: e1003740.
- Høiby, N., Ciofu, O., Johansen, H.K., Song, Z.-J., Moser, C., Jensen, P.Ø., *et al.* (2011) The clinical impact of bacterial biofilms. *Int J Oral Sci* **3**: 55–65.
- Ivanova, M.I., Sawaya, M.R., Gingery, M., Attinger, A., and Eisenberg, D. (2004) An amyloid-forming segment of beta2-microglobulin suggests a molecular model for the fibril. *Proc Natl Acad Sci USA* **101**: 10584–10589.
- Janzon, L., Löfdahl, S., and Arvidson, S. (1989) Identification and nucleotide sequence of the delta-lysin gene, *hld*, adjacent to the accessory gene regulator (*agr*) of *Staphylococcus aureus*. *Mol Gen Genet* **219**: 480–485.

- Jefferson, K.K. (2004) What drives bacteria to produce a biofilm? *FEMS Microbiol Lett* **236**: 163–173.
- Jones, R.N. (2008) Key considerations in the treatment of complicated staphylococcal infections. *Clin Microbiol Infect* **14 Suppl 2**: 3–9.
- Jubelin, G., Vianney, A., Beloin, C., Ghigo, J.-M., Lazzaroni, J.-C., Lejeune, P., and Dorel, C. (2005) CpxR/OmpR interplay regulates curli gene expression in response to osmolarity in *Escherichia coli*. *J Bacteriol* **187**: 2038–2049.
- Kaplan, J.B., Ragunath, C., Velliyagounder, K., Fine, D.H., and Ramasubbu, N. (2004) Enzymatic detachment of *Staphylococcus epidermidis* biofilms. *Antimicrob Agents Chemother* **48**: 2633–2636.
- Kato, M., Han, T.W., Xie, S., Shi, K., Du, X., Wu, L.C., *et al.* (2012) Cell-free formation of RNA granules: low complexity sequence domains form dynamic fibers within hydrogels. *Cell* **149**: 753–767.
- Kearns, D.B., Chu, F., Branda, S.S., Kolter, R., and Losick, R. (2005) A master regulator for biofilm formation by *Bacillus subtilis*. *Mol Microbiol* **55**: 739–749.
- Keppler, A., Gendreizig, S., Gronemeyer, T., Pick, H., Vogel, H., and Johnsson, K. (2002) A general method for the covalent labeling of fusion proteins with small molecules *in vivo*. *Nat Biotechnol* **21**: 86–89.
- Keppler, A., Pick, H., Arrivoli, C., Vogel, H., and Johnsson, K. (2004) Labeling of fusion proteins with synthetic fluorophores in live cells. *Proc Natl Acad Sci USA* **101**: 9955–9959.
- Kisiday, J., Jin, M., Kurz, B., Hung, H., Semino, C., Zhang, S., and Grodzinsky, A.J. (2002) Self-assembling peptide hydrogel fosters chondrocyte extracellular matrix production and cell division: implications for cartilage tissue repair. *Proc Natl Acad Sci USA* **99**: 9996–10001.
- Klein, R.D., and Hultgren, S.J. (2015) Chaos controlled: discovery of a powerful amyloid inhibitor. *Mol Cell* **57**: 391–393.
- Klemm, P., Hjerrild, L., Gjermansen, M., and Schembri, M.A. (2004) Structure-function analysis of the self-recognizing Antigen 43 autotransporter protein from *Escherichia coli*. *Mol Microbiol* **51**: 283–296.
- Klevens, R.M., Morrison, M.A., Nadle, J., Petit, S., Gershman, K., Ray,



- S., *et al.* (2007) Invasive methicillin-resistant *Staphylococcus aureus* infections in the United States. *JAMA* **298**: 1763–1771.
- Knudsen, S.K., Stensballe, A., Franzmann, M., Westergaard, U.B., and Otzen, D.E. (2008) Effect of glycosylation on the extracellular domain of the Ag43 bacterial autotransporter: enhanced stability and reduced cellular aggregation. *Biochem J* **412**: 563.
  - Kolenbrander, P.E. (2000) Oral microbial communities: biofilms, interactions, and genetic systems. *Annu Rev Microbiol* **54**: 413–437.
  - Kreiswirth, B., Kornblum, J., Arbeit, R.D., Eisner, W., Maslow, J.N., McGeer, A., *et al.* (1993) Evidence for a clonal origin of methicillin resistance in *Staphylococcus aureus*. *Science* **259**: 227–230.
  - Kuhlman, B., and Baker, D. (2000) Native protein sequences are close to optimal for their structures. *Proc Natl Acad Sci USA* **97**: 10383–10388.
  - Kuroda, M., Yamashita, A., Hiramawa, H., Kumano, M., Morikawa, K., Higashide, M., *et al.* (2005) Whole genome sequence of *Staphylococcus saprophyticus* reveals the pathogenesis of uncomplicated urinary tract infection. *Proc Natl Acad Sci USA* **102**: 13272–13277.
  - Lardner, A. (2001) The effects of extracellular pH on immune function. *J Leukoc Biol* **69**: 522–530.
  - Larson, M.R., Rajashankar, K.R., Crowley, P.J., Kelly, C., Mitchell, T.J., Brady, L.J., and Deivanayagam, C. (2011) Crystal structure of the C-terminal region of *Streptococcus mutans* antigen I/II and characterization of salivary agglutinin adherence domains. *J Biol Chem* **286**: 21657–21666.
  - Larson, M.R., Rajashankar, K.R., Patel, M.H., Robinette, R.A., Crowley, P.J., Michalek, S., *et al.* (2010) Elongated fibrillar structure of a streptococcal adhesin assembled by the high-affinity association of alpha- and PPII-helices. *Proc Natl Acad Sci USA* **107**: 5983–5988.
  - Lasa, I. (2006) Towards the identification of the common features of bacterial biofilm development. *Int Microbiol* **9**: 21–28.
  - Lasa, I., and Penadés, J. (2006) Bap: a family of surface proteins involved in biofilm formation. *Res Microbiol* **157**: 99–107.
  - Latasa, C., Roux, A., Toledo-Arana, A., Ghigo, J.-M., Gamazo, C., Penadés, J.R., and Lasa, I. (2005) BapA, a large secreted protein required for biofilm formation and host colonization of *Salmonella*

- enterica* serovar Enteritidis. *Mol Microbiol* **58**: 1322–1339.
- Latasa, C., Solano, C., Penadés, J.R., and Lasa, I. (2006) Biofilm-associated proteins. *C R Biol* **329**: 849–857.
  - Le, K.Y., Dastgheyb, S., Ho, T.V., and Otto, M. (2014) Molecular determinants of staphylococcal biofilm dispersal and structuring. *Front Cell Infect Microbiol* **4**: 167–167.
  - Leal, S.S., Botelho, H.M., and Gomes, C.M. (2012) Metal ions as modulators of protein conformation and misfolding in neurodegeneration. *Coord Chem Rev* **256**: 2253–2270.
  - Li, Q., Kumar, A., Makhija, E., and Shivashankar, G.V. (2014) The regulation of dynamic mechanical coupling between actin cytoskeleton and nucleus by matrix geometry. *Biomaterials* **35**: 961–969.
  - Loehfelm, T.W., Luke, N.R., and Campagnari, A.A. (2008) Identification and characterization of an *Acinetobacter baumannii* biofilm-associated protein. *J Bacteriol* **190**: 1036–1044.
  - Macintosh, R.L., Brittan, J.L., Bhattacharya, R., Jenkinson, H.F., Derrick, J., Upton, M., and Handley, P.S. (2009) The terminal A domain of the fibrillar accumulation-associated protein (Aap) of *Staphylococcus epidermidis* mediates adhesion to human corneocytes. *J Bacteriol* **191**: 7007–7016.
  - Mack, D., Haeder, M., Siemssen, N., and Laufs, R. (1996) Association of biofilm production of coagulase-negative staphylococci with expression of a specific polysaccharide intercellular adhesin. *J Infect Dis* **174**: 881–884.
  - Mackaness, G.B. (1964) The immunological basis of acquired cellular resistance. *J Exp Med* **120**: 105–120.
  - Maher, M.C., Lim, J.Y., Gunawan, C., and Cegelski, L. (2015) Cell-based high-throughput screening identifies rifapentine as an inhibitor of amyloid and biofilm formation in *Escherichia coli*. *ACS Infect Dis* **1**: 460–468.
  - Maji, S.K., Schubert, D., Rivier, C., Lee, S., Rivier, J.E., and Riek, R. (2008) Amyloid as a depot for the formulation of long acting drugs. *PLoS Biol* **6**: e17.
  - Mankar, S., Anoop, A., Sen, S., and Maji, S.K. (2011) Nanomaterials: amyloids reflect their brighter side. *Nano Rev* **2**: 6032.

- Mann, E.E., Rice, K.C., Boles, B.R., Endres, J.L., Ranjit, D., Chandramohan, L., *et al.* (2009) Modulation of eDNA Release and Degradation Affects *Staphylococcus aureus* Biofilm Maturation. *PLoS ONE* **4**: e5822.
- Martí, M., Trotonda, M.P., Tormo-Más, M.Á., Vergara-Irigaray, M., Cheung, A.L., Lasa, I., and Penadés, J.R. (2010) Extracellular proteases inhibit protein-dependent biofilm formation in *Staphylococcus aureus*. *Microb Infect* **12**: 55–64.
- Maurer, P., Hohenester, E., and Engel, J. (1996) Extracellular calcium-binding proteins. *Curr Opin Cell Biol* **8**: 609–617.
- McCarthy, H., Rudkin, J.K., Black, N.S., Gallagher, L., O'Neill, E., and O'Gara, J.P. (2015) Methicillin resistance and the biofilm phenotype in *Staphylococcus aureus*. *Front Cell Infect Microbiol* **5**: 1.
- McKenney, D., Pouliot, K.L., Wang, Y., Murthy, V., Ulrich, M., Döring, G., *et al.* (1999) Broadly protective vaccine for *Staphylococcus aureus* based on an *in vivo*-expressed antigen. *Science* **284**: 1523–1527.
- Merino, N., Toledo-Arana, A., Vergara-Irigaray, M., Valle, J., Solano, C., Calvo, E., *et al.* (2009) Protein A-mediated multicellular behavior in *Staphylococcus aureus*. *J Bacteriol* **191**: 832–843.
- Morikawa, M. (2006) Beneficial biofilm formation by industrial bacteria *Bacillus subtilis* and related species. *J Biosci Bioeng* **101**: 1–8.
- Navarro, S., and Ventura, S. (2014) Fluorescent dye ProteoStat to detect and discriminate intracellular amyloid-like aggregates in *Escherichia coli*. *Biotechnol J* **9**: 1259–1266.
- Nguyen, P.Q., Botyanszki, Z., Tay, P.K.R., and Joshi, N.S. (2014) Programmable biofilm-based materials from engineered curli nanofibres. *Nat Commun* **5**: 4945.
- O'Gara, J.P. (2007) *ica* and beyond: biofilm mechanisms and regulation in *Staphylococcus epidermidis* and *Staphylococcus aureus*. *FEMS Microbiol Lett* **270**: 179–188.
- O'Toole, G., Kaplan, H.B., and Kolter, R. (2000) Biofilm formation as microbial development. *Annu Rev Microbiol* **54**: 49–79.
- Oli, M.W., Otoo, H.N., Crowley, P.J., Heim, K.P., Nascimento, M.M., Ramsook, C.B., *et al.* (2012) Functional amyloid formation by *Streptococcus mutans*. *Microbiology* **158**: 2903–2916.

## References

---

- Oliveberg, M. (2010) Waltz, an exciting new move in amyloid prediction. *Nat Methods* **7**: 187–188.
- Oshida, T., Sugai, M., Komatsuzawa, H., Hong, Y.M., Suginaka, H., and Tomasz, A. (1995) A *Staphylococcus aureus* autolysin that has an N-acetylmuramoyl-L-alanine amidase domain and an endo-beta-N-acetylglucosaminidase domain: cloning, sequence analysis, and characterization. *Proc Natl Acad Sci USA* **92**: 285–289.
- Otzen, D.E. (2012) Amyloid Fibrils and Prefibrillar aggregates. 1–500.
- Pamp, S.J., and Gjermansen, M. (2007) The biofilm matrix: a sticky framework. *The biofilm mode of life: mechanisms and adaptations*. Norfolk, UK: Horizon Scientific Press 37-69.
- Pantůček, R., Sedláček, I., Petrás, P., Koukalová, D., Svec, P., Stetina, V., *et al.* (2005) *Staphylococcus simiae* sp. nov., isolated from South American squirrel monkeys. *Int J Syst Evol Microbiol* **55**: 1953–1958.
- Park, S., Kelley, K.A., Vinogradov, E., Solinga, R., Weidenmaier, C., Misawa, Y., and Lee, J.C. (2010) Characterization of the structure and biological functions of a capsular polysaccharide produced by *Staphylococcus saprophyticus*. *J Bacteriol* **192**: 4618–4626.
- Paterson, G.K., and Mitchell, T.J. (2004) The biology of Gram-positive sortase enzymes. *Trends Microbiol* **12**: 89–95.
- Prigent-Combaret, C., Brombacher, E., Vidal, O., Ambert, A., Lejeune, P., Landini, P., and Dorel, C. (2001) Complex regulatory network controls initial adhesion and biofilm formation in *Escherichia coli* via regulation of the *csgD* gene. *J Bacteriol* **183**: 7213–7223.
- Qin, Z., Ou, Y., Yang, L., Zhu, Y., Tolker-Nielsen, T., Molin, S., and Qu, D. (2007) Role of autolysin-mediated DNA release in biofilm formation of *Staphylococcus epidermidis*. *Microbiology* **153**: 2083–2092.
- Queck, S.Y., Jameson-Lee, M., Villaruz, A.E., Bach, T.-H.L., Khan, B.A., Sturdevant, D.E., *et al.* (2008) RNAIII-independent target gene control by the *agr* quorum-sensing system: insight into the evolution of virulence regulation in *Staphylococcus aureus*. *Mol Cell* **32**: 150–158.
- Radostits, O.M., Gay, C.C., Hinchcliff, K.W., and Constable, P.D. (2006) *Veterinary Medicine: A textbook of the diseases of cattle, horses, sheep, pigs and goats*.
- Reid, G. (1999) Biofilms in infectious disease and on medical devices. *Int J Antimicrob Agents* **11**: 223–6– discussion 237–9.

- Rice, K.C., Mann, E.E., Endres, J.L., Weiss, E.C., Cassat, J.E., Smeltzer, M.S., and Bayles, K.W. (2007) The *cidA* murein hydrolase regulator contributes to DNA release and biofilm development in *Staphylococcus aureus*. *Proc Natl Acad Sci USA* **104**: 8113–8118.
- Roche, F.M., Meehan, M., and Foster, T.J. (2003) The *Staphylococcus aureus* surface protein SasG and its homologues promote bacterial adherence to human desquamated nasal epithelial cells. *Microbiology* **149**: 2759–2767.
- Rohde, H.H., Burdelski, C.C., Bartscht, K.K., Hussain, M.M., Buck, F.F., Horstkotte, M.A.M., *et al.* (2005) Induction of *Staphylococcus epidermidis* biofilm formation via proteolytic processing of the accumulation-associated protein by staphylococcal and host proteases. *Mol Microbiol* **55**: 1883–1895.
- Romero, D., Aguilar, C., Losick, R., and Kolter, R. (2010) Amyloid fibers provide structural integrity to *Bacillus subtilis* biofilms. *Proc Natl Acad Sci USA* **107**: 2230–2234.
- Romero, D., and Kolter, R. (2014) Functional amyloids in bacteria. *Int Microbiol* **17**: 65–73.
- Romero, D., Sanabria-Valentín, E., Vlamakis, H., and Kolter, R. (2013) Biofilm inhibitors that target amyloid proteins. *Chem Biol* **20**: 102–110.
- Romero, D., Vlamakis, H., Losick, R., and Kolter, R. (2011) An accessory protein required for anchoring and assembly of amyloid fibres in *B. subtilis* biofilms. *Mol Microbiol* **80**: 1155–1168.
- Romero, D., Vlamakis, H., Losick, R., and Kolter, R. (2014) Functional analysis of the accessory protein TapA in *Bacillus subtilis* amyloid fiber assembly. *J Bacteriol* **196**: 1505–1513.
- Romling, U., Rohde, M., Olsén, A., Normark, S., and Reinköster, J. (2000) AgfD, the checkpoint of multicellular and aggregative behaviour in *Salmonella typhimurium* regulates at least two independent pathways. *Mol Microbiol* **36**: 10–23.
- Rosenstein, R., Nerz, C., Biswas, L., Resch, A., Raddatz, G., Schuster, S.C., and Götz, F. (2009) Genome analysis of the meat starter culture bacterium *Staphylococcus carnosus* TM300. *Appl Environ Microbiol* **75**: 811–822.
- Sambrook, J., Fritsch, E.F., and Maniatis, T. (1989) *Molecular Cloning*.

## References

---

- Sawyer, E.B., Claessen, D., Gras, S.L., and Perrett, S. (2012) Exploiting amyloid: how and why bacteria use cross- $\beta$  fibrils. *Biochem Soc Trans* **40**: 728–734.
- Sánchez-Magraner, L., Cortajarena, A.L., García-Pacios, M., Arrondo, J.-L.R., Agirre, J., Guérin, D.M.A., *et al.* (2010) Interdomain  $\text{Ca}^{2+}$  effects in *Escherichia coli* alpha-haemolysin:  $\text{Ca}^{2+}$  binding to the C-terminal domain stabilizes both C- and N-terminal domains. *Biochim Biophys Acta* **1798**: 1225–1233.
- Schenk, S., and Laddaga, R.A. (1992) Improved method for electroporation of *Staphylococcus aureus*. *FEMS Microbiol Lett* **73**: 133–138.
- Schmittschmitt, J.P., and Scholtz, J.M. (2003) The role of protein stability, solubility, and net charge in amyloid fibril formation. *Protein Sci* **12**: 2374–2378.
- Schoene, C., Fierer, J.O., Bennett, S.P., and Howarth, M. (2014) SpyTag/SpyCatcher cyclization confers resilience to boiling on a mesophilic enzyme. *Angew Chem Int Ed Engl* **53**: 6101–6104.
- Schroeder, K., Jularic, M., Horsburgh, S.M., Hirschhausen, N., Neumann, C., Bertling, A., *et al.* (2009) Molecular characterization of a novel *Staphylococcus aureus* surface protein (SasC) involved in cell aggregation and biofilm accumulation. *PLoS ONE* **4**: e7567.
- Schuck, P. (2000) Size-distribution analysis of macromolecules by sedimentation velocity ultracentrifugation and Lamm equation modeling. *Biophys J* **78**: 1606–1619.
- Schwartz, K., Ganesan, M., Payne, D.E., Solomon, M.J., and Boles, B.R. (2016) Extracellular DNA facilitates the formation of functional amyloids in *Staphylococcus aureus* biofilms. *Mol Microbiol* **99**: 123–134.
- Schwartz, K., Sekedat, M.D., Syed, A.K., O'Hara, B., Payne, D.E., Lamb, A., and Boles, B.R. (2014) The AgrD N-terminal leader peptide of *Staphylococcus aureus* has cytolytic and amyloidogenic properties. *Infect Immun* **82**: 3837–3844.
- Schwartz, K., Syed, A.K., Stephenson, R.E., Rickard, A.H., and Boles, B.R. (2012) Functional amyloids composed of phenol soluble modulins stabilize *Staphylococcus aureus* biofilms. *PLoS Pathog* **8**: e1002744.
- Shahnawaz, M., and Soto, C. (2012) Microcin Amyloid Fibrils A Are Reservoir of Toxic Oligomeric Species. *J Biol Chem* **287**: 11665–11676.

- Shankar, N., Lockatell, C.V., Baghdayan, A.S., Drachenberg, C., Gilmore, M.S., and Johnson, D.E. (2001) Role of *Enterococcus faecalis* surface protein Esp in the pathogenesis of ascending urinary tract infection. *Infect Immun* **69**: 4366–4372.
- Simm, R., Morr, M., Kader, A., Nimtz, M., and Romling, U. (2004) GGDEF and EAL domains inversely regulate cyclic di-GMP levels and transition from sessility to motility. *Mol Microbiol* **53**: 1123–1134.
- Sivanathan, V., and Hochschild, A. (2013) A bacterial export system for generating extracellular amyloid aggregates. *Nat Protoc* **8**: 1381–1390.
- Solano, C., Sesma, B., Alvarez, M., Humphrey, T.J., Thorns, C.J., and Gamazo, C. (1998) Discrimination of strains of *Salmonella enteritidis* with differing levels of virulence by an in vitro glass adherence test. *J Clin Microbiol* **36**: 674–678.
- Sonohara, R., Muramatsu, N., Ohshima, H., and Kondo, T. (1995) Difference in surface properties between *Escherichia coli* and *Staphylococcus aureus* as revealed by electrophoretic mobility measurements. *Biophys Chem* **55**: 273–277.
- Speziale, P., Pietrocola, G., Foster, T.J., and Geoghegan, J.A. (2014) Protein-based biofilm matrices in Staphylococci. *Front Cell Infect Microbiol* **4**.
- Sreerama, N., and Woody, R.W. (2000) Estimation of protein secondary structure from circular dichroism spectra: comparison of CONTIN, SELCON, and CDSSTR methods with an expanded reference set. *Anal Biochem* **287**: 252–260.
- Sung, J.M.-L., Lloyd, D.H., and Lindsay, J.A. (2008) *Staphylococcus aureus* host specificity: comparative genomics of human versus animal isolates by multi-strain microarray. *Microbiology* **154**: 1949–1959.
- Sutherland, I. (2001) The biofilm matrix - an immobilized but dynamic microbial environment. *Trends Microbiol* **9**: 222–227.
- Syed, A.K., and Boles, B.R. (2014) Fold modulating function: bacterial toxins to functional amyloids. *Front Microbiol* **5**: 401.
- Tendolkar, P.M., Baghdayan, A.S., Gilmore, M.S., and Shankar, N. (2004) Enterococcal surface protein, Esp, enhances biofilm formation by *Enterococcus faecalis*. *Infect Immun* **72**: 6032–6039.
- Terra, R., Stanley-Wall, N.R., Cao, G., and Lazazzera, B.A. (2012) Identification of *Bacillus subtilis* SipW as a bifunctional signal peptidase

- that controls surface-adhered biofilm formation. *J Bacteriol* **194**: 2781–2790.
- Thompson, M.J., Sievers, S.A., Karanicolas, J., Ivanova, M.I., Baker, D., and Eisenberg, D. (2006) The 3D profile method for identifying fibril-forming segments of proteins. *Proc Natl Acad Sci USA* **103**: 4074–4078.
  - Toledo-Arana, A., Valle, J., Solano, C., Arrizubieta, M.J., Cucarella, C., Lamata, M., *et al.* (2001) The enterococcal surface protein, Esp, is involved in *Enterococcus faecalis* biofilm formation. *Appl Environ Microbiol* **67**: 4538–4545.
  - Tong, S.Y.C., Davis, J.S., Eichenberger, E., Holland, T.L., and Fowler, V.G. (2015) *Staphylococcus aureus* infections: epidemiology, pathophysiology, clinical manifestations, and management. *Clin Microbiol Rev* **28**: 603–661.
  - Tormo, M.A., Knecht, E., Götz, F., Lasa, I., and Penadés, J.R. (2005) Bap-dependent biofilm formation by pathogenic species of *Staphylococcus*: evidence of horizontal gene transfer? *Microbiology* **151**: 2465–2475.
  - Tournu, H., and Van Dijck, P. (2012) *Candida* biofilms and the host: models and new concepts for eradication. *Int J Microbiol* **2012**: 845352.
  - Troffer-Charlier, N., Ogier, J., Moras, D., and Cavarelli, J. (2002) Crystal structure of the V-region of *Streptococcus mutans* antigen I/II at 2.4 Å resolution suggests a sugar preformed binding site. *J Mol Biol* **318**: 179–188.
  - Trotonda, M.P., Manna, A.C., Cheung, A.L., Lasa, I., and Penades, J.R. (2005) SarA positively controls Bap-dependent biofilm formation in *Staphylococcus aureus*. *J Bacteriol* **187**: 5790–5798.
  - Ubeda, C., Tormo, M.A., Cucarella, C., Trotonda, P., Foster, T.J., Lasa, I., and Penadés, J.R. (2003) Sip, an integrase protein with excision, circularization and integration activities, defines a new family of mobile *Staphylococcus aureus* pathogenicity islands. *Mol Microbiol* **49**: 193–210.
  - Uhlich, G.A., Cooke, P.H., and Solomon, E.B. (2006) Analyses of the Red-Dry-Rough Phenotype of an *Escherichia coli* O157:H7 Strain and Its Role in Biofilm Formation and Resistance to Antibacterial Agents. *Appl Environ Microbiol* **72**: 2564–2572.
  - Valle, J., Latasa, C., Gil, C., Toledo-Arana, A., Solano, C., Penadés, J.R., and Lasa, I. (2012) Bap, a biofilm matrix protein of *Staphylococcus aureus* prevents cellular internalization through binding to GP96 host



receptor. *PLoS Pathog* **8**: e1002843.

- Valle, J., Toledo-Arana, A., Berasain, C., Ghigo, J.-M., Amorena, B., Penadés, J.R., and Lasa, I. (2003) SarA and not  $\sigma^B$  is essential for biofilm development by *Staphylococcus aureus*. *Mol Microbiol* **48**: 1075–1087.
- Van Gerven, N., Klein, R.D., Hultgren, S.J., and Remaut, H. (2015) Bacterial amyloid formation: structural insights into curli biogenesis. *Trends Microbiol* **23**: 693–706.
- Veh, K.A., Klein, R.C., Ster, C., Keefe, G., Lacasse, P., Scholl, D., *et al.* (2015) Genotypic and phenotypic characterization of *Staphylococcus aureus* causing persistent and nonpersistent subclinical bovine intramammary infections during lactation or the dry period. *J Dairy Sci* **98**: 155–168.
- Ventura, S., Zurdo, J., Narayanan, S., Parreno, M., Mangues, R., Reif, B., *et al.* (2004) Short amino acid stretches can mediate amyloid formation in globular proteins: The Src homology 3 (SH3) case. *Proc Natl Acad Sci USA* **101**: 7258–7263.
- Vergara-Irigaray, M., Maira-Litrán, T., Merino, N., Pier, G.B., Penadés, J.R., and Lasa, I. (2008) Wall teichoic acids are dispensable for anchoring the PNAG exopolysaccharide to the *Staphylococcus aureus* cell surface. *Microbiology* **154**: 865–877.
- Vergara-Irigaray, M., Valle, J., Merino, N., Latasa, C., García, B., de Los Mozos, I.R., *et al.* (2009) Relevant role of fibronectin-binding proteins in *Staphylococcus aureus* biofilm-associated foreign-body infections. *Infect Immun* **77**: 3978–3991.
- Vilain, S., Pretorius, J.M., Theron, J., and Brözel, V.S. (2009) DNA as an adhesin: *Bacillus cereus* requires extracellular DNA to form biofilms. *Appl Environ Microbiol* **75**: 2861–2868.
- Vuong, C., Kocianova, S., Voyich, J.M., Yao, Y., Fischer, E.R., DeLeo, F.R., and Otto, M. (2004) A Crucial Role for Exopolysaccharide Modification in Bacterial Biofilm Formation, Immune Evasion, and Virulence. *J Biol Chem* **279**: 54881–54886.
- Walsh, I., Seno, F., Tosatto, S.C.E., and Trovato, A. (2014) PASTA 2.0: an improved server for protein aggregation prediction. *Nucleic Acids Res* **42**: W301–W307.
- Walter, J., Chagnaud, P., Tannock, G.W., Loach, D.M., Dal Bello, F., Jenkinson, H.F., *et al.* (2005) A high-molecular-mass surface protein (Lsp) and methionine sulfoxide reductase B (MsrB) contribute to the

- ecological performance of *Lactobacillus reuteri* in the murine gut. *Appl Environ Microbiol* **71**: 979–986.
- Wang, Hammer, N.D., and Chapman, M.R. (2008) The molecular basis of functional bacterial amyloid polymerization and nucleation. *J Biol Chem* **283**: 21530–21539.
  - Wang, R., Braughton, K.R., Kretschmer, D., Bach, T.-H.L., Queck, S.Y., Li, M., *et al.* (2007) Identification of novel cytolytic peptides as key virulence determinants for community-associated MRSA. *Nat Med* **13**: 1510–1514.
  - Wang, W., and Roberts, C.J. (2010) *Aggregation of therapeutic proteins.*
  - Wang, X., Smith, D.R., Jones, J.W., and Chapman, M.R. (2007) *In vitro* polymerization of a functional *Escherichia coli* amyloid protein. *J Biol Chem* **282**: 3713–3719.
  - Weidenmaier, C., Goerke, C., and Wolz, C. (2012) *Staphylococcus aureus* determinants for nasal colonization. *Trends Microbiol* **20**: 243–250.
  - Weinrick, B., Dunman, P.M., McAleese, F., Murphy, E., Projan, S.J., Fang, Y., and Novick, R.P. (2004) Effect of mild acid on gene expression in *Staphylococcus aureus*. *J Bacteriol* **186**: 8407–8423.
  - Wertheim, H.F.L., Melles, D.C., Vos, M.C., van Leeuwen, W., van Belkum, A., Verbrugh, H.A., and Nouwen, J.L. (2005) The role of nasal carriage in *Staphylococcus aureus* infections. *Lancet Infect Dis* **5**: 751–762.
  - Whitmore, L., and Wallace, B.A. (2004) DICHROWEB, an online server for protein secondary structure analyses from circular dichroism spectroscopic data. *Nucleic Acids Res* **32**: W668–73.
  - Wimpenny, J., Manz, W., and Szewzyk, U. (2000) Heterogeneity in biofilms. *FEMS Microbiol Rev* **24**: 661–671.
  - Wollenberg, M.S., Claesen, J., Escapa, I.F., Aldridge, K.L., Fischbach, M.A., and Lemon, K.P. (2014) *Propionibacterium*-produced coproporphyrin III induces *Staphylococcus aureus* aggregation and biofilm formation. *mBio* **5**: e01286–14–e01286–14.
  - Woodard, D., Bell, D., Tipton, D., Durrance, S., Burnett, L.C., Cole, L., *et al.* (2014) Gel formation in protein amyloid aggregation: a physical mechanism for cytotoxicity. *PLoS ONE* **9**: e94789.

- 
- Yang, Y.-H., Jiang, Y.-L., Zhang, J., Wang, L., Bai, X.-H., Zhang, S.-J., *et al.* (2014) Structural insights into SraP-mediated *Staphylococcus aureus* adhesion to host cells. *PLoS Pathog* **10**: e1004169.
  - Zakeri, B., Fierer, J.O., Celik, E., Chittock, E.C., Schwarz-Linek, U., Moy, V.T., and Howarth, M. (2012) Peptide tag forming a rapid covalent bond to a protein, through engineering a bacterial adhesin. *Proc Natl Acad Sci USA* **109**: E690–7.
  - Zogaj, X., Bokranz, W., Nimitz, M., and Romling, U. (2003) Production of cellulose and curli fimbriae by members of the family *Enterobacteriaceae* isolated from the human gastrointestinal tract. *Infect Immun* **71**: 4151–4158.
  - Zuo, R. (2007) Biofilms: strategies for metal corrosion inhibition employing microorganisms. *Appl Microbiol Biotechnol* **76**: 1245–1253.